

Some pages of this thesis may have been removed for copyright restrictions.

If you have discovered material in Aston Research Explorer which is unlawful e.g. breaches copyright, (either yours or that of a third party) or any other law, including but not limited to those relating to patent, trademark, confidentiality, data protection, obscenity, defamation, libel, then please read our [Takedown policy](#) and contact the service immediately (openaccess@aston.ac.uk)

A STUDY OF THE INFLUENCE OF DIECASTING

MACHINE INJECTION CHARACTERISTICS UPON

METAL FLOW IN RUNNER : GATING SYSTEMS

A Thesis submitted to

THE UNIVERSITY OF ASTON IN BIRMINGHAM

as Partial Requirement for

the Degree of

DOCTOR OF PHILOSOPHY

by

193853 = 9 AUG 1976

Thesis 621.74 0432 MAI

JOHN DENIS MAIDEN, B.Sc.(Hons), M.I.Mech.E., M.I.Prod.E

Production Engineering Department

October 1975

SUMMARY

The object of the thesis is to examine the influence of machine injection systems, and of mould runner : gate systems, upon metal flow in the pressure diecasting process, to enable design of these to be optimized. An analytical framework covering those flow variables which significantly influence casting quality is developed for this purpose and experimental evidence offered in support. The work is presented in two parts:

In part 1, an analysis of machine : mould influence upon flow rate, energy rate and flow state of the casting alloy is presented. Flow rate, (both of the casting alloy and mould gases), is an aspect of pressure casting which has received much attention in previous studies. Consequently in dealing with this aspect comparison is made, where appropriate, with any significant past work both as a means of correlation and also to resolve any anomalies which may exist. A theoretical examination of a number of machine : mould combinations is made, demonstrating the interdependence of injection system and (mould) runner : gate design in establishing flow conditions. Finally the analysis is applied to an experimental diecasting machine and mould and the results of this compared with measured performance.

In part 2, a loss coefficient equation applicable to runner : gating systems is developed for use in the analysis of part 1. This is compared with reported information and with the results of experimentation using a water model. The model is further used to examine state of flow through gating systems both as a corollary to the machine experimentation reported in part 1 and also to enable the flow state criteria proposed in the analysis to be assessed. A range of gating systems are used and flow is examined in both infinite and finite cavity conditions.

CONTENTS

Summary	
Acknowledgments	
Declaration	
List of Figures	

INTRODUCTION

1.	Background	1
1.1	Process definition	1
1.2	Machine : Mould configuration	1
1.3	Quality considerations	3
2.	Definition of Problem	4
2.1	Literature Survey	5
2.1.1	Reported Analysis of Metal Flow	5
2.1.2	Theories Advanced	7
2.1.3	Machine experimentation and Model studies	8
2.2	Research Objectives	12

PART 1

Development of Analytical Framework and application to
Diecasting Systems.

3.	Development of Analysis	15
3.1	Flow rate	15
3.2	Energy rate	32
3.2.1	Resistance coefficients constant	37
3.2.2	Resistance coefficients variable	39
3.3	Flow state	42
3.4	Venting	47
3.5	Conclusions	58

4.	Application of Flow Rate Analysis to General	
	Diecasting Systems	59
4.1	Re-examination of Sachs	59
4.2	Examination of factors affecting transition from	
	unsteady to steady flow conditions	68
4.2.1	Influence of machine : metal system	
	factors	68
4.2.2	Influence of vent closure and cavity	
	resistance	80
4.3	Note on two-stage injection	89
4.4	Conclusions	100
5.	Application of Energy Rate and Flow State Analysis to	
	General Diecasting Systems	103
5.1	Energy Rate Calculations	103
5.2	Flow State Calculations	113
5.3	Conclusions	
6.	Application of Flow Rate Analysis to Experimental Die-	
	casting Machine and Comparison with Measurement	120
6.1	Determination of Machine Resistance and Inertia	
	Factors	121
6.2	Determination of Metal System Resistance and Inertia	
	Factors	125
6.3	Comparison of Calculation and Experimentation	130
6.4	Conclusions	133
7.	Application of Energy Rate and Flow State Analysis to	
	Experimental Diecasting Machine : Mould combination	135
7.1	Energy Rate	135
7.2	Flow State	138
7.3	Conclusions	142

PART 2

Ancillary Studies including the Development of a Loss
Coefficient Equation and Water Model Examination of
Aspects of Flow

8.	Experimental Equipment and Instrumentation	145
8.1	Diecasting Equipment	145
8.1.1	Machine	145
8.1.2	Tooling	145
8.1.3	Casting Alloy	145
8.2	Analogue Equipment	146
8.2.1	Flow Rig	146
8.2.2	Tooling	147
8.2.3	Note on Equipment Limitations	147
8.3	Instrumentation	148
8.3.1	Variables Examined	148
8.3.2	Temperature Measurement	149
8.3.3	Pressure Measurement	150
8.3.4	Displacement and Velocity Measurement	150
8.3.5	Recorder and Galvanometers	151
8.3.6	Timer	152
8.4	Overall Recording and Measurement Accuracy	153
8.4.1	System Response	153
8.4.2	Effect of Siting	153
8.4.3	Measurement of Traces	155
8.5	Photographic Equipment	155
8.5.1	High Speed Filming	155
8.5.2	Still Photography	156


8.6	Experimental Procedure	157
8.6.1	Casting Tests	157
8.6.2	Analogue Studies	158
9.	Loss Factor Assessment in the Metal System	159
9.1	Loss Features	159
9.2	Coefficients for Combined Loss Features	161
9.3	Loss Coefficient Equation	168
9.4	Application to Nussey Gating Systems	169
9.5	Comparison with Sachs Loss coefficient Equation	174
9.6	Application to Experimental Mould	177
9.7	Conclusions	181
10.	Quantitative Study of Nussey Gate Range	182
10.1	Check of Efficiency Values	182
10.2	Loss Coefficient Variation under Unsteady Flow							
	Conditions	184
11.	Experimental Studies of Flow State in Gating Systems using							
	a Water Model	186
11.1	Influence of Gate Geometry	187
11.1.1	Gate Length : Depth Ratio	188
11.1.2	Approach Angle	189
11.1.3	Gate Exit Semi Angle	190
11.1.4	Runner : Gate Width ratio	191
11.1.5	Runner : Gate Asymmetry	192
11.1.6	Comparison of Flow State with Weber							
	Number	193
11.2	Influence of Free Piston Travel	194
11.3	Conclusions	195

12.	Pilot Studies of Cavity Influence upon Flow	197
12.1	Influence of Boundaries Parallel to Flow	197
12.2	Effect of Boundary Obstruction Perpendicular to Mean Flow Direction from Gate	199
12.3	Conclusions	202
13.	General Conclusions	203
14.	Future Work	207
	References	209

DECLARATION

No part of the work described in this thesis has been submitted in support of an application for another degree or qualification of this or any other University or other institute of learning.

No part of the work described in this thesis has been done in collaboration with any other person.



A C K N O W L E D G E M E N T S

I would like to thank Professor H.J. Pick for acting as Supervisor and Professor R.H. Thornley for permitting the work to be carried out in the Production Engineering Department.

Thanks are also due to the Electronics Section of the Department for their assistance with instrumentation, the Communications Media Unit for advice on photographic techniques, and to Mr. R. Rignall, Chief Technician in the Casting Laboratory who so ably assisted in the testing and photographic work.

Finally, my thanks to Mrs. M. Bellamy who typed the bulk of the thesis.

LIST OF FIGURES

Fig No.

- 1 (a) Diagrammatic representation of injection system of hot chamber diecasting machine.
- (b) Diagrammatic representation of injection system of cold chamber diecasting machine.
- 2 Example of poor casting finish due to flow breakdown.
- 3 (a) Example of solidification porosity.
- (b) Example of gas entrapment due to flow pattern.
- 4 Flow in rectangular cavity, after Frommer.
- 5 B-6 test shape.
- 6 Experimental procedure, after Babington and Kleppinger.
- 7 Tensile strength vs. metal pressure, after Babington and Kleppinger.
- 8 Quality index vs. metal pressure, after Babington and Kleppinger.
- 9 Quality indices, after Babington and Kleppinger.
- 10 Tensile strength vs. gate thickness, after Overas and Badone.
- 11 Tensile properties v. plunger speed, after Overas and Badone.
- 12 Surface quality vs. machine variables, after Sanders.
- 13 (a) Diagrammatic representation of diecasting system.
- (b) Idealized diagram of injection system, after Sachs.
- 14 Metal system filling stages, after Sachs.
- 15 (a) Table 2, flow equations.
- (b) Energy rate vs. piston stroke.
- 16 Table 3, details of diecasting machine range.
- 17 Table 4, after Sachs.
- 18 Table 5, Vent size and filling time.
- 19 Velocity characteristics vs. stroke.
- 20 Velocity characteristics vs. time.
- 21 Velocity characteristics vs. time.
- 22 Velocity characteristics vs. time.

- 23 Steady state velocity analysis, machine 1A.
- 24 Comparison of calculations for filling time and vent size vs. gate thickness for machine 1.
- 25 Comparison of calculations for filling time and vent size vs. gate thickness for machine 2.
- 26 Non-dimensional illustration of the variation of venting area ratios with proportional variation of machine and of gating system resistance factors.
- 27 Free-running injection curves for machine 1A for various conditions in stage 1.
- 28 Free-running injection curves for machines 1A and 5 showing influence on velocity build-up of the ratio of resistance to inertia factor.
- 29 Filling characteristic machine 5.
- 30 Percentage difference between steady estimation and transient filling time for B-6 test die.
- 31 Filling characteristic for B-6 test die on machine 2.
- 32 (a) Filling characteristic for B-6 test die on machine 1A.
 - (b) Effect on filling time of gate area and of metal piston changes on machine 1A.
- 33 (a) Filling characteristic, zero venting, machine 1A.
 - (b) Comparison of steady state, optimum vent and zero vent fill times using machine 1A.
 - (c) Percentage difference optimum vent, zero vent fill times using machine 1A.
- 34 (a) Filling characteristic, zero venting, machine 1.
 - (b) Comparison of steady state, optimum vent and zero vent fill times using machine 1.
 - (c) Percentage difference optimum vent, zero vent, fill times using machine 1.
- 35 Volume compression under adiabatic conditions.
- 36 Comparison of fixed and variable cavity resistance using machine 2.
- 37 Comparison of fixed and variable cavity resistance using machine 5.
- 38 Filling times for fixed and for variable cavity resistance using machines 5 and 2 for comparison.

- 39 Two stage injection characteristics.
- 40 Free running piston velocity curves for hypothetical two stage injection system.
- 41 Piston velocity characteristic for a range of gate size and changeover positions using machine 1A.
- 42 Piston velocity characteristic for a range of gate size and changeover positions using machine 2.
- 43 Piston velocity characteristics for a range of gate size and changeover positions using machine 5.
- 44 (a) Energy rate vs. gate size, machine 1A, changeover position 15.25 mm.
- (b) Energy rate vs. gate size, machine 1A, changeover position 61.00 mm.
- (c) Energy rate vs. gate size, machine 1A, changeover position 122.00 mm.
- 45 Maximum and steady state energy rates for machine 1A.
- 46 Maximum and steady state energy rates for machine 2.
- 47 Maximum and steady state energy rates for machine 5.
- 48 Energy rate vs. changeover position.
- 49 Energy rate vs. filling stroke.
- 50 Energy rate, Piston velocity vs. net drive force.
- 51 Weber number vs. gate size for a range of changeover position, machine 1A.
- 52 Weber number vs. gate size for a range of changeover position, machine 2.
- 53 Weber number vs. gate size for a range of changeover position, machine 5.
- 54 Weber number ratios for machines 1A, 2 and 5.
- 55 Diagrammatic illustration of experimental cavity and associated runner : gate
- 56 Diagrammatic layout of injection cylinder.
- 57 Stages of piston movement.
- 58 Trace record of piston velocity characteristic under free running conditions.

- 59 Trace record of piston velocity characteristic under injection conditions.
- 60 Comparison of calculated and measured piston speed for EMB 10 machine (free running).
- 61 Comparison of calculated and measured piston speed for EMB 10 machine (using gate size 25.4 mm x 0.635 mm).
- 62 Comparison of calculated and measured piston speed for EMB 10 machine (using gate size 25.4 mm x 2.54 mm).
- 63 Composite figure for range of piston conditions.
- 64 Comparison of calculation and measurement of elapsed time vs. stroke for experimental tool on EMB 10.
- 65 Comparison of calculation and measurement of injection cylinder drive pressure vs. stroke for experimental tool on EMB 10.
- 66 Energy rate vs. gate size.
- 67 Cavity fill time, piston velocity vs. reservoir pressure.
- 68 (a) Photograph of castings produced using nominal gate size, 25.4 mm x 2.54 mm.
(b) Photograph of castings produced using nominal gate size, 25.4 mm x 0.635 mm.
- 69 Total energy input for different Piston size and for different Runner size.
- 70 Weber number vs. gate area for steady flow conditions on experimental machine : mould set up.
- 71 Photograph of Front faces of sample castings H and A.
- 72 Photograph of Back faces of sample castings H and A.
- 73 Photograph of Front and Back face of sample casting D.
- 74 Photograph, X-ray positive of sample castings H, A and D.
- 75 Photograph, general view of EMB 10 diecasting machine and instrumentation.
- 76 Photograph, experimental tooling for diecasting machine.
- 77 Photograph, general view of water flow rig.
- 78 Photograph, experimental tooling for rig.

- 79 Trace record of free piston velocity characteristic for rig.
- 80 Comparison of calculation and measurement of piston speed - single stage injection.
- 81 Comparison of calculation and measurement of piston speed - two stage injection.
- 82 Typical rig trace.
- 83 Still photographic set up.
- 84 Typical combination loss features.
- 85 (a) Diagram of system comprising bend : contraction, sudden expansion and gate contraction.
(b) Diagram of system comprising bend : contraction, tapered expansion.
- 86 Gate geometry, after Nussey.
- 87 Runner geometry, after Nussey.
- 88 Typical runner : gate combination.
- 89 Table 6, Range of runner : gate combinations, after Nussey.
- 90 Comparison of calculated and measured efficiency for variation of gate width (P).
- 91 Comparison of calculated and measured efficiency for variation of gate depth (Q).
- 92 Comparison of calculated and measured efficiency for land approach angle (R).
- 93 Comparison of calculated and measured efficiency for gate exit semi-angle (S).
- 94 Comparison of calculated and measured efficiency for land length (T).
- 95 Table 7, Dimensions of side runners, after Nussey.
- 96 Least square regression plot of efficiency vs. length for side runners.
- 97 Calculated efficiency for side runner range.
- 98 Bend loss coefficient curve, after Sachs.
- 99 Taper gate, after Sachs.
- 100 Comparison of efficiency estimates.

- 101 Comparison of efficiency measurements for gate depth variation using 25.4 mm gate width.
- 102 Comparison of efficiency measurements for gate depth variation using 76.2 mm gate width.
- 103 Comparison of efficiency measurements for variation of land approach angle.
- 104 Comparison of efficiency measurements for variation of gate exit semi-angle.
- 105 Comparison of efficiency measurements for variation of land length.
- 106 Diagrammatic representation of 'line' and 'point' source flow, after Nussey.
- 107 Photograph, transition stages of flow through runner : gate combination C1.
- 108 Photograph, transition stages of flow through runner : gate combination A1.
- 109 Photograph, side view of runner : gate combination A2.
- 110 Photograph, full flow runner : gate combination C31.
- 111 Photograph, transition stages for flow through runner : gate combination C17.
- 112 Photograph, transition stages for flow through runner : gate combination C36.
- 113 Weber number curve for rig.
- 114 Photograph, flow state at varying Weber number.
- 115 Photograph, general flow under 'short shot' conditions for runner : gate combination C1.
- 116 Photograph, 'explosive' breakdown of flow through runner : gate combinations B9, C17.
- 117 Photographic comparison of free and restricted flow from runner : gate combination C6.
- 118 Photographic casting defects related to breakdown effects.
- 119 Photograph 'explosive' effects in restricted flow from C6.
- 120 Diagrammatic representation of impingement conditions.

INTRODUCTION

1. BACKGROUND

Before examining the research problem a brief examination will be made of the process, machine/mould relationship and quality considerations, to establish the manufacturing context to the work.

1.1 PROCESS DEFINITION

Casting processes may be generally defined as those processes in which components are produced by introducing molten metal into a suitable mould cavity and causing it to solidify therein in some preferred manner. Pressure diecasting, as its name implies, differs most significantly from other processes in the pressure levels employed to force the molten metal into the cavity. Most processes utilize gravitational pressure or applied pressure of a similar order (e.g. low pressure casting). Pressure diecasting employs pressures such that gravitational influence is negligible. In process terms the use of high pressures (potentially) enables complex, thin-walled castings to be produced to a high order of dimensional accuracy and surface finish. The equipment (diecasting machine) which provides both the high injection pressures and the necessary support and control of the tooling is generally designed with a capacity to cycle at high rates for rapid production. The cost of machine and tooling limits the use of the process to volume production situations.

1.2 MACHINE/MOULD CONFIGURATION

In the context of fluid flow studies the most significant feature on the diecasting machine is the injection system.

Due to the corrosive effect of metal alloys upon (metal) container walls under prolonged contact, the form of an injection system is tailored to this propensity in the metal to be cast. For the lower melting point alloys (zinc, lead, etc.) 'hot chamber' machines are employed Fig. 1(a) in which the injection system operates in the alloy holding furnace. For higher melting point alloys (aluminium, copper and latterly, ferrous alloys) 'cold chamber' machines are used Fig. 1(b). In these machines the holding furnace is separated from the injection system. Thus the alloy to be cast has to be ladled by hand or some automated equivalent to the shot sleeve. The injection systems of 'hot chamber' machines may be activated by compressed air or pressured hydraulic fluid, whereas cold chamber systems are almost invariably hydraulically activated.

In both types of diecasting machine the injection system connects to the mould via a feed channel through the fixed platen of the machine. The rest of the feed system, which is cut into the mould and connects with the cavity, is usually referred to as the runner and/or gating system. It comprises feed channels (runners) connected to the feed entry point (gate) into the cavity and follows the parting line of the mould to the cavity. At the point of connection of runner and cavity there is a considerable contraction of dimension to enable waste material to be clipped off evenly from the cast component. This point is referred to as the gate. Thus the form of the casting metal feed system comprises a fixed element built into the injection system of the machine and a connecting element cut into the mould which varies with every mould put on to the diecasting machine.

1.3 QUALITY CONSIDERATIONS

(i) Surface finish. The surface finish of a casting is largely determined by the finish of the mould cavity. Metal moulds with high standards of finish enable castings of generally equivalent (finish) standards to be produced. However the manner of entry and filling of a cavity by the casting metal can influence the surface condition of the resulting component in localized areas. Metal flowing at high rates can break down into a metal spray on entering the mould cavity. Under unfavourable thermal conditions the individual droplets may not completely coalesce. The result may be a surface covered in discontinuities which are the boundaries of the lamellar platelets formed by the solidified spray. Fig.(2) illustrates this effect.

(ii) Structure. The control of the porosity level in a cast component is clearly important for mechanical applications. The metallurgical condition of the casting and the presence or otherwise of voids in the cast structure are determined by the way in which the cavity is filled and the control of the resulting solidification. Purely solidification voids can occur where there are local imbalances in solidification Fig. (3a). A more usual source of voids (due to the high metal injection rates) arises from the entrapment of gas by the metal filling and solidifying in the the cavity. Fig. (3b).

(iii) Dimensional accuracy. To a large extent dimensional accuracy is a function of the accuracy of mould construction, location and assembly.⁽¹⁾ However the positions at which metal is fed into the cavity can exert a significant influence⁽¹⁾ upon dimensional stability due to the temperature gradients

established, and localized contraction effects.

2. DEFINITION OF THE PROBLEM.

From the diecaster's point of view it is necessary to control defects in surface condition and structure, together with variation of dimension, within limits which are acceptable functionally and economically. When substandard components are produced it is generally a consequence of failure satisfactorily to control the way in which casting metal enters and fills the cavity and the way in which it loses heat in that time. The basic physical features of significance in metal flow have been defined ⁽²⁾ as rate, state and direction, coupled with rate of gas venting from the cavity. To this should be added the feature of energy rate input to the metal entering the cavity since this must determine the completeness of filling of the cavity. It is evident that all these features are influenced both by the diecasting machine (design and condition of the injection system) and by the mould design. Flow of metal is initiated by the metal injection system and is influenced by the vagaries of the system. When the molten metal reaches the runner/gate/cavity system embodied in the mould, its motion, energy level and general condition are affected by their orientation, the hydraulic resistance they generate and the back pressure of gas venting from the cavity.

Clearly a mathematical model would be of considerable benefit in the planning and execution of research to provide a general understanding of flow in pressure casting. The current state of development of such a model and the impact of such analysis upon experimental work in the field are examined in the following literature survey.

2.1 LITERATURE SURVEY

2.1.1 PUBLISHED ANALYSIS OF METAL FLOW

In analytical terms the diecasting system can be broken down into essentially four elements

- (i) the machine injection system
- (ii) the runner/gating system
- (iii) the cavity
- (iv) the venting system

As already stated these features in combination influence flow conditions in the casting metal. The degree of comprehensiveness of reported analysis varies considerably whilst the emphasis is, with minor exception⁽¹¹⁾ devoted to the examination of flow rate in the metal and/or vented gas.

Flow rate formulae based upon analysis covering the gate alone have been proposed by a number of researchers⁽³⁻⁸⁾. This kind of examination is far too simplistic and has little value.

Frommer⁽⁹⁾ presented a (steady state) analysis of metal flow rate considering (i) and (ii) in combination. He made the assumptions that no energy losses occur in the injection or runner system and that no resistance occurs due to air back pressure in the cavity.

Jacobi⁽¹⁰⁾ and more recently Uehara⁽¹¹⁾, also using steady state analysis, extended Frommer's work to take account of losses in the runner/gating system.

Sachs⁽¹²⁾ has made the most rigorous examination to date of flow rate in diecasting systems. He examined the combination of elements (i), (ii) and (iv) in some detail. Equations for both steady and unsteady flow conditions were developed by

examining the change of conditions on an incremental basis. Sachs stated that trapped cavity air represented the most serious threat to the integrity of structural castings and focussed his analysis upon filling and venting rates. His work purported to show that venting requirements differed considerably in steady and unsteady flow conditions and that venting back pressure under optimum conditions was significant.

Veinik ⁽¹³⁾ carried out a similar, but somewhat less detailed analysis of flow rate. He, also, examined the venting problem and showed that the build-up of air pressure does not affect metal flow rate significantly.

Some researchers have confined themselves to the study of venting problems, basing their examination upon the assumption of steady filling conditions and using the compressible gas laws ^(12,13,14) or empirical considerations ^(15,16,17,39,40). The end result of this kind of approach is a formula to predict vent size in relation to cavity filling rate. The more rigorously derived of them ⁽¹²⁻¹⁴⁾ are identical in form, differing only in the magnitude of a constant appearing in the equation. Draper ⁽³⁾ examined these but was unable to resolve the differences and suggested the need for experimental studies to provide clarification.

In terms of energy rate analysis Uehara ⁽¹¹⁾ has made a limited study of energy rate input to a simple gating system assuming steady flow conditions and fixed gate loss coefficient.

Only Belov ⁽¹⁸⁾ et al have appeared to make any quantitative study of flow breakdown in the diecasting metal system, attempting to relate thermal and fluid flow conditions for droplet coalescence.

2.1.2 THEORIES ADVANCED

Both Frommer ⁽⁹⁾ and Veinik ⁽¹³⁾ have advanced theories of casting which have been widely disseminated though neither have been derived from the analytical studies of their authors.

Frommer's theory concerns flow circulation in a simple cavity. It suggests that for flow into a rectangular cavity the ratio of gate/cavity width influences the way in which a metal stream enters and fills the cavity and that this ratio has a critical value. Frommer claims that the initial flow pattern is smooth, the metal moving in a jet, having the same cross-section as the gate until it meets an obstruction. The jet then splits and sends fore-runners (Fig. 4) up the end walls. Pulsations at the end walls cause turbulence so that a well of metal and entrapped air grow at the end wall fast enough to catch-up and engulf the forerunners, which slow down due to friction and cooling. This theory has received qualified support from a number of researchers ⁽¹⁹⁻²²⁾ using model and short shot techniques, although Brandts ⁽²³⁾ experimental results are at variance with it.

Veinik's theory centres around the need to preserve superheat for complete coalescence of the casting and has two basic principles i.e. maximum and minimum friction. Veinik suggests that in minimum friction superheat is preserved by rapid pouring and at maximum friction by the addition of friction heat to the moving metal. He states that minimum friction conditions are obtained using streamlined runners and large gates and has the benefit of giving solid front rather than spray filling of the mould, requires lower pressures

although control of directional solidification is necessary. This approach is arguably best for the production of structural components. The principal of maximum friction involves the use of highly resistive (narrow) gates to cause metal reheat. Narrow gates might also be expected to be associated with flow breakdown i.e. spray filling. Veinik suggests that spray filling can well be advantageous in that it eliminates the need for control of directional solidification. He argues that the air/metal mixture will fill the cavity, that the air will be uniformly distributed as microporosity and that the pressure in the trapped air will force the metal against the cavity wall to produce sound finish and eliminate sinkage.

2.1.3. MACHINE EXPERIMENTATION AND MODEL STUDIES

(a) Experimentation

The reported experimental work was repetitious and was not oriented with respect to an analytical framework or theory. Consequently little progress has been made from these studies in achieving a basic understanding of the process. Instrumented machines were used in conjunction with (usually) complex cavity forms. Machine controls (of pressure or temperature) were adjusted over a spectrum, and of sample castings produced at the various settings. Trend relationships were established between (usually) subjective indices of quality and machine settings. The following examples selected from that published in the last thirty years serves to illustrate the above.

In 1947 ASTM Committee B-6 set up a sub-committee (24) whose terms of reference were to devise methods and instruments

for a number of factors involved in diecasting "..... to achieve a better understanding, and ultimately, control, of the variables involved in the process." The Committee recommended a test shape Fig. (5) to be used for evaluation purposes. The test shape was intended to allow the examination of

thin and thick wall sections
large flat areas
abrupt changes in section
cored holes

Babington & Kleppinger ⁽²⁴⁾ used the ASTM test die for detailed machine studies. Fig. (6) illustrates the investigative procedure and typical results from this study are shown in Fig. (7) and Fig. (8). Mean values of injection features (packing pressure, plunger velocity) were compared with indices of casting quality Fig. (9). The authors realised that the complexity of the test cavity would have an unquantifiable effect upon their results and consequent conclusions which could only be roughly deduced from 'short shots'.

Overath and Badone ⁽²⁵⁾ performed a series of instrumented machine tests using a test bar cavity and employing the same casting alloy as Babington & Kleppinger. They produced a series of curves relating mechanical properties to gate thicknesses and plunger speeds. (Figs. (10) and (11)). It is difficult to relate their work to that of Babington and Kleppinger. It tends to be complementary since the variables examined by Overath and Badone were fixed in the latter's experimentation and vice-versa, although where comparisons can be drawn they are essentially in agreement.

More recently Sanders et al ⁽²⁶⁾ examined the influence of metal temperature, die temperature, hydraulic line pressure and shot valve opening upon the surface quality of a production casting. Surface quality was statistically related to the

measured machine variables (Table 1, Fig.(12)).

These pieces of work are typical of that taking place over the last 25 years or so and whilst the sophistication of the instrumentation has increased, the philosophy of approach has not. No quantifiable extrapolation can be made from this type of work to different machine/mould situations since they have no common frame of reference. This view is, in a sense, supported by the change of emphasis in instrumented experimentation in recent years which places more emphasis on the role of instrumentation for 'feedback' control purposes and the development of instrumentation packages to that end. The most prominent organisation associated with this work is currently the British Non-Ferrous Metals Research Association. (27)

(b) Model studies

The virtue of using a fluid flow analogue is of course that provided the dimensional comparisons are in order, then by using transparent dies and appropriate photographic techniques flow conditions may be visually examined. When combined with experimental studies in the casting environment this approach can therefore be a powerful investigative tool.

There are a number of reports of fluid model studies in the literature (28,19,22,29,30,41). Most are concerned simply with very generalized examination of flow patterns in specific moulds (22,30,41) or the validation of (Frommer's)

flow theory (28,29).

None have been used to substantiate any analytical or indeed experimentally derived model predicting flow. A possible, albeit peripheral, exception to this is the work of Wallace (30) who made limited use of Sachs analysis to calculate piston velocity in his model.

Few reported any dimensional justification of the systems they used and the resulting information is of minor interest. The one exception to this, and indeed (in the author's opinion) the only useful and scientifically based model study to date is that of Nussey (19). Having made a most comprehensive review of diecasting literature on aspects of metal flow he concluded that the (fluid model) examination of gating systems in steady state flow conditions, and in the absence of cavity or injection system influences, would be of benefit. His study mainly centred on a gating profile for end-on gating systems, although he did include a limited appraisal of manifold systems. Nussey examined the influence of gate geometry and pressure levels upon efficiency of flow, defining from a photographic appraisal different kinds of flow regime. The value of the work lies in the insight into loss coefficients in simple gating systems which it provides and also the information on the influence of the gate/runner systems upon flow state.

2.2 RESEARCH OBJECTIVES

From an examination of the literature two main conclusions emerge

1. Some part of an analytical framework of the diecasting process exists. There is an almost complete lack of the sort of information on machines and moulds (loss coefficient, etc.) which enable this to be applied. There are also a number of contradictions arising from this (e.g. whether gas back pressure is or is not significant for optimum venting rates).

2. There have been no experimental studies designed to validate the existing analysis nor has it been used as a basis for experimentation.

The ideal approach to any experimental study of a system arguably requires the development of a coherent mathematical model from which the experimental investigation is planned. Thus the experimentation is capable of both interpolation and extrapolation within the frame of reference provided by the model. In turn the model is refined as a consequence of information feedback from the experimentation. It is suggested that this is not happening currently in diecasting research for several reasons viz.

- (i) The lack of a sufficiently comprehensive framework embracing all the flow features influencing casting quality inhibits the planning of experimentation.
- (ii) Lack of information regarding machines and moulds inhibits the use of any existing analysis.

- (iii) No attempt has been made where such information does exist to use analysis to highlight machine/mould influences and their significance which would suggest potentially beneficial lines of experimentation.

Consequently the objectives proposed for the investigation are as follows:

Principally

- a) to develop a coherent body of analysis embracing flow rate, energy rate, flow state in diecasting systems, resolving current contradictions in the existing framework.
- b) to examine machine/mould relationships to highlight the significance of, and interrelationship between, machine injection and gating system characteristics.
- c) to provide experimental validation.

Secondary objectives are

- d) to examine the means by which machine information necessary for the analysis may be experimentally derived.
- e) to suggest a loss coefficient equation for gating systems and provide experimental validation for it.
- f) to use a fluid flow model to provide support information for c) and e), extending existing information on flow state through gating systems particularly with respect to cavity influence.

PART 1

DEVELOPMENT OF ANALYTICAL FRAMEWORK AND ITS APPLICATION TO

DIECASTING SYSTEMS

The objective of Part 1 of this report is to satisfy points a-d raised in 2.2.

In section 3 the basic analysis is derived.

In sections 4-5 calculations are performed on general diecasting systems for the purpose of establishing injection system/gating system interactions and the implications of these.

In sections 6-7 calculations are checked with experimentally derived information for validation purposes. In the course of section 6 an experimental approach is suggested whereby machine/metal system coefficients, necessary for the analysis, may be measured.

3. DEVELOPMENT OF ANALYSIS

3.1 FLOW RATE

The object of this section is to develop analysis of metal flow rate in both steady and unsteady conditions. It will have been noted from 2.1.1 that the main body of published analysis is concentrated upon this aspect of metal flow. The most detailed work reported is that of Sachs who also examined steady and unsteady flow conditions. His work is unnecessarily complex and cumbersome due to the nature of his assumptions and is indeed significantly in error with regard to certain aspects of the analysis. Nevertheless it has received wide publicity and it is useful to compare it with that developed herein to highlight the above point.

In order to enable comparison with Sachs' analysis the identifying symbols used in the analysis will be essentially as defined by Frommer ⁽⁹⁾ and used by Sachs.

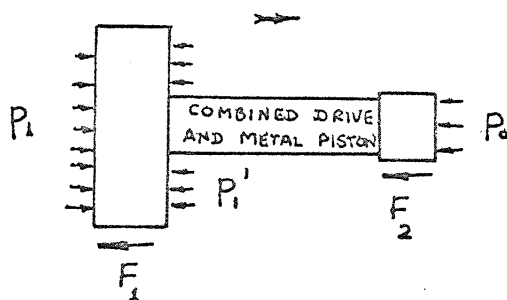
The casting system can be represented diagrammatically as shown in Fig. 13. The way metal fills a cavity and the evacuation of gas from it are determined by a number of features principally

- i. The machine injection system.
- ii. The runner/gate feed system comprising a fixed element in the machine and a connecting element designed into the tooling.
- iii) The runner/gate/cavity orientation.
- iv) The cavity geometry.
- v) The venting system.

Basically the total system comprises three interrelated flow 'circuits'

- a) the drive circuit)
- b) the exhaust circuit) (1)
- c) the metal system (ii) - (v)

The pressure and velocity distributions in the fluid in each 'circuit' are related by flow continuity and energy laws. These 'circuits' are interdependent since they share common or related boundary conditions (the linked drive and metal pistons). Thus at these boundaries force balances can be set up for steady or unsteady conditions which link circuit boundary pressures. viz.



c.f. FIG 13

p_1 = cylinder drive pressure

f_k = area of drive side of piston

p_1 = exhaust back pressure

p_0 = pressure in metal system

f_0 = area of metal piston

$$p_1 f_k - p_1' (f_k - f_0) - F_1 - F_2 - p_0 \cdot f_0 = 0, F_1, F_2 = \text{frictional resistance of piston and plunger.}$$

(steady flow)-1(a)

$$p_1 f_k - p_1' (f_k - f_0) - F_1 - F_2 - p_0 f_0 = M \cdot \frac{dv}{dt}, \quad M = \text{mass of piston and plunger.}$$

(unsteady flow)-1(b)

$\frac{dv}{dt}$ = piston acceln.

Thus by using equations 1(a) and 1(b) pressure/velocity conditions in one circuit can be linked with conditions in the other two enabling flow conditions in the metal system for instance, to be related to the conditions in the injection system.

The greatest body of analysis of filling rate has been based upon the assumption of steady filling conditions and the most elementary form of the analysis revolves around the examination of the metal system without extrapolation to other circuits.

The unit energy at any point in a flow system under steady conditions is expressed by the equation

$$\frac{p}{\gamma_L} + \frac{v^2}{2g} + \text{energy losses} = \text{constant} \quad -2, \quad \frac{p}{\gamma_L} = \text{static pressure head at point considered}$$

v = velocity of flow at point considered

If this is applied to the gate of the metal system (fig.13)

$$\frac{p_o}{\gamma_L} + \frac{v^2}{2g} = \frac{v_g^2}{2g} + \Sigma c \frac{v_g^2}{2g} + \frac{p}{\gamma_L}$$

v = piston velocity

v_g = gate velocity

Σc = losses in the metal system referred to gate velocity

p = pressure in metal in cavity

$$\text{yielding } v_g = \sqrt{\frac{2g(P_o - p)}{\gamma_L \left[1 + \Sigma c - \left(\frac{f}{f_o} \right)^2 \right]}} \quad - (3)$$

The term $\left(\frac{f}{f_o} \right)^2$ represents the translation of the velocity head $\frac{v^2}{2g}$ to relate to gate velocity using continuity flow consideration i.e. $f \cdot v_g = f_o \cdot v_o$.

Assuming a knowledge of p_o, p and Σc therefore the gate velocity (and hence rate of flow) into the cavity under steady state conditions may be calculated. This stage of analysis is typical of the earliest published attempt to analyse metal flow⁽³⁻⁸⁾. Its application depends upon a detailed knowledge of its components but more importantly its accuracy depends upon the validity of the assumption of steady state conditions.

The flow circuits are, as mentioned, interdependent, and by applying the energy and continuity equations to these and using the force balance equations it is possible to arrive at an equation relating gate velocity to injection system conditions and thus be able to relate machine characteristics to flow rate viz.

Applying the Bernoulli equation (2) to each of the flow circuits in turn yields the following (ref. to fig. 13.)

Drive circuit

$$P = \gamma_f \cdot \frac{v^2}{2g} \cdot \left\{ 1 + K_d \cdot \left(\frac{f_k}{q} \right)^2 \right\} + p_1$$

P = reservoir pressure

p_1 = pressure in drive side of cylinder

K_e, K_d = loss coefficients for systems referred to average pipe area.

f_k = drive piston area

Exhaust circuit

$$p_1^1 = \gamma_f \frac{v^2}{2g} \left\{ \{1 + K_e\} \left(\frac{f_k - f_o}{q^1} \right)^2 - 1 \right\}$$

q^1, q = pipe area

v = piston velocity

Metal circuit

$$p_o = \gamma_L \frac{v^2}{2g} \cdot \left\{ (1 + K_m) \left(\frac{f_o}{f} \right)^2 - 1 \right\} + p$$

p_o = pressure in metal at metal piston

K_m = loss coefficients for system referred to gate

Substitution in 1(a) for p_1 , p_1^1 and p_o yields

$$P f_k - p f_o = \left[\left(1 + K_D \left(\frac{f_k}{q} \right)^2 \right) f_k + \left((1 + K_E) \frac{(f_k - f_o)^2}{q^{(1)2}} - 1 \right) (f_k - f_o) \right] \gamma_f \frac{V^2}{2g}$$

$$+ \left[(1 + K_m) \left(\frac{f_o}{f} \right)^2 - 1 \right] f_o \gamma_f \frac{V^2}{2g} + (F_1 + F_2)$$

Under all practical circumstances

$$K_D \cdot \left(\frac{f_k}{q} \right)^2 \gg 1 \text{ hence } \left[1 + K_D \left(\frac{f_k}{q} \right)^2 \right] \text{ may be written } K_D \left(\frac{f_k}{q} \right)^2$$

Similarly

$$\left[(1 + K_E) \frac{(f_k - f_o)^2}{q^{(1)2}} - 1 \right] \text{ may be written } (1 + K_E) \frac{(f_k - f_o)^2}{q^{(1)2}}$$

$$\left[(1 + K_m) \left(\frac{f_o}{f} \right)^2 - 1 \right] \text{ may be written } (1 + K_m) \left(\frac{f_o}{f} \right)^2$$

Hence

$$P \cdot f_k - p f_o = \left[\left[K_D \cdot \left(\frac{f_k^3}{q^2} \right) + (1 + K_E) \frac{(f_k - f_o)^3}{q^{(1)2}} \right] \cdot \frac{\gamma_f}{2g} + (1 + K_m) \frac{(f_o)^3}{(f)^2} \frac{\gamma_L}{2g} \right] \frac{V^2}{2g}$$

$$+ (F_1 + F_2)$$

Write

$$(P \cdot f_k - p f_o - F_1 - F_2) = Q$$

$$\frac{\gamma_f}{2g} \left[K_D \frac{f_k^3}{q^2} + (1 + K_E) \frac{(f_k - f_o)^3}{q^{(1)2}} \right] = C_1$$

(C_1 defined as machine resistance factor)

$$\frac{\gamma_L}{2g} \left[\left(1 + K_m \right) \frac{f_o^3}{f^2} \right] = C_{m_3} \text{ (defined as metal system resistance factor)}$$

$$\text{Hence } Q = (C_1 + C_{m_3}) v^2 \quad \text{-----} \quad 4(a)$$

Note v = piston velocity

$$f_o v = f \cdot v_g$$

($C_1 + C_{m_3}$ defined as total resistance factor for system)

Sachs made exactly the same approach, however he substituted for F_1, F_2 using published information on the relationship between friction forces and system pressure in piston operated systems. By substituting these relationships he obtained an equivalent expression viz.

$$0.97 f_k \cdot P - p(1+1.15\mu_o) f_o = \left[0.97 \frac{f_k^3}{q^2} \cdot K_D + (1+K_E)(1.03f_k - 0.88f_o) \cdot \frac{(f_k - f_o)^2}{q^{0.2}} \right] \cdot \frac{v^2 \gamma_f}{2g} + \left[(1+K_m) \left(\frac{f_o}{f} \right)^2 - 1 \right] f_o \cdot \frac{\gamma_L \cdot v^2}{2g}$$

Substitute

$$Q' = 0.97 f_k P - p(1+1.15\mu_o) f_o$$

$$C_1^1 = \frac{\gamma_f}{2g} \left[0.97 \frac{f_k^3}{q^2} \cdot K_D + (1+K_E)(1.03f_k - 0.88f_o) \cdot \frac{(f_k - f_o)^2}{q^{0.2}} \right]$$

$$C_{m_3}^1 = \left[(1+K_m) \left(\frac{f_o}{f} \right)^2 - 1 \right] f_o \cdot \frac{\gamma_L}{2g}$$

$$\text{Hence } Q^1 = (C_1^1 + C_{m_3}^1) v^2 \quad \text{-----} \quad 4(b)$$

The odd numbers arising in the Sachs equation occur due to the values of friction coefficient employed for the drive cylinder. (μ_o = friction coefficient of metal piston/cold chamber contact surfaces). The significance of the terms $p f_o$ and $p(1+1.15\mu_o)f_o$ in terms Q and Q^1 of 4(a) and 4(b) respectively has to be carefully considered. A conceptual error made by Sachs in his examination of certain aspects of flow (the relationship between optimum vent size and piston velocity) arose from his assumption that this term is a necessarily significant one even for optimum venting conditions. It has been demonstrated and will be confirmed in section (3.4) that this is not so. For optimum venting the gas back pressure is negligible and significant back pressure will only occur in those conditions which good casting practice seeks to avoid. However, this aspect will be discussed at some length in section (3.4). If one disregards the back pressure terms in equations 4(a) and 4(b) and substitutes representative values for dimensions it becomes clear that the friction components built into the Sachs equation are negligible and almost exactly the same result can be obtained from 4(a) simply by putting $F_1+F_2 = 0$. This is clearly illustrated in the table below.

DRIVE PISTON DIA $f_k = \pi d^2/4$	METAL PISTON DIA $f_o = \pi d^2/4$	C_1/C_1^1		
		$K_D = K_E$	$K_D \ll K_E$	$K_D \gg K_E$
12	2	1.00	.97	1.03
8	2	1.01	.97	1.03
6	2	1.00	.96	1.03
4	2	1.01	.96	1.03

	C_1/C_1^1	$V(4a)/V(4b)$
$K_D = K_E$	1.00	1.015
$K_D < K_E$.97	1.030
$K_D > K_E$	1.03	1.000

It may be seen that putting $F_1, F_2 = 0$ in 4(a) yields piston values very close to those based on 4(b) for the whole spectrum of loss factor proportion. It is obviously desirable that friction in the system be as small as possible and on this basis there is no significant difference between 4(a) and 4(b) Sachs.

The foregoing relates to steady state conditions. Whilst there is a large body of published opinion that this assumption may be used there is as yet no theoretical or experimental justification.

Thus the analysis of rate of flow under unsteady conditions will be examined. Sachs' layout will be used for comparative purposes (see figs. 14 and 15). The analysis is performed on a 'lump' basis. The movement of the piston is broken down into stages and each stage is analysed consecutively. Sach broke the piston movement into four effective stages and the breakdown will be maintained since the technique would be the same for any number. These stages are as follows (using fig. 15 for reference).

- i. piston movement to shut off shot sleeve filler hole diagrams (1-2), no metal system resistance, no gas back pressure.

- ii. piston movement until metal just enters gating system diagrams (2-4), no metal system resistance, no gas back pressure.
- iii. piston movement to fill runner and gate diagrams (4-5), metal system resistance
- iv. piston movement to fill cavity diagrams (5-6), metal system resistance.

Note.

(For ease of analysis, sections (iii) and (iv) were considered by Sachs as one lump. In the charts of Sach's work and its extension using his machine information this assumption has been maintained. However, in later experimental evaluation (section 6) it was clear that these stages are evident as separate features on the velocity characteristics and are of sufficiently significant duration to warrant treating separately).

Applying the Bernoullian equation for irrotational flow in unsteady conditions to each of the flow circuits in turn (ref. figs. 13-15) and substitution in 1(b) for each of the stages in turn yields the following

Stage (a)

Drive circuit

$$P = \gamma_f \cdot \frac{V^2}{2g} \left[(1+K_D) \left(\frac{f_K}{q} \right)^2 \right] + \frac{\gamma_f}{g} \cdot \frac{dV}{dt} \left[(\ell_4 - \ell_1 - \ell_E) + \ell_2 \cdot \frac{f_K}{q} \right] + p_1$$

Exhaust circuit

$$p^1 = \gamma_f \cdot \frac{v^2}{2g} \left[(1+K_E) \left(\frac{f_k - f_o}{q^1} \right)^2 - 1 \right] + \frac{\gamma_f}{g} \cdot \frac{dV}{dt} \left[\ell_E + \ell_2^1 \left(\frac{f - f_o}{q^1} \right) \right]$$

Metal circuit

$$p_o = 0 \quad (\text{closed channel flow not yet established})$$

- Assumptions (i) resistance factor for injection circuits
as for any other stage of movement, i.e.
no initial damper effect (c.f. Sachs equation)
- (ii) the acceleration terms are established
on the assumption that acceleration in
the pipe network is the same at any point
i.e. few changes in pipe section size.

Substitution in 1b yields

$$P \cdot f_k = \frac{\gamma_f}{2g} \left[\left(1+K_D \left(\frac{f_k}{q} \right)^2 \right) f_k + \left[(1+K_E) \left(\frac{f_k - f_o}{q^1} \right)^2 - 1 \right] (f_k - f_o) \right] v^2$$

$$+ \left[\frac{\gamma_f}{g} \left[\frac{\ell_2 f_k^2}{q} + \ell_2^1 \left(\frac{f_k - f_o}{q^1} \right)^2 + (\ell_4 - \ell_1 - \ell_E) f_k + \ell_E (f_k - f_o) \right] + \frac{W}{g} \right] \frac{dV}{dt}$$

$$+ (F_1 + F_2)$$

This expression can be simplified without undue loss of accuracy

$$(1+K_E) \left[\frac{f_k - f_o}{q^1} \right]^2 \gg 1 \quad \therefore (1+K_E) \left[\frac{f_k - f_o}{q^1} \right]^2 - 1 \doteq (1+K_E) \left[\frac{f_k - f_o}{q^1} \right]^2$$

$$K_D \cdot \left(\frac{f_k}{q} \right)^2 \gg 1 \quad \therefore \left[K_D \left(\frac{f_k}{q} \right)^2 + 1 \right] \doteq K_D \left(\frac{f_k}{q} \right)^2$$

$\left[(\ell_4 - \ell_1 - \ell_E) f_k + \ell_E (f_k - f_o) \right]$ would usually be negligible in relation to the other terms. Hence the expression can be simplified to

$$P \cdot f_k = \frac{\gamma_f}{2g} \left[K_D \frac{f_k^3}{q^2} + (1+K_E) \left(\frac{f_k - f_o}{q^1} \right)^3 \right] v^2 + \left[\frac{\gamma_f}{g} \left[\ell_2 \frac{f_k^2}{q} + \ell_2^1 \left(\frac{f_k - f_o}{q^1} \right)^2 \right] + \frac{W}{g} \right] \frac{dv}{dt} + (F_1 + F_2)$$

$$\text{Put } C_1 = \left[K_D \cdot \frac{f_k^3}{q^2} + (1+K_E) \left(\frac{f_k - f_o}{q^1} \right)^3 \right] \frac{\gamma_f}{2g} \quad (\text{c.f. steady state})$$

$$a_1 = \left[\ell_2 \frac{f_k^2}{q} + \ell_2^1 \left(\frac{f_k - f_o}{q^1} \right)^2 \right] \frac{\gamma_f}{g} + \frac{W}{g}$$

$$\text{Put } P f_k - (F_1 + F_2) = Q$$

$$\text{Thus } Q = C_1 v^2 + a_1 \frac{dv}{dt} \quad \text{5(a)}$$

(Note: a_1 defined as machine inertial factor)

Sachs equivalent is as follows

$$0.97 P \cdot f_k = \frac{\gamma_f}{2g} \cdot \frac{1}{q^2} \left[(1.03 f_k - 0.88 f_o) (f_k - f_o)^2 (1+K_E) + 0.97 f_k^3 K_D \right] \frac{x_1}{x} \cdot v^2 + \left[\frac{\gamma_f}{g} \cdot \frac{1}{q} \left[(1.03 f_k - 0.88 f_o) (f_k - f_o) \ell_2^1 + 0.97 f_k^2 \ell_2 \right] + \frac{W}{g} \right] \frac{dv}{dt}$$

$$Q^1 = C_1^1 \cdot \frac{x_1}{x} v^2 + a_1^1 \frac{dv}{dt} \quad \text{5(b)}$$

In his analysis Sachs introduced the ratio of $\frac{x_1}{x}$ as a multiplier of the resistance factor term C_1^1 . The value x_1 represents the stroke length to complete stage (a) and he did this to simulate

valve opening effects during that stage. Some compensating factor is probably appropriate for this first stage since in practice some sort of damper system invariably operates to prevent metal splashing through the filler hole and/or surge effects leading to premature mould tilling. Whether this is an appropriate means of compensation for a given machine configuration will very much depend upon the damping arrangement.

If one puts $(F_1 + F_2) = 0$ in 5(a) then $C_1 = C_1^1$, $a_1 = a_1^1$ for a range of machine dimensions.

The general solution of an equation of the form

$\alpha = \beta p^2 + \phi \frac{dp}{dt}$ ($\alpha, \beta, \phi = \text{constants}$) can be shown⁽³²⁾ to be

$$p = e^{-\frac{\beta}{\phi} \int dx} \sqrt{\frac{2}{\phi} \int \alpha e^{\left[\frac{2\beta}{\phi} \int dx\right]} + \text{const.}}$$

Thus the equation for piston velocity may be obtained from 5(a)/5(b) and clearly the expressions for acceleration and elapsed time also. There will, in practice, be a significant difference between piston velocity values as determined by 5(a), 5(b) in view of the damping compensation factor in 5(b). Different forms of damping are briefly considered in section (4.2) and fig. (27) indicates the results.

Stage (b)

In stage (b) the equation for velocity will be exactly the same as 5(a) viz

$$Q = C_1 v^2 + a_1 \frac{dv}{dt}$$

Note: Sachs' equation 5(b) reduces to

$$Q^1 = C_1^1 v^2 + a_1^1 \frac{dV}{dt} \quad \text{since as soon as the piston clears the filler hole } \frac{x_1}{x} = 1.$$

Stage (c & d)

Here for the first time the metal system will be expected to develop significant back pressure as closed channel flow develops.

Hence

$$P_o = \frac{\gamma_L}{2g} \left| \left(\frac{f_o}{f} \right)^2 (K_m + 1) - 1 \right| + (\text{acceleration term}) + p$$

The acceleration term will be expected in practice to vary somewhat, (referring to figs. 15 and 16), it will initially

$$= \frac{\gamma_L}{g} (H - x_2) \frac{dV}{dt} \quad \text{At the instant of filling termination it will be approximately}$$

$$= \frac{\gamma_L}{g} \cdot \left\{ \frac{\text{runner volume}}{\text{average runner area}} \right\} \left\{ \frac{f_k}{\text{average runner area}} \right\} \cdot \frac{dV}{dt}$$

If steady flow conditions prevail rapidly then

$\frac{\gamma_L}{g} \cdot (H - x_2) \frac{dV}{dt}$ will be a reasonable assumption for unit acceleration in the metal system. If unsteady conditions prevail for the filling operation then some intermediate value must be established. For the purposes of the analysis the value of

$$\frac{\gamma_L}{g} (H - x_2) \frac{dV}{dt} \quad \text{will be used.}$$

Should this not be the case, when applied to an experimentally verifiable situation, this will be readily seen from the difference in the gradient of the velocity time curve.

Now

$$P_o = \frac{\gamma_L}{2g} \left[\left(\frac{f_o}{f} \right)^2 (K_m + 1) - 1 \right] V^2 + \frac{\gamma_L}{g} (H - x_2) \frac{dV}{dt} + p$$

Substituting this together with equation for p_1 and p_2 already expressed in stage (a) in 1(b) yields.

$$P \cdot f_k - p f_o = \left[C_1 + \frac{\gamma_L}{2g} \cdot f_o \cdot \left[\left(\frac{f_o}{f} \right)^2 (K_m + 1) - 1 \right] \right] V^2 + \left[a_1 + \frac{\gamma_L}{g} \cdot f_o \cdot (H - x_2) \right] \frac{dV}{dt} + (F_1 + F_2)$$

Write

$$\frac{\gamma_L}{2g} \cdot f_o \left[\left(\frac{f_o}{f} \right)^2 (K_m + 1) \right] = C_{m_3}, \left(\left(\frac{f_o}{f} \right)^2 (K_m + 1) \gg 1 \right)$$

$$\frac{\gamma_L}{g} \cdot f_o \cdot (H - x_2) = a_{m_3} \text{ (defined as metal system inertial factor)}$$

$$P \cdot f_k - p f_o - (F_1 + F_2) = Q$$

Yields

$$Q = (C_1 + C_{m_3}) V^2 + (a_1 + a_{m_3}) \frac{dV}{dt} \quad \text{--- (6a)}$$

Again, the Sachs equivalent is as follows:

$$0.97 P \cdot f_k - p(1 + 1.15 v_o) f_o = \left[C_1 + \frac{\gamma_L}{2g} \cdot f_o \left[\left(\frac{f_o}{f} \right)^2 (K_m + 1) - 1 \right] \right] V^2$$

$$+ \left[a_1 + \frac{\gamma_L}{g} \cdot f_o (H - x_2) \right] \frac{dV}{dt}$$

Sachs, (after some complex manipulation), effectively discarded the term $f_o(1+1.15\mu_o)p$ as negligible (a reverse of his attitude in his approach to the steady state analysis).

Hence

$$Q^1 = \left[C_1^1 + C_{m_3}^1 \right] V^2 + \left[a_1 + a_{m_3}^1 \right] \frac{dV}{dt} \quad \text{6(b)}$$

Sachs' estimation for unit acceleration in the metal stream $\left[H + f_o \int_0^{\lambda_3} \frac{d\gamma}{fx} \right] \frac{\gamma}{g} \cdot f_o \cdot \frac{dV}{dt}$, represents an overestimate since the term should actually be $\left[(H-x) + f_o \cdot \int_0^{\lambda_3} \frac{d\gamma}{fx} \right] \frac{\gamma}{g} \cdot f_o \cdot \frac{dV}{dt}$, the variable x would have created some difficulty in the solution of the equation and he discarded it on the grounds of insignificance. A summary of equations for flow rate etc. in unsteady conditions is given in table (2).

Certain points emerge from the analysis developed in this section and its comparison with Sachs' work. It is clear that the friction equations used by Sachs which add so much to the complexity of his equation coefficients yield negligible friction values. An almost identical effect could be achieved simply by assuming zero friction and setting up the equation accordingly, thus 4(a) = 4(b). Clearly it is a desirable feature that friction should be negligible and on that basis the equations listed in table 2 should be adequate for the determination of flow rate etc. It may be that 'stick'-friction for instance could be a significant factor in the creation of surge effects in metal flow in cold chamber machines, and that friction levels generally might well be of significance. With this in mind it is arguable that the equation forms 4(a), 5(a) etc. are the most comprehensive since friction forces are included as separate terms. The problem

would be to establish the relationship of piston movement to friction force in the circumstances. For constant friction a weighting factor would be adequate. Where some more complex relationship existed the solution of the differential equation could be much more difficult. This point will be considered in the validation tests.

Further subsidiary points are:

- i. In transient flow in which the metal is moving in closed system conditions the value of the inertial factor varies with stroke. If transition to steady state is very rapid then it can be approximated with reasonable accuracy to $(H-x_2) \frac{\gamma_L}{g}$. If not, then determination depends upon the extent of the transition period and the size of the runner gate system. In any case its overall significance will depend upon its magnitude in relation to the machine inertial factor (a_1). In circumstances when it is of significance ($> a_1$) the assumption $a_{m3} = \frac{\gamma_L}{g} (H-x_2)$ can be checked for accuracy by a velocity/time gradient comparison with experimentally derived information.
- ii. In the first stage of piston movement to close off filler holes in shot sleeve/gooseneck, there is invariably some valve or damper system in operation to prevent metal splashback and/or surge effects. Thus the effective resistance factor varies. It could be allowed for by a weighting of the value of C_1 by a lump addition or by using a multiplying factor (The comparative effect of both these possibilities is

shown in fig. 27). Sachs assumed that C_1 during this stage varied according to a multiplying factor $\frac{x_1}{x}$.

Other points emerging from the examination.

- a) The work of Sachs on flow rate is generally in agreement with the analysis produced in this section, (although exhibiting some unnecessary degree of complexity), assuming negligible friction in the systems considered. His work on flow rate was aimed at the examination of piston velocity/(gas) vent size relationships. A conceptual error (examined in detail in section 3.4) created a situation whereby calculations based on steady state and on transient conditions indicated differences which do not exist. Since his work and conclusions have been widely disseminated it is worthwhile to repeat this work to correct these errors.
- b) The literature reveals a large body ⁽³⁻¹¹⁾ of work analysing the diecasting system on a steady state basis. However no justification is offered and it is clearly as much a matter of convenience as of belief. Sachs felt that the conditions in diecasting were of unsteady flow and regarded the transient analysis as the significant part of his work. No effort has been made to examine the factors influencing variations from unsteady to steady conditions in diecasting and it would be clearly worthwhile to repair this omission.

- c) The detailed information necessary for the application of flow analysis is considerable. Some information could only be obtained by experimentation. Experiments used to validate the analysis can also be used to determine the model approach to the acquisition of such information.

3.2 ENERGY RATE

The object of this section is to develop equations for injection/gating system balancing for maximum rates of energy input to the metal system.

The energy put into the metal system during casting is dissipated in overcoming system resistance. Any residual energy at the end of cavity filling is absorbed in compressing gas voids in the (solidifying) metal and elastic deformation of the mould. It is important that the rate of energy input is sufficient to overcome local resistance at any instant during cavity filling. The casting metal behaves as a liquid for a relatively short period of time. A check in the filling pattern at a casting section can cause sufficient delay for significant heat loss to take place. The metal front at that point may well lose fluidity with a consequent enormous increase in resistance to further flow into the section. The result at any section where this occurs (invariably the narrower sections) may well be incomplete filling.

The rate of energy input into the metal system at any instant during cavity filling is given by

$$N_e = p_o \cdot f_o \cdot V$$

7

N_e = total energy input rate with respect to time

p_o = pressure in metal system at piston face

f_o = metal piston area

V = piston velocity

$$p_o = \frac{C_{m3}}{f_o} \cdot V^2 + \frac{a_{m3}}{f_o} \cdot \frac{dV}{dt} \quad (\text{see previous section})$$

piston velocity can be obtained from the general solution to the equation $Q = c_3 V^2 + a_3 \frac{dV}{dt}$ viz.

$$V = \left[\frac{Q}{C_3} + K e^{\frac{2C_3}{a_3}(x)} \right]^{\frac{1}{2}}$$

K = constant

if piston velocity at the instant at which cavity filling is initiated is V_i (piston position x_2)

substituting in the above yields

$$V = \left[\frac{Q}{C_3} + (V_i^2 - \frac{Q}{C_3}) e^{\frac{2C_3}{a_3}(x_2-x)} \right]^{\frac{1}{2}} \quad \text{_____} \quad 8$$

It follows from this that

$$\frac{dV}{dt} = - \left[V_i^2 - \frac{Q}{C_3} \right] \left[\frac{C_3}{a_3} \right] e^{\frac{2C_3}{a_3}(x_2-x)} \quad \text{_____} \quad 9$$

Substitution in 7 yields

$$N_e = C_{m3} \left[\frac{Q}{C_3} + (V_i^2 - \frac{Q}{C_3}) e^{\frac{2C_3}{a_3}(x_2-x)} \right]^{\frac{3}{2}} - a_{m3} \left[(V_i^2 - \frac{Q}{C_3}) \frac{C_3}{a_3} e^{\frac{2C_3}{a_3}(x_2-x)} \right] \text{_____} 10$$

$$\times \left[\frac{Q}{C_3} + (V_i^2 - \frac{Q}{C_3}) e^{\frac{2C_3}{a_3}(x_2-x)} \right]^{\frac{1}{2}}$$

In practice the second term on the right hand side of the expression is small compared with the first term. Even with the most favourable of dimensional conditions its influence is of the order of 10% diminishing rapidly as

$$\frac{\frac{2C_3}{a_3} (x_2 - x)}{e} \rightarrow 0.$$

This point is illustrated in fig. (17). Two machines, one having high values of C_1, a_1 (m/c 2 see table 3 for details) and one having low values (m/c 5 table 3) are examined in combination with a 68.3 mm. x .762 mm. gate $\left[C_{m_3} = 5160, a_{m_3} = 5.26 \right]$

The ratio of N_e calculated on the basis of equation 10 to that calculated from

$$N_e = C_{m_3} \left[\frac{Q}{C_3} + (V_i^2 - \frac{Q}{C_3}) e^{\frac{2C_3}{a_3} (x_2 - x)} \right] \text{ ————— } 10(a)$$

is plotted against piston stroke. Thus, depending upon the size of casting to be filled the use of equation 10(a) for calculating energy rates will not lead to significant error.

Section (4.2) will show that the rate of transition to steady flow conditions is dependent upon the magnitude of the ratio of overall system resistance factor to the overall system inertial factor. For the broad range of machines examined this was extremely rapid

At initiation of cavity fill $(x = x_2)$

$$N_{ein} = C_{m_3} \cdot V_i^3$$

At steady flow conditions $((V_i^2 - \frac{Q}{C_3}) e^{\frac{2C_3}{a_3} (x_2 - x)} \rightarrow 0)$

$$N_{est} = C_{m_3} \left(\frac{Q}{C_3} \right)^{3/2}$$

Now the ratio $N_e \text{ in } N_{e \text{ st}}$ may be greater or less than 1 depending upon whether V_i is greater or less than the steady piston velocity $V = \sqrt{\frac{Q}{C_3}}$

In conditions of rapid transition the influence of a high or low initial energy rate, (even when filling comparatively small volume castings), has little influence on total energy input into the system which will be largely determined by the steady energy rate input

$$\text{i.e. } N_e = C_{m_3} \left[\frac{Q}{C_3} \right]^{3/2}$$

[This point is illustrated in section (4.2)]

Thus for the examination of machine/mould relationships for optimum energy rate input the steady state equations will be used.

Optimum energy input to the metal system.

The energy put into the metal system by the diecasting machine is absorbed.

- (i) overcoming resistance in that element of the metal circuit contained in the body of the machine. i.e. cold chamber or gooseneck and nozzle.
- (ii) overcoming resistance in that element of the metal circuit contained in the mould. i.e. runner and gating system.
- (iii) passed into the cavity in the form of kinetic energy in the metal stream.

Now energy dissipated in (i) is wasted. It has been argued⁽¹³⁾ that the resistance of a gate can benefit filling in that the energy loss to gate resistance will take the form of frictional reheating of the metal. Thus (ii) may be of some peripheral benefit in aiding thermal balancing. The level of kinetic energy of the metal stream entering the mould will, for a given set of thermal conditions, determine whether or not the cavity fills satisfactorily. Thus it is not sufficient to examine overall energy input to the metal system. It is more important to examine the proportional distribution.

This can be expressed in the form of resistance coefficient ratios i.e.

$$\text{Let } K_m = K_R + K_G$$

K_R = loss coeff. in gooseneck/
nozzle or cold chamber

K_G = loss coeff. in the gate/mould

Hence

Rate of energy dissipated in machine section of metal system (N_{eR})

$$N_{eR} = \frac{K_R}{1+K_m} \cdot N_e \quad \text{-----} \quad (11)$$

Rate of energy dissipated in runner/gating section of metal system N_{eG}

$$N_{eG} = \frac{K_G}{1+K_m} \cdot N_e \quad \text{-----} \quad (12)$$

Kinetic energy passed on in metal stream K.E.

$$K.E. = \frac{1}{1+K_m} \cdot N_e \quad \text{_____} \quad (13)$$

$$\left[\text{i.e. } N_{eR} + N_{eG} + K.E. = N_e \right]$$

N_{eR} should be minimized, and N_{eG} and K.E. optimized. This proposition will be examined using

$$N_e = C_{m3} \cdot \left[\frac{Q}{C_3} \right]^{3/2}$$

yielding

$$N_{eG} = \frac{K_G}{1+K_m} \cdot C_{m3} \left[\frac{Q}{C_3} \right]^{3/2}$$

$$K.E. = \frac{1}{1+K_m} \cdot C_{m3} \cdot \left[\frac{Q}{C_3} \right]^{3/2}$$

Uehara⁽ⁱⁱ⁾ examined overall energy input to a simple metal system assuming the resistance coefficients of the system to be fixed and independent of gate size variations. Whilst this could be achieved up to a point in practice by proportional scaling of system dimensions a more practical approach would be to consider the system resistance coefficients as variable with respect to gate size. Separate analyses will therefore be carried out

- a) assuming $K_m = \text{constant}$
- b) assuming $K_m = \text{function of gate/runner area ratios.}$

3.2.1 Analysis based on $K_m = \text{Constant}$

The most obvious point arising from this assumption is that N_e , N_{eG} and K.E. are directly proportional to each other

since the multiplying factors will be constant. Thus the optimum gate size for N_e will also be the optimum size for $N_e G$ and K.E.

$$N_e = C_{m_3} \left[\frac{Q}{C_3} \right]^{3/2}$$

From the previous section

$$C_{m_3} = \frac{\gamma_L}{2g} \cdot \frac{f_o^3}{f^2} (1+K_m)$$

Rearranging

$$C_{m_3} = \frac{\gamma_L}{2g} \cdot \frac{f_o^3}{f_R^2} \cdot \frac{f_R^2}{f^2} (1+K_m)$$

f_R = runner cross-sectional area

Putting $\frac{\gamma_L}{2g} \cdot \frac{f_o^3}{f_R^2} (1+K_m) = A$, $\frac{f}{f_R} = F$ and

Substituting for C_{m_3} in the energy equation yields

$$N_e = Q^{3/2} \left[\frac{(A/F^2)^{2/3}}{C_1 + A/F^2} \right]^{3/2} \quad (14)$$

Differentiating equation 14 w.r.t. F yields

$$\frac{dN_e}{dF} = 1.5 Q^{3/2} \left[\frac{\left[(C_1 + A/F^2)^{-1/3} \cdot \frac{2}{3} (A/F^2)^{2/3} - (A/F^2)^{2/3} \right] \left[-2A/F^3 \right]}{(C_1 + A/F^2)^2} \times \left[\frac{(A/F^2)^{2/3}}{C_1 + A/F^2} \right]^{1/2} \right]$$

Equating the above to zero (to obtain a point of flexure) and eliminating common terms yields

$$0 = 2C_1 - A/F^2$$

i.e. $F = \left[A/2C_1 \right]^{1/2} \quad (15a)$

This value of F is the value at which energy rate input to the metal system is a maximum since $\frac{dN_e}{dF} = 0$.

$$\text{Thus } f_{\text{opt}} = f_R \left[A/2C_1 \right]^{1/2} \quad (15b)$$

By plotting A against F (15a) between the limits $0 < F \leq 1$ (in practice $f \neq f_R$) for a machine of known resistance factor (C_1) the resulting curve enables f_{opt} to be selected for a range of combination of f_R and f_o .

3.2.2 Analysis based upon K_m = function of Gate Size Variation

Section (9) is devoted to the examination of gate system loss coefficients / efficiencies. It is established in that section that K_m for conventional gating systems follows the relationship

$$K_m = BF^2 + a(1-F)$$

B, a are constants

The first term on the righthand side of the expression refers to runner loss coefficients and the second term to the loss coefficient at the gate itself. Clearly optimum gate sizes for N_e , N_{ea} and K.E. will no longer coincide and must be determined separately.

(a) Total rate of energy input N_e .

$$N_e = C_{m3} \left[\frac{Q}{C_3} \right]^{3/2}$$

Writing $\frac{Y_L}{2g} \cdot \frac{f_o^3}{f_R^2} = \bar{A}$, $\frac{f}{f_R} = F$ and

substituting in the expression for C_{m3} yields

$$C_{m_3} = \bar{A} \left[(1+a)F^{-2} + B - aF^{-1} \right]$$

Substitute into the expression for N_e

$$N_e = Q^{3/2} \cdot \bar{A} \left[(1+a)F^{-2} + B - aF^{-1} \right] \frac{1}{\left[C_1 + \bar{A} \left[(1+a)F^{-2} + B - aF^{-1} \right] \right]^{3/2}} \quad \text{--- 16}$$

Differentiating the equation 16 w.r.t. F and equating to zero to find maximum $\left[\frac{d^2 N_e}{dF^2} < 0 \right]$, assuming f_R fixed

yields

$$F^2(2C_1 - B\bar{A}) + FaA^{-1} - (1+a)\bar{A} = 0$$

Rearranging

$$f_{\text{optimum}} = f_R \left[\frac{-a\bar{A} \pm \sqrt{(\bar{A} a)^2 + 4\bar{A}(1+a)(2C_1 - B\bar{A})}}{2(2C_1 - B\bar{A})} \right] \quad \text{--- 17}$$

There are several points worth noting

(i) For optimum energy rate input to the metal system

$$\bar{A} \left[(1+a)F^{-2} + B - aF^{-1} \right] = 2C_1$$

Thus although changes in f_o and/or f_R will alter \bar{A} and consequently F , the magnitude of the term $\bar{A}[(1+a)F^{-2} + B - aF^{-1}]$ will remain constant for a given machine resistance setting. Consequently for a given net drive force the optimum rate will be constant in magnitude and will be equal to $.385 C_1^{-1/2} Q^{3/2}$ (obtained by substitution from the above equation into the energy equation).

(ii) if $B\bar{A} > C_1$ it will not be possible to achieve optimum rates of energy input for a given net drive force. Thus the metal piston area (f_o) and the runner area (f_R) are critical in establishing whether maximum energy rates can be achieved.

(iii) it follows that the gate size at which maximum energy dissipation at the gate occurs and the gate size at which maximum kinetic energy rates can be applied to the metal system are not the same. This is because the multiplying factors are themselves functions of gate size.

Arising from point (iii) the equations for optimum gate size for energy dissipation and for kinetic energy input will now be established.

(b) Maximum rate of energy dissipation at the gate.

In the expression $K_m = BF^2 + a(1-F)$ the term $a(1-F)$ refers directly to the resistance at the gate itself, hence $K_g = a(1-F)$

$$\begin{aligned} \text{Thus } N_{eg} &= \frac{K_g}{1+K_m} \cdot N_e \\ &= \frac{a(1-F)}{[1+BF^2 + a(1-F)]} \cdot \frac{Q^{3/2} \bar{A} [(1+a)F^{-2} + B - aF^{-1}]}{[C_1 + \bar{A} [(1+a)F^{-2} + B - aF^{-1}]]^{3/2}} \end{aligned}$$

Differentiating this expression with respect to F and equating the result to zero yields

$$(C_1 + B\bar{A})F^3 - (-0.5\bar{A}a + 2C_1 + 2B\bar{A})F^2 - (2\bar{A}(1+a) - 0.5\bar{A}a)F + \bar{A}(1+a) = 0 \quad \text{--- 18}$$

The first real value obtained from the solution of this equation will be the optimum value of F at which maximum rates of energy dissipation occur at the gate $\left[\frac{d^2 N_e}{dF^2} < 0 \right]$

(c) Maximum rate of energy input to the metal stream entering the cavity.

$$\begin{aligned} \text{K.E.} &= \frac{1}{1+K_m} \cdot N_e \\ &= \frac{1}{[1+BF^2+a(1-F)]} \cdot \frac{Q^{3/2} \bar{A} \cdot [(1+a)F^{-2}+B-aF^{-1}]}{[C_1+\bar{A}[(1+a)F^{-2}+B-aF^{-1}]]^{3/2}} \end{aligned}$$

Differentiating this with respect to F and equating to zero yields

$$F = \frac{\bar{A}a \pm \sqrt{(\bar{A}a)^2 + 16\bar{A}(1+a)(2C_1+2\bar{A}B)}}{4(2C_1 + 2\bar{A}B)} \quad 19$$

3.3 CONDITIONS GOVERNING STREAM BREAKDOWN (STATE OF FLOW)

In this section a general index for defining flow breakdown is proposed with a view to providing a basis for defining machine/gate conditions for solid front and for spray filling and an equation is developed for that purpose.

Analysis of flow rates in casting invariably assumes, if only by implication, that metal flowing through a gate into a mould will do so as a solid stream. This assumption is for example implicit in Sachs' work. Clearly from the point of view of gas venting, and to some extent temperature control, this is a desirable condition, particularly where porosity free castings are required.

Veinik⁽¹³⁾ has postulated two principles of gating practice:

- a) solid front filling (principle of minimum friction)
- b) spray filling (principle of maximum friction)

In the latter case he argued that benefits could be obtained from using highly resistive gates. He claimed that such gates would cause the breakdown of the metal stream into a spray, filling the cavity in such a way that the resulting casting would have uniformly distributed microporosity, reducing its strength by a factor but without macroporosity concentrations which might lead to failure. The postulate was that a casting so produced would have a coherent surface skin (good surface finish) and good dimensional stability.

In practice filling conditions tend to fall between the conditions of spray and solid front filling even in highly resistive gates. Evidence of this can be seen in the photographs of section (7.2).

In general hydrodynamics flow breakdown can be related to a dimensionless number grouping known as the Weber number expressed as follows

$$W_e = \frac{\rho V^2 d}{T}$$

It is basically a number which measures the ratio of unit inertial to unit surface tension force. Clearly the higher this ratio the greater the probability of flow breakdown. The diecasting system will therefore be analysed on the basis of this dimensionless number.

Using the symbols of the previous section the Weber number can be written

$$W_e = \frac{\gamma_L}{g} \cdot \frac{V_g^2 \cdot d}{T}$$

γ_L = wt. density of metal

V_g = gate velocity

d = hydraulic mean diameter for gate

T = surface tension of metal assumed constant

Now $V_g \cdot f = V \cdot f_o$

$$\text{and } V = \sqrt{\frac{Q}{C_3} + (V_i^2 - \frac{Q}{C_3}) e^{\frac{2C_3}{a^3}(x_2 - x)}}$$

Assuming a rectangular gate of length L and thickness t

$$d = \frac{4 \cdot L \cdot t}{2(L+t)} = \frac{2L \cdot t}{(L+t)} ; \text{ note } f = L \cdot t$$

Substituting for these in the above expression for W_e yields

$$W_e = \frac{\gamma_L}{g} \cdot \left[\frac{f_o}{f} \right]^2 \left[\frac{Q}{C_3} + (V_i^2 - \frac{Q}{C_3}) e^{\frac{2C_3}{a^3}(x_2 - x)} \right] \cdot \frac{2L \cdot t}{(L+t)} \cdot \frac{1}{T} \quad \text{--- 20}$$

At the point at which metal is about to enter the cavity (piston position $x = x_2$)

$$W_e = \frac{\gamma_L}{g} \cdot \left[\frac{f_o}{f} \right]^2 \cdot V_i^2 \cdot \frac{2f}{(L+t)} \cdot \frac{1}{T} \quad \text{--- 21(a)}$$

If and when steady flow conditions are attained

$$W_e = \frac{\gamma_L}{g} \cdot \left[\frac{f_o}{f} \right]^2 \cdot \frac{Q}{C_3} \cdot \frac{2f}{(L+t)} \cdot \frac{1}{T} \quad \text{--- 21(b)}$$

Now W_e (21(a)) may be greater or less than W_e (21(b)) depending upon the point on the piston 'free running curve' at which filling is initiated (see section (4.2) for illustration).

Where $W_e (21(a)) \gg W_e (21(b))$ spray filling could well occur initially reducing to solid front filling if $W_e (21(b)) < \text{minimum level for flow breakdown to occur}$.

Where $W_e (21(a)) \ll W_e (21(b))$ solid front filling may occur initially if $W_e (21(a)) < \text{minimum level for flow breakdown to occur}$ and will continue provided $W_e (21(b))$ is also below the minimum values.

In the absence, as yet, of experimental information it is not possible to specify quantitatively limiting values of W_e . However, these premises are advanced :

- i. It is not desirable practice for $V_i \gg \frac{Q}{C_3}$ since, depending upon the machine power it may yield a value of $W_e (21(a))$ at which spraying takes place. This could lead to isolated spray type defects in the casting.
- ii. To ensure solid front filling $V_i \leq \frac{Q}{C_3}$ and $W_e (21(b)) < \text{that value at which spraying occurs}$. This has to be correlated with energy requirements for filling and requires experimentation to quantify.
- iii. To ensure consistent spray type filling the value of W_e should be as large as possible consistent with machine capacity. For consistency this level should be stabilized rapidly. Thus ideally $V_i = \sqrt{\frac{Q}{C_3}}$ and $W_e (21(b))$ would prevail throughout filling.

Although, again, experimental evidence is as yet lacking to quantify breakdown levels it is possible, in similar fashion to the examination of energy rates, to determine gate

size for maximum value of W_e . This expansion of premise (iii) will now be considered.

Gate size for maximum (steady state) W_e

Equation 21(b) may be rewritten

$$W_e = \frac{\gamma_L}{g} \cdot \left[\frac{f_o}{f_R} \right]^2 \cdot \left[\frac{f_R}{f} \right]^2 \cdot \frac{Q}{(C_1 + C_{m_3})} \cdot \frac{1}{T} \cdot \frac{2f}{(L+t)}$$

Substituting for C_{m_3} and writing $\frac{f}{f_R} = F$ yields

$$W_e = \left[2 \frac{\gamma_L}{g} \cdot \left[\frac{f_o}{f_R} \right]^2 \cdot \frac{Q}{T} \right] \cdot \frac{1}{(L+t)} \cdot \frac{F}{[(C_1 + \bar{A}B)F^2 - a\bar{A}F + A(1+a)]}$$

Assume L fixed and f varying as t allows the expression to be further modified to

$$W_e = \left[\frac{2\gamma_L}{g} \cdot f_o^2 \cdot \frac{Q}{T} \right] \cdot \frac{F \cdot L}{[(C_1 + \bar{A}B)F^2 - aAF + A(1+a)] [L^2 + Ff_R]} \cdot f_R \quad 22$$

Differentiating equation 22 with respect to F and equating the result to zero yields

$$+2(C_1 + \bar{A}B)f_R F^3 + [(C_1 + \bar{A}B)L^2 - aAf_R]F^2 - AL^2(1+a) = 0 \quad 23$$

The first real root of equation 23 yields the gate size at which maximum W_e occurs ($\frac{d^2 W_e}{dF^2} < 0$).

3.4 VENTING OF THE MOULD

In this section an equation for mould venting is developed from basic principles and compared with existing equations of the same type.

Analytical solutions to the problem of venting of mould gases have been proposed by several research workers principally Veinik⁽¹³⁾, Sachs⁽¹²⁾ and Draper et al.⁽¹⁴⁾ The basic assumptions for these analyses are similar viz.

- (i) the application of perfect gas laws to the problem.
- (ii) the assumption of adiabatic conditions in the mould and in the vent passage for gas flow.
- (iii) Veinik and Draper relate their analysis to steady filling conditions. Sachs' work purports to examine steady and unsteady filling conditions.

In each case the end result was an equation relating the theoretical vent area (f_v) for total gas removal to the volumetric displacement rate by the metal piston ($f_o.v$) and the initial temperature of the mould gases (T_d). These are as follows

$$f_v = \frac{\text{Imp. units}}{.05 \frac{f_{o.v}}{\sqrt{T_d}}} = \frac{\text{S.I. units}}{.131 \frac{f_{o.v}}{\sqrt{T_d}}} \quad (\text{Sachs, unsteady flow})$$

$$f_v = f_o \cdot \left[\frac{(0.97 f_{KP})^{5/7} [f_o (1 + 1.15 \mu_o)]}{67.1 [C_1 + C_{m_3}] T_d} \right]^{1/2}$$

(Sachs, steady flow analysis)

$$f_v = \frac{\text{Imp. units}}{.02 \frac{f_o.v}{\sqrt{T_d}}} = \frac{\text{S.I. units}}{.049 \frac{f_o.v}{\sqrt{T_d}}} \quad (\text{Veinik})$$

$$f_v = .01 \frac{f_o.v}{\sqrt{T_d}} = .025 \frac{f_o.v}{\sqrt{T_d}} \quad (\text{Draper and Peikart})$$

As can be seen, three of the equations differ only by a multiplying factor. However there is a much more significant division of philosophy underlying these equations between Sachs and Veinik in particular. Veinik states that high gas back pressures in the cavity during die filling "..... lead to an increase in the weight of gas retained in the cavity, producing blown castings and porosity." His equation is based therefore on maximum gas evacuation at the lowest cavity gas pressure which will achieve this. Sachs' steady flow analysis starts from identical assumptions yet appears to demonstrate that very high cavity gas pressures are necessary to achieve maximum evacuation rates. In order to resolve these differences and to isolate a viable gas venting equation this problem will now be re-examined.

The assumptions on which the analysis will be based are identical to those already stated i.e. perfect gas behaviour, adiabatic flow under essentially steady flow conditions. The assumption of steady rather than unsteady flow is based upon the evidence of section (4.2). In that section it is demonstrated that transition from unsteady to steady flow is extremely rapid over a broad range of casting conditions.

Thus the assumption of essentially steady filling for even comparatively small castings is a reasonable one.

Analysis of the venting problem

The problem is one of essentially one-dimensional flow of a compressible fluid through a converging nozzle from a pressure chamber. The cavity represents the pressure chamber and the vent the nozzle. The general energy equation for one-dimensional flow of a compressible fluid between position 1 and 2 in a system can be written as follows

$$J E_1 + \frac{V_1^2}{2g} + Jq = J E_2 + \frac{V_2^2}{2g}$$

J = work constant i.e. mechanical equivalent of heat

E = enthalpy

$V_{1,2}$ = stream velocity at position 1,2.

q = heat input

In adiabatic flow conditions $q = 0$ and the expression reduces to

$$J E_1 + \frac{V_1^2}{2g} = J E_2 + \frac{V_2^2}{2g} \quad \text{_____} \quad (24)$$

From fundamental thermodynamics it can be shown that

$$E = C_p \cdot T$$

$$C_p = \frac{K}{K-1} \cdot \frac{R}{J}$$

C_p = specific heat of fluid at constant pressure

T = absolute gas temperature

R = universal gas constant

$$K = \frac{C_p}{C_v}$$

C_v = specific heat of fluid at constant volume

Substitution into (24) yields

$$\frac{V_2^2 - V_1^2}{2g} = \frac{K}{K-1} (RT_1 - RT_2)$$

Substituting pressure, specific weight for RT_1 , RT_2 according to the equation of state and further rearranging according to the adiabatic relationship between pressure and specific weight yields:

$$\frac{V_2^2 - V_1^2}{2g} = \frac{K}{K-1} \cdot \frac{P_2}{\gamma_2} \left[\left(\frac{P_1}{P_2} \right)^{\frac{K-1}{K}} - 1 \right] \quad (25)$$

γ_2 = specific weight at position 2

NOTE: This equation can also be derived by integrating the Euler equation $\frac{dp}{\gamma} + \frac{VdV}{g} = 0$ along a stream tube and noting that $pV^K = \text{constant}$.

Equation (25) may now be used to examine mould venting

Vent position 2 corresponds to vent exit

position 1 to the cavity

γ_2 = specific weight of vented gas = γ_v

V_2 = exit velocity of vented gas = V_v

V_1 = velocity of approach of gas in cavity to vent (considered to be negligible)

$P_2 = P_v + P_{at}$ where P_v = gauge pressure of gas jet entering the surrounding medium considered to be at ambient pressure (P_{at})

$P_1 = P + P_{at}$ where P = gauge pressure of cavity gases

Substituting into equation (25) yields

$$V_v^2 = 2g \cdot \frac{K}{K-1} \cdot \frac{P_v + P_{at}}{\gamma_v} \left[\frac{P_v + P_{at}}{P_v + P_{at}}^{\frac{K-1}{K}} - 1 \right] \quad (26)$$

It can be shown from fundamental thermodynamics⁽³³⁾

- a) the maximum possible gas speed attainable at a converging nozzle is sonic
- b) sonic velocity (C) is related to the absolute pressure and wt. density at any point in a gas stream by the expression

$$C = \sqrt{g \cdot K \cdot (\text{abs. press}) (\text{wt. density})^{-1}}$$

Thus the magnitude of sonic velocity in the vent exit is given by

$$C = \sqrt{g \cdot K \cdot (P_v + P_{at}) (\gamma_v)^{-1}} \quad (27)$$

Using this information and rearranging (26) yields

$$\frac{V_v^2}{C^2} = \frac{2}{K-1} \left[\left[\frac{P_v + P_{at}}{P_v + P_{at}} \right]^{\frac{K-1}{K}} - 1 \right]$$

The critical pressure ratio at which sonic velocity is achieved in the vent exit can be determined from this expression by substituting $V_v = C$, yielding

$$\left[\frac{P_v + P_{at}}{P_v + P_{at}} \right]_{\text{critical}} = \left[\frac{K+1}{2} \right]^{\frac{K}{K-1}} \quad (28)$$

The minimum value of P at which this is achieved will be when $P_v = 0$

$$\text{i.e. } P = P_{at} \cdot \left[\left[\frac{K+1}{2} \right]^{\frac{K}{K-1}} - 1 \right]$$

for air $K = 1.4$, $P = .89 P_{at}$

Since supersonic velocities are not attainable in the vent any increase in P beyond this level simply causes an increase in P_v according to the relationship expressed in equation (28).

Now the weight flow rate of gas through the vent is given by

$$\frac{dW}{dt} = C_D \cdot f_v \cdot V_v \cdot \gamma_v$$

f_v = vent area

C_D = coefficient of discharge for orifice

Substituting from (26) and rearranging yields

$$\frac{dW}{dt} = C_d \cdot f_v \cdot \left[2g \cdot \frac{K}{K-1} (P+P_{at}) \gamma_1 \left[\left(\frac{P_v+P_{at}}{P+P_{at}} \right)^{\frac{2}{K}} - \left(\frac{P_v+P_{at}}{P+P_{at}} \right)^{\frac{K+1}{K}} \right] \right]^{\frac{1}{2}}$$

γ_1 = wt. density of gas in cavity

This expression is applicable so long as

$$\frac{P_v+P_{at}}{P+P_{at}} < \text{the critical ratio}$$

$\frac{dW}{dt}$ will be a maximum when sonic velocity is achieved in the vent exit i.e. at the critical pressure ratio, substituting in the above expression yields

$$\frac{dW}{dt}_{\max} = C_d \cdot f_v \cdot \frac{P+P_{at}}{\sqrt{T_1}} \left[\frac{gK}{R} \left[\frac{2}{K+1} \right]^{\frac{K+1}{K-1}} \right]^{\frac{1}{2}} \quad (29)$$

T_1 = absolute temp. of gas in cavity

R = universal gas constant

It is clear that provided cavity gauge pressure (P) is greater than $0.89 P_{at}$ that optimum flow rate conditions exist, the magnitude being dependent upon the cavity pressure. Good venting practices demand that gas back pressure should be as small as possible, (consistent with complete venting), to avoid restricting metal flow into the cavity. For the purpose of selecting vent size therefore the lower bound value of P for optimum flow rate will be used.

Now the volume rate of flow air from the cavity into the vent must equal the volume rate of approach of the metal piston i.e.

$$\frac{dW}{dt}_{\max} \times \text{specific volume of cavity air} = f_o \cdot V$$

Let specific volume of cavity air at pressure $(P+P_{at})$ be v_1

$$\text{Hence } \frac{dW}{dt}_{\max} \cdot v_1 = f_o \cdot V \quad (30)$$

$$C_d \cdot f_v \cdot \frac{(P+P_{at})v_1}{\sqrt{T_1}} \left[\frac{gK}{R} \left[\frac{2}{K+1} \right]^{\frac{K+1}{K-1}} \right]^{\frac{1}{2}} = f_o \cdot V$$

Now $(P+P_{at})v_1 = RT_1$, the temperature of cavity air under ambient conditions is assumed to approach to the die(average) temperature T_d . Ignoring heating influence of incoming metal and assuming adiabatic conditions of compression yields:

$$T_1 = T_d \cdot \left[\frac{P+P_{at}}{P_{at}} \right]^{\frac{K-1}{K}}$$

Substituting in the above equation yields

$$C_d \cdot f_v \cdot \sqrt{T_d} \cdot \left[R \cdot \left[\frac{P+P_{at}}{P_{at}} \right]^{\frac{K-1}{K}} \cdot g \cdot K \cdot \left[\frac{2}{(K+1)} \right]^{\frac{K+1}{K-1}} \right]^{\frac{1}{2}} = f_o V \quad (31)$$

Now at the lower bound value of P , $\left[\frac{P+P_{at}}{P_{at}} \right] = 1.89$

In the metric system $R = 29.28 \text{ m/}^\circ\text{C}$, $g = 9.81 \text{ m/s}$.

Substituting these values in the above and rearranging yields

$$f_v = \frac{f_o \cdot V}{12.7 C_d \cdot \sqrt{T_d}} = \frac{.0787 f_o}{C_d \cdot \sqrt{T_d}} \quad (32)$$

This equation will now be compared with the equation of Veinik, and Sachs. Draper's equation is incorrect due to a fundamental mistake, conceded by the authors, and will be discounted.

Comparison with Veinik analysis

Veinik equation $f_v = .049 \frac{f_o \cdot V}{\sqrt{T_d}}$

Equation (32) $f_v = .0787 \frac{f_o \cdot V}{C_d \sqrt{T_d}}$

Veinik assumed that $C_d = 1$ in his analysis. His coefficient (.02) differs from that of equation (32) due to a variation of assumption for volumetric flow rates viz.

Equation (32) was based upon the relationship

$$\frac{dW}{dt}_{\text{max}} \times \text{specific volume of cavity gas at pressure } (P+P_{\text{at}}) = f_o \cdot V$$

Veinik's equation was based upon the assumption of the relationship

$$\frac{dW}{dt}_{\text{max}} \times \text{specific volume of cavity gas at ambient pressure } (P_{\text{at}}) = f_o \cdot V$$

If one compares these two statements it is clear that the former is the more realistic of the two. It follows that the Veinik coefficient is low.

Comparison with Sachs' analysis

Steady flow

Sachs developed an equation identical to equation (32) without apparently associating the form of the rate of flow equation he used with the optimum condition it represents. His major conceptual error lay in this and was exacerbated by the manipulative line he then pursued. He rearranged equation (30) to yield

$$\frac{dW}{dt} = f_o \cdot V \cdot \left[\frac{P+P_{\text{at}}}{P_{\text{at}}} \right]^{\frac{1}{K}} \cdot \frac{P_{\text{at}}}{T_d} \quad (33)$$

He then compared this with equation 4(b) section 3.1

$$0.97 \cdot f_K \cdot P - p(1 + 1.15\mu_o) f_o = (C_1 + C_{m_3}) V^2 \quad (4b)$$

i.e. he assumed back pressure to be necessarily significant for optimum venting.

He substituted for V from 4(b) in (33) and differentiated the result with respect to $(P+P_{at})$ to find an "optimum" value of $\frac{dW}{dt}$ and the values of piston velocity, gas pressure and vent size associated with it viz.

$$V_{opt} = \left[\frac{7}{17} \cdot \frac{0.97 \cdot f_K \cdot P}{[C_1 + C_{m_3}]} \right]^{\frac{1}{2}} \quad \text{--- (34(a))}$$

$$P_{opt} = \frac{10}{17} \cdot \frac{0.97 \cdot f_K \cdot P}{f_o (1+1.15\mu_o)} \quad \text{--- (34(b))}$$

$$f_V = f_o \left[\frac{(0.97 \cdot f_K \cdot P)^{1/K} [f_o (1+1.15\mu_o)]}{67.1 [C_1 + C_{m_3}] T_d} \right]^{\frac{1}{2}} \quad \text{--- (34(c))}$$

The manipulation from which these equations were developed may now be seen to be based upon a false premise and are therefore meaningless. An intuitive appreciation of this may be gained from an appraisal of the equation for P_{opt} which purports to prove that optimum venting can only be achieved at a back force equivalent to $\frac{10}{17}$ of the net drive force!

Unsteady state

Sachs' more rigorous examination of venting under unsteady conditions did not fall into the conceptual error of the steady state analysis. After much complex manipulation and having "..... to sacrifice exactness of analysis for lucidity and to make reasonable assumptions susceptible to analytical treatment" he finally obtained the equation

$$\frac{.53 \cdot f_V \cdot C_d \cdot R \cdot \sqrt{T_d}}{f_o \cdot V} \left[\frac{P+P_{at}}{P_{at}} \right]^{\frac{K-1}{2K}} = \text{a constant} = 'n'$$

'n' was defined as the vent factor having a possible spectrum

of value ranging from 0 (zero venting) to 1 (total venting).

If one substitutes $n=1$ into the above it becomes identical to (32) yielding the same result i.e.

$$f_V = .0787 \cdot \frac{f_o \cdot V}{\sqrt{T_d} \cdot C_d}$$

$$\left[\text{Sachs assumed } C_d = 0.6 \text{ yielding } f_V = .131 \cdot \frac{f_o \cdot V}{\sqrt{T_d}} \right]$$

Thus the equations for steady and unsteady conditions are identical in form.

Having re-examined the venting problem and compared the result with Sachs and Veinik analyses the following conclusions may be drawn:

- i. For optimum venting cavity gas pressure need not be large $[P + P_{at} = 1.89 P_{at}]$. Under optimum venting conditions the gas back pressure component in the general force equation governing piston movement may be ignored.
- ii. The Sachs equation for vent size, piston velocity, gas pressure under steady flow conditions are based upon a false premise and should be discarded.
- iii. The vent equation, applicable to both unsteady and steady flow conditions is

$$f_V = .0787 \cdot \frac{f_o \cdot V}{\sqrt{T_d} \cdot C_d} \quad (\text{S.I. units})$$

iv. The analysis of vent size represents the limit of useful (analytical) examination of venting systems. In practice, successful gas evacuation from a cavity depends upon vent siting as well as size. The site, ideally, must be such that the vent remains open during the whole of cavity filling and requires that gases be moved progressively toward it. Thus this aspect of venting is a function of cavity filling patterns and metal flow state and is not realistically susceptible to mathematical analysis.

3.5 CONCLUSIONS

An analytical framework has been developed in 3.1 - 3.4 which covers the most significant features of metal flow in pressure casting. It remains now to apply this analysis to general diecasting systems to establish machine/mould influences and their implications, particularly with respect to amplitude and duration of transition from unsteady to steady flow.

In the case of the flow rate analysis it is necessary before examining the above to repeat the body of calculations carried out by Sachs. This is necessary because of the error in the work and the widespread dissemination and acceptance of the resulting (erroneous) conclusions.

4. APPLICATION OF FLOW RATE ANALYSIS TO GENERAL DIECASTING SYSTEMS

To build up a complete picture of machine/mould influence during the transition phase of the casting cycle requires a 'step by step' approach involving the repetitious use of the equations, (particularly of flow rate), discussed in section 3. The use of a computer for this purpose eased the burden of computations and allowed very small step sizes to be used. The initial programme used had three calculation loops in series corresponding to stages a,b,c/d. of figure 15 and based on the equations of table 2. This programme was used initially to re-examine the work carried out by Sachs. A fourth loop was later added to this programme to allow runner and gate influence to be considered separately rather than lumped together (c/d).

4.1 EXAMINATION OF SACHS' CONCLUSIONS

In view of the anomalies discovered in his analysis it was decided to repeat these calculations using the modified equation developed in 3.1. As already mentioned, a computer was used for this purpose in view of the tedious nature of the work and also to reduce the time involved. The programme was arranged to run until steady state conditions were attained. Thus not only could calculations comparable to those of Sachs be made but further information on transition effects was available from the computer print-out.

Sachs ⁽⁸⁾ applied his calculations to the A.S.T.M. B-6 test casting (fig.5) assumed to be produced under equal thermal conditions in aluminium alloy of approximately 13% silicon with four different gate thicknesses, .76, 1.02, 1.27 and 1.52 mm. on different machines, the details of which are specified in table 3, fig. 18. Machines (1-4) inclusive were hydraulically operated cold chamber machines, whilst machines (5-7) inclusive were pneumatically operated cold chamber machines. The calculations for these machines were repeated and the comparative results are shown in tables 4 and 5. (Figs. 19, 20). Examples of velocity/stroke/time characteristics obtained from the computer print-out are shown in figs. (21) and (22). The point on the stroke at which runner/cavity fill began varied somewhat from machine to machine. To bring the filling sections of the curves into phase for comparative purposes the velocity/stroke characteristic fig. (21) was split into two sections.

Certain differences are apparent from a comparison of the tables of results, which throw some doubt upon certain of Sachs' main conclusions. One discrepancy which, although significant in itself, does not fall into this category is the difference between the calculations of the time taken for piston travel between positions x_1 and x_2 . Sachs' estimates are almost exactly ten times the computer result. There is general agreement between Sachs' transient velocity calculations and the computer prediction. In view of the interdependant nature of the computer calculations it is clear that it is Sachs' stage time estimate which is incorrect. This

error is intuitively obvious without the backing of the computer calculations viz. The ratio $\frac{x_1}{x_2 - x_1}$ is anywhere between 6 and 8 for the machines considered. Fig. (21) shows the velocity build-up to x_1 for the range of machines and the subsequent change in piston velocity between x_1 and x_2 . It is clear that the elapsed time for the two stages cannot be of the same order as Sachs' results appear to indicate.

Having eliminated this point the significant difference occurring between the calculations will now be discussed:

Steady state velocity

Sachs' estimate of steady state velocity was based on the equation

$$V_{opt} = \sqrt{\frac{7}{17} \cdot \frac{P \cdot f_K}{C_3}}$$

P = reservoir/accumulator pressure

f_K = drive piston area

$C_3 = C_1 + C_{m3}$

V_{opt} = steady piston velocity for optimum vent conditions

which in turn derived from two equations

$$f_K \cdot P - f_o \cdot (1 + 1.15\mu_o) \cdot P_{opt} = C_3 \cdot \frac{V_{opt}^2}{2g}, \quad f_o = \text{metal piston area}$$

μ_o = metal piston function

$$f_o (1 + 1.15\mu_o) P_{opt} = \frac{10}{17} \cdot P \cdot f_K$$

P_{opt} = gas pressure in the cavity under optimum venting

The erroneous assumptions made by Sachs in the derivation of the equations for V_{opt} and P_{opt} have been discussed in section 3.4. It has been demonstrated that for optimum venting

conditions P_{opt} is negligible. Thus

$$V_{opt} = \sqrt{\frac{P \cdot f_K}{C_3}}$$

Sachs' values for steady state velocity should therefore be corrected by a factor of $\sqrt{\frac{17}{7}} = 1.558$. If this is done excellent agreement is found between the computer estimate for steady state velocity and the corrected values for all machines. Fig. (23) illustrates the closeness of the agreement for machine 1A.

Filling time estimates for steady filling conditions.

This discrepancy is accounted for by the difference between steady filling velocities. Sachs' time values require correction by a factor of $\frac{1}{1.558}$. Excellent agreement exists between the corrected values and the computer prediction for steady conditions.

Vent calculations for steady filling conditions.

The equation for vent area used by Sachs in his calculations was

$$f_{vo} = \frac{f_o \cdot V_{opt}}{.71 C \cdot R \cdot \sqrt{T_d}} \left[\frac{P_{at}}{P_{opt} + P_{at}} \right]^{1/7} \quad (\text{S.I. units})$$

Into this correct (theoretical) expression he substituted values for P_{opt} and V_{opt} from equation 34a,b which are incorrect. This leads to a gross under-estimate of vent area. The implications are discussed in conjunction with the transient

stage calculations.

Vent area estimate for transient conditions

Sachs based his calculations for optimum vent area under transient conditions upon the equation

$$f_{vo} = \frac{V \cdot f_o \cdot n}{7.62 \sqrt{T_d}} \quad n = \text{so-called venting factor assumed to be } \approx 0.9$$

The piston velocity he used for his calculations was that achieved by the piston at position x_2^1 i.e. at the entrance to the cavity. He clearly did not envisage any major change of velocity during cavity filling. Figure 21 shows that this is only partially true. It is the case for machines 2,3,4 but is emphatically not so for machines 1, 1A,5,6,7. The computer prediction used the same equation but used average piston velocity during filling for the calculations. Thus there is reasonable agreement between the two calculations for machines 2,3,4 and significant difference for machines 1,1A,5,6 & 7.

Amongst other things, Sachs concluded that:

- (i) for optimum vent conditions the actual cavity fill time is approximately 2/3 of the cavity filling time calculated for steady state for all types of machine.
- (ii) the optimum vent size required for hydraulically driven machines for a given die is 2.7 to 3.8 greater under actual as opposed to steady state conditions and for air driven machines the differences are greater.

(iii) in hydraulically operated machines the optimum vent size does not vary much with gate size but some significant variations occur with air-operated machines.

In view of the errors in Sachs' steady state calculations these conclusions must be revised somewhat. Taking each point in turn, the differences in optimum vent size requirement between transient and steady state conditions are essentially a measure of the difference between steady state and average filling velocities. For the range of machines examined the difference between steady state and average filling velocities is generally small (c.f. steady state and transient filling times in table 5). Figs. 24b and 25b compare the computer calculations of steady state and transient state vent size requirements for machine 1 and machine 5 respectively with those of Sachs. The computer prediction demonstrates that the state differences are comparatively small and will only be of significance where there are extended acceleration or deceleration periods during cavity fill.

Clearly cavity fill time under optimum vent conditions will be influenced by similar considerations. Thus where average fill and steady state velocities are of a similar order then filling times will be correspondingly so. The computer prediction of transient filling times generally shows good agreement with Sachs. The computer prediction of steady state filling times approximate fairly closely to the transient calculations (as do Sachs when appropriately corrected).

Figs. 24(a) and 25(a) compare steady and transient filling times for machines 1 to 5.

Finally, there is the conclusion relating to the sensitivity of the relationship between vent and gate size. This point is worthy of detailed examination since it contains a valid, if somewhat distorted point. The distortion lies in Sachs' use of the results to distinguish specifically between air-operated and hydraulic machines as this is, to some extent, misleading. For the purposes of explaining this comment, venting under steady state conditions will be used for illustration and arithmetic convenience.

The venting equation can be written

$$f_{vo} = \frac{.131 f_o V}{\sqrt{T_d}}, \text{ Assuming } C_d = 0.6 \text{ (See section 3.4 for identification of symbols)}$$

for steady conditions

$$V = \sqrt{\frac{A}{C_1 + C_{m_3}}} \quad \begin{array}{l} A = P \cdot f_K \\ C_1 = \text{machine resistance factor} \\ C_{m_3} = \text{metal system resistance factor} \end{array}$$

$$= \frac{A}{C_1 + \frac{\gamma_L}{2g} \cdot \frac{f_o^3}{f^2} (1 + K_m)}$$

Substituting in the expression for venting size yields

$$f_{vo} = \frac{B}{C_1 + \frac{\gamma_L}{2g} \cdot \frac{f_o^3}{f^2} (1 + K_m)}, \quad B = \frac{.131 f_o \cdot \sqrt{A}}{\sqrt{T_d}}$$

If $C_1 \ll C_{m_3}$

$$f_{vo} \approx \frac{B}{\sqrt{\frac{l}{2g} \cdot \frac{f_o^3}{f^2} (1+K_m)}} \approx B^1 f \text{ for fixed resistance}$$

Thus under conditions where a range of gate sizes are employed upon a machine in which the statement $C_1 \ll C_{m_3}$ is not compromised then vent size requirement varies directly as gate size. If $C_1 \gg C_{m_3}$ then clearly

$$f_{vo} \approx \frac{B}{\sqrt{C_1}}$$

Under these conditions vent size requirement is independent of gate size. Figure 28 illustrates this point on a non-dimensional basis. The y-axis represents the ratio $\frac{f_{vu}}{f_{vl}}$ where

f_{vu} = optimum vent size for the largest gate considered (f_u)

f_{vl} = optimum vent size for the smallest gate considered (f_l)

The x-axis represents the ratio $\frac{C_1 - C_{m_3 av}}{C_{3 av}}$ where

C_1 is the machine resistance factor

$C_{m_3 av}$ is the average resistance factor for the range of gate size considered. $C_{3 av}$ is the average resistance factor for the system for the range considered. The two curves plotted are for a range of gate size variation of 2.0 and of 8.0. For

$\frac{C_1 - C_{m_3 av}}{C_{3 av}} \rightarrow 1$ (i.e. C_{m_3} negligible) the vent size ratio

$\frac{f_{vu}}{f_{vl}} \rightarrow 1$ also. For $\frac{C_1 - C_{m_3 av}}{C_{3 av}} \rightarrow -1$ (i.e. C_1 negligible)

$\frac{f_{vu}}{f_{vl}} \rightarrow \frac{f_u}{f_l}$ i.e. 2.0 and 8.0 respectively.

THE UNIVERSITY OF ASTON
IN BIRMINGHAM
LIBRARY

Thus the assessment of vent/gate size relationships is better done in the context of machine/gating factor relationships rather than of drive fluid type since although pneumatic machines would tend towards -1 on the $\frac{C_1 - C_{m_3 av}}{C_1 av}$ scale and hydraulic machines to the +1 point. this is not exclusively so and there can be considerable overlap. For example consider machine 1A for which $K_D = K_E \approx 50$. This machine would give an x-ordinate value tending towards +1 for any range of gating considered thus tending toward minimum vent size sensitivity. However if the length of drive, exhaust piping were reduced and its diameter increased so that $K_D + K_E$ is very small; the machine resistance factor would drop and would yield an x-ordinate similar say, to machine 5 i.e. tending toward -1 where vent size is very sensitive to gate size variation. Conversely, if the resistance of machine 5 were increased (reduced pipe size, longer pipes, etc.) its C_1 value would move well into the hydraulic machine range. Thus it is an over simplification to suggest as Sachs does, that optimum vent/size requirements vary significantly with gate size for pneumatically operated machines. The more generally correct statement would be that where machine resistance is small in relation to a spectrum of gate resistance then optimum vent size requirement varies with gate size within that spectrum. Where the converse is true then vent size requirement is essentially independent of gate size variation.

Summarising therefore, the three points raised by Sachs are either incorrect or insufficiently qualified and the correct conclusions from the spectrum of results are

- i. For optimum vent conditions actual cavity fill time was approximately the same as fill time estimated for steady flow conditions for the machine range considered.
- ii. Optimum vent size requirements were essentially the same for both actual filling and assumed steady fill conditions. Any difference was due to the difference between the steady fill velocity as compared to the average fill velocity.
- iii. Where machine resistance is small in relation to a spectrum of gate resistance, then optimum vent size requirement varies with gate size within that spectrum. Where the converse is true then vent size requirement is essentially independent of gate size variations.

4.2. EXAMINATION OF FACTORS AFFECTING TRANSITION FROM UNSTEADY TO STEADY FLOW CONDITIONS

The object of this section is to determine the influence of injection system and metal system factors upon transition under ideal conditions, and also under conditions of vent closure and of cavity resistance.

4.2.1. INFLUENCE OF INJECTION AND METAL SYSTEM FACTORS

In the initial stages of piston movement the piston motion may be described as 'free running' in the sense that no metal system resistance is involved. During this phase the form of the velocity curve is determined by the driving force and by the resistance and inertia of the injection system alone. At the point on the piston stroke, where metal system resistance becomes significant 'free running' conditions cease and the curve form is then determined by

the combined resistance and inertia of injection and metal systems. It is clear that the point of changeover will have a significant effect upon acceleration/deceleration conditions during filling. There are three factors to be considered

- a) The form of the 'free-running' curve for an injection system
- b) The influence of the combined effects of injection and metal systems upon the form of the filling curve
- c) The influence of the changeover position.

These will be examined in turn.

"Free-running' conditions.

The equations of table 2, (clarified by examination in conjunction with figure 15), show the putative relationships for velocity etc. during the stages of movement considered. Consider the relationships embodied in stages 1 and 2 which relate to 'free' piston movement. Although derived from basic considerations the velocity equation for stage 1 contains an assumption by Sachs that injection system resistance varies linearly with piston movement during that stage. Although this relationship was accepted for the purpose of comparative calculation there are other possible conditions equally valid. Stage 1 covers the piston movement necessary to cover the metal filler hole. In order to avoid metal splashing from the hole the movement of a piston during this stage may be controlled by an adjustable damper element in the injection system which

increases injection system resistance by a factor and consequently reduces the rate of piston motion. Thus there are two possibilities for the velocity equation of stage 1

- i. $V = \sqrt{A_1 x}$, Sachs, linear variations of injection system resistance
- ii. $V = \left[A_1 \left(1 - e^{-\frac{2C_1^1}{a_1} x} \right) \right]^{1/2}$, fixed injection system resistance raised from its normal values of C_1 to C_1^1 by the influence of a damper!

To illustrate the effect this would have on piston motion the computer programme was modified and calculations performed using machine 1A as an example. It was assumed that the machine had unlimited stroke in order that the whole of the 'free running' curve covering the transition from transient to steady state could be observed. Figure 27, shows the result. Curve I represents the free running velocity characteristic using Sachs assumptions. Curves II and III illustrate extremes of velocity characteristics for fixed injection resistance during stage 1. Curve II was determined for zero damper resistance (i.e. C_1 during stage 1 as quoted for machine 1A in table 3). Curve III was based upon high damper resistance (C_1^1 during stage 1 = 10 times the value quoted in table 3). Since the net driving force (Q) and the system resistance after stage 1 are the same for all three cases the curves approach the same steady state value ($= \sqrt{\frac{Q}{C_1}}$).

Curves II and III represent probable extremes of curve form for piston characteristics in 'free running' conditions.

When high temporary resistance (or low initial drive forces) are involved the free running curve will have two distinct phases similar to curve III. Curve II represents the other extreme of a condition where no difference exists between initial and second stage conditions. Sachs' curve which differentiates in the manner already indicated between stage 1 and stage 2 lies between these two extremes.

Where the ratio of injection system resistance to inertia is small there is a tendency for the velocity build-up to steady state to be relatively long. When it is large the period of build up is reduced and there is a rapid transition from transient to steady state in the free-running condition. (See stage 1 of curve III). The rapidity of transition is also influenced by the terminal steady velocity for the injection system in free movement ($=\sqrt{\frac{Q}{C_1}}$, C_1 = injection system resistance factor). Figure 28 illustrates this point using machines 1A and 5. The curves are based upon Sachs' assumptions for stage 1 conditions.

Filling phase (stage 3 of table 2) and injection point.

Consider now the situation in which metal injection takes place. i.e. extra resistance and inertia comes in at x_2 due to the filling of runner and cavity. The equations of stage 3 determine conditions during the cavity fill stage. In order to assess the components influencing steady state transition consider the velocity/stroke equations for stages 2 and 3 rewritten in slightly different form.

$$V_{s2} = \sqrt{\frac{Q}{C_1} + (V_{s1}^2 - \frac{Q}{C_1}) e^{\frac{2C_1}{a_1} \cdot (x_1 - x_2)}} \quad (i)$$

V_{s1} = velocity of piston at the end of stage 1.

V_{s2} = velocity of piston at the end of stage 2 i.e. beginning of cavity fill.

$$V_{s3} = \sqrt{\frac{Q}{C_3} (V_{s2}^2 - \frac{Q}{C_3}) e^{\frac{2C_3}{a_3} \cdot (x_2 - x)}} \quad (ii)$$

V_{s3} = piston velocity at any point in the filling phase.

Consider equation (i) first. The form of the equation V_{s2} remains the same regardless of the resistive conditions of stage 1 although clearly the magnitude of any result is affected. If the exponential index $\frac{2C_1}{a_1} \cdot (x_1 - x_2)$ is > 3 then V_{s2} will be closely approximate to the terminal steady state value for 'free running' conditions i.e. $V_{s2} = \sqrt{\frac{Q}{C_1}}$. This will be approached in systems having high resistance and relatively low inertia and in systems employing small pistons and large strokes (i.e. $(x_1 - x_2)$. large)

Consider now equation (ii)

It is immediately apparent from the form of the equation that if $V_{s2} = \sqrt{\frac{Q}{C_3}}$ the piston velocity will, theoretically at least, stabilize instantaneously to steady state conditions. This point has some significance in relation to slow-fast control systems and will be discussed in detail later in the section. The point on the 'free running' curve for an injection system at which the velocity value is equal to the system steady state velocity for a given combination of that injection

system and a selected metal gating system will be defined as the nodal position. Either side of the nodal position the stroke (and consequently period of time) for which V_{s3} continues to change significantly depends upon the magnitude of the term $(V_{s2}^2 - \frac{Q}{C_3}) \cdot e^{\frac{2C_3}{a_3}(x_2 - x)}$. Whilst this term represents a significant part of the equation for V_{s3} , then unsteady flow conditions will prevail. Consider the various permutations:

Where the magnitude of the exponential index is small then the rate of change of the exponential component will also be comparatively small and the significance of the term will depend upon $(V_{s2}^2 - \frac{Q}{C_3})$. Where this is large then an extended transition period will occur. For small values (in the limit 0) then the significance of the variable term is much reduced and essentially steady state conditions rapidly attained.

Where the magnitude of the exponential index is large (highly resistive injection system and/or metal gating system) then regardless of the magnitude of $(V_{s2}^2 - \frac{Q}{C_3})$ the rate of change of the variable term will be rapid and steady state velocity conditions rapidly attained.

Thus the attainment of steady flow conditions in a die depends on the point in the above spectrum into which its relationship with the machine fits. The proximity of average filling conditions to steady state will depend also upon the volume of cavity to be filled i.e. length of filling stroke.

The following examples clearly illustrate these points:

Figure 29 uses machine 5 to illustrate variations upon a machine having a low resistance to inertia ratio. The machine's 'free running' characteristic is plotted. Superimposed upon it are (filling) curves for high resistance gate (.762m.m.x 68.25m.m. feeding the B-6 test die) and for a gate of only one fiftieth that resistance (5.334 m.m. x 68.25 m.m. feeding the B-6 test die). Injection is considered for five different starting positions on the stroke i.e. 40,80,122, 183 and 244 m.m.. Consider first the curves relating to the 5.334 m.m. gate. For this gate the system resistance/inertia ratio is comparatively small and the transition period is mainly dependent upon the magnitude of the term $(V_{s2}^2 - \frac{Q}{C_3})$. The further from the nodal position the greater the percentage difference between actual cavity fill time and that estimated on the basis of steady flow conditions. The magnitude of difference will of course depend upon the filling stroke length. The following figures are based upon a filling stroke of 85.34 m.m. (equivalent to the stroke necessary to fill the B-6 test die using the metal piston size listed for machine 5 in table 3).

Stroke to initiation of injection (M.M.)	Actual fill time (secs)	Steady state fill time(secs)	% diff.
40	.0067	.0057	-15.0
80	.0062	.0057	- 8.0
122	.0058	.0057	- 1.7
183	.0055	.0057	+ 3.6
244	.0054	.0057	+ 5.5

Figure 30 shows the percentage variations between actual and steady state fill times for injection stroke initiation at positions 40,80,122,183 and 244 m.m. and for filling stroke lengths of 30.5,61,85,122,152 m.m. The nodal position for the gate in question can be seen to be around 15 metres per second (its value is $V_{s2} = \sqrt{\frac{Q}{C_3}} = 14.94$ metres/sec.) The family of curves clearly show the influence of filling stroke length and displacement from the nodal position. Thus for a filling stroke of 152 m.m. initiated @ 40 m.m. the percentage underestimate is approximately ten per cent whilst for a filling stroke of 30.5 m.m. initiated at the same position the error is nearly double. Clearly for a system having similar resistance but a higher inertia factor the percentage error will be greater.

The curves for the .762 m.m. gate shown in the same graph illustrate the point that when system resistance/inertia ratios are high (in this case due to high gate resistance) stability is reached fairly quickly, see below (based on a filling stroke of 85 m.m.).

Stroke to initiation of cavity m.m	Actual fill fill time (secs)	Steady state fill time (secs)	% diff.
40	.0257	.0267	3.8
80	.0254	.0267	5.0
122	.0252	.0267	5.9

These figures are more significant when compared with the nodal position for the gate, which is at 3.24 metres per second. Thus for an injection initiation point 122 m.m. at which the initial injection velocity is over four times greater than the nodal value the percentage is only 5.9%. Further, this error would not increase by very much even if the injection initiation point were higher up the stroke. In machines in which injection system resistance factor is very high the transition takes place very rapidly for a very wide range of gate resistance. Figure 31 illustrates this quite dramatically. The curves are based on machine No. 2 with an injection initiation point of 52 m.m. for three gate sizes .20 m.m., .76 m.m., 1.52 m.m. x 68.25 m.m. Where a machine has a very high resistance factor the build up to terminal velocity is, in stroke terms, very rapid. Consequently the value of V_{s2} for even moderate pre-injection stroke is likely to be close to the terminal value. Until very large gate resistances are considered the nodal values for a large range of gate resistance are likely to be very close together in the narrow spectrum of values between V_{s2} and terminal velocity value for the injection system. As an example consider the curves for the .76 m.m. and 1.52 m.m. gates. On machine 5 their nodal values were 3.24 and 14.94 m/s respectively. On machine 2 they were 1.28 and 1.36 m/s. (indeed the initiation points coincide almost exactly with the nodal value for the .76 m.m. gate). Thus transition to steady state is very rapid. Where gate resistance is very large indeed the nodal position may be well below the value of V_{s2} as for

example the .20 m.m. gate for which the nodal value is .21m/s. Even so, the transition from transient to steady flow is exceptionally rapid due to the combination of a very high injection resistance factor with a very high metal system resistance factor. The figures given below (based on a stroke of 85 m.m.) illustrates this.

Gate size	Actual filling time (secs)	Steady filling time (secs)	% diff.
1.52mmx68.25mm	.0610	.0628	1.6
.76mmx68.25mm	.0661	.0664	0
.20mmx68.25mm	.384	.390	1.6

Thus the spectrum of variation for gate resistance factors as widely dispersed as 336 (gate 1.52 m.m.) and 82600 (gate .200mm) is only about 3.0%.

Summarizing, therefore, it is true to say that steady state filling conditions will prevail in diecasting under conditions of ideal venting and negligible cavity resistance as follows:

- a) On all diecasting machines where piston velocity at injection is equal to the steady state velocity for the complete system (i.e. changeover at nodal position).
- b) Approximately, on machines having a high injection system resistance to inertia ratio.

c) Approximately, where the resistance/inertia ratio for the metal system is very large.

As far as points b) and c) are concerned the larger the filling stroke the better the approximation.

Steady state filling will not take place where the overall system resistance to inertia ratio is low and where injection is initiated at a piston velocity well away from the nodal position. The degree of difference will vary with the stroke necessary to fill the cavity but the statement is true for a wide range of cavity size.

Before considering the effect of vent closure etc. (section 4.2.2.) there is a further, peripheral, point regarding filling velocity characteristics which is worthy of note. The form of the filling characteristic depends upon the changeover position and the magnitude of system resistance etc. The metal system resistance factor is a function of metal density, piston area, gate size and loss coefficient i.e.

$$C_{m_3} \div \frac{\gamma_m}{2g} \cdot \frac{f_o^3}{f^2} \cdot (1+K_m)$$

For a fixed value of C_{m_3} the filling characteristic will be fixed also (on a given machine at a given change point).

However, since the magnitude of this factor can be made up in a variety of ways, a given velocity characteristic can apply to a number of circumstances (although other characteristics may be different). To illustrate this consider two possible permutations in the context of machine 1A. Fig. 32a illustrates

the casting of aluminium through a gate .76m.m. x 68.25 m.m. using a metal piston of 50.5 m.m. dia. (system resistance factor = 5160). If the casting metal were changed, for a fixed piston size and loss coefficient the resistance factor could be maintained at its original magnitude by changing the gate size appropriately viz.

Metal	Gate size (m.m.)	C_{m_3} (N.sec ² m ⁻²)
Al	.76mm x 68.25mm	5160
Mg	.58mm x 68.25mm	5160
Zn	1.19mm x 68.25mm	5160
Brass	1.42mm x 68.25mm	5160

For all these combinations the velocity, pressure, energy rate curves and filling time for a given cavity size would be identical.

Consider, however, the case where metal piston size is changed and compensated for by an appropriate change of gate size to maintain C_{m_3} i.e.

Metal : aluminium

f	metal piston dia.	C_{m_3} (N.sec ² m ⁻²)
.76mm x 68.25mm	50.8 mm	5160
.20mm x 68.25mm	80.8 mm	5160
.38mm x 68.25mm	64.0 mm	5160
3.05mm x 68.25mm	32.0 mm	5160

Whilst the velocity characteristic remains the same, pressure energy rate and cavity filling time do not ($P_o, N_e, t \propto \frac{1}{f_o}$ for

fixed C_{m_3}). Fig. 32(b) illustrates this point. The figure shows that filling time for a given cavity reduces with increasing gate size and increases with decreasing piston size for a fixed velocity characteristic. Hence for the case considered filling times are increased by reducing gate size below the datum value ($f = .76\text{mm} \times 68.25\text{mm}$.) but change comparatively little for increasing piston size above the datum value 50.8mm. Increasing gate size above the datum reduces the filling time whilst decreasing piston size below datum value increases filling time.

4.2.2. EFFECT OF VENT CLOSURE AND CAVITY RESISTANCE

The previous section considered steady state transition under 'ideal' conditions of optimum venting and negligible cavity resistance during filling. Under these conditions metal system resistance is constant and gas pressure insignificant. Clearly casting does not necessarily take place under ideal conditions and there are undoubtedly instances in which metal system resistance varies and/or in which gas pressure is significant in relation to cavity flow. It is instructive therefore to consider these possibilities.

Premature vent closure.

As has been previously remarked, the problem of vent design is one of size and site. The ideal site is one which is at the last point in the cavity to fill. Even so, complete evacuation can only occur if the cavity gas is moved progressively toward the vent site by the metal filling pattern. Where metal filling the cavity blocks off the vent prematurely than the trapped gases will offer increasing resistance to

flow as further metal is forced into the cavity and it is compressed. In the limit this resistance will cancel out the driving force and bring the piston to rest.

Depending upon the conditions in the cavity during filling the compression of the gas may be under isothermal or adiabatic conditions. Veinik argues that in spray filling (maximum friction) conditions are essentially isothermal whilst in solid front filling (minimum friction) conditions will be adiabatic. The resistance to compression under adiabatic conditions is greater than for isothermal conditions. To examine the effect of premature vent closure the analysis and computer programme was modified to accommodate the following assumptions.

- i. No escape of gas from the cavity during filling (Zero venting).
- ii. Gas compression takes place under adiabatic conditions.
- iii. The effects of gas back pressure remain negligible until the cavity fill stage (Stage 3 in the analysis see table 2).

The equation for piston motion for stage 3 in optimum vent conditions has the form

$Q = C_3 V^2 + a_3 \frac{dV}{dt}$, where Q is the net driving force assured constant. Under zero venting conditions the equation is modified to include a back pressure term i.e.

$$[Q - f_0 \cdot p] = C_3 V^2 + a_3 \frac{dV}{dt}, \quad \begin{array}{l} f_0 = \text{metal piston area} \\ p = \text{back pressure} \end{array}$$

Since p varies with piston position the net driving force $Q' (= Q - f_0 p)$ is a function of x . Solutions of the differential equation becomes more complex and an approximation was adopted

which gave sufficiently accurate results for the exercise. The solution yielded values for velocity etc., which had the same form as those for optimum conditions (stage 3 table 2) but in which the coefficient A_3 was modified thus

$$A_3 = \frac{1}{C_3} \left[Q - p_a \cdot \left[\frac{1}{1 - \frac{f_o(x-x_1)}{V_a}} \right]^\gamma \right]$$

p_a = ambient pressure
in cavity

V_a = volume of runner
and cavity

f_o = metal piston area

x = piston position at
any instant

x_1 = piston stroke to
cover filler hole

The degree of significance that gas back pressure is likely to have can be seen from the analytical statement for A_3 to depend upon the net driving force under optimum conditions (Q) and upon the cavity volume (i.e. overall length of stroke).

Machines 1 and 1A (table 3.) differ only in their net driving force. It was decided therefore to apply the modified computer program to these machines. There was no indication in the analysis of any significant influence by gate size under zero venting conditions and this was fixed for the purpose of the computer analysis at .76mm x 68.25mm. (the smallest size examined by Sachs). Using the volume of the B-6 test die as a datum ($V_{B6} = 246\text{cc.}$), filling characteristics were computed for values $\frac{1}{4} V_{B6}$, $\frac{1}{2} V_{B6}$, V_{B6} and $4 V_{B6}$ on machines 1 and 1A. The results of the computations are shown in figs. 33-35.

Figures 33(a) and 34(a) show the velocity characteristics for optimum and for zero venting. It can be seen that back pressure effects do not become significant until late in the filling stage. Divergence of zero and optimum vent velocity characteristics occurs slightly sooner for machine 1A and is somewhat greater. This is to be expected since an analysis of back pressure development under adiabatic conditions shows that back pressure does not reach a magnitude of 10% of net drive pressure until 90% of fill stroke on machine 1A and 94% of fill stroke on machine 1.

Figures 33(b)(c), and 34(b)(c) compare percentage difference between zero and optimum vent cavity fill times. Under conditions of optimum venting (33b and 34b) the percentage difference between steady and transient fill times tend toward zero for increasing fill stroke (NOTE. if cavity fill had been initiated at the nodal point then the percentage difference would have been zero for all strokes). With zero venting, for the machine(s) conditions examined the percentage difference between steady and transient filling times is less than for optimum vent conditions. Thus filling times under zero vent conditions approximated fairly closely to those for steady state filling for the stroke range considered.

However this is only so because in the cases considered the changeover point is well above the nodal position for the machine/gate combination. This leads to a velocity drop down to the nodal value during the first stage of piston movement which is partly cancelled out in averaging terms by the fall of the velocity characteristic below the nodal position due

to the onset of significant gas back pressure. Had the changeover been on or below the nodal position the percentage difference between zero vent and steady state fill times for a given stroke would be higher than the corresponding difference for optimum vent conditions.

The curves (33c and 34c) examining the percentage difference between fill times under zero and optimum conditions show a tendency to increase with increasing fill stroke. The percentage difference is small for the range examined but was largest for machine 1A. Spot calculations were carried out for driving forces of 26700 and 13350 N, (for machine No. 1, $Q = 107000$ N; for 1A, $Q = 53400$ N), to examine the degree to which the percentage difference might vary. The results of these calculations are given in the table below, together with the values on which figures 33c and 34c are based.

CAVITY VOL.	STROKE m.m.	PERCENTAGE DIFFERENCE IN FILL TIMES			
		$Q=107000$ N	$Q=53400$ N	$Q=26700$ N	$Q=13350$ N
$\frac{1}{4} \cdot V_{B_6}$	21.3	.35	1.1	-	-
$\frac{1}{2} \cdot V_{B_6}$	42.6	.50	1.2	-	-
V_{B_6}	85.2	1.05	1.55	1.64	-
$2 \cdot V_{B_6}$	170.4	-	1.65	-	2.33

The percentage differences overall remains small. The trend indicates a tendency to increase for reduced drive force and/or long fill strokes. The conclusion reached is that in terms of fill time there is little difference between conditions of optimum and of zero venting since the initiation of significant gas resistance in zero venting occupies a very small

part of the filling stroke. However, it is well to remember that, of course, in terms of casting quality there is a considerable difference in castings produced under each of these conditions. Figure 35 is a salutary reminder of the degree to which percentage porosity by volume (theoretically) changes with drive force for zero vent and for optimum vent conditions.

Variable runner/cavity resistance.

The predominating resistance feature in a runner/cavity system is generally the gate since this represents (dimensionally) the greatest step change in the system. In hydraulic terms the gate remains as the controlling influence on flow until or unless a greater resistance is encountered downstream (in the cavity). This could conceivably happen in castings of complex shape in which the average section size approaches that of the gate and/or partial solidification reduces section size as filling proceeds. Under these circumstances the flow rate will be modified as if the effective gate resistance had changed. Clearly under these circumstances steady flow will never occur but it is interesting to speculate on the degree of deviation from it.

In view of the loop form of the computer programme it was comparatively easy to adapt it to examine the effect of resistance variation. Basically, the programme as initially developed repeats itself to calculate piston velocity, elapsed time etc. for preselected step values of stroke through various stages of filling. In the original programme the resistance of

the runner/cavity was assumed to come in at the start of stage 3. (cavity fill stage, see table 2) and remain constant from then on. It was an easy matter to modify the programme to examine a case of variable filling resistance according to any functional relationship for any or every step value of stroke comprising stage 3. Further, the step values could be reduced to any size (for example in considering the problem of zero venting step values of .00003m were used).

In order to assess the influence of variable runner/cavity resistance the following assumptions were made and the computer programme adopted accordingly.

- i. Cavity resistance was assumed to increase by 10% of its original value for every (calculation) increment of stroke. The value for stroke increment was fixed at .003 m.
- ii. Filling was assumed to take place with optimum vent conditions.

In examining the relationship between machine and gating systems and the influence these have on filling times under fixed resistive conditions (section 4.2.1.) it was clear that the proportional relationship of system resistance factors was of considerable significance. It was decided therefore to carry out the analysis of variable resistance effects using a permutation of two machines having high and low resistance factors with two gates also at opposite ends of the resistance spectrum. The details of these are given in the following table:

Machines See table 3	Resistance factor $N \cdot sec^2 / m^2$	Inertial factor $N \cdot sec^2 / m$
No. 2	$C_1 = 28000$	$a_1 = 461$
No. 5	$C_1 = 138$	$a_1 = 45$
Gating size (based on B-6)	Initial value	
.76mmx68.25mm.	$C_{m_3} = 5160$	$a_3 = 5.25$
5.33mm.x68.25mm.	$C_{m_3} = 105$	$a_3 = 4.38$

Figures 36-38 show the results of the analysis applied to the various combinations.

Figure 36 (Machine 2)

Machine 2 has a very high resistance and the form and plateau magnitude of its 'free running' piston velocity curve show this. The larger gate has an insignificant initial resistance factor (105). A rate of increase of 10% per 3.05 mm. yields a resistance value of approximately 1000 after 265 mm. of filling stroke. This is not sufficient to influence the overall system resistance value significantly and deviation of the filling characteristic from the machine's 'free running' curve is marginal. For the .76 mm. gate the changeover position (stage (2) to stage (3)) is at the nodal point for the combination and the piston (filling) velocity characteristic is horizontal for fixed gate/cavity resistance ($C_{m_3} = 5160$). Since the base value of gate resistance is significant vis-a-vis machine resistance, a 10% step increase in its value has an immediate and perceptible influence upon the velocity characteristic i.e. piston velocity 265 mm. of stroke from inception

of filling is only about 60% of the fixed resistance value.

Figure 37 (Machine No. 5)

This machine has a very low resistance factor, of similar order to that for the 5.33 mm. gate. Consequently a 10% incremental rate of increase of gate resistance has an obvious influence for low as well as high resistance gating systems. Figure 38 (a) compares the percentage difference existing between fill time based upon fixed resistance and fill time based upon variable resistance. Figure 38 (b) compares the fill time based upon an averaging of the variable resistance situation with actual fill time for the variable resistance situation. Consider first the results for machine No. 2: For a gate system of low initial resistance (5.33 mm. gate) the influence of 10% cumulative step increases of this resistance over the range considered is negligible. Even for a highly resistive gate (.76mm.) varying in a similar manner the percentage differences are not as large as might have been anticipated. Indeed in fig. 38b the maximum percentage deviation is only about 8% at the maximum filling stroke considered. The same gates examined in conjunction with machine No. 5 show a very different picture. The percentage differences are considerable for both gates, particularly so for the high resistance gate.

The information gained from this examination may be summarised as follows: Clearly variation of runner/cavity resistance will influence piston velocity characteristic and

filling time. The (magnitude) difference as compared with a filling characteristic based upon fixed or average resistance will depend upon a number of factors viz.

- i. the functional relationship of resistance change with piston movement.
- ii. the magnitude of the initial resistance factor of the gate
- iii. the magnitude of the machine resistance factor
- iv. the length of filling stroke.

For the example considered, which was that of a high linear rate of resistance change it was clear that for machines of high resistance factors there will be very little difference in filling times until or unless the gate resistance factor approaches a similar order of value. Machine 2 had a resistance factor of 28000, the 5.33 mm. gate had a resistance change of 105 to approximately 1000 over the maximum stroke considered; this was not sufficient to have any effect. The .76 mm. gate changed in resistance from 5160 to 9650 over the maximum stroke and this led to a relatively significant deviation of value. It follows that for machines of low resistance factor significant differences would occur over a broad spectrum of gate sizes and the results using machine No. 5 confirm this.

4.3 NOTE ON TWO STAGE INJECTION

The object of 'slow-fast' control on a diecasting machine is to prevent excessive turbulence in the metal moving into the runner/gating system prior to the initiation of cavity fill

which could lead to air entrapment and premature splashing of metal into the cavity. As the name suggest, the controls allow the adjustment of piston speed to give a relatively slow movement during the initial progression of metal into the runner/gating system followed by a faster piston movement whilst the cavity is filled. The usual method of achieving this is by means of a damper unit built into the injection head. This allows the machine resistance factor to be adjusted, the damper cutting out at a preset piston position corresponding to the beginning of cavity fill.

The author's experience of these types of control is that they provide only very crude adjustment of resistance values and cut-out position. A more fundamental criticism, however, is that they are equally crude in terms of design principle viz. It is generally accepted that rough relationships exist between alloy type, gate size and filling rate for good casting. Indeed the literature abounds in references to range of gate velocity necessary for the production of good casting practice. These are well summarised in Nussey's survey of die-casting literature. The analysis in the foregoing sections showsthat the attainment of a required filling rate in a given time or piston stroke is a function of the resistance/inertial factors in both the injection and the metal(gating) system. Low rates of resistance/inertial factor give long build up times whilst low resistance factors yield high terminal filling velocities, the converse being true for both statements. Thus a slow/fast control should, ideally, combine the desirable feature of a slow approach with the ability to rapidly

attain optimum filling conditions for a given gate and metal piston size. Current design practice in these types of control takes no quantitative account of these factors at all. Despite this, it is general experience (including the author's) that slow/fast systems do help in the attainment of good casting quality. This poses the question as to how much more benefit such systems might provide if they are properly designed. Two possibilities are examined in the following

- i. The combination of the conclusions from the analysis with existing control 'hardware'
- ii. The specification of an alternative to 'slow-fast' systems based upon the previous analysis.

'Good practice' in the use of existing systems

As previously stated, existing systems are invariably based upon the use of a damper unit built into the machine injection head. Their 'control' extends only to the slow stage. The damper setting determines the largest element of machine resistance factor and the point (fill initiation) at which it cuts out. Filling proceeds at a rate which is a function of net drive force and the combination of the machine 'residual' resistance factor with the resistance factor of the metal gating system. The best use of such a system would be as follows:

Slow stage: very high resistance factors reduce the transition to steady conditions to a minimum. By using a relatively high damper resistance the slow stage filling becomes essentially steady state, the piston velocity being given by

$$V_{s.s.} = \sqrt{\frac{Q}{C_{1m} + C_R}}$$

Q = net drive force
(variable)

C_R = damper resistance
factor (variable)

C_{1m} = machine 'residual'
resistance factor

This would avoid transient effect compromising the intention of the slow stage. The value of piston velocity would have to be high enough to avoid excessive metal heat losses during this stage.

Fast stage: the damper cuts out ($C_R \rightarrow 0$), the metal system resistance factor (C_{m_3}) comes into play and the piston accelerates toward its terminal condition. The piston velocity in this stage is given by

$$V_{f.s.} = \left[\frac{Q}{C_{1m} + C_{m_3}} + \left[V_{s.s.}^2 - \frac{Q}{(C_{1m} + C_{m_3})} \right] e^{\frac{2C_{1m} + C_{m_3}}{a_1 + a_{m_3}} (x^* - x)} \right]^{\frac{1}{2}}$$

a_1, a_{m_3} = inertial factors
of machine and
gating system
respectively

x^* = slow/fast change-
over position

When terminal conditions are attained

$$V_{f.s. \text{ steady}} = \sqrt{\frac{Q}{C_{1m} + C_{m_3}}}$$

If the ideal gate velocity (obtained from practice/literature) is V_g

$$V_g \cdot f = f_o \cdot V_{f.s. \text{ steady}} \quad f = \text{gate area}$$

$$\text{Hence } V_g = \frac{f_o}{f} \sqrt{\frac{Q}{C_{1m} + \frac{\gamma}{2g} \cdot \frac{f_o^3}{f^2} (1+K_m)}, C_{m3} = \frac{\gamma}{2g} \cdot \frac{f_o^3}{f^2} (1+K_m)}$$

Knowing the required value (or more probably) spectrum of value for V_g , the appropriate metal piston size and/or gate size, resistance factor may be selected for the attainment of this. Two points arise:

- i. Consider the following
 - a) gate size is limited by casting dimensions
 - b) there is a limit to the allowable variation of metal piston size on a given machine.

Thus it may not be possible to attain appropriate gate velocities for a given casting on a given machine. Or, using the same information more positively, it is possible to specify for a given machine the range of casting systems it can cover.

ii. Where a machine is capable of producing the right conditions there is a further point to consider. Figure 39 indicates the idealized range of form of piston velocity curve under slow/fast filling for fixed cavity resistance. Filling will be partially unsteady. The proportion depends

upon the resistance/inertial factor for the system and the cavity volume. Low resistance/inertial factors give long transition periods and, depending upon cavity size, may take up the whole of the filling stroke (c.f. cavity fill positions 1 and 2). Thus for smaller cavity volumes ideal filling velocities may not be attained and the average may be significantly different. Adjustment of net drive force (raising the potential terminal piston velocity above the value $V_f = \text{steady} = V_g \cdot f / f_o$) would cause the average gate velocity to tend towards the ideal.

Alternative approach

The analysis of transition effects (section 4.2.) has shown that where a nodal changeover position is achieved for the initiation of cavity filling, then filling is completely steady state. Thus the possibility of premature filling or of unnecessary flow breakdown is avoided. A variable resistance system built into the injection unit which allows adjustment to a nodal position, (consistent with ideal fill rates), for any gating system to be run on the machine would therefore seem desirable.

This would require the injection mechanism to be capable of independent adjustment (in resistance factor terms) in two stroke phases i.e. during runner fill and during cavity fill. Firstly the resistance factor must be capable of adjustment so that the piston velocity, appropriate to the gate size, (of the metal system to which it is connected), is achieved by the point of fill initiation. Secondly the overall system resistance during cavity fill must be such as to maintain the

piston velocity constant, i.e. so that the changeover point is the nodal position for the gate (for ideal filling rate).

The magnitude of the variables which the designed system has to cover may be deduced as follows:

i. Stroke to fill initiation point (1st phase)

In practice the piston movement to fill initiation is given by x^* where

$$x^* = \frac{|\text{Vol. of metal system} - \text{vol. of metal shot}|}{\text{metal piston area}}$$

This varies with shot volume and metal piston size. The range of these can be specified for a machine, hence yielding a spectrum of value for x^* .

ii. Piston velocity at the initiation of cavity fill

The piston velocity at this point should be that which yields the ideal filling rate i.e.

$$V = V_g \cdot \frac{f}{f_o}$$

V = piston velocity

f_o = piston area

V_g = ideal gate velocity

f = gate area

This is related to the machine resistance and inertial parameters by the expression for piston velocity

$$V = \left[\frac{Q}{C_{1m} + C_R} \cdot \left[1 - e^{-\frac{2C_{1m} + C_R}{a_1} (x^*)} \right] \right]^{\frac{1}{2}}$$

Q = net drive force
 C_{1m} = residual resistance factor

a_1 = machine inertial factor

C_R = variable resistance factor

(NOTE: this expression is obtained from the equation

$$V = \left[\frac{Q}{C_{1m} + C_R} + \left[V_{s1}^2 - \frac{Q}{C_{1m} + C_R} \right] \cdot e^{\frac{2C_{1m} + C_R}{a_1}(x_c - x^*)} \right]^{1/2}$$

where x_c is the stroke to cover the filler hole and V_{s1} is the velocity of the piston immediately after it has been cleared. There is normally a provision in most machines to allow the piston to inch forward until the filler hole is covered to prevent metal splashing. For the purpose of a general specification this stage has been assumed negligible. Should this not be the case this factor can be included without any change in the design philosophy).

The maximum range of piston velocity of which the machine needs to be capable is given by

$$V = V_g \cdot \frac{f_{\min}}{f_{o_{\max}}} \quad \text{---} \quad V = V_g \cdot \frac{f_{\max}}{f_{o_{\min}}}$$

The range of resistance factors which the injection system would require to cover this can be specified from the second equation. This will also be dependent upon the net drive force range of which the machine is capable and the range of value of x^* .

iii. Maintenance of piston velocity at steady (ideal) value during filling.

If the filling is to be completely steady state i.e. the nodal position for the gate size considered then the introduction of metal system resistance must be balanced by some proportional reduction in the machine resistance factor, given by the equation

$$V = \sqrt{\frac{Q}{C_{1m} + C_R^1 + C_{m3}}} = V_g \cdot \frac{f}{f_o}$$

$$\begin{aligned} C_{m3} &= \text{metal system resistance factor} \\ &= \frac{\gamma_L}{2g} \cdot \frac{f_o^3}{f^2} (1 + K_m) \end{aligned}$$

Yielding

$$C_R^1 = Q \left\{ \frac{f_o \cdot 1}{f V_g} \right\}^2 - \left[C_{1m} + \frac{\gamma_L}{2g} \cdot \frac{f_o^3}{f^2} \cdot (1 + K_m) \right]$$

The necessary range of machine injection system resistance factor (C_R^1) may be deduced from the above on the basis

$$\left. \begin{array}{l} C_R^1 \rightarrow \max, \quad \frac{f_o}{f} \rightarrow \max \\ C_R^1 \rightarrow \min, \quad \frac{f_o}{f} \rightarrow \min \end{array} \right\} \text{ for given value of } Q$$

An illustration of the setting technique for an injection system based on the above is given in the following example of aluminium casting.

Machine specification: (combination of detail from machines 5 and 2, table 2)

$$C_{1m} = 144 \frac{\text{Nsec}^2}{\text{m}^2} \quad (\text{based on machine 5})$$

$$C_{R_{\min}} = 0$$

$$C_{R_{\max}} = 28000 \frac{\text{Nsec}^2}{\text{m}^2} \quad (\text{based on machine 2})$$

$$Q = 54000 \text{ N}$$

$$f_o = .002 \text{ m}^2$$

$$x^* = .052 - .06 \text{ metres}$$

Gating specification

$$f = .76\text{mm.} \times 68.25\text{mm.} = .000052 \text{ m}^2, C_{m_3} = 5160$$

$$V_g = 60 \text{ m/s}$$

required value of $x^* = .052\text{m}$

Examination of the literature by Nussey reveals various opinions as to optimum gating velocity for aluminium. Significant differences exist between American and European practice. For the purpose of the exercise a representative value $V_g = 60 \text{ m/s}$ is used |.

Setting machine resistance factor for 1st phase

$$V = V_g \cdot \frac{f}{f_o} = 60. \cdot \frac{.000052}{.002}$$

$$V = 1.56 \text{ m/s}$$

Figure 40 shows curves of free piston velocity based on various settings for C_R . Examination shows that a piston velocity of 1.56 m/s is attained at $x^* = .052 \text{ m}$ for a value of $C_R = 20200$.

∴ Resistance setting for 1st phase = $C_R = 20200$

Setting machine resistance factor for 2nd phase (filling)

$$C_R^1 = Q \left\{ \frac{f_o}{f} \cdot \frac{1}{V_g} \right\}^2 - \{C_{1m} + C_{m_3}\}$$

Yields $C_R^1 = 16900$

∴ Resistance factor setting for 2nd phase = $C_R^1 = 16900$

NOTE: it is possible under some circumstances for the equation for C_R^1 to yield a negative value indicating impossible conditions. For example, if $V_g = 150$ m/s then $C_R^1 = -1780$. The only conclusion to be drawn would be that if gate size were fixed, then either

1. f_o would have to be changed (and the setting process repeated.)
- or 2. if the machine possessed the capacity for introducing step change in Q (i.e. pressure intensification) then this factor could be changed in appropriate proportion.

Should neither of these possibilities redress the balance then it would be impossible to run a die having a gating system of the size and resistance factor specified at the ideal gating velocity during filling.

4.4 CONCLUSIONS

Re-examination of the body of Sachs' work (4.1.) confirmed the differences which were predicted would arise as a result of his conceptual error in the development of steady state equations for velocity and vent size. The modifications to Sachs' conclusions made necessary by this are reported in detail in section 4.1 and are essentially as follows:

- i. Vent size differences for steady state and transient filling conditions are directly related to the difference between steady and average filling velocities. Fill times have a similar relationship.
- ii. The general relationship between gate and vent size for a cavity can be expressed thus: where machine resistance factor is small in relation to a spectrum of gate resistance then optimum vent size requirement varies with gate size within that spectrum. Where the converse is true then vent size requirement is essentially independent of gate size variation.

Examination of transition conditions (4.2.) was carried out in two stages. Firstly, transition was considered in the context of ideal filling conditions, i.e. optimum venting and negligible cavity resistance. Secondly, non-ideal conditions of zero venting and of variable cavity resistance were considered. In the former the shape of the filling characteristic was significantly influenced by the point on the piston 'free running' curve at which cavity fill was initiated. The magnitude and rate of change of (piston)

velocity is a function of the resistance/inertial factors of the system. Where changeover (fill initiation) position coincided with the steady state filling velocity for a particular machine/gate combination filling conditions were completely steady. The further changeover was from this (nodal) position then the greater the magnitude of change during transition to steady conditions. The length of transition period was found to be dependent upon the ratio of resistance factor to inertial factor for the system. When the resistance was high the transition was extremely rapid, when low it could take a significant period. It will be noted that the form of a piston (filling) velocity curve is not unique to one set of casting conditions. Any metal system having the same resistance factor and essentially the same inertial factor has the same velocity characteristics. In some instances pressure, energy rate curves would be the same also. The reason for this together with an example are reported in 4.2.

Under the heading of non-ideal conditions, zero venting and variable cavity resistance were considered separately. The examination of zero venting conditions showed that back pressure (resistance) did not become significant until late in the filling stroke. The influence on piston velocity is therefore limited to the last 10% or so of filling stroke depending on cavity volume. Consequently the difference between zero and optimum vent conditions in terms of cavity fill time was small although the practical difference in terms of casting porosity is obviously large.

Clearly variation of metal system resistance factor during cavity fill will prevent steady flow conditions from being achieved, the degree of difference depending upon the magnitude of resistance factor variation. When the machine resistance factor is large in relation to the metal system resistance and its variation, the influence of such variation upon filling rates is negligible.

It has been shown that it is possible to avoid transition effects completely if the machine and gating system are matched to ensure 'nodal' fill initiation conditions. This ensures that velocity, pressure etc. are constant throughout filling for ideal conditions. This has some significance from the point of view of injection system design, and its application to two stage controls is examined in 4.3.

5. APPLICATION OF ENERGY AND FLOW STATE EQUATIONS TO GENERAL DIECASTING SYSTEMS

The machines used for illustration are machines 1A, 2 and 5 from table 3. The first two machines are hydraulically operated and have high machine resistance and inertial factors, whilst the latter is pneumatically operated and has low values for these factors. This enables the influence of the spectrum of machine factor magnitude to be examined. The metal system influence is represented by the runner/gate configuration as used in test die B-6 (fig. 5). The effects of gate size variation will be considered in the context of this configuration.

5.1. ENERGY RATE CALCULATIONS

Two points should be noted in conjunction with this subsection.

- a) No information exists as to metal system resistance (K_R) in the machine section of the metal 'circuit' for the machine used. The experimental examination reported in section 6 will show that this can be significant. This limitation cannot be rectified and it will be assumed that $K_R=0$. To compensate to some extent for this, Sachs' assumption for friction conditions will be used (i.e. in C_{m_3} replace $(1+K_m)$ by $(1+1.15\mu_o)(1+K_m)$ where μ_o = metal piston resistance coefficient = .12)
- b) The form of the B-6 gate configuration is such that gate resistance is negligible (i.e. $K_g = 0$). Consequently

N_e , K.E. will have their optimum values at the same gate size given by

$$f = f_R \left[\frac{A}{2C_1} \right]^{\frac{1}{2}} \quad (\text{equation 15b, 3.2})$$

Thus the curves of overall energy rate only will be examined, as the magnitude of K.E. rate at a given size will only differ by a constant multiplying factor and the curve forms will be identical.

The analysis covered a broad range of gate size for the metal system and the effects of the range of machine/gate combinations are examined for several changeover positions (fill initiation). The details are as follows:

Machines

Machine No.	Resistance factor (N sec ² m ⁻²)	Inertial factor (N sec ² m ⁻¹)
1A	4000	200
2	28000	460
5	140	45

Gates.

Gate size is plotted as multiples or sub-multiples of a normal gate size 'f'. The reason for this is as follows: Resistance factors for a gate size spectrum were originally calculated on the assumption of aluminium as the casting alloy and the B-6 test die normal gate size as nominal. Now metal system resistance factors are a function of alloy density and

gate size. Thus alloy/gate combinations having the same resistance factor will have the same (total) energy rate curves (and if their efficiencies are the same then this will apply to K.E. curves also). Consequently the curves computed for aluminium will apply to any alloy provided the gate size spectrum to which they apply is suitably adjusted. This adjustment consists simply of multiplying the 'aluminium' gate sizes by $\sqrt{\frac{\gamma_{\text{alloy}}}{\gamma_{\text{aluminium alloy}}}}$ For illustration the gate sizes for

both zinc and aluminium having the same resistance factors and therefore energy curves are tabulated below

GATE	SIZE m.m. ²		C _{m3} N.sec ² m ⁻²	a _{m3} N.sec ² m ⁻¹
	Zinc	Aluminium		
f/4	.305x68.25	.203x68.25	82500	6.13
f/2	.584x68.25	.381x68.25	20600	5.84
f	1.194x68.25	.762x68.25	5160	5.26
2f	2.362x68.25	1.524x68.25	1280	4.67
4f	4.724x68.25	3.050x68.25	322	4.53

NOTE: the inertial factor will differ for different alloys on a similar shot size. However for steady flow conditions this factor does not apply and for unsteady conditions the influence of this difference is only significant for very low values of C_{m3}. The inertial factors computed for aluminium can be used with negligible error resulting.

The calculations were carried out on the basis of optimum vent conditions (i.e. negligible gas back pressure in the cavity). The results are plotted in graph form and will be discussed in the following.

Figures 41-43

These graphs contain the velocity characteristics for the complete permutation of conditions examined. The form and relationships for similar families of velocity curves are discussed in detail in section 4 sub-section 2. They are used in this section to establish a reference framework within which the energy relationships can be discussed.

Figures 44 (a-c)

This set of figures show the energy rate variations with piston movement over the range of gate sizes and changeover positions for machine 1A. Compare these with the equivalent family of velocity curves (fig.41). The changeover velocities for positions 15.25, 61.00 and 122.00 mm. cover the nodal range (steady velocities) for gate sizes f - $4f$. The nodal values for gate size $\frac{f}{2}$ and $\frac{f}{4}$ are significantly less than the nearest changeover point (15.25 mm.). Thus the difference between initial and steady energy rates are largest (for m/c 1A) at the bottom end of the range of gate size considered. The biggest difference occurred for changeover position 122mm. (fig.44c) and least for changeover position 15.25mm. (fig.44a). The curve families intersect, indicating no difference in initial and steady energy rates at positions corresponding to $.875 f$ for changeover position 15.25mm. and

2f for changeover position 61.00mm. The curves for changeover position 122.00mm. do not intersect within the range of gate size plotted although approaching it at the larger end of the gate range. These intersection points indicate the values of gate size for which the steady state piston velocity corresponds to that at the changeover position, i.e. for which the changeover position is the nodal point on the piston velocity curve.

The steady state energy rate curves are identical for all changeover positions. This arises because the changeover (or fill initiation) position can only influence transition conditions.

Figures 45-47

The same information as is contained in fig. 44(a-c) is plotted in fig. 45. To enable comparison with the equivalent information from machine 2 (fig. 46) and machine 5 (fig. 47) the energy rate is plotted on a \log_{10} basis. It is immediately clear that although energy rate varies with changeover position, the largest differences are associated with the machine type (this point will be discussed in the context of fig. 48). Over the spectrum of gate sizes considered the steady state energy rate curves for each machine indicate a gate size for which energy rate input would be a maximum (predictable from equation 15b). As in fig. 44(a-c) 'nodal' gate size for a given changeover position is indicated by the intersection of steady state with initial energy rate curve plotted for that position.

Figure 48

The energy rates (initial/steady state) for all three machines are plotted against changeover (fill initiation) position. Again, in view of the tremendous variation in these values the energy rate ratio is plotted on a \log_{10} basis. The point where each gate curve cuts the horizontal axis indicates the nodal changeover position for that gate (c.f. velocity curves).

The graph clearly highlights the influence of machine resistance factor. Machine 5 has a low machine resistance factor (and consequently a high free piston velocity ceiling see fig. 43). Thus there is a significant velocity variation for the changeover positions and an equally broad range of steady state (piston) velocities for the range of gate size. The result is that the ratio of energy rates varies enormously over the range of gate size and changeover position. At the opposite end of the scale machine 2 has a comparatively large machine resistance factor. This reduces the influence of gate resistance to relative insignificance over the gate size range and is the major determinant of the magnitude of the piston velocity. Consequently, although energy rates vary with changeover position, the spectrum of variation across the range of gate size is small.

Transition rates were high for all the combinations considered and the greatest part of the change from initial to steady energy rate conditions occurred within about 3.05mm. of piston stroke. It is thus clear that even for comparatively small castings the total energy input would not be

significantly different from the input for completely steady flow conditions. However where initial and steady state energy rates differ significantly, that difference might contribute to the production of a defective casting. viz.

a) $N_{e_{\text{initial}}} \ll N_{e_{\text{steady}}}$

Where the initial energy rate is significantly less than the steady value there is the possibility that premature solidification may occur due to the lower piston velocity and consequent increased heat loss from the incoming metal. This could lead to defective castings.

b) $N_{e_{\text{initial}}} \gg N_{e_{\text{steady}}}$

Where initial energy rates are very high there is a distinct possibility that this could lead to mould damage, consequently reflected in the castings produced in the mould. It has been demonstrated ⁽³⁴⁾ that mould erosion in the pressure casting of zinc alloys is principally due to the phenomena of cavitation taking place in the metal stream during mould filling. It has been the author's experience in a foundry producing both zinc and aluminium pressure castings that whilst cavitation erosion is a common experience in the moulds used for zinc it is non-existent in those used for the production of aluminium castings. Further, where erosion occurred in a zinc casting mould, the only attempt which could be made to alleviate the condition was by reducing the net drive force. More often than not the reduction would have little effect upon erosion rates but significant

heat loss problems could well occur due to the lowering of injection velocities. Now zinc casting practice uses thin gates (average thickness .635mm.) whilst aluminium practice is to use comparatively thick gates (average thickness 3.175mm.). Also hot chamber machines are commonly pneumatically operated and cold chamber machines commonly hydraulically operated. Thus the alloy/gate size/machine type involved in zinc casting (potentially) involves very high initial energy rates and severe transition conditions, whereas for aluminium this would be considerably less so. It may well be that the cavitation phenomena in zinc pressure casting arises largely as a result of high initial energy rate and exists largely during the transition period. Clearly this would have to be confirmed experimentally but it is instructive to examine the energy rate applicable for aluminium and for zinc alloys casting with the same gate size. To illustrate this point calculations of energy rates were made for zinc casting under conditions listed in the table below and compared with those for aluminium casting under identical conditions.

MACHINE No.	CHANGE OVER POS ⁿ (m.m. OF PISTON STROKE)	GATE SIZE (m.m.)
1A	61.00	.762x68.25
5	61.00	.762x68.25

The results of the comparison are shown in figures 49 and 50.

Figure 49 (Machine 1A). Both initial and steady energy rates are low on this (high resistance factor) machine. There is a factor of difference of approximately 2.5 between the initial energy rates for zinc and aluminium reducing to approximately 1 under steady conditions. The almost identical energy input under steady conditions arises simply because the very high machine resistance factor reduces to relative insignificance the differences in metal system resistance factor for the two casting alloys. The ratio of difference between initial and steady conditions is 5.56 for zinc and 2.3 for aluminium.

Figure 49 (Machine 5). Energy rates are high on this (low resistance factor) machine. The factor of difference between zinc and aluminium is 1.5 reducing to .67. The ratio of difference between initial and steady conditions is 102.5 for zinc and 43 for aluminium. It is an interesting point that after the transition stage the steady state energy input is greater for aluminium than for zinc. This arises of course because the lower metal system resistance factor (in aluminium casting) gives a higher steady state piston velocity than zinc. One might be tempted to argue that this supports the theory of cavitation as a transition phenomena. However it must be remembered that the gate size used in the calculations is below conventional aluminium gating practice.

Figure 50 shows the variation of initial energy rate and injection velocity with reducing net drive force Q . The piston velocities for casting zinc and aluminium drop by 25%

for a drop of 40% in net drive force. Over the same range the initial energy rate for zinc drops by 50% whilst for aluminium the drop is rather greater at 68%. Thus not only does aluminium cast under identical conditions absorb significantly less energy than zinc initially, the rate reduces more quickly with reducing drive pressure.

Summarising the information gained from the curves it is evident that enormous changes in energy rate input can take place in the initial stages of filling a cavity. The order of difference between initial and steady energy rate values depends, for a given net drive force, upon

- (i) changeover position
- (ii) machine resistance and inertial factors
- (iii) gate resistance and inertial factors

The influence of changeover position depends upon the degree of its displacement from the nodal position of the machine/gate combination considered. Where changeover position is chosen to coincide with the nodal position, (i.e. the point on the piston velocity curve where the velocity coincides with the steady state value for the machine/gate combination), initial and steady energy rates are identical. Where displacement exists the order of difference will depend upon the resistance and inertial factors for the machine/gate combination considered. When a machine has a very high resistance factor (e.g. m/c^2) the energy input rates both initial and steady over a relatively broad range of gate size are limited. In conditions of low machine resistance there can be an

enormous variation over a small range of gate size.

The steady state energy curves all had a point of inflection corresponding to maximum energy rate input. The gate size at which this occurs is predictable from the equation of section 3.2.

In terms of total energy, high or low rates of energy input initially do not significantly influence total energy input to a cavity for other than very small castings. However there are grounds for suggesting that very high or very low rates of energy input contribute materially to the incidence of defects in the resulting castings.

This section demonstrates the factors influencing initial energy rate magnitudes and in so doing indicates how they might be brought into line with steady state conditions. Further, the section analysis allows machines and moulds to be matched for optimum (steady flow) rates of energy input to a cavity.

5.2. STATE OF FLOW CALCULATIONS

In section (3.3) the (dimensionless) Weber number has been advanced as a possible index of state of flow in casting gating systems. In the absence of experimentally derived information it is not as yet possible to specify limiting values of Weber number for spray or for solid front filling. However it is possible to examine machine/mould influence upon these (numbers) and to isolate the factors of greatest significance. A range of machine/mould combinations are considered for this purpose. Flow conditions are examined

in connection with the same range of gate size and machine.
The details are as follows:

Machines

MACHINE No.	RESISTANCE FACTOR $\text{N} \cdot \text{sec}^{-2} \cdot \text{m}^{-2}$	INERTIAL FACTOR $\text{N} \cdot \text{sec}^{-2} \cdot \text{m}^{-1}$
1A	4000	200
2	28000	460
5	140	45

(Net drive force for all machines 54,290 N)

Gate dimensions

GATE AREA m.m.	MEAN HYDRAULIC DIA. m.m.	RESISTANCE FACTOR	
		ALUMINIUM	ZINC
f/4 .203x68.25	.406	82500	198144
f/2 .381x68.25	.760	20600	49536
f .762x68.25	1.507	5160	12384
2f 1.524x68.25	2.982	1280	3072
4f 3.050x68.25	5.841	322	768

Changeover settings

15.25 m.m.

61.00 m.m.

122.00 m.m.

Material properties

DENSITY (Kg/m ³)		SURFACE TENSION N/M	
ZINC	ALUMINIUM	ZINC	ALUMINIUM
7200	2712	.831	.905

Figures 51-53 show the variation of initial and steady flow Weber numbers for the range considered and figure 54 the ratios of Weber number for the three machines.

Figures 51-53

Comparing first the ratio of Weber numbers for zinc and aluminium in equivalent machine/mould conditions it may be seen that the ratio between the two lies somewhere between 1.1 and 2.62 for any combination. These spectrum limits may be readily deduced from a consideration of the dimensions of the Weber number equation

$$W_e = \frac{\rho \cdot V_g^2 \cdot d}{T}$$

$$\frac{\rho_{\text{zinc}}}{\rho_{\text{al}}} \cdot \frac{T_{\text{al}}}{T_{\text{zinc}}} = 2.62$$

$$\left[\frac{V_{g_{\text{zinc}}}}{V_{g_{\text{al}}}} \right]^2 = \frac{C_1 + Y \cdot \rho_{\text{al}}}{C_1 + Y \cdot \rho_{\text{zinc}}}, \quad Y = \frac{1}{2} \cdot \frac{f_o^3}{f^2} \cdot (1 + K_m)$$

$$= 1 \quad \text{for} \quad C_1 \gg Y \cdot \rho$$

$$= 1/2.4 \quad \text{for} \quad C_1 \ll Y \cdot \rho$$

Thus in conditions of high machine resistance factor relative to a given gate size

$$\frac{W_{e_{zinc}}}{W_{e_{al}}} \rightarrow 2.62$$

In conditions of low machine resistance factor relative to a given gate size

$$\frac{W_{e_{zinc}}}{W_{e_{al}}} \rightarrow \frac{2.62}{2.4} \rightarrow 1.1$$

Machine 2 has a high machine resistance factor relative to the larger gate sizes. Consequently the Weber number ratio is about 1.1 at the lower end of the gate size range but increases rapidly to approximately 2.6 as gate size is increased. Machine 5 has a very low machine resistance factor and consequently the ratio remains around 1.1/1.3 throughout the range considered. Machine 1A behaves similarly to machine 2.

The highest value of Weber number for steady flow conditions and the gate size at which it is attainable for a given machine are predictable from the equations of section (3.3). As may be seen from equation (23) the gate size for maximum Weber number is density dependent. Consequently the gate sizes for maximum W_e do not coincide (see steady state curves).

One of the more significant features displayed by the graphs lies in the magnitude of W_e attained in the different machine conditions. Steady state values are of similar order for all three machines at the smaller end of the gate size range although the difference increased at the larger gate sizes. Clearly, where the gate resistance is such that $C_{m_3} \gg C_1$ then steady state gate velocity and hence W_e is

controlled by the gate resistance factor and the machine type is of least significance. As gate size is increased such that $C_{m_3} \ll C_1$ the machine resistance factor determines the value. Within the gate spectrum which this occurs a peak value of W_e is attained. This is true for machines 1A and 2 for the gate spectrum considered. In machine 5 the resistance factor of the largest gate considered is still significant relative to that of the machine. Consequently the steady state curve continues to rise (peaking at values of 6f for zinc and 9f for aluminium). The biggest variation occurs in initial Weber numbers at gate entry. Fig. (54) gives an indication of the factor relationships for initial and steady Weber numbers for the machine/gate combinations. The table below lists these factors for machines 2 and 5.

GATE SIZE (ins)		$W_{e\text{ initial}}/W_{e\text{ steady}}$ (identical for Zn and Al)	
		Machine 2	Machine 5
f/4	.203x68.25	3.96	346
f/2	.381x68.25	1.78	80
f	.762x68.25	1.12	19.6
2f	1.524x68.25	1.0	5.4
4f	3.050x68.25	1.0	1.7

As can be seen from fig (51) and the above table the limited spectrum of 'free piston' velocity on high resistance factor machines (generally hydraulic e.g. m/c 2) limit also the magnitude of variation of the Weber number ratio. The

variation for low resistance factor machines (generally pneumatic, e.g. machine 5) reflects the much larger 'free piston' velocity spectrum (note, the duration of the transition period depends upon the individual system resistance/inertial factor ratios, see section (4.2)).

Zinc gating practice operates generally in the gate size spectrum $\frac{f}{4}$ - f and zinc pressure casting machines are generally pneumatically operated. Aluminium gating practice on the other hand operates in the size spectrum $2f+$ and aluminium casting is generally carried out using hydraulic machines. In practical terms therefore the higher Weber numbers and ratios are more likely to be experienced in zinc pressure casting than in aluminium. This coincides with the author's own experience that evidence of significant breakdown of flow in spray terms is more readily available in zinc than in aluminium pressure castings.

Summarising the information it is clear that, as for energy considerations, relative size of resistance factors for machine types and gates, changeover position and net drive force determine the magnitude of initial and steady flow Weber numbers and the difference between them. The smallest variations will occur on machines of high resistance factor used in conjunction with low resistance factor gates (generally the case in aluminium casting). The bigger variations will occur in machines of low resistance factor used in conjunction with high resistance factor gates.

Without experimental knowledge of the relationship between Weber number and flow breakdown in the casting

environment it is not yet possible to quantify the necessary machine/gate conditions for either spray filling or for solid front filling of a cavity. However the information gained from this section allows speculation. The differing theses behind the practice of spray filling or of solid front filling are such that flow conditions in which both types of flow occur are not likely to be conducive to good casting results. Conditions such as occur with machine 5 might well fall into this category. For this machine at the smallest gate size considered there is a factor difference of 346 between initial and steady flow Weber number. It would seem entirely possible under these conditions for Weber numbers to be attained initially at which flow breakdown occurs, rapidly reducing to solid flow as steady conditions are attained.

Thus the ideal filling conditions from the point of view of control of flow state is likely to be where the changeover i.e. fill initiation position is at the nodal point on the 'free running' piston velocity curve for the machine/gate combination. By adjusting net drive force and selecting an appropriate gate size for either a maximum or a minimal Weber number value conditions of complete spray or complete solid front filling will be most nearly approached. Spray filling will require higher values of Weber number than solid front filling. Fig. (54) indicates that these are most likely to be attained upon low resistance factor (generally pneumatic) machine albeit at the larger end of the gate size spectrum. When gate size is limited to the lower end of the range by casting or finishing consideration there is little or nothing to choose between any of the machine types considered in the study.

6. APPLICATION OF FLOW RATE ANALYSIS TO EXPERIMENTAL
DIECASTING MACHINE AND COMPARISON WITH EXPERIMENTATION

PREAMBLE

Validation experiments were carried out using an experimental mould mounted upon an E.M.B.10 pneumatically operated hot chamber diecasting machine. The experimental mould contained a 76.2mm x 76.2mm. x 6.35mm. cavity having overflows situated about the periphery (see fig. 55). The cavity was not vented i.e. zero venting conditions prevail during casting. Initially the gate size through which the cavity was fed was nominally 25.4mm. x .635 mm. but was modified to 25.4mm. x 2.54mm. (nom.) in the latter part of the test series.

The tests themselves were conducted in two parts. In the initial series the tests were conducted to determine loss factors for the injection system of the diecasting machine, and for that section of the metal system (gooseneck and nozzle) built into the machine, which could not otherwise be established with any accuracy. In the second part of the examination the velocity and pressure characteristics under casting conditions were* measured for the machine/mould combination, for comparison with computed curves (* see equipment section 8 for details of instrumentation).

In the casting series the alloy used was MAZAK 3 zinc alloy and castings were produced using a nom. 25.4mm. x .635mm.

gate and then using a 25.4mm. x 2.54 mm. nom. gate for comparison.

The test procedure was standardized as follows: The mould was heated until monitoring thermocouples placed in it indicated a temperature which preliminary experimentation showed to be the minimum at which castings could be produced without sticking. Sample castings were then produced at that temperature for a range of injection pressure. The castings so produced showed considerable cold finish defects (see figs. 71-3). The vestigial record that these (defects) represented of the original mould filling pattern was examined as a tentative means of assessing energy and breakdown effects.

6.1. DETERMINATION OF MACHINE RESISTANCE AND INERTIA FACTORS.

Injection System Layout

Fig. (56) shows diagrammatically the layout of the injection cylinder. The air inlet port to the injection drive side was situated in a chamber at the top of the cylinder. In the fully withdrawn position the top of the air piston enters this chamber partly blocking off the inlet port. On initiation of the injection stroke, air entering the cylinder seeps past the piston into the upper chamber pressurizing part of the top surface of the piston and forcing it down. As more of the inlet port is revealed the resistance to air flow drops and piston speed slowly increases until after piston movement ' x_1 ' the inlet port is completely clear and the piston itself clears the upper chamber so that the air pressure comes onto the whole of the top surface of the piston driving it down with maximum effect. This damper effect is necessary to ensure that the 'metal' piston has moved past the filler holes in

the gooseneck before rapid movement is initiated. This avoids splashback of liquid metal into the pot (see fig. 57 for overall layout of system). Another damper effect is built into the cylinder to cushion the end of the piston stroke. Towards the termination of the stroke the skirt of the piston cuts off the exhaust exit and enters an annular space at the base of the cylinder. The air thus trapped in this space is progressively compressed and acts as a cushion slowing down the piston movement and preventing impact damage at the end of the stroke. This damping effect takes place over the last part of the stroke equivalent to length 'B'. On the drive side of the piston the resistance to air flow arises due to wall friction in the pipe to the reservoir (4.58m. long, 4.13 cms. diameter) and the various obstacles to air flow (eight right angle bends, one gate valve, one shuttle valve, one moisture trap). On the exhaust side similar resistances to flow occur (3.1 m. pipe length, four right angle bends, one gate valve, one shuttle valve, one moisture trap).

Injection System Inertial Factor (a_1)

The quantitative definition of inertial factor a_1 for the injection system is quoted in table 2. By using this equation the inertial factor for the EMB 10 was calculated to be $7.3 \text{ (N.sec}^2.\text{m}^{-1}\text{)}$.

Injection System Resistance Factor (C_1) (see table 2)

Most of the terms comprising the resistance factor are easily defined quantitatively e.g. drive fluid density, areas of pistons, pipes, etc. The term which presents the most

difficulty is that defining the magnitude of losses in the drive and exhaust system (K_D , K_E in the equation). The following table represents an estimate based on published information.⁽³⁵⁻³⁷⁾

LOSS SOURCE	EMB	10
	K_D	K_E
PIPE WALL FRICTION ($=\frac{4f\ell}{d}$, $f=.016*\text{SACHS}$)	7.1	4.7
RIGHT ANGLE BEND ($K=1.0$)	8.0	4.0
GATE VALVE (OPEN)	.2	.2
SHUTTLE VALVE	2.0-10.0	2.0-10.0
MOISTURE TRAP	10.0-100.0	10.0-100.0
TOTAL	27 - 125	21 - 119

Using the bottom values from the range i.e. $K_D=27$, $K_E=21$ yields a value of $C_1 = 450$. Using the upper range yields a value of $C_1 = 2155$. Clearly this is not adequate for a proper comparison. The relationship between piston velocity and resistance factor for steady conditions is expressed by the equation

$$V = \sqrt{\frac{Q}{C_1}} \quad Q = \text{net drive force}$$

It was decided therefore to run the diecasting machine with the metal piston disconnected (free running mode) to ascertain whether steady running conditions were attained running the air cylinder alone. If this were so then by measuring the

piston velocity and net drive force the value of C_1 could be obtained experimentally.

The diecasting machine was set up (i.e. heated) for normal running conditions, with the metal piston disconnected so that the 'free running' characteristic could be examined. The machine was cycled at different pressures and the velocity characteristics recorded (see section 8 for instrumentation details). A typical characteristic is shown in fig. (58).

There were clearly three phases of motion

- i. movement under the effect of the initial damper
- ii. running under full pressure
- iii. slowing down under the influence of the air cushion

In the middle phase of the piston movement a clear plateau i.e. steady velocity conditions, was evident.

From plateau measurements at three pressure settings the following values of C_1 were obtained

RESERVOIR PRESSURE (N/m^2)	Q (N)	STEADY PISTON VELOCITY (M.P.S.)	C_1 ($\text{N} \cdot \text{sec}^2 \cdot \text{m}^{-2}$)
540,000	9942	3.23	954
700,000	12962	3.73	934
880,000	16232	4.31	876
AVERAGE VALUE			= 922

This value of C_1 corresponds to a combined value ($K_D + K_E$) lying approximately in the middle of the calculated range.

6.2. DETERMINATION OF METAL SYSTEM RESISTANCE AND INERTIAL FACTORS.

Metal System Layout

The EMB 10 used in the experimentation is a hot chamber machine and the diagrammatic layout of the metal system is shown in fig. (57). The metal system has two distinct sections

- (i) The gooseneck and nozzle which are part of the diecasting machine.
- (ii) The runner/gate/cavity system in the diecasting mould.

The former is a constant factor in all metal systems formed by the addition of a diecast mould to the machine and thus makes a constant contribution to the metal system resistance factor. The latter varies according to tooling configuration and determines the terminal value of the metal system resistance factor (C_{m_3}).

Metal System Inertia Factor a_{m_3} (see table 2).

The metal system inertia factor was found to average 1.24. ($N \cdot sec.^2 \cdot m^{-1}$)

Metal System Resistance Factor C_{m_3} (see table 2)

This factor comprises the combined resistance factors of the fixed element of the metal system (gooseneck/nozzle) and the variable element (gating/cavity) and these were determined separately.

Gooseneck/nozzle resistance factor (C_{m_3A})

A similar problem exists in determining the resistance factor for the gooseneck/nozzle element of the metal system as had been the case for the injection system and it was decided to determine this factor experimentally.

If during the movement of metal in the metal system due to piston displacement from position $x = x_1$ to $x = x_2$ (see fig. 57) a velocity plateau occurs (i.e. steady flow conditions) the piston velocity equation will reduce to

$$V = \sqrt{\frac{Q}{C_1 + C_{m_3A}}}$$

Q = net drive force

C_1 = injection system
resistance factor

C_{m_3A} = metal system resistance
factor for nozzle and
gooseneck

The diecasting machine was set up with the experimental mould mounted on it (normal gate size 25.4mm.x.635mm. see fig. (55)). Castings were produced at different (reservoir) pressure settings and recordings made of the injection characteristics. A typical recording is shown in fig (59). There were again three phases to the characteristic

- i. movement under damper action
- ii. piston movement under full pressure forcing metal through gooseneck and nozzle to the mould entrance
- iii. mould filling

In the middle phase of piston movement there was again a steady velocity condition. Plateau measurements were taken

from recordings of casting taken at three different (reservoir) pressures. The following values of C_{m_3A} were obtained using a value of $C_1 = 922$

RESERVOIR PRESS N/m ²	Q N	V m/sec	C_{m_3A} N.sec ² m ⁻²
524,000	9693	1.405	4022
731,000	13465	1.622	4253
945,000	17366	1.811	4387
AVERAGE VALUE			4219

Runner/gate resistance factor (C_{m_3B})

Using the loss coefficient equation developed in section 9.3

$$K_m = \left[K_d \left(1 - \frac{f_N}{f_a}\right)^2 \cdot \left[\frac{f_R}{f_N}\right]^2 + 0.85(1+K_c) \right] \left[\frac{f}{f_R}\right]^2 + 1.6K_{cg} \cdot \sin(R-2\theta)$$

(see 9.3. for defn. of terms)

[Note K_m is the system loss coefficient referred to gate velocity]

Values of K_m were calculated for the two gate sizes (see 9.6 for details)

Using table 2, $C_{m_3B} = \frac{\gamma_m}{2g} \cdot \frac{f_o^3}{f^2} \cdot (1+K_m)$

Note: γ_m = metal density
 f_o = piston area
 f = gate area

Substitution into this equation yielded the following

25.4 mmx.635mm. nominal gate (actual size 25.4mm.x.584mm.)

$$K_m = .546$$

$$C_{m_3B} = 89000$$

25.4mm.x2.54mm. nominal gate (actual size 23.62mm.x2.36mm.)

$$K_m = 1.61$$

$$C_{m_3B} = 10848$$

SUMMARY OF RESISTANCE AND INERTIA FACTORS AND EQUATIONS USED

The equations of table 2 were used to describe piston movements , cavity filling time and energy input.

"Free running" tests

Stage 1 equations were used to describe the period of damper control. These equations are based on the assumption that the resistance factor varies as $C_1 \cdot \frac{x}{x_1}$ to take account of post clearance effect

$$C_1 = 922 \quad a_1 = 7.3 \quad x_1 = 18.3 \text{ mm.}$$

Stage 2 equations were used to describe the middle phase of piston movement

$$C_1 = 922 \quad a_1 = 7.3 \quad x_2 = 152.5 \text{ mm.}$$

No attempt was made to describe the air cushion effect toward the end of the stroke since this should not normally come within the normal range of casting stroke.

Casting tests.

Stage 1 equations were again used to describe the period of damper control. Metal resistance during this period will be negligible and conditions will be the same as for free

running.

$$C_1 = 922 \qquad a_1 = 7.3 \qquad x_1 = 18.3 \text{ mm.}$$

Stage 2 equations were used to describe the stage of piston movement during which metal is forced through gooseneck and nozzle to the sprue. The resistance and inertial factors are thus a combination of those for the injection system and the gooseneck/nozzle portion of the metal system.

$$\begin{aligned} C_1 &= 922 + C_{m_3A} & a_1 &= 0.5 + a_{m_3} & x_2 &= 45.75 \text{ mm.} \\ &= 5136 & &= 8.54 \end{aligned}$$

x_2 represents the piston position at which the molten metal front has reached the sprue position in the metal system.

Stage 3 equations were used to describe the cavity filling stage

Nom. gate size 25.4 mm. x .635mm.

$$\begin{aligned} C_3 &= C_1 + C_{m_3A} + C_{m_3B} & a_3 &= a_1 & x_3 &= 85.4 \text{ mm.} \\ &= 94,224 & &= 8.54 \end{aligned}$$

Nom. gate size 25.4mm. x 2.54 mm.

$$\begin{aligned} C_3 &= C_1 + C_{m_3A} + C_{m_3B} & a_3 &= a_1 & x_3 &= 85.4 \text{ mm.} \\ &= 15960 & &= 8.54 \end{aligned}$$

The stage 3 calculations were carried out for both optimum and zero vent conditions.

The analysis for energy and stream breakdown curves was taken from sections (3.2) and (3.3).

6.3 COMPARISON OF CALCULATION AND EXPERIMENTAL RESULTS

VELOCITY CHARACTERISTICS

(i) 'Free running' curves. In the initial tryout the fit between calculation and measurement was very poor over the first (damper) portion of the piston movement. The basis of this analytical stage was that the effective resistance factor would vary as $C_1 \cdot \frac{x}{x_1}$.

Clearly this conception did not fit the machine conditions. Since the differences were essentially of scale the analysis was repeated on the assumption that the resistance factor would vary as the inlet port was cleared as $|n \cdot C_1 \cdot \frac{x_1}{x}|$. The value of n for the machine condition was estimated to be 40. Comparison between calculation and measured curves using the assumption was good over the relevant portion of piston stroke. No attempt was made to replicate the air cushion effect occurring towards the end of the piston stroke. Figure (60) is representative of the results obtained at various reservoir pressures.

(ii) Casting conditions

a) Using a 25.4mm.x .635mm. (nom.) gate.

Figure (61) compares calculated and experimental curves for three reservoir pressure settings. The calculated curves for zero and for optimum vent conditions are superimposed on each other. The measured piston movement terminated at all three pressure settings well before the theoretical termination point for optimum and even zero vent conditions. In this test

series the overflows did not generally fill and this largely accounts for the discrepancy (this point will be discussed in conjunction with the results of tests on the 25.4mm.x2.54mm. nom. gate and also in the section on energy conditions).

b) Using a 25.4mm.x2.54mm. gate. (Fig. 62)

The overall fit is good and the terminal stages of (measured) piston movement corresponds fairly closely with the calculation based on zero venting conditions. In this test series both casting and overflows filled completely at all test pressures.

The following table compares gate velocities and filling time at three reservoir pressures for the two gate sizes.

RESERVOIR GAUGE PRESSURE N/m ²	GATE VELOCITY(M.P.S)		CAVITY FILL TIME SECS	
	25.4mm. GATE x2.54mm	25.4mm.GATE x.635mm.	25.4mm.GATE x2.54mm.	25.4mm.GATE x.635mm.
524,000	18.56	31.88	.033	.078
703,000	25.54	38.31	.024	.065
945,000	27.55	45.05	.022	.055

It can be seen that, although gate velocities are significantly higher for the smaller gate at all pressures the filling times are significantly lower. Indeed it takes nearly 70% longer to fill the cavity at the highest pressure setting for the smaller gate even when compared with the filling time for the larger

gate at the lower pressure setting. The reason for the premature freezing off during casting with the smaller gate is thus abundantly clear. This feature will be discussed further in the section dealing with energy and breakdown conditions. The tests for the 25.4mm.x.635mm. gate were repeated with the mould temperature raised to a significantly higher level. The castings so produced all had completely filled overflows. The curve fit for this condition was as good as for the larger gate.

Finally fig. (63) is a composite figure for a nominal injection pressure of 703,000 N/m² comparing measurement and calculation for zero vent conditions. It is interesting to compare this with the equivalent idealized curves of section (4).

Filling time and pressure

Figures (64) and (65) compare calculation and measurement of elapsed time, and drive cylinder pressure respectively for the 25.4mm.x.635mm. (nominal) gate test. The curves were plotted on the basis of information derived from the last test series using this gate, i.e. at the higher mould temperature. The elapsed time curves show excellent agreement, the pressure curves less so. (This was also the case for the 25.4mm.x2.54mm. (nominal) gate tests). Further tests indicated that the discrepancy in the pressure curves could be accounted for. The pressure transducer was located in the upper (damper) chamber of the drive cylinder, this being the only reasonably accessible position. Tests showed that at other than low rates of piston movement the pressure in the region sensed by the pressure

transducer did not correspond to the mean piston pressure.

6.4. CONCLUSIONS

To apply the flow rate analysis to diecasting machines it is necessary to derive both machine system loss factor, and the loss factor for the fixed element of the metal system, experimentally. (Note: In the case of the latter it is possible that the value thus obtained (6.2.) actually represents the combined influence of actual loss factor and metal piston friction i.e.

$$C_{m_3A}(\text{calc}) = C_{m_3A}(\text{Act}) + \frac{F}{V^2}, \quad \begin{array}{l} F = \text{friction} \\ \text{force} \\ V = \text{piston} \\ \text{velocity} \end{array}$$

However this is not important since the magnitude of $C_{m_3A}(\text{calc})$ accurately represents the influence if not the specific source of resistance effect from the fixed element). The technique for measurement is described in 6.1, 6.2. The loss coefficient equation developed in 9.3. gave good agreement with experimentally derived values.

The test castings were produced under zero venting conditions and the experimentally derived curves of piston velocity etc. agreed closely * with calculation. (* Also, in a paper by Luis and Draper⁽³⁸⁾, the authors included sufficient information on their hydraulically actuated die-casting machine for the analysis to be applied. Again good agreement was obtained).

It is concluded that the analysis of section 3.1. is soundly based. Further, the information requirements for the application of such analysis should, in the case of the machine element be derived as described in 6.1. and 6.2. The relevant information for the runner/gate system is capable of estimation from 9.3. Thus, having obtained the necessary information for a given machine it is possible in flow rate terms to predict the performance of a given runner/gate system placed on the machine.

7. APPLICATION OF ENERGY RATE AND FLOW STATE ANALYSIS TO EXPERIMENTAL MACHINE/MOULD COMBINATION.

7.1. ENERGY RATE

Energy rate curves were calculated on the basis of the information generated in section 6. The results are shown in fig. (66). Since the value of Q (net drive force) does not influence the optimum gate size the points of flexure on the various curves coincide for all three pressure settings. The optimum gate sizes are given in the table below.

	N_e	N_{eg}	K.E.
f_{opt}	not reached		
	$B\bar{A} > C_1$ (9000) (922)	.965mm. x25.4mm.	1.600mm. x25.4mm.

The experimental gate sizes were nominally 25.4mm. x .635mm. and 25.4mm. x 2.54 mm. The calculated rates of energy consumption are shown below.

Injection pressure N/m ²	Energy rates N.m./sec					
	N_e 25.4mm.x 2.54mm.	N_e 25.4mm.x .635mm.	N_{eg} 25.4mm.x 2.54mm.	N_{eg} 25.4mm.x .635mm.	K.E. 25.4mm.x .2.54mm.	K.E. 25.4mm.x .635mm.
524,000	7171	3033	0	849	2129	1734
703,000	11149	4717	0	1320	3308	2695
945,000	17355	7342	0	2054	5150	4196

Since the 25.4mm. x 2.54mm. gate is the same size as the runner there is no loss at the gate entrance and hence no energy dissipation rate (N_{eg}). The rate of energy dissipation at the nominal 25.4mm. x .635mm. gate is about 28% of the total energy input rate. In terms of kinetic energy the rate of input for the nominal 25.4mm. x .635mm. gate is just over 80% that of the nominal 25.4mm. x 2.54mm. gate. However the total energy input to the cavity during filling is considerably greater. The reason for this is that the overall cavity filling time for the smaller gate is significantly larger(fig.67).

In view of this it is interesting to consider the castings produced during experimentation with these two gate sizes. All castings produced using the nominal 25.4mm. x 2.54mm. gate were complete. That is to say that the overflow wells filled completely, as exemplified by fig. (68a), at all injection pressures (524,000, 703,000, 945,000 N/m²). The overflow wells did not generally fill using the nominal 25.4mm. x .635mm. gate even at the highest injection pressure (fig. 68b). In assessing this situation it must be concluded that the problem does not lie in differences in K.E. rate. After all the K.E. rate at 524,000 N/m² for the nominal 25.4mm. x 2.54mm. gate was considerably less than that at 945,000 N/m² for the 25.4mm. x .635mm. gate. Yet under the former conditions the casting and overflow filled completely whilst under the latter the overflows generally did not. The major determinant of this difference must lie in the difference in thermal condition of the metal entering the cavity. In the transmission of liquid metal from the hot chamber to the cavity, heat loss is greatest when the 25.4mm. x .635mm. gate is employed since transmission

times are longer and there is less general frictional reheat (see table) to compensate. Clearly the frictional reheat at the gate itself is not sufficient to compensate for this.

The tests from which the sample castings were obtained were carried out with the general mould temperature as low as possible consistent with successful ejection of the casting. This condition was set for two reasons

- i. To assess cavity resistance during filling under maximum heat loss conditions.
- ii. In order that the resulting 'cold finish' on the castings so produced would preserve a vestigial record of the filling pattern and state of metal flow.

In later tests the mould temperature was raised to normal running levels. Castings produced using the nominal 25.4mm. x .635mm. gate filled completely including overflow wells, supporting the conclusions drawn in the previous paragraph.

Two conclusions may therefore be drawn from this limited experimentation.

- a) Gate frictional reheating will not compensate for heat loss during the long transmission times associated with small gate sizes.
- b) The quantity of energy required to fill a cavity completely varies according to the condition of the casting metal. Thus the benefits of gate selection for optimum K.E. rates will only be fully realised when casting is carried out under conditions of consistent temperature control at an appropriate temperature level.

Using the experimental mould/machine layout as a model calculations were performed to illustrate one or two of the points raised in the energy analysis, based on the injection pressure of 52400 N/m^2 . Fig. (69) shows curves for total energy input based on changes in metal piston size (f_o) and on runner size (f_R). It can be seen that the curve peaks will occur within the machine range when $\bar{A}B \neq C_1$ and that the magnitude of these peaks will be the same. It is interesting to note that raising the value of f_R from $25.4\text{mm.} \times 2.54\text{mm.}$ to $25.4\text{mm.} \times 10.2 \text{ mm.}$ places the peak K.E. rate at the nominal $25.4\text{mm.} \times .635 \text{ mm.}$ gate size. It would have been interesting to check whether the increased energy rate would in practice have enabled complete castings to be produced. Unfortunately the dimensional adjustments of sprue, nozzle and gooseneck necessary to maintain efficiency relationships were not feasible.

7.2. FLOW STATE

Curves of W_e vs gate size were plotted for the experimental machine/mould configuration and are illustrated in fig. (70). Since Q does not affect the F -value at which the maximum point of inflection occurs the gate size for maximum W_e is the same for all three injection pressure levels i.e.

$$f_{\text{opt}} = 25.4\text{mm.} \times 2.00 \text{ mm.}$$

To properly assess breakdown phenomena requires the direct visual examination of metal flow through the gate or of an analogue fluid through a dimensionally similar system.

As far as analogue systems are concerned this point is discussed in sections 10 and 11. However, for the actual casting metal, in the absence of a specialised rig this is not currently possible. The only means of assessment of flow state available from the casting environment was by means of a visual/x-ray assessment of the vestigial record preserved in the 'cold finish' castings produced in the early test series. The problem with this approach is that the casting is a summation of both fluid flow and of thermal influences. The surface texture of the casting for example is not only a vestigial indication of flow pattern but also of the degree of coalescence achieved. Thus apparent evidence of mixed solid/spray type flow conditions may be as much an indicator of variable rates of coalescence. Bearing this stricture in mind, and in the absence of any other direct means of examination in situ, representative castings were selected from the test series for X-ray and visual examination. Samples were examined from those produced at :

- (i) 945,000 N/m² injection pressure using the feeder gate of nominal size 25.4mm. x .635mm. (identifying symbol for sample: H)
- (ii) 524,000 N/m² injection pressure using the feeder gate of nominal size 25.4mm. x 2.54mm. (identifying symbol for sample : A)
- (iii) 945,000 N/m² injection pressure using the feeder gate of nominal size 25.4mm. x 2.54mm. (identifying symbol for sample: D).

As may be seen from fig. (70) the value of W_e casting into the 25.4mm. x .635mm. gate at 945000 N/m² is close to that obtaining whilst casting at 524000 N/m² into the 25.4mm. x 2.54mm gate. Thus (i) and (ii) enable comparison to be made of castings produced at essentially the same values of W_e but at different pressures and gate sizes. Castings produced at 945000 N/m² using the 25.4mm. x 2.54 mm. gate ((iii)) had the highest N_e and W_e values and were included for this reason. The values of energy rate and W_e value at which these castings were produced are shown in the table below.

Sample	K.E. N.m./sec	N_{eg} N.m./sec	W_e (dimensionless)
H	2351	1151	18.8×10^3
A	2885	0	18.8×10^3
D	6985	0	34.0×10^3

For the purpose of identification the face of a sample casting coplanar with the top surface of the gate will be referred to as the front face. The appearance of the front face of all castings is exemplified by a central zone free from defects, indicating the general flow path of metal into the mould in contact with the mould surface. The opposite face of the casting will be referred to as the back face. Metal does not feed directly across the mould surface forming this face and as a consequence, in the 'cold finish' samples this surface of the casting shows considerable foliation.

Fig. (71) shows the front and fig. (72) the back faces of samples H and A whilst fig (73) shows the front and back views of sample D.

Samples H and A

As previously stated the kinetic energy levels are of similar order and the W_e numbers used as an index of flow state are almost identical. As far as can be judged visually the vestigial evidence of flow shows that breakdown occurs to about the same degree in both gates. It would appear that droplet size ranges are approximately the same with perhaps a slight bias in size distribution towards droplet diameters of a similar order to the gate thickness. This is most evident in fig. (72).

Sample D (compare with A)

The difference in the KE levels at which the samples were produced is clearly evident in the greater degree of droplet smearing that has taken place along the front face of D and in the greater level of coalescence. The distribution of droplet size appears to be about the same although a comparison of back face views would perhaps indicate a slight change in the bias of droplet size distribution in D toward the small end of the spectrum.

The x-ray pictures of the samples fig. (74) showed two categories of porosity

- a) Gross porosity contained in the centres of the two lobes of the original flow pattern filling the cavity in which the samples were produced.

b) Distributed microporosity.

The gross porosity arose to some extent due to the lack of venting and partly due to the introverted nature of the flow pattern. The gross porosity is less in sample H than in A or D due possibly to the avoidance of gas entrainment from the overflow wells. The extent and distribution of microporosity seems to be of similar order for all three samples although x-ray examination of ten castings from each of categories (i), (ii), (iii) seemed to indicate greater microporosity in those from category (iii).

7.3. CONCLUSION

The appraisal of energy rate influences and flow index using the experimental machine/mould set-up was limited in scope. Its utility lies in the number of points which it raises which are worthy of more detailed investigations. These are as follows:

Energy rate

- i. The use of energy rate indices for the determination of cavity filling may not necessarily guarantee successful filling even where optimum gate sizes are employed when significant imbalances in thermal conditions exist. This was clearly indicated in the tests in which the extended filling time for castings produced using the smaller gate led to premature freeze off of the overflow wells. This occurred despite higher rates of energy input in terms of $(N_{eg} + K.E.)$.

ii. Following from this it is clear that the benefits to be gained from gate frictional reheating are nullified by the increase in heat loss in the casting metal prior to reaching the cavity arising from the extension of filling time when using highly restrictive gates.

Flow state index.

iii. The information gained from the visual and x-ray examination of sample castings leads to the conclusion that equivalence of Weber number between gating systems indicates similar degrees of flow breakdown for flow into a cavity. It seems possible that the size of droplet bears some slight relationship with gate thickness (there is some support for this in the analogue studies of section (11)).

iv. There are indications that as Weber number increases for a given gating system any slight dependancy of droplet size upon gate thickness disappears.

PART 2

Part 2 comprises sections 8-12 inclusive. A (gate system) loss coefficient equation, necessary for the practical application of the analysis of Part 1, is developed. Water model studies are described which confirm published information used in the development of loss coefficient values. Further experimentation is reported which examines aspects of flow state in the gating system and cavity in the context of the predictions of analysis and experiment in Part 1.

The sections may be briefly summarized as follows:

- Section 8. describes the equipment used in experimental studies.
- Section 9. outlines the development of a loss coefficient equation for gating systems together with a comparison with published information.
- Section 10. reports an experimental investigation of gating efficiencies, essentially confirming published information used in 9.
- Section 11. examines flow state in a gate range, assessing the influence of gate geometry, and comparing the results with the analytical criteria.
- Section 12. outlines a pilot study of the influence of cavity geometry upon flow state and upon resistance to flow.

8. EXPERIMENTAL EQUIPMENT AND INSTRUMENTATION.

8.1. DIECASTING EQUIPMENT

8.1.1. Machine

The experimental machine used was a standard E.M.B. 10 pneumatically operated hot chamber type. It was equipped for fully automatic operation but in the test series was operated on a semi-automatic basis. A recirculating conveyor was used to return unwanted castings to the melting unit. The general arrangement of machine and instrumentation is shown in fig.(75).

8.1.2. Tooling

The experimental tooling was of unit die construction allowing various inserts to be used in a general bolster. Two sets were employed in the experimental work. One covered a 76.2mm.x76.2mm.x6.35mm. cavity with overflows and the other a 76.2mm.x76.2mm.x1.59mm. cavity without overflows. In the former two gate sizes were used nom. 25.4mm.x.635mm. and nom. 25.4mm. x2.54mm. whilst in the latter only the 25.4mm.x.635mm. gate size was tested.

The 76.2mm.x76.2mm.x6.35mm. insert set is shown in fig. (76). Neither set of inserts had vents cut into them so that all castings were produced under zero vent conditions.

8.1.3. Casting alloy.

The casting alloy used during the tests was MAZAK 3 zinc alloy to B.S. 1004A. The specification is as follows:

<u>Constituent</u>	<u>Percentage</u>
Al	4.1
Cu	1.0
Mn	.04
Fe	.75
Pb, C	.003
Sn	.001
Zn	remainder

8.2. FLOW MODEL EQUIPMENT

8.2.1. Flow Rig

A general view of the flow rig and instrumentation is shown in fig.(77). The rig was built by the firm of Joseph Lucas to simulate the injection system of a pneumatically operated diecasting machine. Basically the system is as follows. An eight inch diameter air cylinder with a six-inch stroke is fitted with a coupling and linked to a standard E.M.B. 10 plunger and sleeve, which in turn is linked to the model with a copper tube. The sleeve is fitted with a heater (not shown in fig. (77)) so that wax can be used as an analogue fluid if necessary. Air is supplied by a Worthington-Simpson compressor to the rig via an accumulator and filter. The rig is equipped to allow two stage injection to be studied. The slow stroke is obtained by using reduced air pressure, changeover being accomplished to full pressure as an arm on the piston trips a micro-switch to open the main air valve (which the reduced air supply bypasses). The original micro-switch arrangement devised by Joseph Lucas Ltd. was crude and difficult to set. This was replaced so that the trip

(* the rig did not provide a representative simulation of pneumatic injection systems and as a consequence placed a limit on certain aspects of the experimental work. This is discussed in 8.2.3.)

position could be set by micrometer, and was infinitely adjustable.

In the test series reported the analogue fluid used was water.

8.2.2. Tooling

The tooling used on the analogue rig consisted of runner plates and gates devised by Nussey⁽¹²⁾ and acquired through Joseph Lucas Ltd., who sponsored his work. The original die block used by Nussey was arranged to allow infinite cavity studies (i.e. injection into atmosphere) or closed cavity studies. Although perfectly satisfactory for the former it is quite impractical for the latter since the perspex plates used to form the closed cavity are far too thin and easily deform under pressure. A new die block having greater rigidity was built which utilized 50 mm. perspex blocks to form a closed cavity for filling studies. This is shown in fig. (78) together with samples of runner and gate plates. (Dimensional details of the runner and gate plates are given in fig. (89) section 9.4.) The new die block was also more flexible in the sense that as well as allowing cavity depth to be varied by spacer plates it also allowed gate position to be adjusted from a feed position symmetrically disposed between the cavity walls to one in which the feed position lay almost in the plane of one of the cavity surfaces.

8.2.3. Note on rig limitation

Two factors in the rig characteristics placed a limit on its use for validation of the analysis

- i. The resistance factor for the rig was abnormally high and the resistance factors for the available gate range were, with one exception, insignificant compared with this. It was impossible therefore to establish wide ranges of transition condition for the rig:gate combinations available.
- ii. The combination of a highly resistive drive system combined with a compressible drive fluid increased the effect of stiction in the system to a significant level. Fig. (79) illustrates the piston velocity characteristic with the 'metal' piston disconnected. The large initial velocity peak is the result of stiction combined with inadequate mean flow rates from the air reservoir. The effect also manifested itself at the changeover point where the two stage control system was used. Figs. (80) and (81) illustrate the comparison of analysis and measurement with and without two stage control.

It was not considered necessary to adapt the analysis to cope with these vagaries since practical experience with pneumatic diecasting machines did not show anything like that effect (see fig. (58) for the pneumatically operated E.M.B.10 used in the experimental work).

This meant however that the system was not satisfactory for a quantitative assessment of transition effects and the experimentation was confined to a largely subjective assessment of transition conditions for the experimental gating systems.

8.3. INSTRUMENTATION

8.3.1. Variables Examined

For reasons of economic and experimental convenience it was arranged that as much of the instrumentation as possible

was common to both diecasting machine and flow rig. The diecasting machine had extra instrumentation in the form of thermocouples and associated equipment but the pressure, displacement and velocity measuring equipment was common to both. The variables measured were as follows:

Diecasting machine (see fig. (75) for general view)

- Die temperature
- Metal temperature in the pot
- Piston displacement and velocity
- Drive and exhaust pressures in the pneumatic cylinder

Rig (see fig. (77) for general view)

- Piston displacement and velocity
- Drive and exhaust pressures in pneumatic cylinder
- Static pressure in the analogue fluid at the model entrance

8.3.2. Temperature measurement in die block

The thermocouples used were intended for monitoring and setting purposes and high response was not required. Mineral insulated BICC chromel-alumel thermocouples of .062" outer diameter were used (manufactured to B.S. 1827:1952). The signal from each thermocouple was passed to Fenlow amplifiers type AD103/3 and then to a recorder where the strengthened signal drove an SMI 'A' type galvanometer (see 8.3.5.).

One thermocouple was placed in the fixed and one in the moving half of the inserts. They were disposed at the centre of the 76.2mm.x76.2mm. walls to within 3.18mm. of the cavity surface. The thermocouples were inserted through holes

drilled from the back of the inserts and good thermal contact was obtained by setting the thermocouple tips in dental amalgam manufactured by Johnson-Mathey.

8.3.3. Pressure Measurement

14mm. Kistler piezo-electric type transducers having a range of $0-24 \times 10^6 \text{ N/m}^2$, (and a rise time of 10 μsec to maximum), were used. On the diecasting machine and on the rig, two such transducers recorded cylinder pressures whilst, additionally on the rig, one was used to detect mean static pressure in the analogue fluid at the entrance to the model. The signal from the transducer was taken to a Kistler charge amplifier and the strengthened signal used to drive an 'L' type galvanometer in the recorder. A resolution to .015 N is claimed by the manufacturer for the transducers. Calibration was carried out by means of an adapted Budenberg test gauge, gain factors being selected on the amplifier to give satisfactory galvanometer deflection over the expected measurement range.

8.3.4. Displacement and Velocity Measurement for Piston

In the earlier tests the combined displacement/velocity transducer had not been delivered and a standard displacement transducer was used to measure piston movement. This was a Honeywell L.D. 112 differential inductance transducer. The signal from the transducer was fed to a Boulton and Paul type C.51 meter and thence to an SMI 'N' type galvanometer in the recorder. The required amplification of signal was obtained simply by adjusting the gain factor on the meter until at maximum displacement of the transducer arm there was a satisfactory galvanometer deflection at the recorder. Calibration was carried out by moving the arm on an incremental basis over the range and recording the galvanometer deflection. This

gave a check on linearity of the transducer/recorder combination.

The combined displacement/velocity transducer used in the later tests was a Penny and Giles type UP21/85/5. The displacement and velocity signals were generated independently in the transducer. Displacement was measured by means of a wire wound potentiometer across which was connected a V battery and balancing resistor, the resulting output being fed direct to an 'A' type galvanometer in the recorder. Velocity was sensed by a coil and magnet arrangement. The magnet, mounted upon the moving arm of the transducer, induces an e.m.f. in the coils as it passes. This output was fed to a Sanborn 8875A differential amplifier and thence to an SMI 'N' type pen. The linearity of the two elements is quoted by the manufacturers as being between .05 and 0.5% depending upon stroke length used. Calibration of displacement element was as already described. The velocity element was calibrated by comparing its output with displacement-time curves on an incremental basis.

8.3.5. Recording Equipment

The recorder used was a direct recording ultra-violet oscillograph type M 1310 manufactured by Southern Instruments Ltd. (see fig. 75 for general view). It is extremely versatile, accommodating any number of information channels from 1-50 and any paper width up to 305 mm. Generally speaking, 5 channels were employed for the tests and for maximum trace dispersal 305 mm. wide paper was used. In this way the gain of the various recording circuits could be balanced to give maximum

galvanometer deflection within the limits of recorder linearity without excessive trace overlap. The manufacturers claim that S.M.I. galvanometers will give a linearity of amplitude to current within $\pm 1\%$ over a 10 cm. deflection peak to peak. 10 cms. was therefore selected to be the usual limit for signal amplification. Where for any reason this had to be exceeded compensation was made from calibration curves when analysing the information.

The galvanometers used in conjunction with the recorder are listed below

Information sensed	Galvanometer type	Natural frequency (Hz)
temperature	SMI/A	60
displacement	SMI/N	500
velocity } pressure }	SMI/L (fluid damped)	1650

The overshoot quoted for the galvanometer when correctly damped was 7% on a step-input although the manufacturers claim this to be an upperbound value.

The recording paper used was Agfa/Gevaert Oscilloscript 'D'.

8.3.6. Timer

In the early tests high speed filming techniques were used to record flow conditions on the model rig. Later photographic work was carried out using open shutter still photography. In the latter, in order to relate the photographic evidence of flow with measured characteristics (pressure, piston velocity etc.) it was necessary to have some means of identifying the point on the injection characteristic

(as recorded on the oscillograph), at which a photograph was taken. A timer was developed by the Electronics section for this purpose. In service the timer is triggered by a photo cell operated by the movement of the piston. The timer unit itself is a quartz crystal clock operating at a natural frequency of 100 KHz. The clock can be set for delays of 0.- 99.9ms in increments of 0.1ms. After a preset time the clock triggers two thyratrons (gas filled triode switching devices). One thyatron fires a flash unit in a lightproof tent surrounding the model. The other simultaneously puts a step input into an 'A' type galvanometer in the recorder. Thus, the cameras (on open shutter) in the lightproof tent record the event illuminated by the flash whilst the galvanometer displacement recorded on the light sensitive paper identifies the point on the characteristic at which the photograph is taken. The accuracy of the system is claimed to be $\pm 3 \times 10^{-6}$ seconds.

8.4. OVERALL RECORDING AND MEASUREMENT ACCURACY

8.4.1. System response

On all the systems used the response of the system elements excepting galvanometers was of the order of microseconds. The galvanometers were selected to ensure that their natural frequency was in excess of the maximum in the event measured. Thus, the recordings obtained were free of any influence arising from the recording equipment used.

8.4.2. Effect of siting

The siting of instrumentation to measure the desired variable presented certain problems, viz. The velocity/displacement transducer was mounted in line with the piston on

the E.M.B. 10 diecasting machine (see fig. 75) and no problems of extraneous movement were encountered. However on the rig it had to be attached to the piston by an outrigger and this had to be stiffened considerably to avoid vibration. The siting of pressure transducers in the drive cylinders of both rig and diecasting machine was never entirely satisfactory. Particularly on the drive side of the cylinder it was difficult to find an accessible site at which mean pressure conditions existed at all times. Thus the pressure recordings although accurate in themselves did not always relate to the original objectives. It was particularly important that this situation should be avoided in the case of the transducer located in the pipe connecting the rig to the model. It was desired that this transducer should record mean pipe pressure for the analogue fluid and a test was devised to check this. The model was removed from the copper pipe containing the transducer and a rigidly supported plate was placed close to the pipe exit perpendicular to its axis so that a small annular exit space was formed between the plate face and the end of the pipe, this space being set by feeler gauges. A second transducer was mounted in the plate at a position on the axis of the pipe with its sensing face flush with the surface of the plate. Thus any flow along the pipe would directly impinge upon the second transducer which would record the stagnation pressure at that point. Several injection shots were taken at different reservoir pressures and the pressure readings at the pipe and plate mounted transducers recorded. By deducting the measured velocity head from the stagnation head (measured on the plate transducer) it was possible to determine the mean

static pressure in the region of the pipe mounted transducer. When the results of this calculation were compared with the transducer measurements agreement was better than $\pm 1\%$.

8.4.3. Measurement of traces.

A typical trace is shown in fig. (82). In order to make use of the recorded information for calculation purposes it was necessary to translate the various curves into numerical information. This was done by direct measurement of curve ordinates. Timer lines were marked on recordings at intervals of .1 seconds. The accuracy of the recorder timer actuating the marking of timer lines was $\pm 0.2\%$. Any required time increment could be scaled off by reference to these timer lines. Over the average trace displacement it is considered that measurements can be made with an accuracy of $\pm 1\%$.

The biggest influence of this potential error lies in the use of such measured information for the determination of gating efficiency. This is defined (for zero acceleration) as the ratio of gate exit velocity head to the total head at the gate entrance. For this calculation the velocity measurement taken from the trace would have to be squared. If one includes also the potential error in pressure measurements from the trace record this leads to a potential error envelope in efficiency estimation of $\pm 3\%$.

8.5. PHOTOGRAPHIC EQUIPMENT

8.5.1. High Speed Filming

In the early tests a commercial high speed filming system was employed. This consisted of a Wollensack W.F.17 Fastax

camera operating at 5000 frames per second. Illumination was provided by 3 x 1KW and 1 X 0.75KW lighting units, the operation of the whole being controlled by a W.F.358 unit. The film duration at this film speed is approximately 1 second and in order to record initial and steady conditions it was necessary to trigger the camera control unit by the rig piston movement. The system worked fairly well. However it was abandoned in favour of a timed still photographic technique. There were several reasons for this. The system only allowed a film record to be obtained in one plane at a time, stills taken from the film tended to be very grainy and difficult to analyse and finally the cost of film (Kodak Tri-X) was relatively high.

8.5.2. Still Photography

The system finally adopted is shown in fig. (83). Two still cameras are mounted in mutually perpendicular planes, one perpendicular to the major plane of the gate and one parallel to it. The model and cameras are enclosed in a light-proof tent so that the cameras can be operated on open shutter. The operation of the timer (8.3.6.) triggers a flash unit set to provide a flash of short duration (1/40,000 secs). The flow illuminated by the flash is recorded on the camera film. There is no shutter delay in this as the camera shutter is not used. During test periods the rig required two operators, one in the light-proof tent to operate the cameras and one outside to operate the rig and recording equipment.

Cameras : Minolta S.R.T. 101

Flashgun: Mecablitz model 402

Film : 35mm. Tri-X, 400 A.S.A.

8.6 EXPERIMENTAL PROCEDURE

8.6.1. Casting Tests

It was the object in the first series of tests to produce castings having surface defects which could be used to deduce flow conditions as well as provide general validating information on flow. Preliminary tests were therefore conducted on the diecasting machine to find the minimum temperature as recorded by the mould thermocouples at which castings could be consistently produced. This level was found to be when the fixed half thermocouple recorded 100°C (at which point the corresponding temperature indicated by the moving half thermocouple was 75°C .)

In the tests themselves the tooling was warmed up until the mould temperature was around the desired level. The machine was then cycled on a semi-automatic basis at a selected injection reservoir pressure until the required temperature conditions were obtained, this being noted by reference to the galvanometer movement in the recorder. The castings produced during this period were returned to the melting pot by the conveyor. As soon as the required conditions were attained samples were collected and recordings made of the injection conditions. Twenty five to thirty castings were taken at each test run. The overall length of the casting cycle was continually adjusted during this period to ensure that the monitor temperature remained within $\pm 5^{\circ}\text{C}$ of the selected value. Any castings taken on a cycle when the mould was lubricated were rejected. The instrumentation was calibrated before each test run.

8.6.2. Analogue Studies

Two operators were required to operate the system, one to regulate the camera equipment in the lightproof tent and one to operate the rig and instrumentation. The test procedure was as follows:

The operator in the light-proof tent sets and checks cameras and flash gun. The operator outside fills the shot sleeve with the analogue fluid (water), sets the air reservoir pressure to the appropriate value for the tests, sets the timer to the appropriate delay, zeroes the equipment and finally triggers both rig and recording equipment.

Since still cameras were used it was necessary to repeat the test a number of times for different timer delay settings to build up a series of pictures to cover the behaviour of a given gating system during transition. In order to ensure that the final series of pictures taken in this way, from a number of shots, could be used to represent the sequential history of flow for a single shot, the recorded instrumentation characteristics were used as a check.

A number of shots were taken without photographic record to establish the usual form of characteristic for the system. In the tests themselves, if, for some reason, the measured characteristic for a given shot differed from the established norm, that particular setting was examined for several shots to establish the reason. Whenever this occurred the reason was usually due to incomplete filling of the shot sleeve or air aspiration.

As for the casting tests the instrumentation was calibrated before each test run.

9. LOSS FACTOR ASSESSMENT IN THE METAL SYSTEM.

Analysis of the pressure diecasting system requires accurate knowledge of resistance factors for the machine drive/exhaust circuits and for the metal system. It is possible to measure these for the casting machine drive/exhaust circuits and also for that portion of the metal system contained in the machine itself by means of instrumented tests along the line reported in Section (6.). These factors remain essentially constant (for a given machine setting) for any machine/mould combination. However the portion of the metal system (runner/gate) contained in the mould will vary according to the cavity configuration and consequent parting line. Thus resistance coefficients and hence resistance factors can and do vary considerably between moulds. Clearly if the flow conditions for the filling of a particular mould on a given diecasting machine are to be predicted some means has to be found for determining loss coefficients in that part of the system. Text books on fluid dynamics quote information from individual loss features (sudden bends, changes in section etc.) but runner/gating systems generally consist of combinations of such loss associated features and it is for this sort of situation that information is lacking. This section will attempt to remedy at least some part of the deficiency by examining such work as exists (in reported casting studies) and extrapolating from the information contained therein.

9.1 LOSS FEATURES IN THE METAL SYSTEM

Runner/gating systems contain a number of loss elements the most common of which are discussed in the following and illustrated diagrammatically in Fig. (84).

- (i) The parting line for a pressure casting is generally perpendicular to the axis of the metal entry channel to the mould. The casting metal has to negotiate this (approx.) 90° bend on entry to the runner/gating system. (In hot chamber casting there is some slight blending effect by means of a flow spreader (sprue pin) see Fig. 55 for illustration). In addition the area of runner leading out of the bend is commonly less than the area of the channel feeding in. There is therefore (a further) sudden contraction type of loss feature associated with the bend. In systems where expansion does take place from the bend this is achieved generally by means of a taper. (These changes in dimension whether for expansion or contraction are usually obtained by varying the dimensions of the runner in the plane of the parting line and keeping the runner thickness constant).
- (ii) The runner system in the plane of the parting line commonly contain sudden expansions or contractions. These occur where the width of attachment to the cavity is greater or less than the runner. Such sudden changes in runner dimensions are common where unit mould systems are used. In this form of mould construction the design arranges the cavity in a replaceable unit. This allows different castings to be produced using essentially the same mould simply by replacing the insert. Considerable economy can be achieved in this way although the system imposes considerable restriction on gating and cooling design. One such restriction is that of mismatch between the runner systems cut into the replaceable cavity inserts and the fixed runner element of the mould to which they have to connect. Hence the sudden expansion or contraction which occurs.

(iii) There are basically two types of runner/gate configuration 'end-on' and 'side-on'. In 'end-on' gating systems the runner axis is perpendicular to the gate and in 'side-on' systems it is parallel to it. In the gate region the runner contracts down to the gate dimension in a generally graduated manner. This is a fairly complex loss feature since in 'end-on' systems it may be combined with an expansive effect perpendicular to the general flow direction and in 'side-on' systems there is significant flow rate/directional variation along its length.

The above represent the most commonly encountered loss elements in a pressure casting system in the mould region. There will be others of similar nature in the more complex systems in which the parting line of the mould and hence the runner/gating system does not lie in a single plane. Wall friction will not generally be a significant source of loss in runner systems due to the high quality of finish imparted to the tooling in manufacture.

9.2 LOSS COEFFICIENT FOR COMBINED LOSS FEATURES

The experimental work of Nussey⁽¹⁹⁾ offers the best opportunity currently to quantify loss coefficients in general systems. Nussey examined gating systems containing loss feature combinations similar to those described in 9.1 using a water flow model. He measured runner/gate efficiencies under steady flow conditions for a number of combinations and his work provides a fund of information from which a generalized form of loss factor equation may be deduced. In this section therefore quantitative values are suggested for these features based on information obtained from general hydraulic literature and on information derived from Nussey's experimental work.

Combined bend and contraction loss (K_{bc})

The loss coefficient for a 90° bend (K_b) varies between 0.6 and 1.0 depending on the radius of the bend whilst the loss coefficient for sudden contractions have values of the order quoted in the table below⁽³⁵⁻³⁷⁾.

Contraction ratio	0.1	0.2	0.3	0.4	0.5	0.6	0.7	0.8	0.9
K_c^*	.46	.41	.36	.30	.24	.18	.12	.06	.03

(* NOTE: This value is referred to the exit velocity from the contraction).

Clearly at extreme ends of the spectra of contraction ratio either K_b or K_c will predominate in a bend/contraction feature. For very severe contractions flow up to the bend will be so slow that the upper arm of the bend will behave as a reservoir and K_b will disappear. Similarly for a contraction ratio of 1 $K_c = 0$. In normal casting situations very severe contraction ratios do not occur and the need therefore is to know what intermediate relationship exists for this feature. It was possible to test this type of configuration over the middle range in the laboratory. The actual values for loss coefficient measured experimentally agreed satisfactorily with the relationship.

$$K_{bc} = 0.85 (1 + K_c)$$

(NOTE: K_c is referred to the exit velocity from the feature)

This relationship is therefore suggested as suitable to represent the bend/contraction type of loss feature in the overall loss equation.

Combined bend and taper expansion or contraction at outlet.

In the case of a tapered contraction pressure is converted to kinetic energy, flow is stable and efficient. Diverging flow in a tapered expansion where kinetic energy is being transferred back into pressure is inherently unstable, subject to eddies and separation with much turbulence, and is inherently less efficient.

Thus for a combined bend and tapered contraction the value suggested is

$$K_{bc} = 0.85$$

The head loss equation related to tapered expansions (diffusers) is

$$h_f = K_d \cdot \frac{V_1^2}{2g} \left[1 - \left(\frac{f_1}{f_2} \right) \right]^2$$

V_1 = velocity at entrance to diffuser

f_1 = actual area at entrance

f_2 = actual area at exit

Thus $K_d \left(1 - \frac{f_1}{f_2} \right)^2$ represents the loss coefficient for a diffuser referred to inlet velocity. The value of K_d is generally expressed in most hydraulic texts as a function of the cone angle of expansion. Typical figures are given below:

Cone angle (degrees)	6	20	40	60	90
K_d	.15	.40	.95	1.15	1.0

Tests on bend/diffuser contractions indicated the relationship.

$$K_{bd} = 0.5 \left[1.0 + K_d \left[1 - \frac{f_1}{f_2} \right]^2 \right]$$

NOTE: The diffusive effect in the configuration studied was limited to two dimensions although the values of K_d are based on three dimensional diffusive flow in the above table).

Combined diffuser/bend/contraction feature.

This particular combination is found in moulds used on hot-chamber diecasting machines. To help control freeze-off in the casting a flow spreader (sprue pin) is employed at the junction of inlet nozzle and runner system i.e. at the entry bend. The form of the sprue pin and the channel section into which it locates for casting are such as to form a diffuser in the metal channel, of annular form (see Fig. 55).

As already noted the loss coefficient for a diffuser is given by $K_d = (1 - f_1/f_2)^2$. It has also been noted that the loss coefficient for a combined bend/contraction feature is given by $K_{bc} = 0.85 (1 + K_c)$. In order to assess the loss coefficient for a feature containing an inlet diffuser juxtaposed on a bend/contraction feature, tests were conducted on water flowing in a perspex model of such a situation. It was found that the following equation gave reasonable agreement with experimentation:

$$K_{dbc} = K_d \left(1 - \frac{f_N}{f_a}\right)^2 \left(\frac{f_R}{f_N}\right)^2 + 0.85 (1 + K_c)$$

f_N = inlet area to diffusive section (nozzle)

f_a = outlet area from diffuser (sprue base)

f_R = outlet area from contraction.

NOTE: K_{dbc} is referred to the outlet velocity from the diffuser/bend/contraction feature.

Sudden expansion

The loss coefficient for this type of feature is given by

$$K_E = \left[1 - \left(\frac{f_1}{f_2} \right) \right]^2$$

f_1 = smaller approach area
 f_2 = Larger exit area

NOTE: this coefficient is referred to the approach velocity.

Sudden contraction

Typical values for this type of feature are quoted in the paragraph dealing with bend/contraction losses.

Gate loss coefficients

The gate acts as a nozzle and the gate loss coefficient is predominantly associated with the contraction zone linking it with the runner, and the manner of presentation of the flowing liquid.

'End-on' gates: The axis of the runner in this type of gate is perpendicular to the gate itself so that the contraction of flow relates directly to the contraction between runner and gate. However for situations where the gate width is greater than the runner, (a common situation), the fluid has some capacity to alleviate the severity of contraction, by flow expansion perpendicular to the general direction of flow. After some experimental trial and error the following relationship was established which gave good agreement generally with experimental results.

$$K_g = 1.6 K_c \sin(R - 2\theta')$$

K_c = contraction coefficient based on sudden contraction from runner to gate area

R = land approach angle

θ' = minimum angle of approach, assuming gate running full
(see Fig. 85 for illustration)

'Side-on' gate: In this type of gating system the axis of the runner is parallel to the gate. Thus, with the evidence currently to hand, it is far more difficult to speculate upon loss coefficient for side gates as, apart from geometry considerations, the flow through the gate varies in direction and rate at every point unless the runner is appropriately tapered. It

can be shown that $\frac{1}{1+K_g} = (C_d)^2$, where

K_g is the loss coefficient referred to gate velocity and

C_d is the coefficient of discharge of the gate. Now

C_d is a function of mean hydraulic diameter and may be written $C_d = (A + Bd)^n$, A, B, constants, d = mean hydraulic diameter

From these relationships

$$K_g = \frac{1 - (A+Bd)^{2n}}{(A+Bd)^{2n}}$$

A check using Nussey's experimental results for this type of gate reveals a slightly less complex relationship for the experimental range viz.

$$K_g = \frac{40d + 3}{70-40} \quad \text{or} \quad \frac{40d + 7.5}{178-40}$$

(d in inches) (d in cms)

In view of the extremely idealized form of the side-on runner system employed by Nussey this must be regarded as specific to them.

Influence of Reynolds Number upon loss coefficient.

Nussey demonstrated experimentally that there were differences in efficiency (and therefore loss coefficients) with extremes of pressure head. Examination of these results

shows the variation to relate both to gate velocity and gate geometry. This implies some relationship between loss coefficient and Reynolds number. Blasius⁽³⁵⁾ investigating pipe friction found a relationship as follows

$$\text{friction loss coefficient} = \frac{.316}{R_e^{\frac{1}{4}}}$$

The foregoing combined loss coefficients have all been validated by comparison with experimentation at gate velocities around 30 mps. The following loss coefficient equation is proposed to cover the spectrum of gate velocity

$$K = K_{30} \cdot \left(\frac{R_{e30}}{R_e} \right)^{\frac{1}{n}}$$

K_{30} = loss coefficient at gate velocities around 30 mps

R_{e30} = Reynolds number at $V_g = 30$ mps

R_e = actual Reynolds number

By limited trial and error the value of the index gave the best overall agreement at a value of $n = 2.22$.

9.3 LOSS COEFFICIENT EQUATION (BASED ON 9.2)

Let K_M = loss coefficient for runner/gate system
referred to gate velocity

$$\text{i.e. } K_M = K_A \cdot \left(\frac{f}{f_A}\right)^2 + K_B \left(\frac{f}{f_B}\right)^2 + \dots$$

$K_{A,B}$ = loss coefficients at position A,B
referred to velocity $V_{A,B}$

f = gate area, $f_{A,B}$ = area section A,B

$$f \cdot V_g = f_{A,B} \cdot V_{A,B} \quad \text{etc.}$$

On this basis the loss coefficient equations for any combination may be written using the information of 9.2 e.g.

(i) System comprising bend/contraction, sudden expansion, and gate contraction (refer to Fig. 85).

$$\begin{aligned} K_M &= K_{bc} \cdot \left(\frac{f}{f_1}\right)^2 + K_c \cdot \left(\frac{f}{f_1}\right)^2 + 1.6 K_{cg} \sin(R-2\theta') \\ &= 0.85(1+K_c) \cdot \left(\frac{f}{f_1}\right)^2 + \left(1 - \frac{f_1}{f_2}\right)^2 \cdot \left(\frac{f}{f_1}\right)^2 + 1.6 K_{cg} \cdot \sin(R-2\theta') \end{aligned}$$

(ii) System comprising bend/contraction into tapered expansion (refer to Fig. 85).

$$\begin{aligned} K_M &= (0.85(1+K_c) \left(\frac{f}{f_1}\right)^2 + 0.5(1+K_d(1 - \frac{f_1}{f_2})^2) \cdot \left(\frac{f}{f_1}\right)^2 \\ &\quad + 1.6 K_{cg} \cdot \sin.(R - 2\theta') \end{aligned}$$

Having developed the value of K_M for a system the value may be used for analysis of flow rate etc. or it can be used to calculate system efficiency for steady flow on the basis of energy transformation etc.

$$\text{Efficiency } E = \frac{V^2}{2g} \cdot \frac{1}{h} \cdot 100 \%$$

$$\text{Now } h = \frac{V^2}{2g} (1 + K_M)$$

$$E = \frac{1}{1 + K_M}$$

NOTE: This is only true for steady flow conditions. see 10.2

By using this relationship to calculate system efficiencies it is possible to assess how effective the estimation of loss factor has been by direct comparison with experimentally measured values (of efficiency) for steady flow conditions.

In Section (3.2, 3.3) it is necessary to express the dependancy of K_m upon f as succinctly as possible in view of the complexity of equation in which it appears. The modified form used in that section is obtained as follows

$$K_M = K_A \left(\frac{f}{f_A}\right)^2 + \dots + K_N \left(\frac{f}{f_N}\right)^2 + K_{cg} (1.6 \sin (R - 2\theta'))$$

Now examination of the quoted tables of contraction ratio Vs K_c indicates a relationship $K_c = \text{constant}$ (runner area adjacent to gate - gate area).

Thus $K_{cg} 1.6 \sin (R - 2\theta')$ may, for a given gate configuration be written $[a (f_R - f)]$, where $a = \text{constant}$.

Thus the equations may be written

$$K_M = \left[K_A \left(\frac{f_R}{f_A}\right)^2 + \dots + K_N \left(\frac{f_R}{f_N}\right)^2 \right] \cdot \left(\frac{f}{f_R}\right)^2 + a \cdot f_R \left(1 - \frac{f}{f_R}\right)$$

$$K_M = BF^2 + a (1 - F), \quad F = \frac{f}{f_R}$$

This is the equation used in Sections (4) and (5) to relate K_m to f .

9.4 APPLICATION TO NUSSEY GATING SYSTEMS

'End-on' gates.

Fig. (86) illustrates the gate geometry used by Nussey, Fig.(87) the range of runner geometry whilst Fig.(88) shows a typical combination of these. Table 6 (89) illustrates the range of combinations considered by Nussey in his experimental work. The efficiency of a broad selection of these gates was calculated using loss coefficient values suggested in 9.3 basing the area ratios on the static values quoted in Table 3. Referring to Fig.(86), Nussey considered the influence on system efficiency, of

- (i) gate width P
- (ii) gate depth Q
- (iii) land approach angle R
- (iv) gate exit semi-angle S
- (v) land length T

From the calculated information, graphs were plotted for the influence of those features upon system efficiency and compared with Nussey's experimental information. The results of this comparison are shown in Figs.(90 - 94 inc.).

Fig.90 (gate width)

For gate sizes of .635 mm and 1.02 mm agreement between calculation and experimentation is good. For the .254 mm gate however it is poor. It may be that for the latter the very high system pressures associated with this particular gate size may distort the gate sufficiently to account for this difference. Or it may simply reflect some effect which the loss coefficient equations does not allow for. If this is the case the gate contraction factor may require modification for the smaller gate size.

Fig. (91) gate depth

Here the agreement is excellent for both runners B and C involving bend/contractions + expansion + gate contraction loss coefficient and for runner D which contains a bend/taper expansion loss coefficient.

Fig. (92) land approach angle

Curves are plotted for high and low head conditions and there is reasonable agreement with experimentation. The biggest difference occurs for values of land approach angle of 40° where the experimental curve showed a sharp drop in efficiency not reflected in the calculation. In the case of runner C the gate efficiency for a 40° approach angle was checked experimentally in the laboratory and a value for efficiency (indicated by the asterisk on the graph) obtained giving much closer agreement with the loss coefficient equation. A point arises from this with regard to the conclusion drawn by Nussey from his experimental results. He says that ".... an approach angle of 20° was the most efficient tested and the one of 40° least so.....". In view of the experimental verification of the theoretical curve value which indicates a gradual fall off of efficiency beyond the 20° approach angle the latter part of this statement must be in some doubt.

Fig. (93) gate exit semi-angle

Although this gate configuration did not correspond exactly to the loss coeff. combination listed in 9.3 it was decided to examine this system as a bend/contraction + sudden expansion + gate contraction and to include the influence of the semi-angle only in so far as it affected gate area. As may be seen quite

good agreement was obtained, the biggest difference occurring for the system containing the largest expansion factor (runner B).

Fig. (94) land length

Again, generally good agreement particularly for the high head values. Experiment and calculation did not agree as well for low head value using runner B as for the others. An interesting point arises from this particular set of curves. On the basis of his results Nussey states that there is a critical land length for the .635 mm gate tested, giving a land/depth ratio of 2.5 for maximum efficiency, which value corresponds roughly with that normally used in practice. Now the loss coefficient for the gate takes no account of land length, (treating the contraction to the gate as a nozzle from which exit efficiency is ideal). The variation in efficiency in the calculations does not arise as a result of land length variation but as a result of variation in the static areas of the gates making up this series (See Table 3.). It has already been noted that a good correlation exists between calculation and experimentation and Nussey's conclusion should be held in doubt pending further experimentation.

Side-on gates

Nussey examined a number of side-on gates on his water analogue flow rig. Runner/gate systems having varying degrees of curvature were examined. In view of the manufacturing expense circular cross-section tubes were used to represent the runner, as the high cost of drawing and bending prohibited

the use of non-standard tube. Thus the runner/gate geometry is far from representative of real systems. Table (7), Fig. (95) shows the range of sizes examined. Nussey concluded that efficiency was influenced by the radius of curvature of the runner depending upon the gate/runner cross-sectional area ratio. He plotted least square regression lines of efficiency against radius to demonstrate this. However he did not include the results for the smallest bend radius (51 mm). If these are included the least square regression lines have almost zero gradient for all combinations considered (See Fig.96). On that basis bend radius does not appear to influence efficiency. The gate loss coefficient quoted for side-on type gates was derived from the efficiency value for straight tube and the results are plotted in Fig. (97).

9.5 COMPARISON WITH SACHS EQUATION FOR LOSS COEFFICIENTS

Sachs⁽¹²⁾ analysed end-on types of gating system of a much simplified form. He assumed that the runner in the plane of the parting line was essentially of graduated expansion or contraction up to the gate. He derived a loss coefficient equation for this type of feature on the basis of wall friction. To complete the loss coefficient equation he added to this a bend loss coefficient obtained from the curve illustrated in Fig.(98). The resulting equation was: (refer to Figs.(98) and (99)).

$$\begin{aligned}
 K_n &= \left[\frac{\lambda \cdot f^2 \cdot L}{2} \cdot \left\{ \frac{1}{(a_1 b - a b_1)^4} \left[3(a-a_1)^2(b-b_1) - 3(a-a_1)(b-b_1)^2 \right] \ln \frac{a_1 b}{a b_1} \right. \right. \\
 &\quad - \frac{1}{(a_1 b - a b_1)^3} \left[\frac{(a-a_1)^3 - 2(a-a_1)^2(b-b_1)}{a a_1} + 2 \frac{(a-a_1)(b-b_1)^2 - (b-b_1)^3}{b b_1} \right] \\
 &\quad + \frac{1}{(a_1 b - a b_1)^2} \left[\frac{(b-b_1)^2(b+b_1)}{2 b^2 b_1^2} + \frac{(a-a_1)^2(a+a_1)}{2 a^2 a_1^2} \right] \left. \right\} \\
 &\quad + K_a \cdot \left(\frac{f}{f_R} \right)^2 \\
 &= K_f + K_a \left(\frac{f}{f_R} \right)^2 \quad (\text{referred to gate velocity})
 \end{aligned}$$

λ = wall friction factor

As may be seen, that part of the expression yielding wall friction is extremely involved and it is instructive to examine the significance of this term. In his original analysis Sachs uses the form of the gating system of the B-6 test die (Fig.5) for illustration. Using therefore the same system and applying Sachs to a spectrum of gate size yields the results given in the

table below

GATE SIZE mm ²	Loss COEFFICIENTS REFERRED TO V _G		
	K _f	K _a (f/f _R) ²	K _M
.203 x 68.25	.010	.002	.012
.762 x 68.29	.009	.029	.038
1.524 x 68.25	.011	.116	.127
3.050 x 68.25	.010	.462	.472

Thus it may be seen that wall friction can be relatively significant at the lower end of the spectrum of gate size. It follows, however, that this will only be the case in a relatively streamlined system in which the number of loss features is small (i.e. in this case a single bend factor).

When expansion or contraction angles are greater than 6° Sachs equation will underestimate the loss coefficient since it does not allow for separation effects.

Examining the gating form for the test die B-6 with the information of section 9.3 suggests that the system represent a combined bend/taper contraction feature for which the loss coefficient equation is

$$K_M = 0.85 \left(\frac{f}{f_R} \right)^2$$

f = gate area

f_R = initial area of taper contraction.

Applying this to the same range of gate size as the Sachs equations yield the results given in the following table.

GATE SIZE mm ²	Loss COEFFICIENT REFERRED TO V _G		
	K _f	K _a (f/f _R) ²	K _M
.203 x 68.25	0	.003	.003
.762 x 68.25	0	.039	.039
1.524 x 68.25	0	.157	.157
3.050 x 68.25	0	.628	.628

The values of K_M calculated from Sach equations and from the information of section 9.3 differ significantly over the upper end of the range of gate size. If the gate size considered were extended there would ultimately be a maximum of about 36% difference between the values. However in terms of efficiency, ($E = 1/1+K_M$), whilst the values of K_M are small the differences in the efficiency calculations are much less as shown by the table below.

GATE SIZE (mm) ²	EFFICIENCY	
	SACHS	9.3
.203 x 68.25	98.6	98.5
.762 x 68.25	96.3	96.2
1.524 x 68.25	88.7	86.4
3.050 x 68.25	67.8	61.5

Thus the loss coefficient equation for test die B-6 taken from 9.3 agrees well with the Sachs equation in efficiency calculations over the gate size range considered. The difference in K_M over the larger gate sizes represent the different allowance for bend loss coefficients in the two equations, the comparison over the range of gates considered is shown in Fig. (100).

9.6 APPLICATION TO EXPERIMENTAL MOULD

Figure (55) shows the general layout of the runner/gate systems employed in the experimental work of Section (6). As the mould was designed for use on a hot chamber machine the bend contains a sprue flow divider so that flow up to the parting line is along a tapered annular channel. According to Section 9.3 the total loss coefficient will be given by

$$K_M = \left[\text{diffuser coefficient in sprue} + \text{bend/contraction coefficient} \right] (\text{referred to gate velocity}) + \text{gate/contraction coefficient.}$$

$$= \left[K_d \left(1 - \frac{f_N}{f_a} \right)^2 \left(\frac{f_R}{f_N} \right)^2 + 0.85 (1 + K_{cb}) \right] \left(\frac{f}{f_R} \right)^2 + 1.6 K_{cg} \sin(R - 2\theta')$$

f_N = area of nozzle leading to sprue

f_a = area of base of annulus

f_R = area of runner immediately after bend

f = gate area

This equation applied to the experimental gating system yields the following information

(i) 25.4 mm x .635 mm nominal gate

$$\begin{array}{llll} f_N = 71.0 \text{ mm}^2 & K_d = 0.4 & & \\ f_a = 253.0 \text{ mm}^2 & K_{c \text{ bend}} = 0.4 & \theta' = 0 & \\ f_R = 56.0 \text{ mm}^2 & K_{c \text{ gate}} = 0.38 & R = 45^\circ & \\ f = 14.8 \text{ mm}^2 & & & \end{array}$$

Total loss coefficient for runner/gate $K_M = .546$

Metal system loss factor for mould $C_{M3} = 89100$

Efficiency of runner/gate system = 64.7%

(ii) 25.4 mm x 2.54 mm

$$\begin{aligned} f_N &= 18.0 \text{ mm}^2 & K_d &= 0.4 & \theta' &= 0 \\ f_a &= 253.0 \text{ mm}^2 & K_{c \text{ bend}} &= 0.4 & R &= 0 \\ f_R &= 56.0 \text{ mm}^2 & K_{c \text{ gate}} &= 0 \\ f &= 56.0 \text{ mm}^2 \end{aligned}$$

Total loss coefficient for runner/gate $K_M = 1.66$

Metal system loss factor for mould $C_{M3} = 10850$

Efficiency of runner/gating system = 37.6%

The values of C_{M3} for the mould section of the metal system compare very favourably with those measured in the experimentations of section (6) as the tables below show.

(i) Experimental value of C_{M3} for mould gate size 25.4mm x 635mm.

RESERVOIR PRESS ₂ N/m ²	NET FORCE N.	PISTON VELOCITY M.B.S.	C_{M3} N.sec ² .M ⁻²
510000	9440	.30	101600
730000	13500	.366	95424
945000	17400	.431	88560

AVERAGE 95040

(ii) Experimental values of C_{M3} for nominal gate size, 25.4mm x 2.54mm.

RESERVOIR PRESS ₂ N/m ²	NET FORCE N.	PISTON VELOCITY M.P.S.	C_{M3} N.sec ² .M ⁻²
510000	9440	.771	10776
650000	11960	.881	10306
793000	14500	.908	12600

AVERAGE 11232

It is worth noting here that the loss coefficient equation had previously only been applied to Nussey's water analogue. It is gratifying to find satisfactory agreement with experiment when applied to areal casting situation, in the casting of a zinc alloy in a hot chamber machine.

It reinforces the view that loss coefficients are essentially the same for flowing liquid metals as for any other fluid.

Total metal system loss coefficient for experimental machine/mould.

The values of K_M calculated in the foregoing, refer only to that part of the metal system contained in the mould. The total metal system loss coefficient includes that attributable to the metal system built into the machine i.e. gooseneck and nozzle. In the tests of Section (6) the metal system loss factor for gooseneck and nozzle was found to be 87.3. If one ignores friction as a significant contributory factor then this is equivalent to a loss coefficient.

$$K'_M = .704 \text{ referred to metal velocity in nozzle}$$

$$= .704 \left(\frac{f}{f_N} \right)^2 \text{ referred to metal velocity in gate}$$

Thus the total loss coefficient for the whole system can be written

$$\begin{aligned} K_{M \text{ TOT}} &= K_M + K_M^1 \\ &= \left[\left[.704 + K_d \left(1 - \frac{f_N}{f_a} \right)^2 \right] \left(\frac{f_R}{f_N} \right)^2 + 0.85 (1 + K_{c \text{ bend}}) \right] \left(\frac{f}{f_R} \right)^2 \\ &\quad + 1.6 K_{c \text{ gate}} \sin (R - 2\theta') \end{aligned}$$

The values of the bracketed element of the first term is 2.1 for the experimental/machine mould. If the second term is plotted against $\frac{f}{f_R}$ using the contraction coefficient values in 9.3 it may be seen that this term may be rewritten; in the form $0.8 (1 - \frac{f}{f_R})$. Thus the total loss factor for the metal system can be expressed simply

$$K_{M \text{ TOT}} = 2.1 \left(\frac{f}{f_R}\right)^2 + 0.8 \left(1 - \frac{f}{f_R}\right)$$

$$= 2.1 F^2 + 0.8 (1 - F) ,$$

$$F = \frac{f}{f_R}$$

This equation and its coefficients are used for the purpose of energy/breakdown calculations for the experimental machine/mould as reported in Section (7).

9.7 CONCLUSION

It is imperative to be able to estimate accurately system loss coefficients if that system is to be properly examined. The analysis of Sections (4,5) requires this knowledge, particularly for the determination of optimum energy rate and of breakdown conditions. Machine loss coefficients can be measured experimentally as can the loss coefficients for the machine element of the metal system (see Section 6). Section 9.3 offers an empirical contribution to the estimation of mould loss coefficients not previously attempted for pressure casting. The use of these loss coefficients compares favourably with other systems (9.5) and yields accurate estimations of runner/gating efficiency when compared with experimental results from a water flow analogue (9.4) or from a real casting situation. (9.6). Until further work has been carried out to extend knowledge of loss coefficients for combined features it is concluded that the approach and estimates suggested in 9.3 will be sufficiently accurate for realistic analysis of diecasting situations to be attempted and viable conclusions drawn.

10. QUANTITATIVE EXAMINATION OF NUSSEY GATE RANGE.

The acquisition of the range of gate and runner plates used by Nussey allowed further experimental work to be carried out. The principal objective of the work was to examine flow state in the system. However it also presented an opportunity to check Nussey's experimental results, which have been used in Section 9, in the context of an entirely different type of flow rig and instrumentation system.

10.1 CHECK OF EFFICIENCY VALUES

A typical trace of velocity, displacement and pressure characteristic for one injection cycle on the flow rig is shown in Fig. (82). The pressure and velocity characteristics show peaks during the initial piston movement and transition settling to approximate plateaus of pressure and of velocity indicating essentially steady flow conditions. Mean value of pressure and velocity taken from these plateaus were used to determine gate efficiency as defined by Nussey for a range of runner/gate combinations.

As already stated the main objective of the test series examining Nussey gating systems was to study state of flow. In order to approach diecasting conditions as nearly as possible the rig was run at its highest reservoir pressure wherever possible (90000N/m^2). The mean injection velocities did not therefore correspond to the values at which Nussey measured efficiency. The graphs for the various tests are presented therefore in two parts. In part (a) the efficiency measurements

are plotted without compensation, in part (b) the efficiencies for the gate velocity limits used by Nussey are extrapolated from the measured result using the formula suggested in 9.2. A series of runner/gate combinations were tested covering the possible range of gating variation specified by Nussey (see 9.4). The results are shown in Figs.(101 - 105) alongside Nussey's measurements.

Examination of the various graphs shows that

(i) The efficiency measurements are generally consistent with the efficiency spectrum implied by Nussey's high and low head measurements (Section (a) of graphs).

(ii) The conversion relationship expressed in 9.2, when applied to the measured results yields fair agreement with Nussey's efficiency values when applied to the measured efficiencies (Section (b) of graphs).

There are odd exceptions where measured values do not agree. One such example is the result for a 40° land approach angle Fig.(103). It was a matter of experimental practice that a number of experimental checks of efficiency were made for each configuration tested and this particular configuration was no exception. It is interesting to note that the value extrapolated from the measured value for $V_g = 31$ m.p.s. i.e. 68% agrees well with that suggested by the loss coefficient equation for a 40° approach angle, see Fig. (92).

(This was also true for the low head value at 50° approach angle. See also Fig.(103)).

10.2 LOSS COEFFICIENT VARIATION UNDER UNSTEADY FLOW CONDITIONS

In the development of equations for gate size for maximum energy rates or Weber numbers the basis of the analysis was the assumption of steady flow conditions since it was considered that by appropriate machine/mould balancing the transition phase could be reduced to negligible proportions or even eliminated. The loss coefficients of Section 9 are adequate for this purpose.

However, it is possible that machine/mould combinations may be encountered which cannot be balanced so that filling conditions are largely unsteady. Dailey et al.⁽⁴²⁾ have found variations of as much as $\pm 20\%$ in loss coefficient for sharp-edged, circular orifices in unsteady flow conditions. Should this be the case for gating systems the plotting of energy rate curves etc. based on Section 9 could be in error. It was decided to check this possibility by examining the pressure/velocity traces taken for the various gating systems used in the work of 10.2.

Some difficulty was encountered in this. Efficiency under steady flow is given by

$$E = \frac{v^2}{2gh} = \frac{1}{1+K_m}$$

V = gate velocity

h = total head at the gate

K_m = loss coefficient for the system referred to gate velocity.

Thus by taking measurement from the steady flow portion of the trace for piston velocity and static head v and h can be computed and hence K_m . However in unsteady flow

$$E = \frac{V^2}{2gh} = \frac{1}{(1+K_m) + \frac{2L}{V^2} \cdot \frac{dV}{dt}}$$

L = length of accelerating column of fluid referred to gate.

$\frac{dV}{dt}$ = acceleration at gate

It was not possible in the short term to find a means of accurately determining the term $\frac{2L}{V^2} \cdot \frac{dV}{dt}$ and K_m could only be determined for points of flexure on the (piston) velocity curve i.e. where $\frac{dV}{dt} = 0$.

Over the range of gates considered the loss coefficients determined for points of flexure did not vary significantly from steady flow values. On this basis it is considered that the possibility of significant loss coefficient variation in gating systems during unsteady flow can be discounted.

11. EXPERIMENTAL STUDIES OF FLOW STATE IN GATING SYSTEMS USING A WATER MODEL.

The gating systems used in the experimentation were those designed by Nussey⁽¹⁹⁾ and used by him in his experimentation. The object of the study was to examine flow state through these systems in the context of the predictive criteria proposed by the analysis of 3.3. The effect of gate geometry variation was examined and photographic evidence of flow state considered in relation to the Weber number curves calculated for the flow rig.

It should be noted that Nussey examined flow state through these systems in some (photographic) detail. There were two reasons for repeating part of this work. Firstly, Nussey's examination was restricted to single plane viewing (parallel to the plane of the gate land, see Fig.(86) 9.4) and it was considered that for the present study it was desirable to view flow state more comprehensively (i.e. both parallel and perpendicular to the gate land). Secondly, certain of Nussey's conclusions relating to transition effects were considered to be a function of his rig design and merited reconsideration.

11.1 INFLUENCE OF GATE GEOMETRY

In order to be able to make reference where necessary to Nussey's work it is necessary to state certain definitions of flow term used by him. Nussey categorised the runner/gate combinations used in terms of the ratio of gate to minimum runner area, which he called the choke (C). Values of C less than 0.9 were defined to be choked, those lying between 0.9 and 1.1 as critically choked and above 1.1 as unchoked. From direct observation he stated that the steady flow appearance of choked and unchoked systems showed distinct differences, choked flow being of a 'line source' nature whilst unchoked flow was generally point source. The flow regimes corresponding to these descriptions are shown, diagrammatically in Fig. (106).

In the test series the normal test configuration was as follows: The model was connected to the shot sleeve by a horizontal copper pipe colinear with the axis of the shot sleeve. For each shot the sleeve and tube were completely filled with water so that the static level was approximately 25.4 mm (1") below the gate. On the initiation of the injection cycle the water did not begin to flow through the gate until the filler hole had been completely shut-off by the piston.

Studies were made of the following parameters

Gate length: depth ratio

Approach angle

Runner: gate width ratio.

Gate exit semi-angle

Runner: gate asymmetry

Dimensional details of the runner:gate combination used may be obtained from figs.(87) and (89) Section 9.4.

11.1.1 GATE LENGTH:DEPTH RATIO

The following combinations were examined

Gate Plate	Runner Plate
1	A, B ₁ , C
2	A, B ₁ , C
3	A, B ₁ , C
4	A, B ₁ , C

Flow through all the gate:runner combinations followed a similar pattern. At flow initiation the flow regime was point source for all configurations. The significant difference between choked and unchoked systems was that the locus of the point source remained essentially the same through transition to steady state for unchoked systems, whilst for choked systems it moved well back from the gate as flow stabilized. A further difference,(arising from differences in jet expansion angles), is that jet breakdown due to air entrainment after leaving the gate occurs much earlier in the unchoked systems. The Weber number values for the combinations tested were approximately 12×10^3 and at this level there was no breakdown at the gate.

Jet expansion angle in the side view plane was not sensibly affected by gate length:depth ratio as might have been expected. It remained the same regardless of land length over a given

series. It was affected to some extent by choke value, being approximately 10^0 for choked (runner C), and 20^0 for unchoked (runner A) systems.

Edge turbulence and breakdown was evident in all combinations tested, being somewhat greater in unchoked systems. This persisted throughout the steady phase of the injection cycle.

Fig. (107) shows transition stages for combination C1 (choked), Fig. (108) for A1 (unchoked) whilst Fig. (109) shows an oblique side view of A2 clearly illustrating edge turbulence.

11.1.2 APPROACH ANGLE

Gate Plate	Runner plate
10	A, B ₁ , C
1	A, B ₁ , C
12	A, B ₁ , C
13	A, B ₁ , C

There was very little difference in the flow regime for any of the combinations. The more severe approach angle (gate 13) caused slightly more initial spray in transition than the others and the jet expansion angle in side view was slightly greater ($+2^0$). Weber number values around 12×10^3 .

11.1.3 GATE EXIT SEMI ANGLE

Gate plate	Runner plate
21	B ₁ , C
31	B ₁ , C

The flow condition through gate plate 21 for both runners was similar to that illustrated in Fig. (107) for gate 1 from which it differs only in gate depth (see 9.4. for dimensional details). The one noticeable difference was in the droplet size as viewed from the side. The free droplet size was larger for flow through gate 21 than gate 1 by a ratio which appears to be roughly equivalent to the ratios of gate depth. It would appear from this that free droplet size is related to gate size for long thin gates (this point is of interest in the context of 7.2). It must be noted however that the Weber number for steady flow through gate 21 was only 75% of that for flow through gate 1 i.e. 9×10^3 .

The major influence of semi-angle upon flow state apparent from the examination was in the stressing of the jet. In gate 31 the expansion of the jet along the semi-angle placed it in a state of tension so that it ruptured in a number of places at a very early stage after leaving the gate. This, combined with air entrainment, caused jet breakdown significantly closer to the gate than was the case for gate 21 (and gate 1). Fig.(110) shows this clearly. (The side view of this figure also shows the larger droplet size discussed in the context of gate 21).

11.1.4 RUNNER:GATE WIDTH RATIO

Gate plate	Runner plate
1	A, B ₁ , C
17	A, B ₁ , C

As far as gate 1 was concerned the influence of the ratio was, for steady flow conditions to cause point source flow in A1 and approximate line source in C1, all systems starting off as point source.

The runner:gate width ratios were much smaller for gate 17 across the runner spectrum than was the case for gate 1. As a consequence there was far less difference in flow regime between A17 and C17 combinations, indeed there was no essential difference at the steady flow stage.

There were however differences in the development of flow regimes for the two gates. In gate 1 flow developed without any noticeable jet rotation, the major feature being edge turbulence and mushrooming. In gate 17, possibly due to the thinness of the emergent jet (.25 mm or .010" .), the jet showed a tendency to rotate at low Weber numbers (4×10^3) for all runner combinations. The initial flow of the jet was as a rectangular lamina emerging from the gate. Depending upon flow pressure the jet plane would show evidence of rotation above the main flow axis. Then as pressure built up the jet became unstable and broke down as air was entrained. In the

tests this occurred at Weber numbers greater than 25×10^3 . Fig.(111) illustrates this sequence of events for C17.

11.1.5 RUNNER: GATE ASYMMETRY

Runner Plate	Gate Plate
1	A, B ₁ , C
36	A, B ₁ , C

In the case of runners A, B, used in conjunction with gate 36 the jet development follows a similar pattern to that illustrated in Fig. (107) for C1, the principal difference being that once steady flow was established there was a bias in the jet direction following the asymmetry of gate:runner relationship, with an increase in jet edge turbulence and breakdown. However in combination C36 jet splitting consistently occurred, see Fig.(112). As can be seen, one part of the jet corresponds to the initial impact zone of the flow from the runner onto the gate. This kind of splitting according to Nussey is normally associated with air aspiration into the system due to faulty sealing of the model. However the system was checked carefully, being disassembled, resealed and assembled on several occasions without eliminating the effect. No explanation can be offered to account for this. The Weber number values were around 12×10^3 for the tests.

11.1.6 COMPARISON OF FLOW STATE WITH WEBER NUMBER.

Curves of Weber number against gate area for the rig are shown in Fig. (113). The curves are based upon runner C and cover 76.2 mm (3") and 25.4 mm (1") gate widths. Asterisks indicate the positions on the curves for various gate runner combinations and Fig. (114) shows front views of flow regimes through 25.4 mm gates, for illustration.

Combination C17 ($W_e = 76 \times 10^3$) and C6 ($W_e = 68 \times 10^3$) show considerable breakdown at the gate as well as due to air entrainment whilst C18 ($W_e = 48 \times 10^3$) does not show anything like as much air entrainment. The vast majority of 76.2 mm (3") gates had gate areas in the region $f = 48.4 \text{ mm}^2$ (.075 ins²) and had similar Weber number values i.e. $W_e = 12 \times 10^3$. None of these gates exhibited any evidence of breakdown in flow at the gate. Breakdown in all cases occurred after the jet had left the gate, the point of breakdown depending upon jet expansion.

11.2 INFLUENCE OF FREE PISTON TRAVEL

Stiction effects on the rig arising from faulty design could not be reduced sufficiently for two-stage injection to be usefully examined (see equipment Section 8). However it was possible to make some examination of the effect of free piston travel upon transition conditions. The normal test procedure for 11.1 involved minimum free piston travel before flow through the gate commenced. This procedure was modified in two separate ways for the purposes of 11.2 :

- (i) injecting a much reduced shot
- (ii) raising the gate level well above the shot sleeve by using a 'swan-neck' rather than straight copper tube.

Reduced shot size. Certain differences in flow state were observed when using reduced shot sizes in conjunction with the test gates. During the transition phase greater breakdown occurred due to the higher piston speeds. As flow stabilized two main differences emerged when compared with the flow regimes observed in the tests reported in 11.1. Firstly, flow was generally more turbulent with greater breakdown, Fig. (115) for C1 illustrates this. If this is compared with the steady flow regime of Fig. (107) for C1 a significant difference can be seen (Note: injection piston speeds were almost identical for both conditions). Secondly, it was frequently the case that there would be an explosive breakdown in steady flow patterns after which the original flow pattern would be resumed. Fig. (116) illustrates this effect for three different runner gate combinations, in each case the explosive effect can be seen,

with a 'stable' flow front emerging from the gate. All these effects were considered to be due to air entrainment in the shot sleeve.

'Swan neck' connector. Again greater breakdown occurred during transition. However the general flow regimes were similar to those noted using the straight connection pipe. There were very occasional 'explosive' effects of the kind commonly encountered in the 'short shot' test.

11.3 CONCLUSIONS

Generally speaking the vizual aspect of flow in the plane of gate land (front view) corresponded to Nussey's findings. Certain differences did occur, however, which are worthy of note.

(i) 'line' and 'point' source systems all started off as 'point' source. Nussey claimed that this was only occasionally the case and that such a change would be indicative of the onset of cavitation. If this is so then the argument raised in 5.1 of cavitation as an essentially transition phenomena would appear to be correct.

(ii) Nussey found side oscillations in the jet (front view) to be a function of applied head and gate width. In the flow rig used in the current tests the small perturbations occurring in the drive system were found to be of greater significance.

(iii) Transition periods differed considerably for gate: runner combinations on the flow rig as compared with Nussey's experience. This confirms the conclusion of 4.3 regarding transition influences. Side views demonstrated the significance of edge effects in the wider gates and of rotational effects in narrow gates. These views also demonstrated that jet expansion

in that plane was not significantly affected by gate geometry.

In terms of general flow state several potential breakdown conditions were discovered viz.

- a) Breakdown at the gate exit. This was dependent upon the generalized Weber number and is (potentially) capable of prediction.
- b) Breakdown as a result of air entrainment. The point at which this occurs after the jet has left the gate is dependent upon jet expansion, the greater this is the sooner breakdown occurs. In badly vented casting conditions it is possible that breakdown of this kind may be increased due to increased air pressure. This would be greatest in conjunction with unchoked systems of large gate exit semi-angle.
- c) Edge breakdown. For gate to runner widths greater than 1 turbulence and breakdown at the jet edges became significant. This must be considered unacceptable in practical casting terms as it is the authors experience that flow related defects are commonly experienced at the edges of feeding gates.
- d) Breakdown associated with free piston travel. When the shot sleeve is not full the entrainment of air in the shot in the sleeve increases flow breakdown at the gate and causes intermittent, explosive breakdown of flow. (This is an interesting finding in view of the practice in industry of using fixed shot sleeves for different shot sizes and in the use of 'short shots' to indicate filling patterns). When the shot sleeve is full the influence of free piston travel is only evident in the transition phase (c.f. 5.2).

12. PILOT STUDIES OF CAVITY INFLUENCE UPON FLOW.

The analysis of Section 3 was applied to the general range of diecasting machines and to the experimental diecasting set-up on the assumption of zero cavity boundary resistance. It was considered that a pilot study of cavity boundary influence would be of value in testing the validity of this premise and as an indication of possible lines of future work. Accordingly two flow conditions were examined:

1. The restrictive effect upon flow of boundaries parallel to the gate land i.e. parallel to the mean plane of flow from the gate.
2. The influence of a boundary plane perpendicular to the mean flow direction i.e. direct impingement.

12.1 INFLUENCE OF BOUNDARIES PARALLEL TO FLOW

The experimental (water flow) die block was designed so that the perspex plates separated by ground spacers could be mounted upon it parallel to the general flow plane from the gate. Fig. (78) illustrates the block set-up in this way. By using different spacer sizes the plates could be set any distance apart up to 38.1 mm ($1\frac{1}{2}$ "). Using the model in this way flow was examined through a number of runner:gate combinations for a range of gap widths from 38.1 mm ($1\frac{1}{2}$ ") down to a minimum, equivalent to the nominal thickness of the gate under examination. The test procedures were as for the test series reported in 11.1

In terms of flow direction and flow state the spacer plates only exerted an influence from the point at which the expanding jet contacted them. This point was determined by the gap

width and the angle of the expanding jet (10° for choked, 20° for unchoked systems see side views Figs.(107-110). From the point at which contact occurred flow in the mean direction slowed, and bulging occurred along planes parallel to the boundaries, to compensate. This was particularly evident in gates having significant edge turbulence in unrestricted flow. Thus, when the gap thickness was around the nominal gate thickness, the whole flow regime was changed as compared with unrestricted flow. It was particularly noticeable also that small perturbations or explosive effects were dramatically emphasized. Breakdown due to air entrainment, although evident in flow through the larger gaps was almost completely inhibited as flow gap thickness was reduced to a value approaching that of the gate under examination.

Measurements of runner pressure and piston velocity for the series showed that, regardless of considerable changes in flow patterns due to the parallel boundary restrictions there was no sensible difference in the injection characteristics.

Illustration of the above points is provided by Figs. (117) - (119).

Fig. (117) shows a direct photographic comparison between unrestricted flow and flow between boundary plates set to a gap thickness equivalent to the nominal gate thickness for runner: gate combination C6 and also typical injection characteristics for both these flow conditions. The difference in flow pattern and yet the close similarity of injection

characteristic are clearly seen. Fig. (118) shows evidence in an experimental casting of surface defects due to edge breakdown and prematurely solidified forerunners, both of which features are clearly evident in the photograph of restricted flow in Fig.(117) (NOTE: the gate size for the experimental casting and for C6 were the same i.e. 25.4 mm x .635 mm, 1" x .025".) Fig. (119) shows the accentuation by the parallel boundaries of 'explosive' effects in the flow as compared with unrestricted flow.

12.2 EFFECT OF BOUNDARY OBSTRUCTION PERPENDICULAR TO MEAN FLOW DIRECTION FROM GATE.

In this test series the flow obstruction was provided by a flat plate clamped on to ground spacers and projecting over the gate exit. A locating lip existed on the die block surface and in order that the general flow regime would not be affected by this it was decided to restrict the gap between gate exit and impingement surface to a range 0-lip height so that the lip acted at all gap sizes as an extra limiting boundary. The range of free flow distance to impingement was thus 0-3.175 mm (.125"). The spacers were set a standard distance apart (76.2 mm, 3") so that both 25.4 mm (1") and 76.2 mm(3") wide gates could be tested. The arrangement is shown diagrammatically in Fig. (120). As in the previous tests flow was examined through a number of runner:gate combinations for a range of gap widths. Recordings of runner pressures and piston velocity were made and photographs taken of flow out of

the gap between the impingement surface and the die block.

These were then assessed in relation to flow in the unrestricted systems.

For gates of the same width as the impingement gap (i.e. 3", 76.2 mm) the deflected jet showed an increase in turbulence and spread for the larger gap areas. As this approached or went below the gate area the flow, although biased through 90° in the choked systems, closely resembled the unrestricted flow pattern, whilst for unchoked systems the flow became more ordered than the originally unrestricted flow had been.

Where gate widths were significantly less than the gap width (i.e. for 25.4 mm, 1" gates) there was a very considerable increase in jet spread, turbulence, and breakdown after impingement for the larger gap areas. As the gap size approached that of the gate both choked and unchoked systems became considerably more ordered although bearing no relation to the unrestricted flow regime. At the smaller gap sizes the deflected jet emerged from the gap of equal width to the gap and of general appearance similar to that noted for unrestricted flow through choked 76.2 mm (3") gates.

Fig. (121) illustrates the above for runner:gate combination C6. It can be seen that for the larger gap sizes the jet, originally 25.4 mm (1") wide is very considerably modified with a central flow 'core' at 90° to the original flow line surrounded by a considerable amount of divergent spray. As gap area drops below that of the gate the flow can be seen to be much more ordered

and although more 'point source' in its nature shows much similarity with, for example, runner: gate combination C1 (Fig.(107)).

It was found that piston velocity and runner pressure were unaffected by the presence of an obstacle in the free jet flow path for impingement distances greater than 2.54 mm (1") for all gates tested but were considerably modified as gap thickness went below this as is shown by the trace record illustrated in Fig.(121) for C6. It is clear from this that where an obstruction in a cavity is below a certain critical distance from the gate significant resistance is created in the cavity which may approach or exceed that of the gate itself. Clearly this cannot be ignored in flow calculations. As an illustration, Fig. (122) shows the effect upon system efficiency as gap thickness is reduced. Initially, at 2.16 mm (.085"), efficiency is almost unaffected. As the gap reduced the zone immediately outside the gate represented an additional unchoked resistive region and efficiency drops until the gap area becomes less than that of the gate and the region becomes choked. At this point there is a significant rise in efficiency albeit to a value which is still significantly less than for the unrestricted gate (see Fig. (122)). The efficiency of the smallest gap size was checked by recalculating the overall system efficiency from 9.4. The asterisk on the figure indicates the calculated value, which agrees well with that measured.

12.3 CONCLUSIONS

The cavity studies, although limited in their scope provided useful information i.e.

(i) Flow rates (into a cavity) are not influenced by jet contact with boundary surfaces parallel to the mean flow plane and are only influenced by obstacles in the flow path if they are less than a certain critical distance from the gate, which, for the gates tested was 2.54 mm (1"). This confirms the test results of section (6), where curves calculated on the basis of zero cavity resistance (other than back pressure due to entrapped gases) agreed very closely with test results.

(ii) Flow patterns and flow breakdown are significantly influenced by cavity boundaries. Boundaries parallel to the mean flow plane through the gate modify the jet form, causing spreading as the jet contacts them, tending also to reduce breakdown due to air entrainment. Obstructions in the line of flow cause considerable turbulence and breakdown unless local resistance is very high.

It is interesting to note in passing that the test results of 11 and 12 offer both an explanation of the differences between Brandt⁽²³⁾ and Frommers⁽⁹⁾ view of cavity flow and also a modification to the general Frommer theory. The gate systems examined in Section 11 showed considerable jet expansion and breakdown could take place with certain gating configurations, which could account for Brandt's results. The tests of 12.1 show that for Frommers view of cavity feeding pattern due to an originally parallel jet to be valid the cavity depth must be significantly greater than that of the gate.

13. GENERAL CONCLUSIONS.

13.1 DEVELOPMENT OF ANALYSIS

A body of analysis covering those flow features considered to influence casting quality has been developed (Section 3). This forms an adequate frame of reference for the development of coherent experimental studies of machine: mould relationships in the diecasting process.

13.2 APPLICATION OF ANALYSIS

The application of the analysis requires information upon resistance and inertial factors of machines and of moulds. The factors for machine injection systems and for the fixed element of the metal system must be derived experimentally. The experimental approach is outlined in Section 6. A loss coefficient equation developed in Section 9 compares favourably with published information and allows resistance coefficients for moulds to be calculated.

13.3 STUDIES OF TRANSITION FROM UNSTEADY TO STEADY FLOW IN GENERAL DIECASTING SYSTEMS.

13.3.1 RATE OF FLOW (METAL)

Ideal filling conditions (optimum venting, zero cavity resistance).

(i) The piston velocity characteristic is a function of the resistance and inertia factors for the system

(ii) The shape of the piston velocity characteristic during runner:cavity filling is significantly influenced by the point on the piston 'free running' velocity curve at which filling is initiated.

(iii) Where piston velocity at changeover (fill initiation) position coincides with the steady state filling velocity for the machine:mould combination, filling will be completely steady.

(iv) The further changeover is from this(nodal) position then the greater the magnitude of velocity change during transition to steady conditions.

(v) The length of transition period is dependant upon the ratio of system resistance to inertia factor.

(vi) The form of a piston (filling) velocity curve is not unique to one set of conditions.

Non-ideal filling conditions (zero venting and/or cavity resistance).

(vii) Gas back pressure in the cavity does not significantly influence piston velocity until the last 10% or less of the filling stroke.

(viii) When machine resistance factor is large in relation to metal system resistance and its variation, the influence of such variation upon filling rate is negligible.

(ix) Cavity boundaries parallel to the mean plane from the gate may modify flow pattern but offer negligible resistance to flow.

(x) Obstacles to flow, adjacent to the gate can generate significant resistance to flow.

13.3.2 RATE OF FLOW (GAS VENTING)

(xi) Optimum vent size requirements for steady state and for unsteady filling conditions differ only as the ratio of steady state to average piston velocity.

(xii) Where machine resistance factor is small in relation to a spectrum of gate resistance then optimum vent size requirement varies with that spectrum. Where the converse is true than vent size is essentially independant of gate size variation.

13.3.3 ENERGY RATE

Energy rates being a function of piston velocity are sensitive to the same variables of resistance, inertia factors, changeover position etc.

(xiii) For conditions where initial energy rates are high relative to steady values there is some evidence to suggest that the mechanism of cavitation may exist during transition.

(xiv) The maximum total rate of energy input to a metal system for a fixed net drive force is independant of metal piston and runner area.

(xv) Gate size for maximum rate of energy input to the metal in the cavity and for maximum rate of energy dissipation at the gate are not the same.

(xvi) Frictional reheating of metal flowing into the cavity; will not compensate for heat loss during the long transmission times associated with highly restricted gates.

(xvii) The quantity of (mechanical) energy required to fill a cavity varies as the thermal condition of the casting metal.

13.3.4 STATE OF FLOW

The use of Weber number for assessing flow state through the gate allowed certain conclusions to be drawn from application of analysis to general systems.

(xviii) Machine:mould combinations to ensure maximum or minimum values of Weber number during flow may be predicted.

(xix) Gate size for maximum Weber number values during flow does not necessarily coincide with that for maximum energy rates.

(xx) Changeover piston velocities greater than the nodal value for a given gate can lead to conditions during transition in which both spray and solid front flow take place.

(xxi) Experimental studies show that the flow state criteria used has the best correlation with runner:gate systems in which the runner:gate width ratio is 1:1.

(xxii) There is some experimental evidence to suggest that average droplet diameter in conditions of flow breakdown approximate to the gate thickness.

(xxiii) State of flow through a system can be dramatically influenced by the presence of large masses of air/gas in the system during flow.

14. FUTURE WORK.

14.1 Piston velocity characteristics measured on the experimental diecasting machine showed good agreement with analytical prediction. For the conclusions drawn from the analytical examination reported in Section 4 to be acceptable it is necessary that this degree of correlation is seen to be representative. The tests reported in Section 6 should therefore be repeated on a larger scale using a range of diecasting machines.

14.2 The water flow rig employed in the study was not suitable for quantitative studies of transition effects (see Section 8). A further programme of work is therefore necessary.

- a) to examine the relationship between energy-rates and cavitation and to determine whether cavitation is largely a transition phenomena and therefore avoidable,
- b) to define quantitatively the relationship between Weber number and flow breakdown.

A suitable flow rig is required for this purpose and the examination should initially be carried out for infinite cavity conditions, (i.e. free flow from the gate), to enable machine: gate influence to be isolated.

14.3 The tests of Section 12 indicated the degree of influence cavity boundaries could have, both upon flow state and flow rate. It is important therefore that a study of transition

and steady flow effect (14.2) should be followed by an examination of cavity influence along the lines suggested by Section 12. In this way cavity influence could be examined in the context of the analytical framework and modifications made where necessary to that framework.

14.4 The practical extension to the work reported in this thesis and to that proposed in 14.1 - 14.3 is to design a prototype injection system embodying the conclusions drawn from this work (and also taking into account problems due to certain transient phenomena reported in 11.2). This design should then logically be realized in the manufacture of a prototype injection system, and results of field tests on this would be the ultimate justification of the work.

REFERENCES

1. A F S, A A F, Casting Design Handbook, McGraw-Hill 1962
2. Nussey, I D, Kondic, V, Metallurgia, Sept 1964, pp 101-109
Oct 1964, pp 165-171
3. Draper, A B, Trans A F S, 1967, 76, pp 727-734
4. Chzhu, Sen-Yuan, Russian Castings Production, Jan 1961, pp 30-32
5. Pokornyy, H H, Technical Paper No 52, 5th National Diecasting Congress, Detroit, Michigan, 1968, Nov 4-7
6. Ambos, E, Technical Paper No 55, 5th National Diecasting Congress, Detroit, Michigan, 1968, Nov 4-7
7. Plyatskii, V M, Russian Castings Production, Jan 1961, 6
8. Kopf, J, Technical Paper No 11, 5th National Diecasting Congress, Detroit, Michigan, 1968, Nov 4-7
9. Frommer, L, Handbuk der Spritzgusstechnik, Springer, Berling, 1933, 633
10. Jacobi, E, ASTM Bulletin, 1950, 166, 127
11. Uehara, T, Technical Paper No 14, 5th National Diecasting Congress, Detroit, Michigan, 1968, Nov 4-7
12. Sachs, B, ASTM Bulletin, 1953, 192, 27
13. Veinik, A I, Theory of Special Casting Methods, Maschgis, Moscow, 1958, pp 143-242
14. Draper, A B, Peikart, F W, Technical Paper B-12, 2nd National Diecasting Congress, 1965
15. Barton, H K, Foundry, July 1963, 91, 75
16. Rearwin, E W, Foundry, Nov 1960, 88, 106
17. Ryzhikov, A A, Zlotin, S Z, Russian Castings Production, March 1965, 113
18. Belov, M, Gassel, K N, Kogan, M G, Foundry, Sept 1968, 96, 172-178
19. Nussey, I D, PhD Thesis, University of Birmingham 1962

20. Belopukov, A K, Lit Proiz, 1958, (7), 3
21. Barton, H K, Metal Industry, Feb 1952, 80, 149
22. Stuhrike, W F, Trans AFS, 1965, 73, 594
Wallace, J F,
23. Brandt, W R, Machinery, Aug 1938, 52, 87
Machinery, Nov 1938, 53, 1
24. Babington, W, ASTM Proc, 1951, 51, 169
Kleppinger, S H,
25. Overas, A S, Badone, L, Foundry, March 1965, 93, 124
26. Sanders, D S, Trans Soc Diecasting Engineers
Kaiser, W D, 6th National Congress, 1970, Paper 51
27. Booth, S E, Aluminium, June 1973, 49, (6), 410
28. Bennett, F C, Foundry, Nov 1961, 89, (11), 105
29. Koster, W, Gohring, K, Die Giessereie, Dec 1941, 28, 521
30. Smith, W E, Modern Castings, 1963, 44, 325
Wallace, J F,
31. Akademischer Verein "Huette", des Ingenieurs Taschenbuch
Huette, 1, Band, 1936
32. Lowry, H V, Hadyn, H A, Advanced Mathematics for Technical
Students, Longmans, Green and Co, 1955
33. Walshaw, A C, Applied Thermodynamics,
Blackie and Son Ltd, 1951
34. Maiden, J D, Confidential Report,
Joseph Lucas Research Centre.
35. Rouse, H, Engineering Hydraulics,
Wiley and Sons, 1949
36. Addison, H, A Treatise on Applied Hydraulics
Chapman and Hall, 1954
37. Daugherty, R L, Fluid Mechanics with Engineering
Franzini, J B, Applications, McGraw-Hill, 1965
38. Luis, L, Draper, A, Modern Casting, June 1966, 49, (6),
163
39. Ryzhikov, A A, Russian Castings Production, March
Zlotin, S Z, 1965, pp 113-114
40. Belopukhov, A, K, Russian Castings Production, March
Korotkov, R A, 1969, pp 121-122.

41. Perkins, N D, Bain, C J, Journal Australian Inst of Metals,
May 1965, 10, (2), pp 161-168
42. Dailey, J W, Trans ASME, 76, 1071
Deemer, K S,

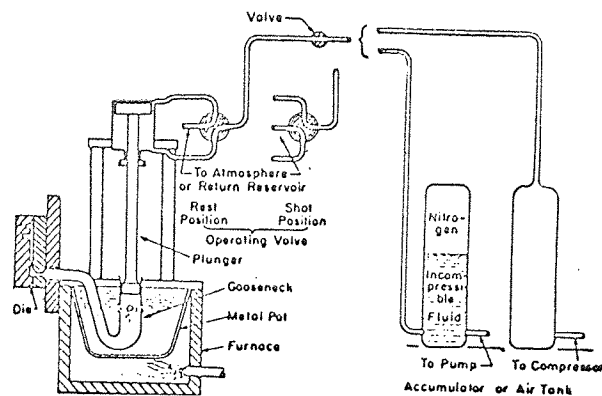


FIG 1 (a) Injection system hot chamber diecasting machine

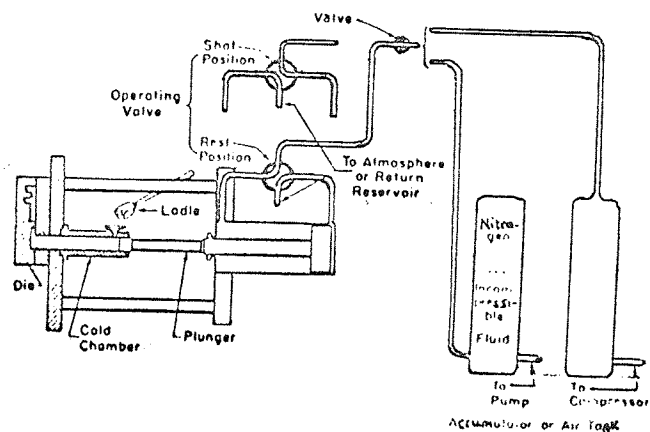
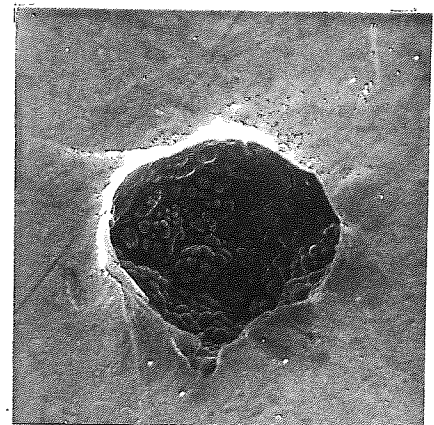
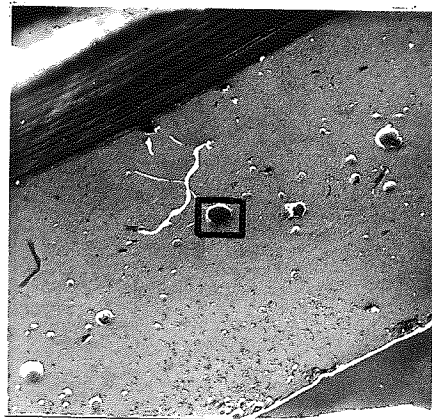


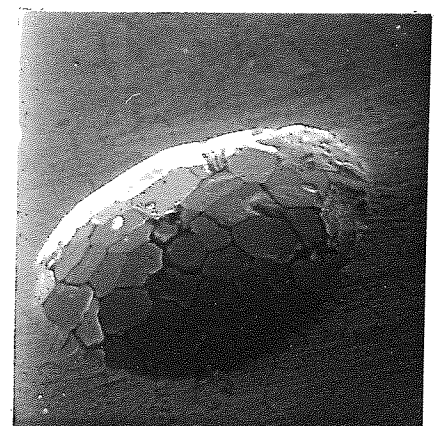
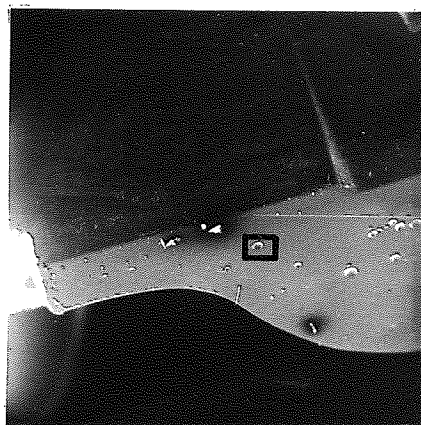
FIG 1 (b) Injection system cold chamber diecasting machine



FIG 2 POOR FINISH DUE TO FLOW BREAKDOWN



a) SOLIDIFICATION POROSITY



b) AIR ENTRAPMENT AT CASTING GATE

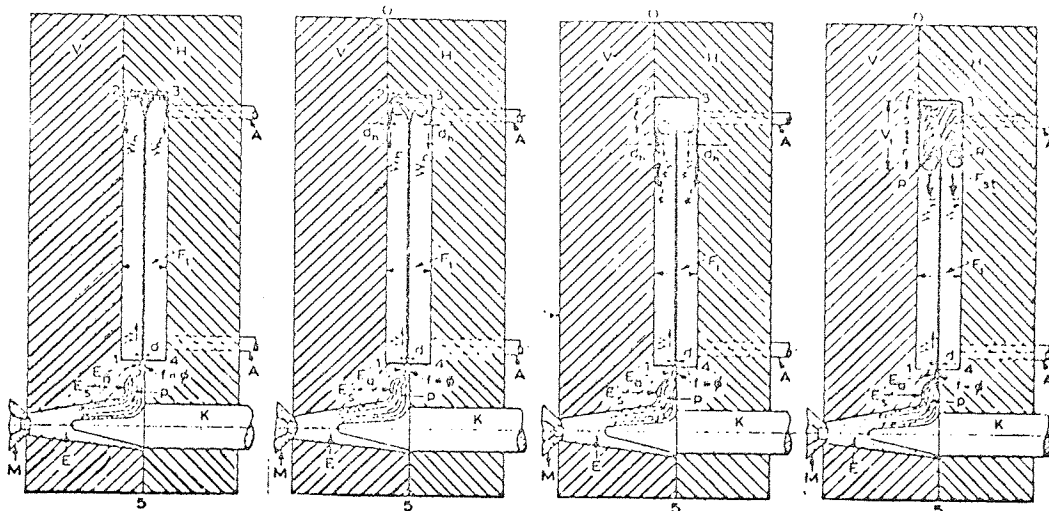


FIG 4 Filling stages of rectangular cavity.
 (after Frommer⁹)

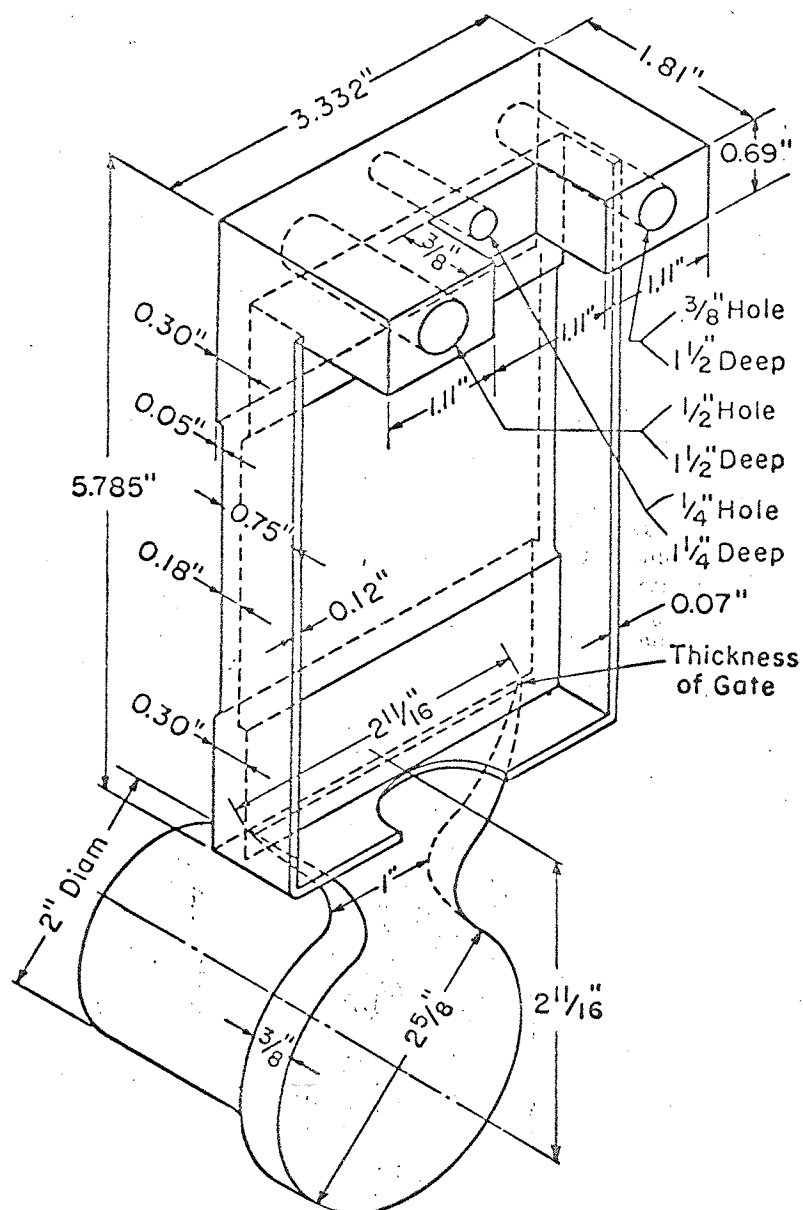


FIG 5 B-6 Test Shape

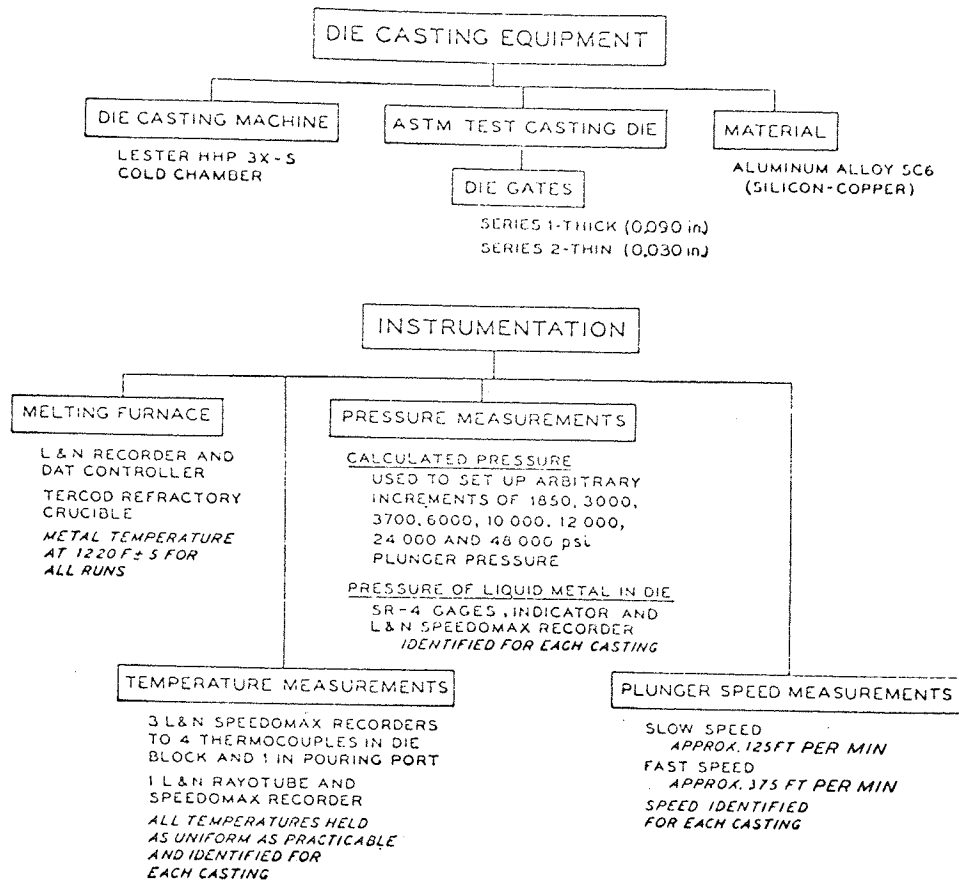


FIG 6 After Babington and Kleppinger (24)

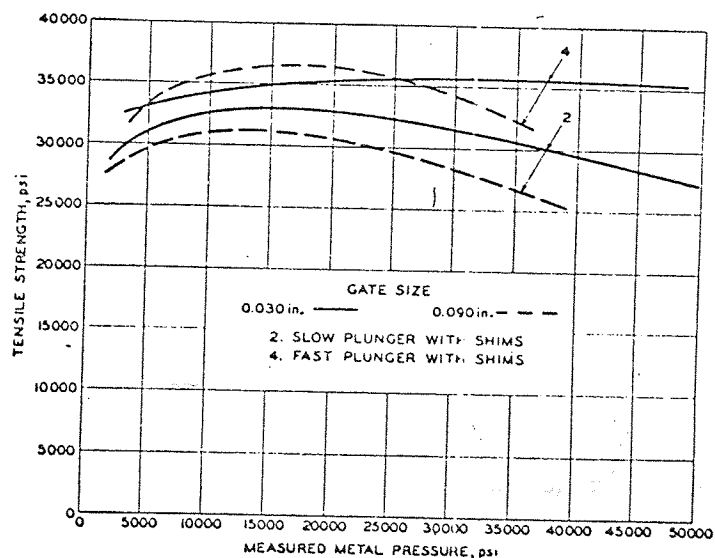


FIG 7 After Babington and Kleppinger (24)

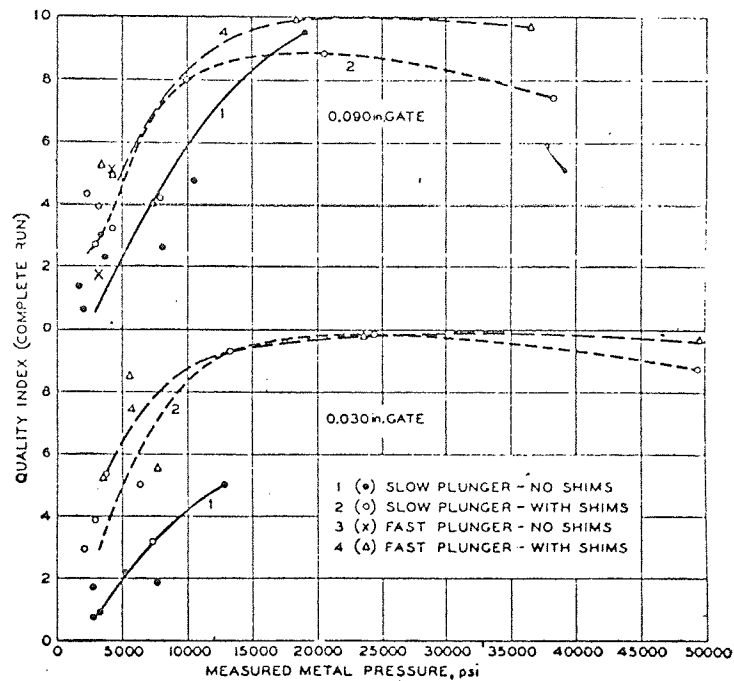


FIG 8 After Babington and Kleppinger (24)

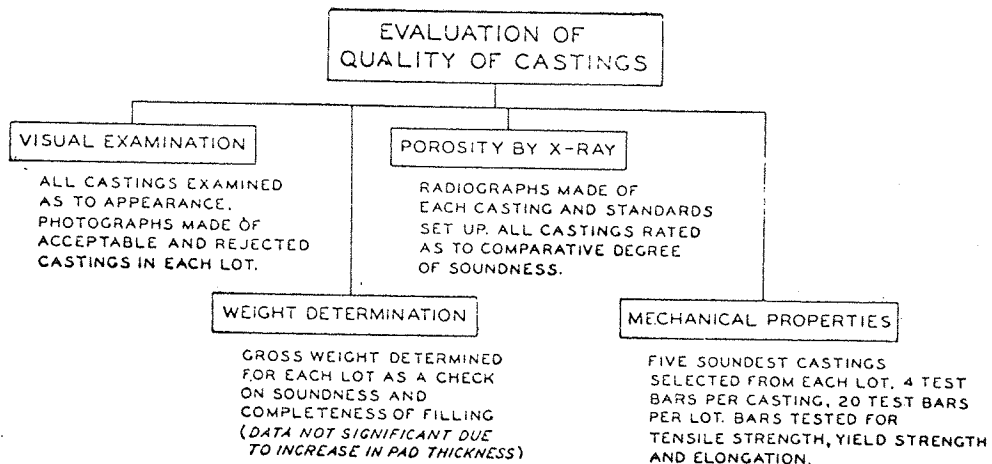


Fig 9 After Babington and Kleppinger (24)

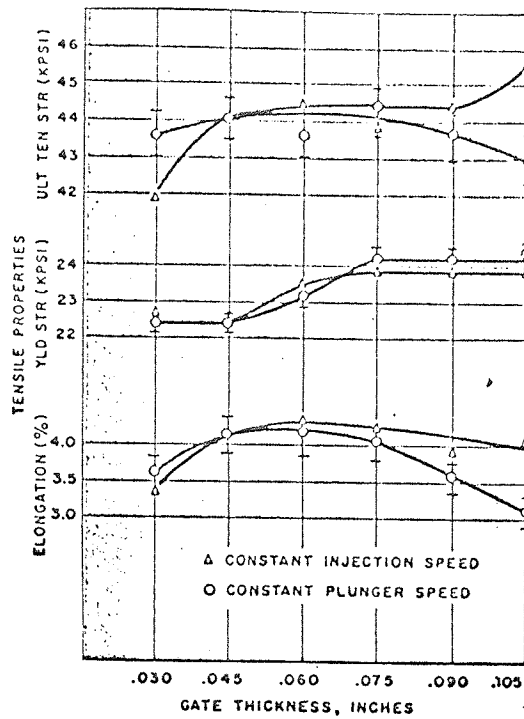


FIG 10 After Overas and Badone⁽²⁵⁾

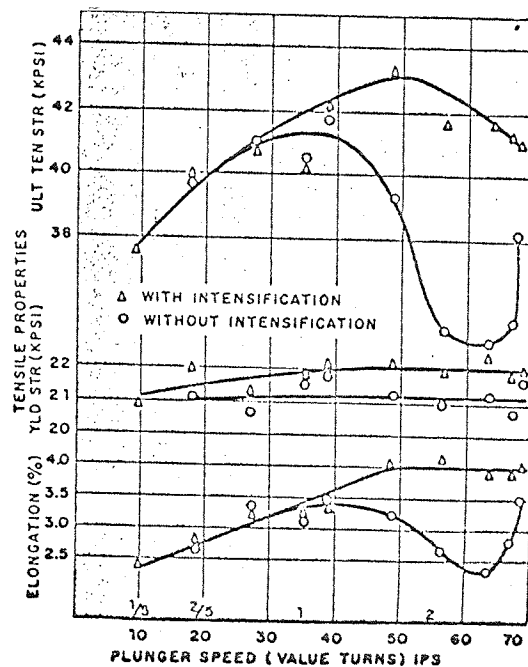


FIG 11 After Overas and Badone⁽²⁵⁾

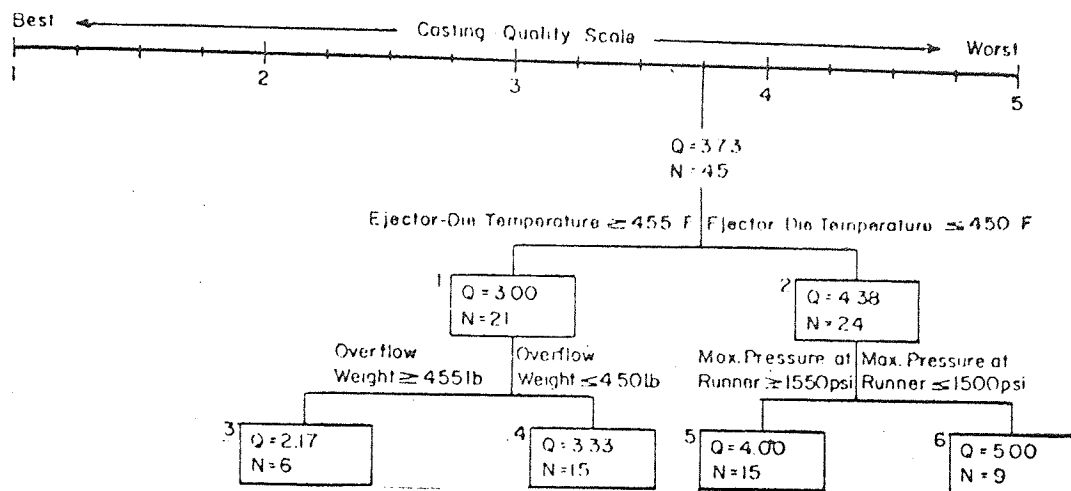
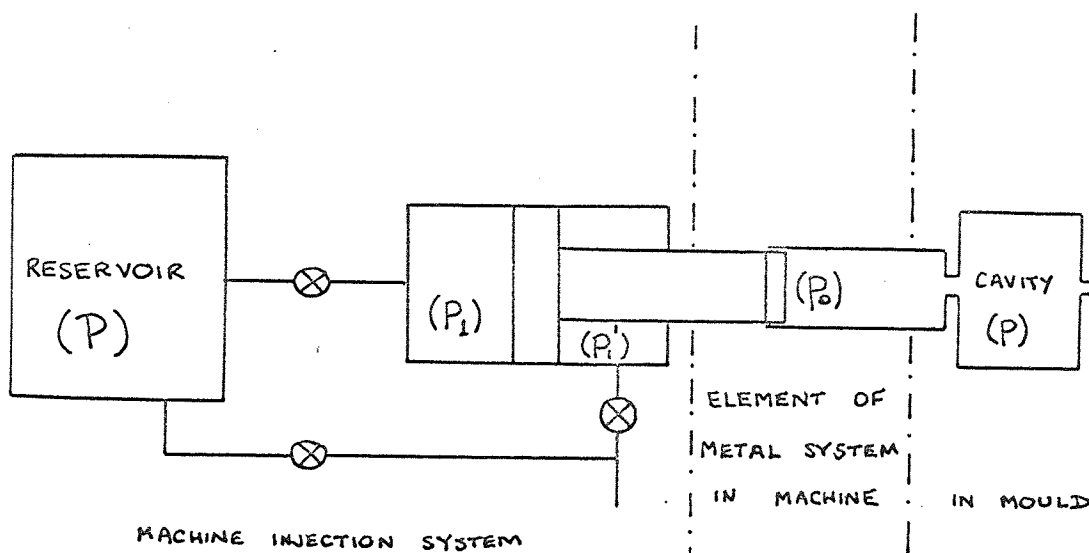


FIG 12

After Sanders (26)



AREA OF DRIVE CYLINDER PISTON = f_k

AREA OF METAL SYSTEM PISTON = f_o

PRESSURE IN RESERVOIR = P

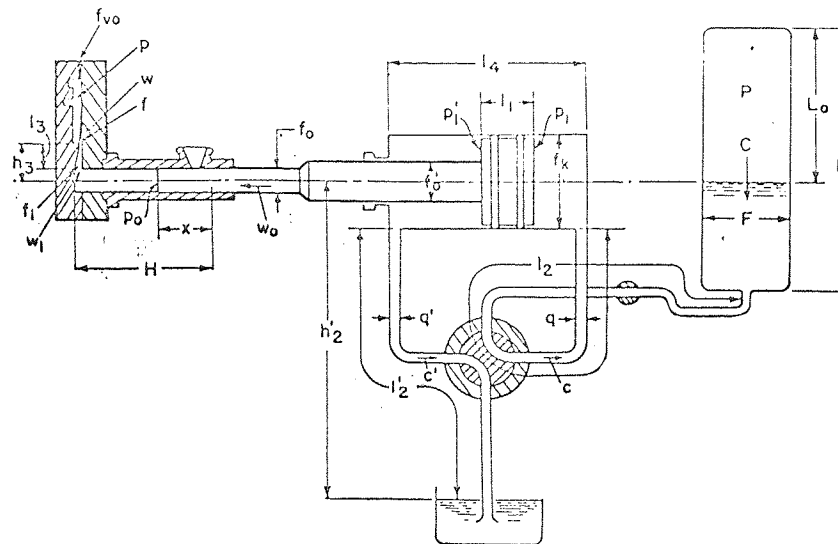
PRESSURE IN DRIVE SIDE OF DRIVE CYLINDER = P_i

" " EXHAUST " " " = P'

" " METAL SYSTEM = P_o

" " CAVITY = P

FIG 13 Diagrammatic representation of diecasting system



—Cold-Chamber Machine Setup.

- | | |
|---|---|
| x = plunger displacement at time t , measured from plunger start $x = 0, t = 0$ | L_0 = height of nitrogen in accumulator at $t = 0$ |
| F = area of accumulator | l_2 = length of drive pipe line |
| f_k = area of piston | l_1' = length of return pipe line |
| f_0' = area of piston rod | l_1 = length of piston |
| f_0 = area of plunger | l_2 = length of gate |
| f_1 = area of gate entrance | l_4 = length of cylinder |
| f_2 = area of gate exit | h_2' = height of plunger axis above reservoir level |
| f_3 = area of vent slots in die | h_1 = height of gate exit above plunger axis |
| f_4 = area of drive pipe line | H = distance of plunger at $x = 0$ to ejector half of die |
| q' = area of return pipe line | C = velocity of drive fluid in accumulator |
| P = pressure in accumulator | c = velocity of drive fluid in drive pipe line |
| p_1 = pressure on piston area f_k | c' = velocity of drive fluid in return pipe line |
| p_1' = pressure on piston area $(f_k - f_0')$ | w_0 = velocity of piston |
| p_0 = pressure on plunger area f_0 | w_1 = velocity of metal in gate entrance |
| p = pressure of air in die cavity | w = velocity of metal in gate exit |
| L = length of accumulator | |

FIG 14

After Sachs⁽¹²⁾

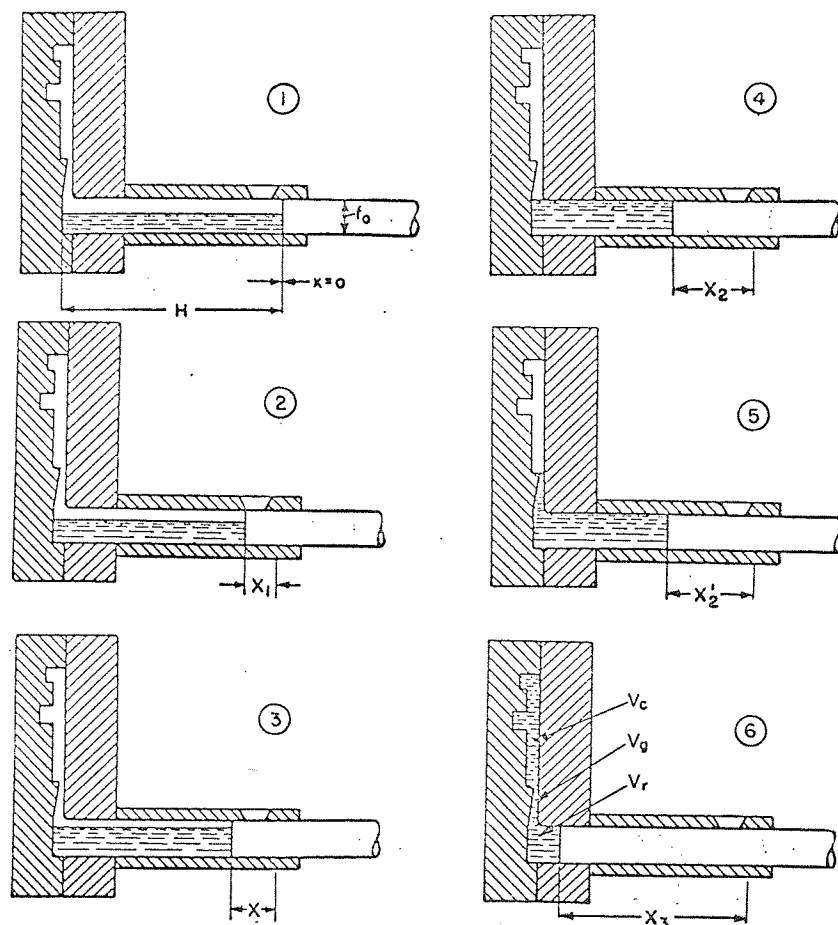


FIG 15 Stages in die filling (after Sachs¹²⁾)

FIG 16 CONTINUED ::

STAGE 1 ($0 < x \leq x_1$)

$$Q = \text{NET DRIVE FORCE} = f_k \cdot P - (F_1 + F_2), \quad f_k = \text{piston area}, \quad P = \text{reservoir pressure}, \quad F_{1,2} = \text{friction effects}$$

$$C_1 = \text{MACHINE RESISTANCE FACTOR} = \frac{\sum f_k}{2g} \cdot \frac{1}{q^{\frac{1}{2}}} \cdot \left[\frac{f^3}{k} \cdot K_D + (1+K_E) \left(\frac{f}{k} - f_0 \right) \right]$$

q_i = mean pipe area (see FIG 14), f_o = metal piston area (fig 14)

$$K_D = \text{loss coefficient for drive side of injection system}$$

exhaust

 $\gamma_i =$ weight density of drive fluid

$$Q_1 = \text{MACHINE INERTIAL FACTOR} = \left[\frac{8}{9} \cdot \frac{1}{9} \cdot \frac{1}{9} \cdot [(f_k - f_o)^2 \ell_2' + f_k^2 \ell_2] \right] + \frac{G}{G_1}$$

L_2	= effective pipe length for drive side of injection system	Fig 14
L'_2	" " " exhaust "	"

$G = \text{weight of moving parts of injection system}$

C_R = ADDITIONAL WEIGHTING RESISTANCE FACTOR DUE TO DAMPER

$$A'_i = 2Q / [2c_i x_i + a_i] \quad , \quad A'_i = Q / c_i \quad , \quad D'_i = 2c'_i / a_i \quad , \quad c'_i = (c_i + c_e)$$

FIG 16 CONTINUED : IDENTIFICATION OF SYMBOLS

STAGE 2 ($x_1 < x \leq x_2$)

IS IDENTIFIED AS THAT STAGE OF PISTON MOVEMENT DURING WHICH DANGER OPERATION IS DISCONTINUED, LASTING UNTIL THE MOLTEN METAL REACHES RUNNER: GATE ENTRANCE (PISTON POSITION x_2)

$$A_2 = Q/C_1, B_2 = [(V_{x_1})^2 - A_2], D_2 = 2C_1/a_1$$

V_{x_1} = piston velocity at the initiation of stage 2

STAGE 3 ($x_2 < x \leq x_3$)

THAT STAGE OF PISTON MOVEMENT COVERING CAVITY FILLING DURING THIS STAGE METAL SYSTEM RESISTANCE COMES INTO PLAY

$$Q' = Q - P_b \cdot f_o, C_{M3} = \text{METAL SYSTEM RESISTANCE FACTOR} = \frac{\gamma_L \cdot (f_o)^3 \cdot (1 + K_M)}{2g \cdot f_o^2}$$

P_b = gas back pressure in cavity

γ_L = weight density of casting alloy

f_o = gate area

K_M = loss coefficient for metal system

$$C_3 = \text{TOTAL SYSTEM RESISTANCE FACTOR} = C_1 + C_{M3}$$

$$Q_{M3} = \text{METAL SYSTEM INERTIAL FACTOR} = \frac{\gamma_L \cdot f_o}{g} [H - x_2]$$

$$Q_3 = \text{TOTAL SYSTEM INERTIAL FACTOR} = Q_1 + Q_{M3}$$

$$A_3 = Q'/C_3, B_3 = [(A_2 - A_3) + B_2 \cdot e^{D_2(x_1 - x_2)}], D_3 = 2C_3/a_3$$

NOTE : IN THE TABLE THE EQUATIONS HAVE BEEN PRESENTED FOR THREE STAGES OF PISTON MOVEMENT. IT CAN BE SEEN THAT THIS SYSTEM IS CAPABLE OF FURTHER SUBDIVISION IF NECESSARY

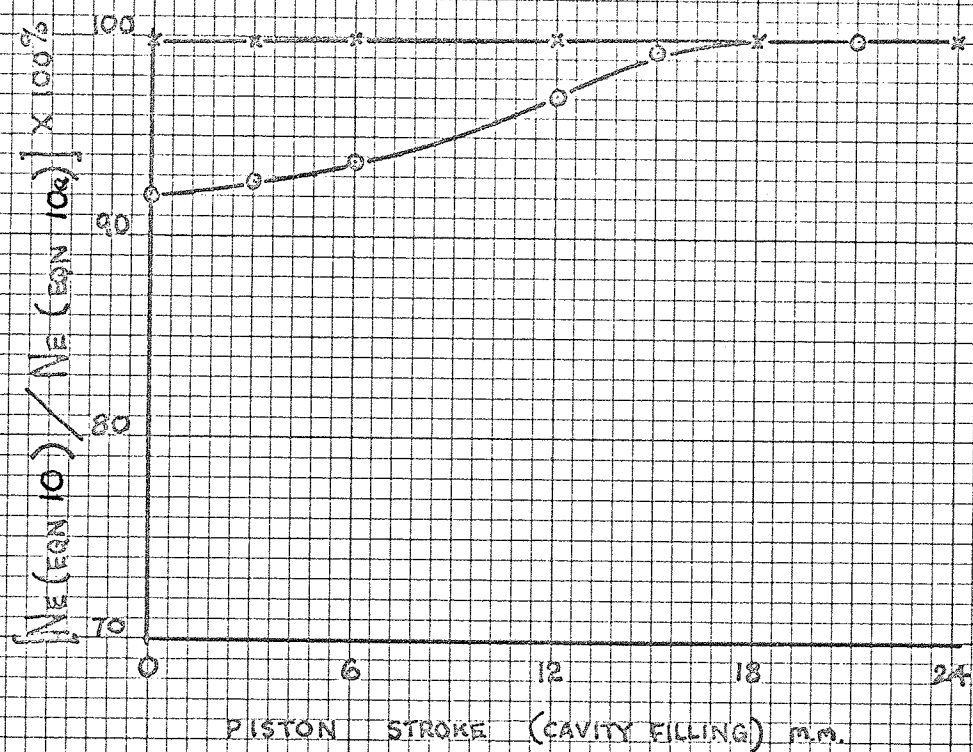


FIG 17 ENERGY RATIO vs. PISTON STROKE

F18 TABLE 3 DETAILS OF DIECASTING MACHINE RANGE

MACHINE NUMBER	DRIVING AGENT	ACCUMULATOR/RESERVOIR PRESSURE [$N/m^2 \times 0.0015$]	LENGTH OF PIPELINE (m. x 3.28)		PIPE/PISTON DIAMETERS (cms x .155)				WT. OF METAL PARTS (N. x .225)	STATIC PRESSURE ON METAL [$N/m^2 \times .00015$]	DRIVE CIRCUIT LOSS COEFFICIENT (K)	EXHAUST CIRCUIT LOSS COEFFICIENT (K')	MACHINE LOSS FACTOR C_L [$N.scc/m^2 \times .021$]	MACHINE INERTIA FACTOR a_i [$N.scc/m^2 \times .069$]
			DRIVE	RETURN	PIPES	PISTON	PISTON ROD	COLD CHAMBER						
1	OIL	2000	13	13	2	4	2 $\frac{3}{4}$	2	85	8000	52	48	83.2	13.8
1A	"	1000	13	13	2	4	2 $\frac{3}{4}$	2	85	4000	52	48	83.2	13.8
2	"	1000	13	13	1 $\frac{1}{4}$	4	2 $\frac{3}{4}$	2	85	4000	53.5	49.5	581.0	31.6
3	"	1000	13	13	1 $\frac{1}{4}$	5	2 $\frac{3}{4}$	2	100	6250	53.2	49.5	2580.0	86.1
4	"	1000	13	13	2	6	2 $\frac{3}{4}$	2	120	9000	52.2	48.2	1260.0	75.5
5	AIR	1000	13	13	2	4	2 $\frac{3}{4}$	2	85	4000	52	48.0	2.87	3.02
6	"	1000	13	13	1 $\frac{1}{4}$	4	2 $\frac{3}{4}$	2	85	4000	53.5	49.5	20.1	3.64
7	"	1000	13	13	1 $\frac{1}{4}$	5	2 $\frac{3}{4}$	2	100	6250	53.5	49.5	89.0	6.0

FIG 19 TABLE 4 (AFTER SACHS)

MACHINE NUMBER	GATE		STEADY STATE				TRANSIENT STATE					
	THICKNESS	AREA	OPTIMUM VENTING				OPTIMUM VENTING					
	m.m.	$(m.)^2 \times 10^4$	PISTON VELOCITY m. p.s.	FILLING TIME SECS.	VENT AREA $m.^2 \times 10^4$		PISTON VELOCITY AT x_1 (m.p.s.)	PISTON VELOCITY AT x_2 (m.p.s.)	TIME FOR PISTON TO REACH x_1 (SECS)	TIME FROM $x_1 \rightarrow x_2$ (SECS)	FILLING TIME (SECS)	VENT AREA $m.^2 \times 10^4$
1	.762	.52	2.20	.0390	.110			4.60			.0234	.420
	1.016	.68	2.55	.0335	.127		4.25	4.88	.0240	.0187	.0204	.446
	1.270	.86	2.74	.0311	.138			4.97			.0191	.453
	1.524	1.04	2.90	.0295	.145			5.08			.0186	.460
1A	AS	AS	1.56	.0510	.086		3.02	3.32	.0336	.0265	.0337	.303
	ABOVE	ABOVE	1.80	.0475	.099			3.44			.0289	.314
			1.90	.0438	.108			3.52			.0271	.321
			2.06	.0415	.113			3.57			.0261	.326
2	AS	AS	.82	.1065	.046		1.29	1.33	.0790	.0671	.0661	.121
	ABOVE	ABOVE	.85	.1050	.047			1.36			.0641	.124
			.87	.0985	.048			1.39			.0632	.127
			.87	.0980	.048			1.42			.0600	.129

TABLE 4 CONT.

3	.762 1.016 1.270 1.524	.52 .68 .86 1.04	.52 .53 .53 .53	.1625 .1620 .1610 .1610	.028 .028 .028 .028	.80	.83 .83 .83 .83	.1275 .1120	.1040 .1040 .1040 .1040	.076 .076 .076 .076
4	.762 1.016 1.270 1.524	.52 .68 .86 1.04	.88 .89 .90 .90	.0915 .0960 .0950 .0945	.043 .044 .044 .044	1.31	1.40 1.43 1.43 1.43	.0776 .0640	.0642 .0610 .0605 .0600	.128 .131 .131 .131
5	AS ABOVE	AS ABOVE	2.06 2.73 3.31 3.89	.0415 .0319 .0258 .0220	.113 .151 .182 .214	9.75	8.84 11.12 12.34 13.26	.0104 .0075	.0238 .0172 .0124 .0111	.805 1.022 1.124 1.208
6	AS ABOVE	AS ABOVE	1.91 2.41 2.82 3.00	.0448 .0355 .0302 .0285	.105 .133 .154 .164	6.07	4.85 5.88 6.31 6.61	.0168 .0131	.0270 .0212 .0183 .0164	.441 .537 .576 .604
7	AS ABOVE	AS ABOVE	1.94 2.26 2.39 2.50	.0440 .0378 .0357 .0341	.104 .120 .128 .133	4.1	3.60 3.96 4.11 4.21	.0247 .0206	.0276 .0241 .0225 .0216	.328 .360 .375 .383

FIG 20 TABLE 5 TABLE OF COMPARATIVE CALCULATIONS c.s. TABLE 4

MACHINE NUMBER	GATE		STEADY STATE				TRANSIENT STATE					
	THICKNESS	AREA $m^2 \times 10^4$	OPTIMUM VENTING				OPTIMUM VENTING					
			PISTON VELOCITY (m.p.s)	FILLING TIME SECS.	VENT AREA $m^2 \times 10^4$		PISTON VELOCITY AT x_1 (m.p.s.)	PISTON VELOCITY AT x_2 (m.p.s.)	TIME FOR PISTON TO REACH x_1 (SECS)	TIME FROM $x_1 \rightarrow x_2$ (SECS)	FILLING TIME (SECS)	VENT AREA $m^2 \times 10^4$
1	.762	.52	3.43	.0249	.313			4.57			.0235	.332
	1.016	.68	3.96	.0216	.361			4.88	.0243	.00191	.0204	.382
	1.270	.86	4.27	.0200	.385			4.88			.0192	.407
	1.524	1.04	4.51	.0189	.396			5.03			.0186	.420
1A	AS ABOVE	AS ABOVE	2.44	.0350	.223			3.08			.0342	.228
			2.81	.0304	.256			3.17	.0343	.00269	.0295	.264
			3.04	.0281	.278		3.02	3.22			.0278	.283
			3.19	.0267	.288			3.24			.0269	.290
2	AS ABOVE	AS ABOVE	1.28	.0664	.117			1.36			.0663	.118
			1.32	.0646	.124			1.37	.0750	.0067	.0640	.123
			1.35	.0630	.125		1.28	1.37			.0630	.125
			1.36	.0628	.129			1.37			.0610	.128

TABLE 5 CONT.

3	.762 1.016 1.270 1.524	.52 .68 .86 1.04	.81 .81 .81 .81	.1054 .1054 .1054 .1054	.074 .074 .074 .074	.80	.82 .82 .82 .82	.153 .00112	.1051 .1051 .1051 .1051	.074 .074 .074 .074
4	AS ABOVE	AS ABOVE	1.37 1.39 1.40 1.41	.0625 .0616 .0610 .0607	.124 .126 .127 .128	1.31	1.38 1.38 1.38 1.39	.079 .0066	.0625 .0615 .0609 .0607	.125 .126 .127 .128
5	AS ABOVE	AS ABOVE	3.20 4.26 5.18 6.04	.0267 .0200 .0165 .0142	.292 .401 .469 .550	9.81	7.77 8.50 9.20 9.66	.0106 .00067	.0254 .0169 .0155 .0132	.306 .413 .500 .590
6	AS ABOVE	AS ABOVE	2.98 3.75 4.36 4.86	.0287 .0227 .0196 .0176	.212 .341 .404 .446	6.07	4.82 5.85 6.19 6.49	.021 .0013	.0278 .0219 .0192 .0172	.280 .355 .413 .455
7	AS ABOVE	AS ABOVE	3.00 3.51 3.72 3.90	.0284 .0243 .0231 .0219	.274 .316 .333 .358	4.11	3.57 3.96 4.08 4.15	.0281 .0021	.0281 .0245 .0228 .0218	.278 .316 .344 .359

FIG 21

PISTON VELOCITY VS PISTON STROKE
FOR RANGE OF MACHINES

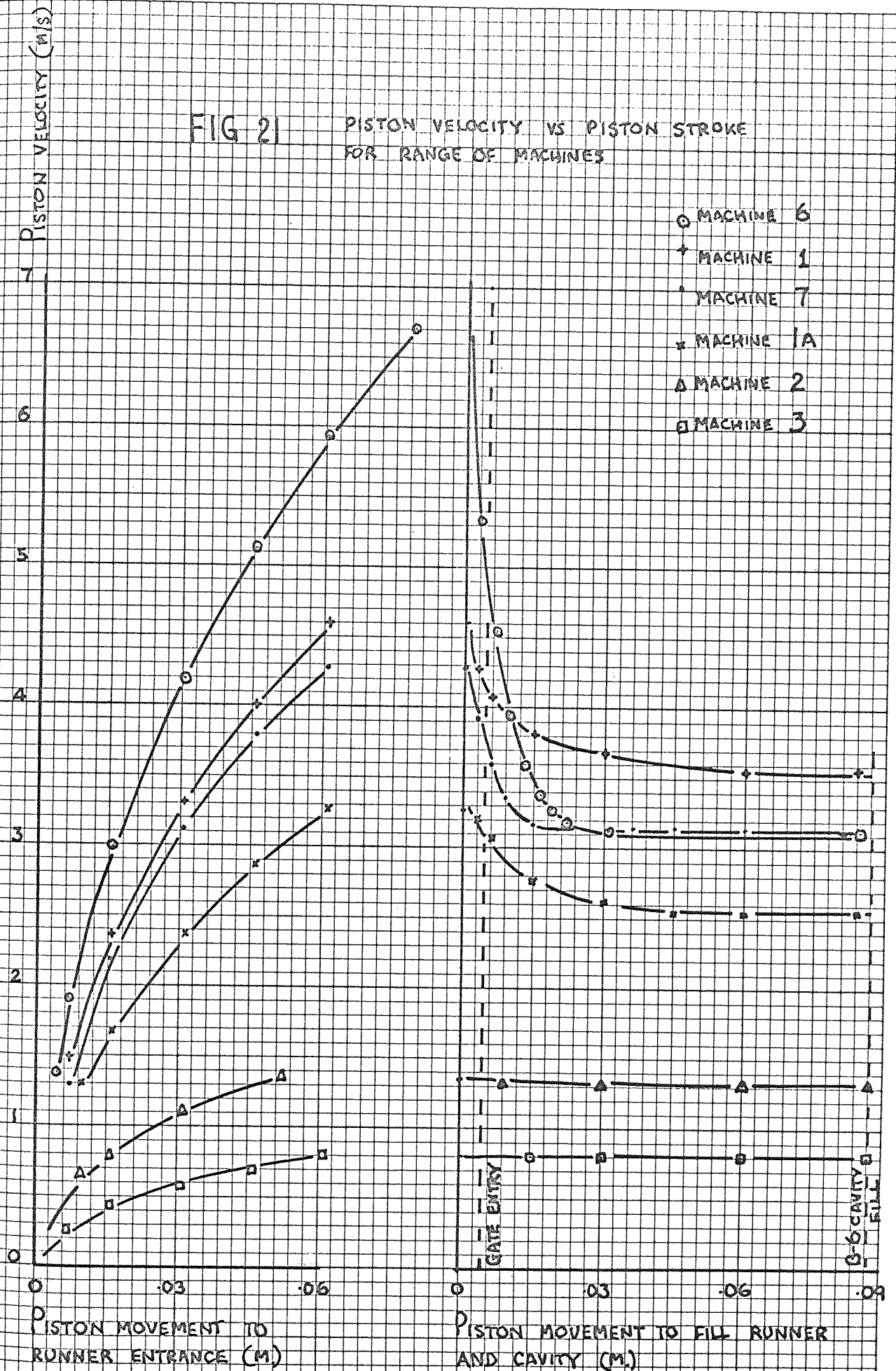


FIG 22

PISTON VELOCITY VS FILLING TIME
FOR B-6 TEST DIE ON RANGE OF
MACHINES

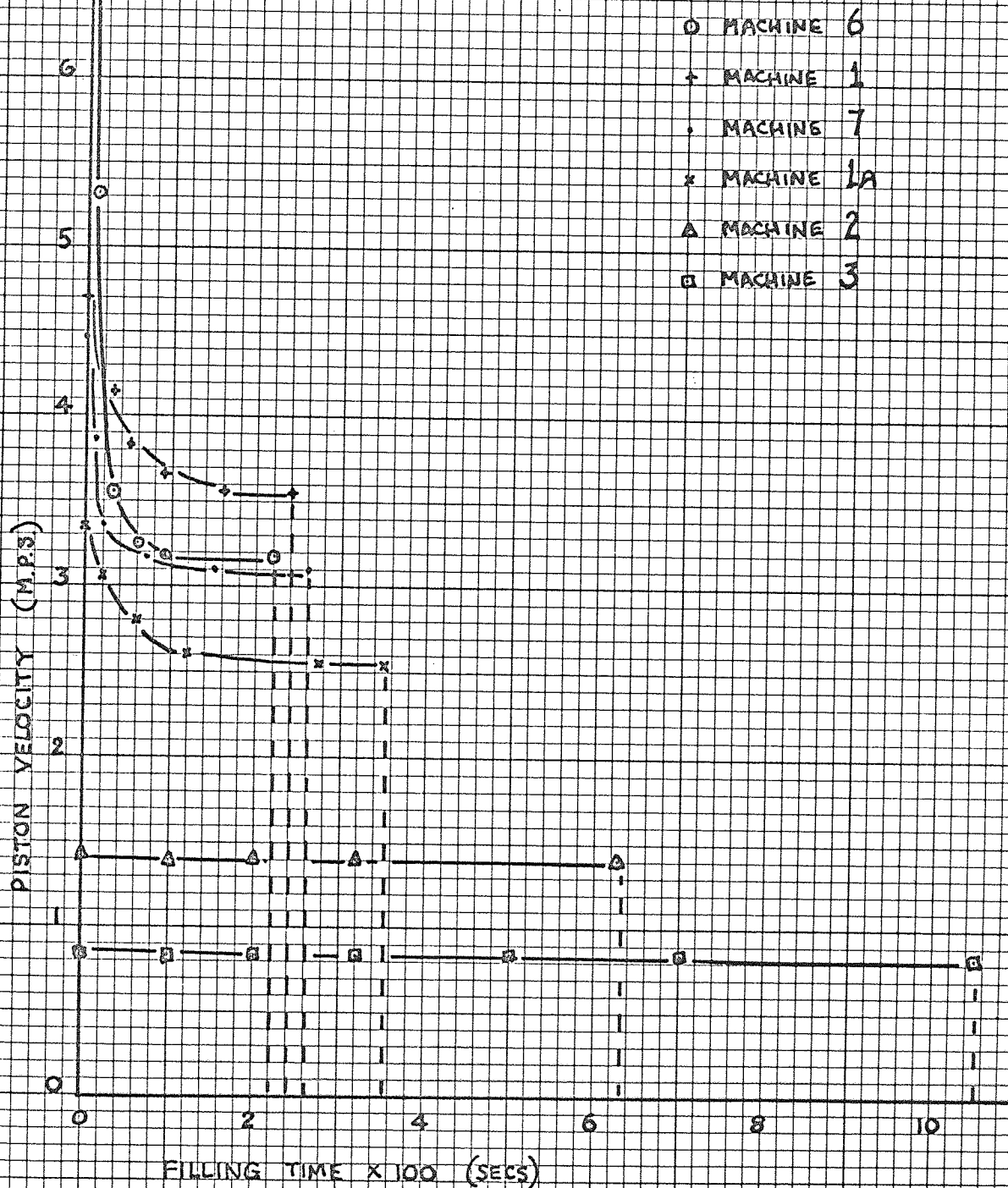


FIG 23 STEADY STATE VELOCITY ANALYSIS
FOR MACHINE 1A.

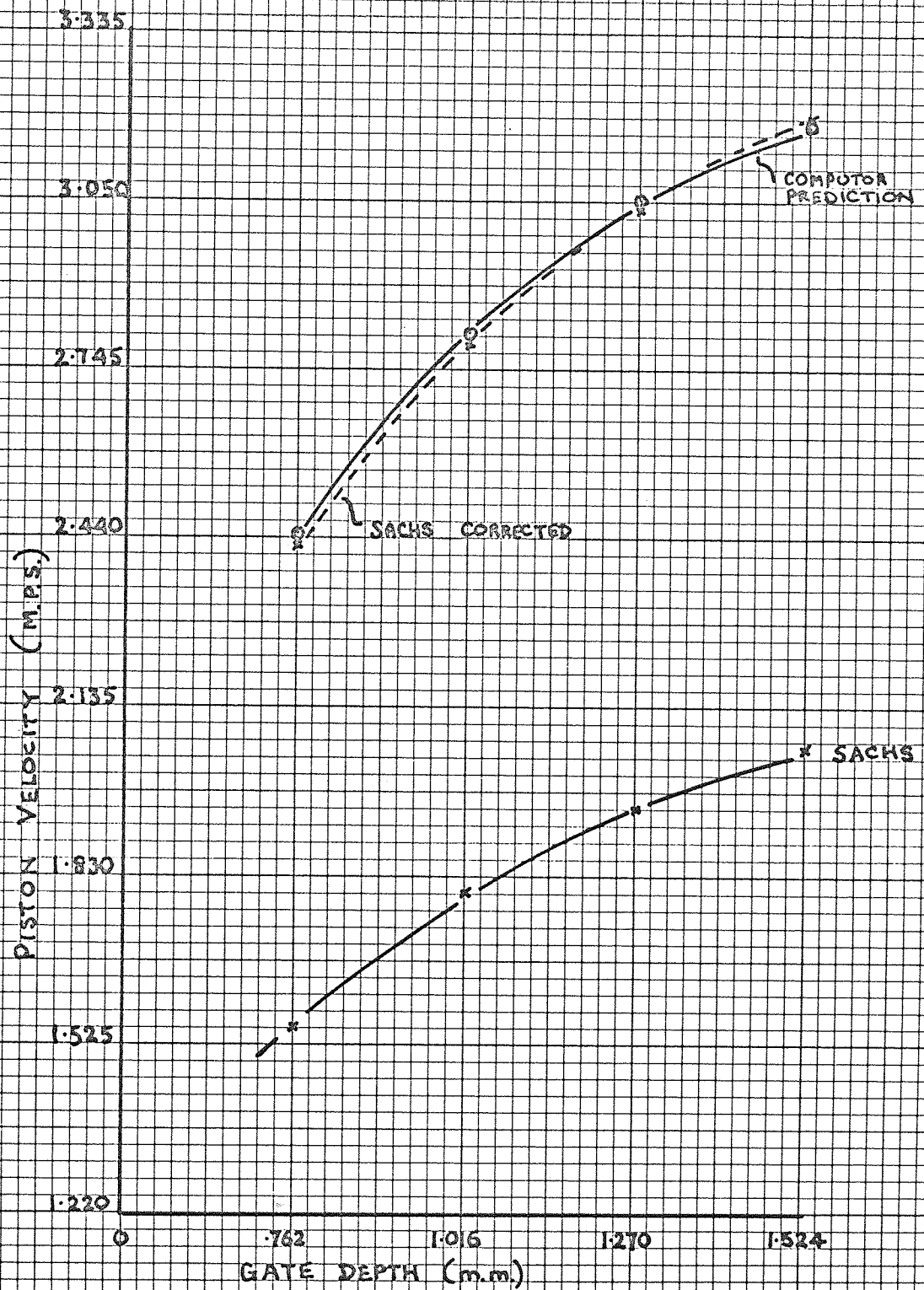
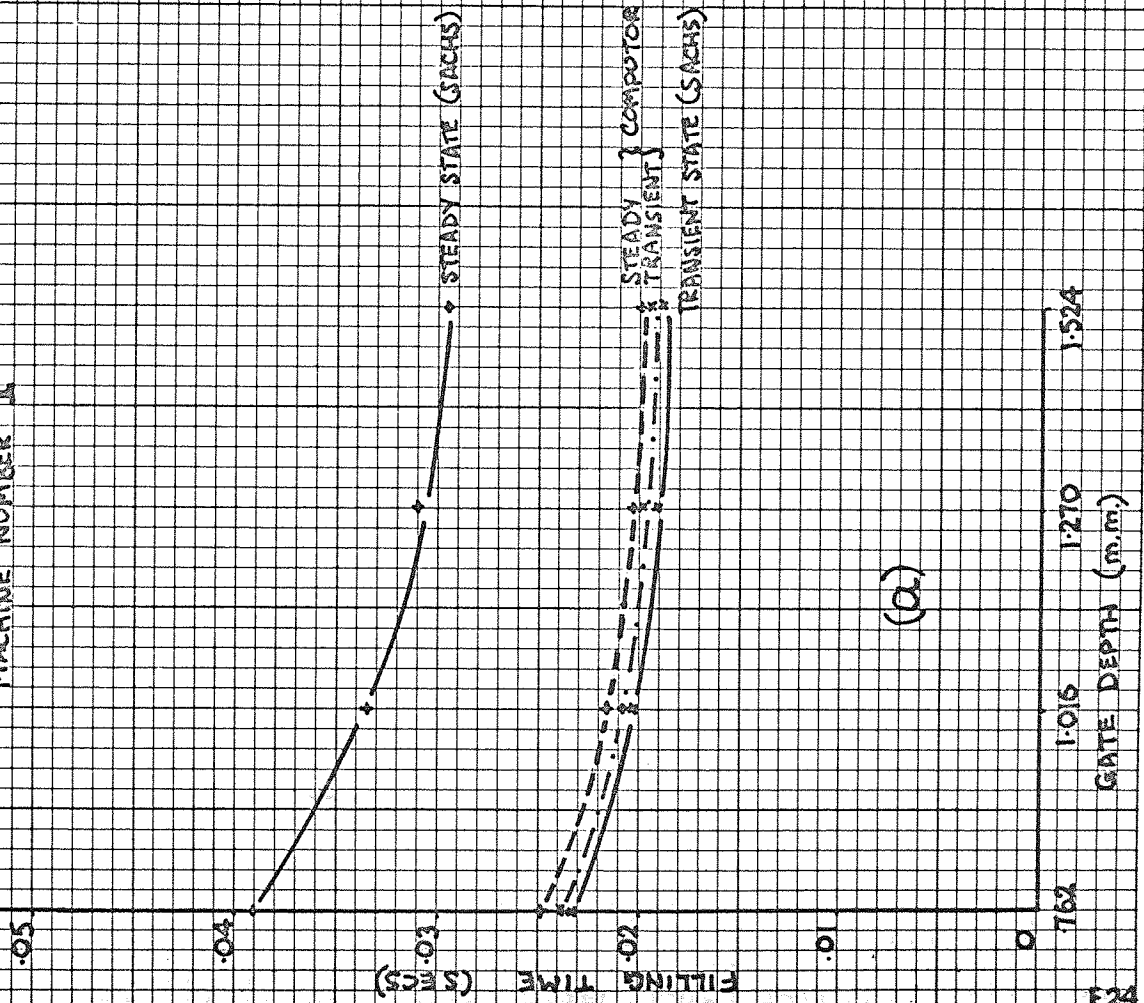
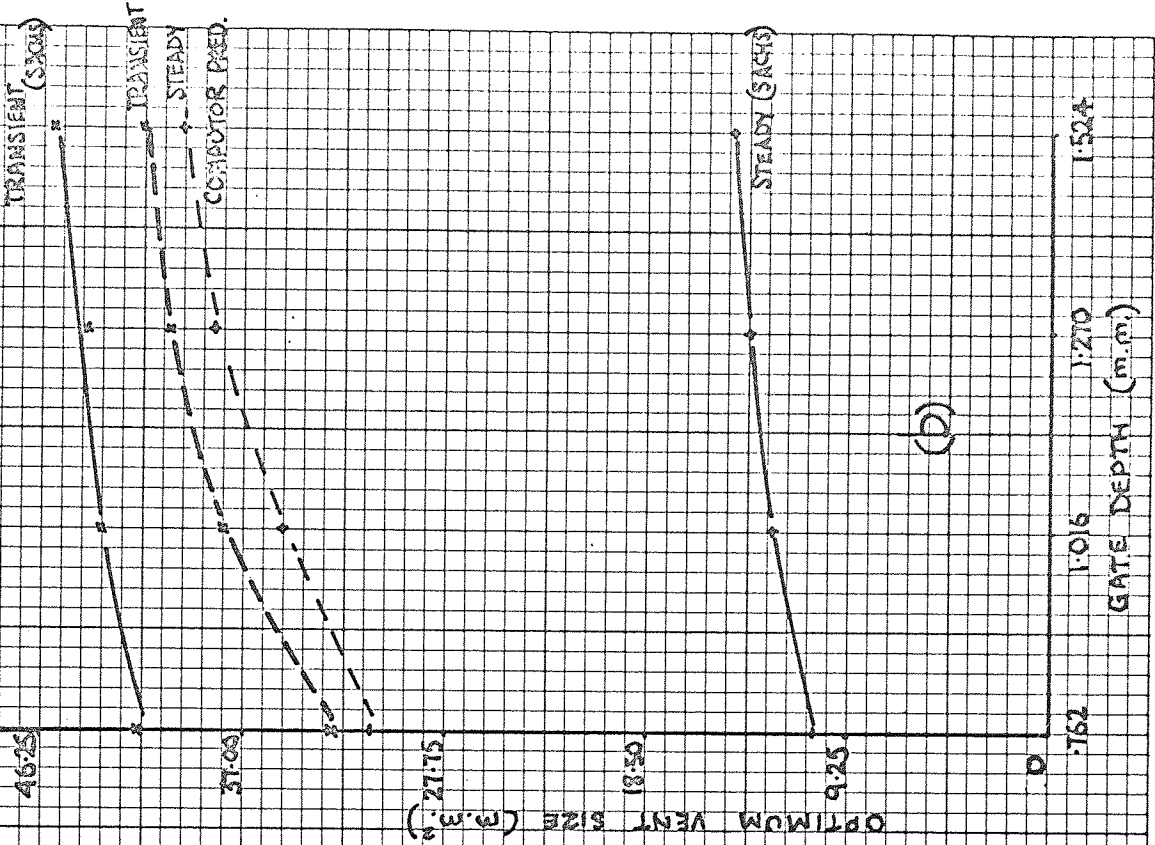


FIG 24 COMPARISON OF CALCULATIONS FOR FILLING TIME AND FOR VENT SIZE VS. GATE DEPTH

MACHINE NUMBER 1



(a)



(b)

FIG 25
COMPARISON OF CALCULATIONS FOR FILLING TIME AND FOR VENT SIZE VS. GATE DEPTH
MACHINE NUMBER 5

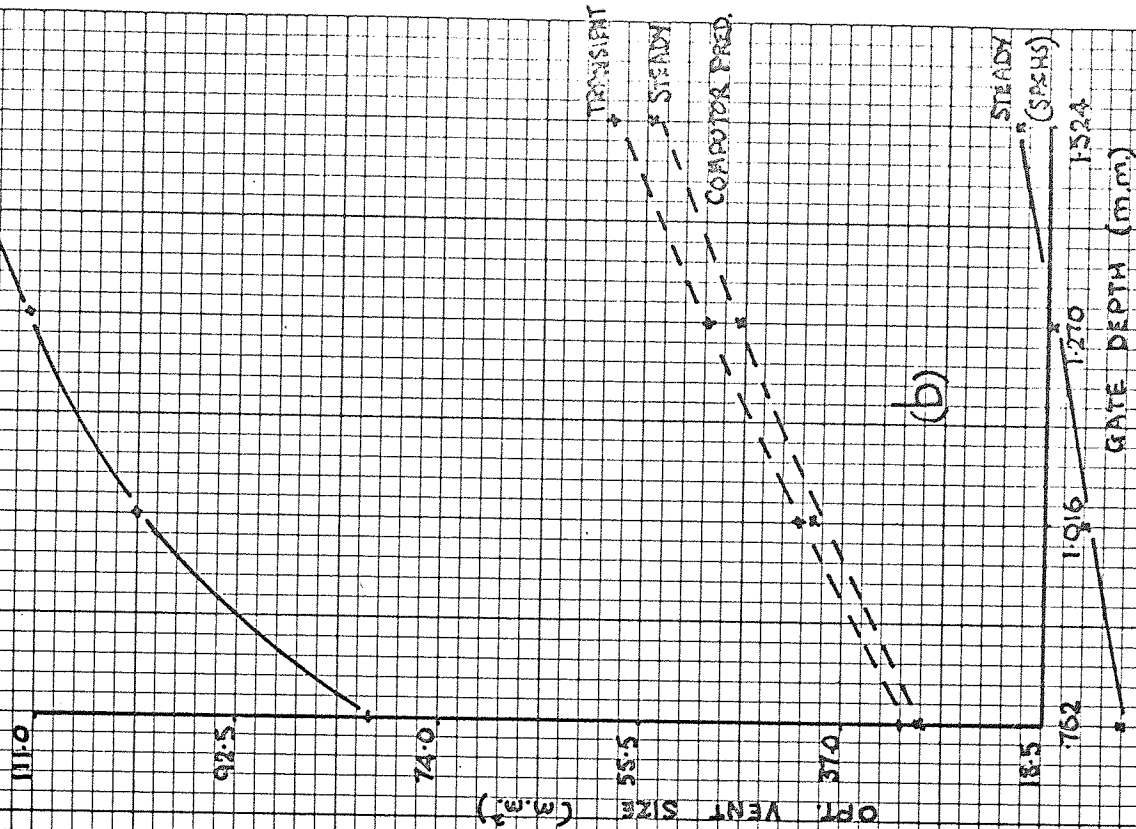
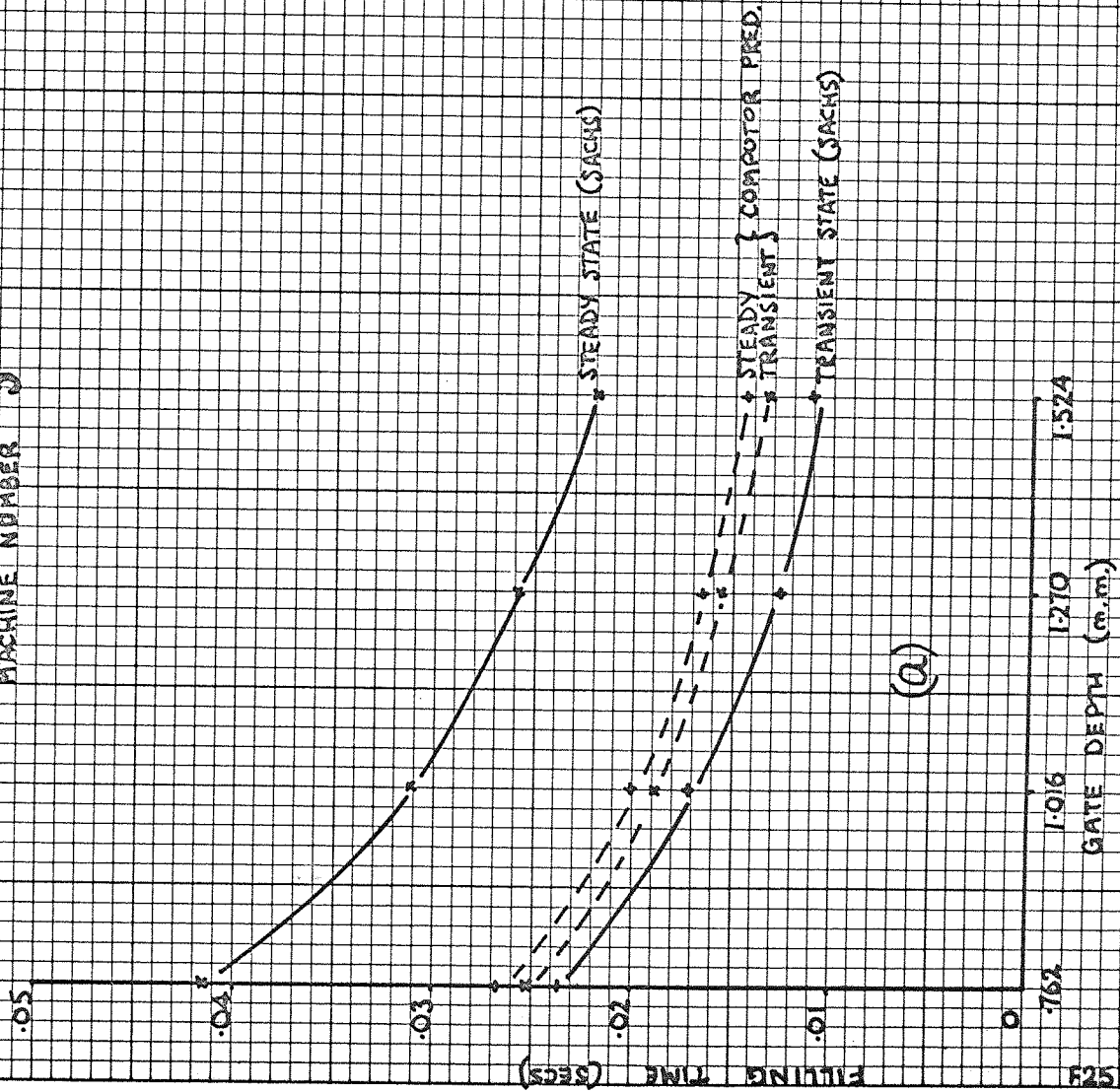


FIG 26 NON-DIMENSIONAL PLOT OF VARIATION OF VENTING AREA RATIOS WITH PROPORTIONAL VARIATION OF MACHINE AND OF GATING SYSTEM RESISTANCE FACTORS

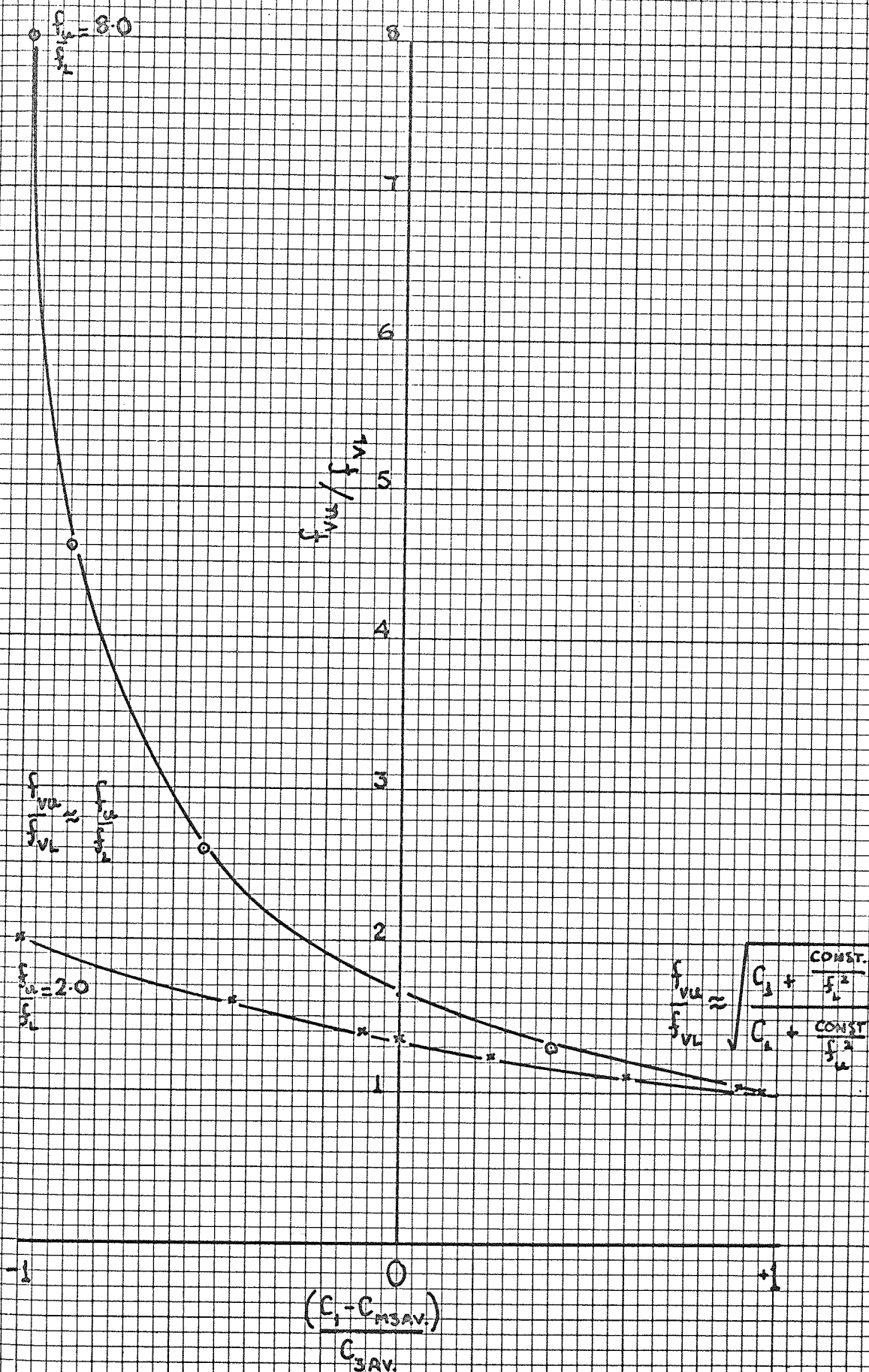


FIG 27 'FREE RUNNING' PISTON VELOCITY CURVES FOR MACHINE 1A FOR VARIOUS DAMPER CONDITIONS IN STAGE 1

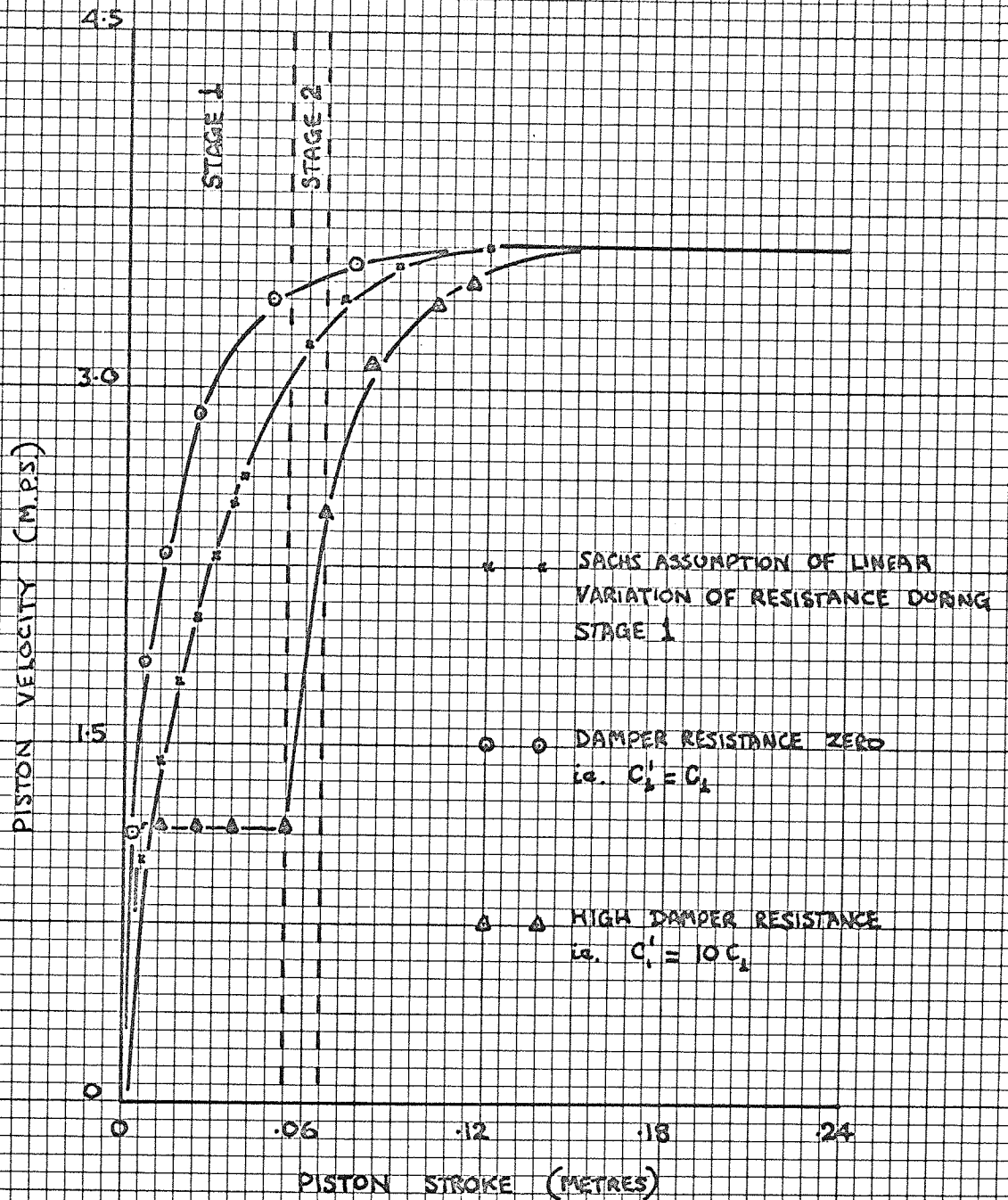


FIG. 28 'FREE RUNNING' CURVES FOR MACHINES 1A AND 5
SHOWING INFLUENCE ON VELOCITY BUILD-UP OF THE
RATIO OF RESISTANCE TO INERTIA FACTOR

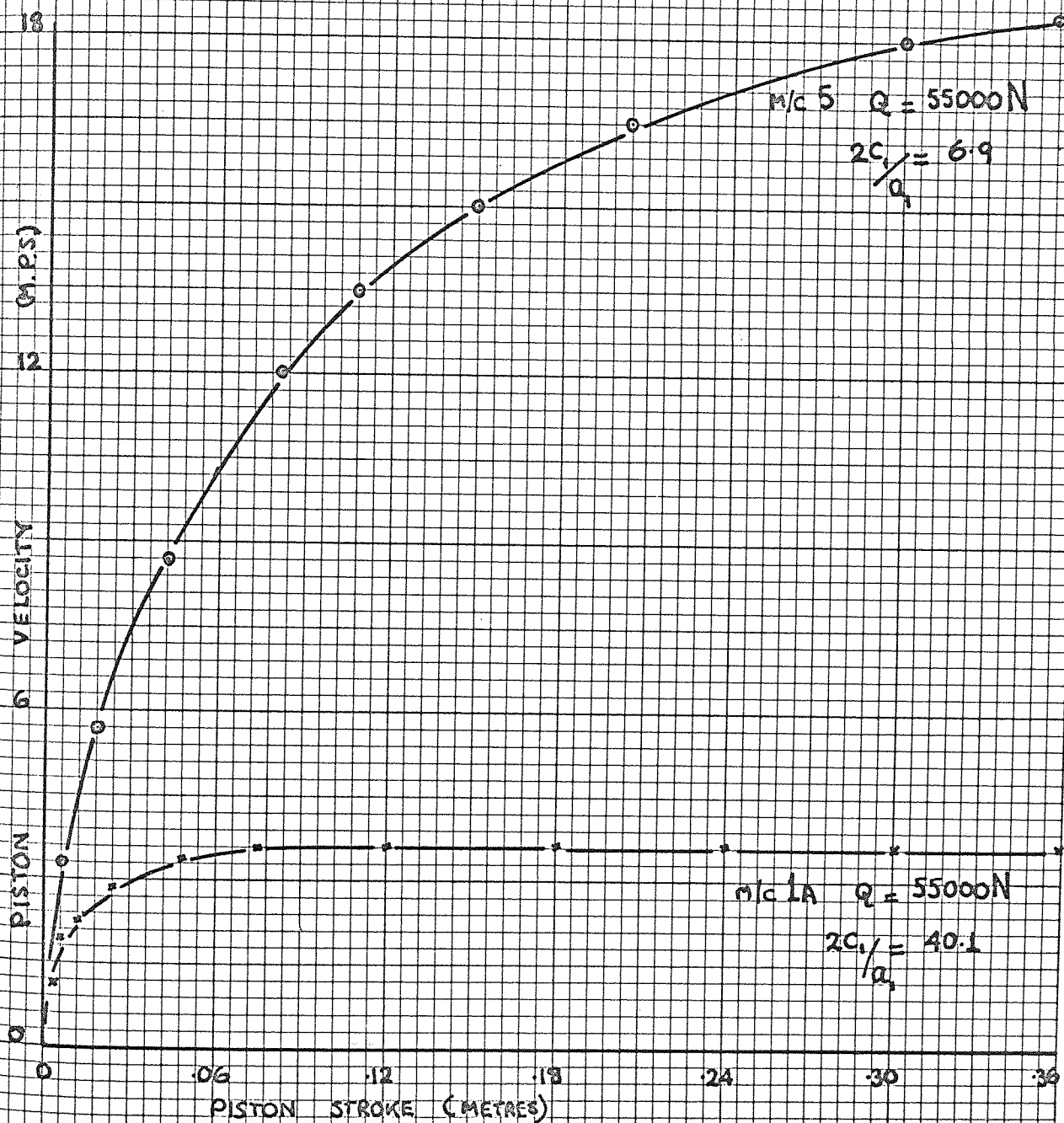


FIG 29 PISTON VELOCITY CHARACTERISTICS FOR MACHINE NUMBER 5
FOR GATE DEPTHS 762 AND 5.33 m.m. AT CHANGEOVER
POSITIONS .04, .08, .122, .183 AND .244 m.

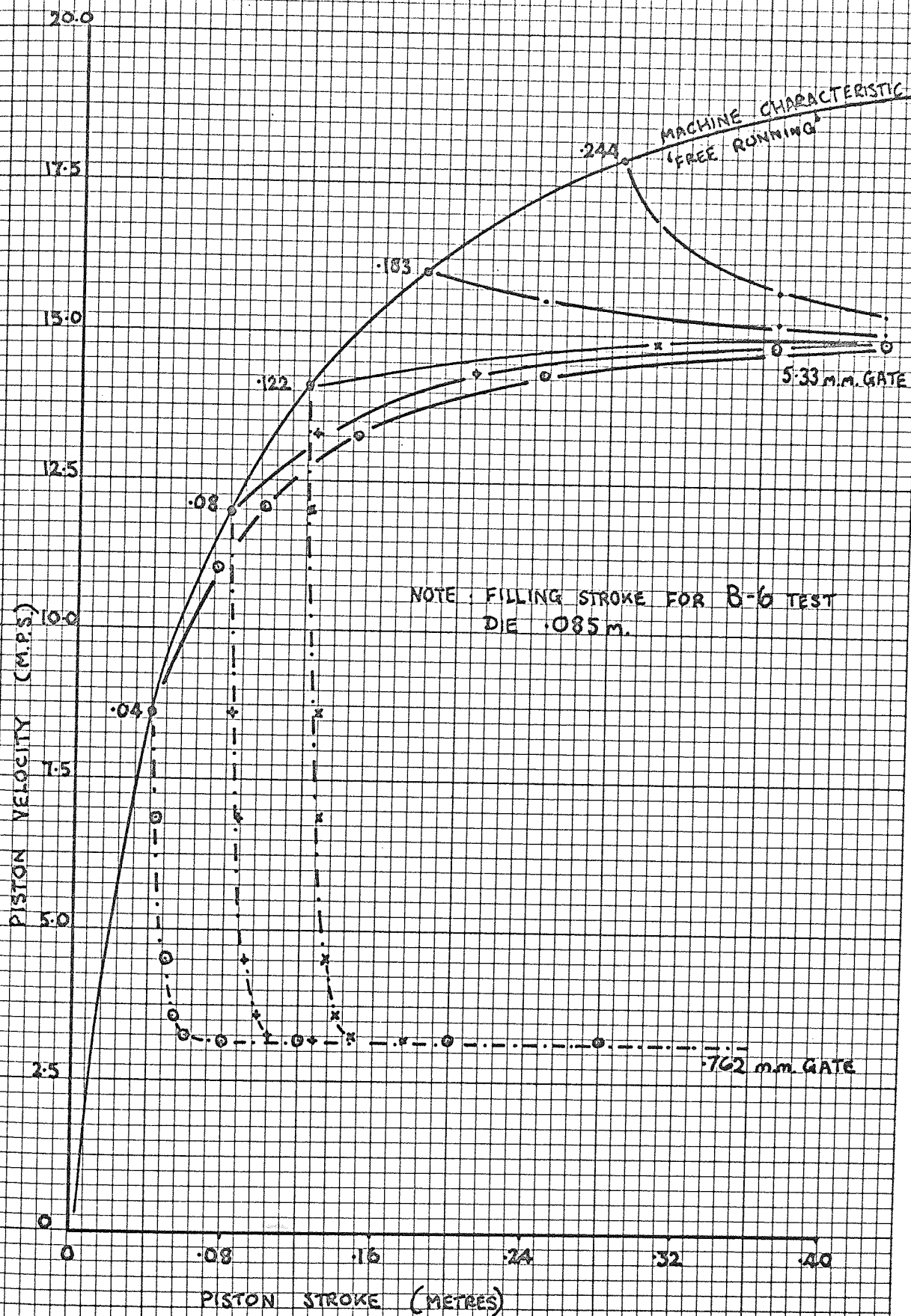


FIG 30

PERCENTAGE DIFFERENCE BETWEEN STEADY STATE AND TRANSIENT FILLING TIMES FOR B-6 TEST DIE AT VARIOUS FILLING STROKES AND CHANGEOVER POSITIONS.

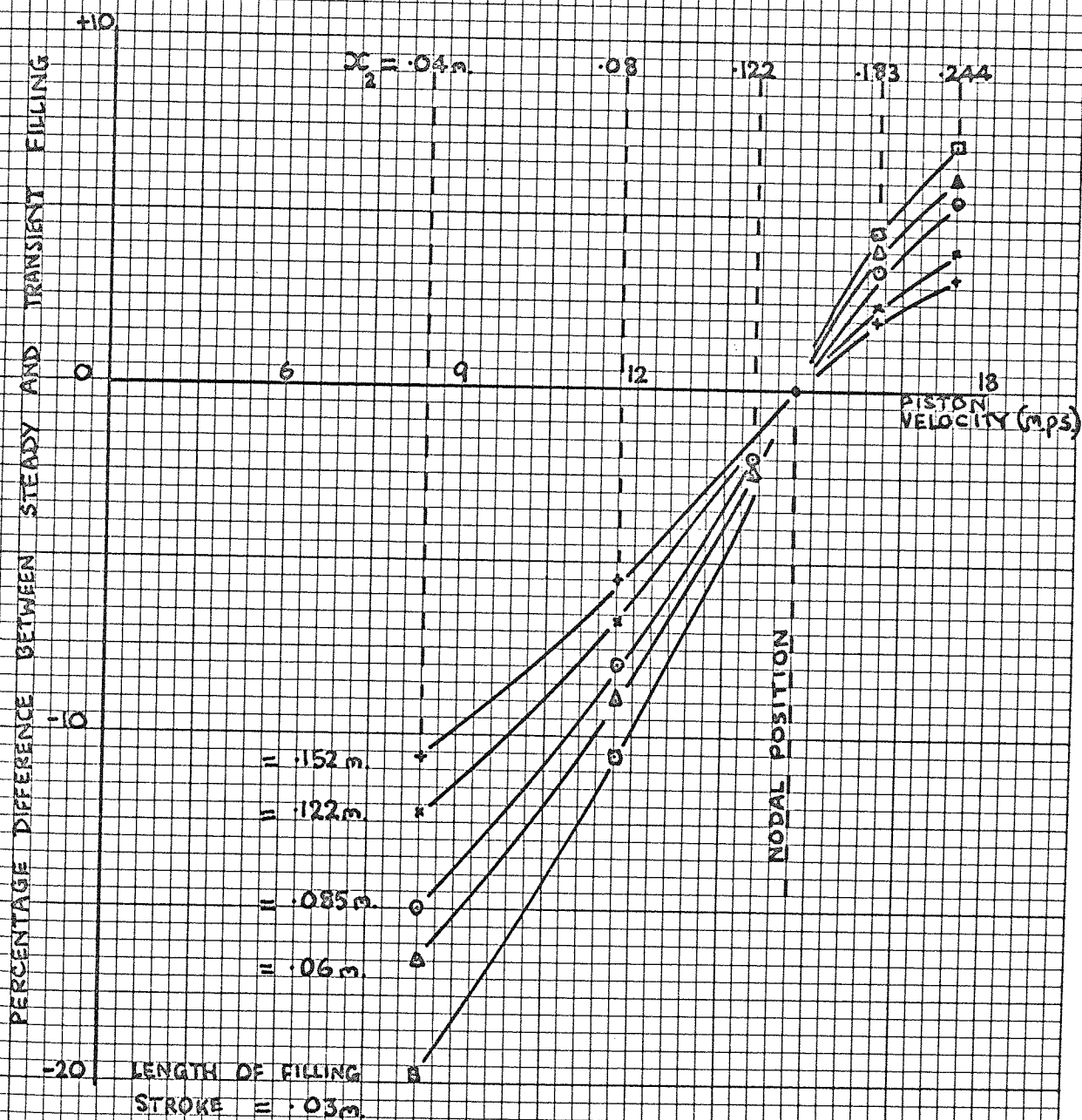
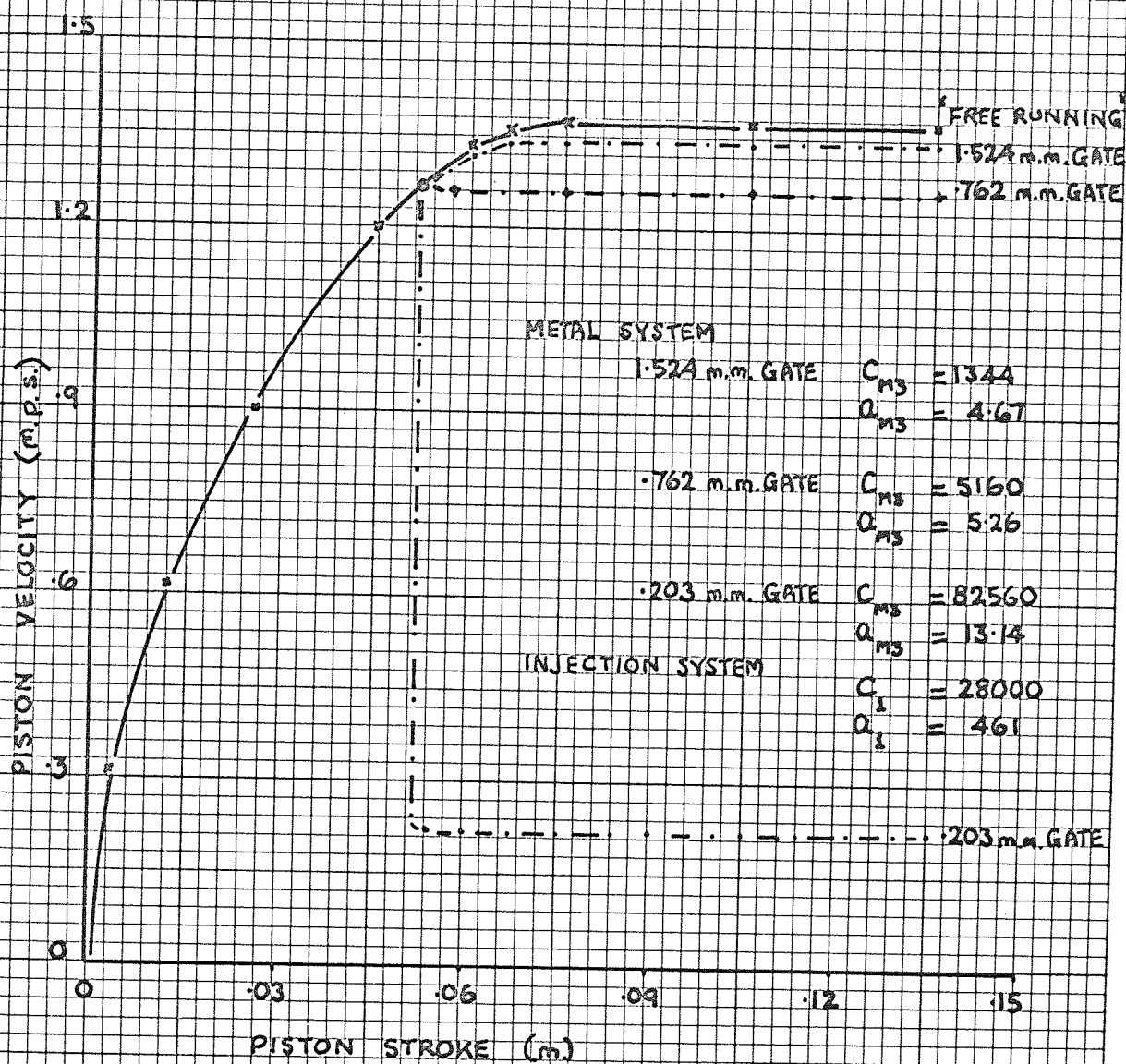


FIG 31 FILLING CHARACTERISTICS FOR B-6 TEST DIE ON MACHINE NUMBER 2 USING DIFFERENT GATE SIZES



NOTE: FILLING STROKE FOR B-6 TEST DIE .085m.

FIG 32(a) FILLING CHARACTERISTIC FOR B-6 TEST DIE
ON MACHINE 1A

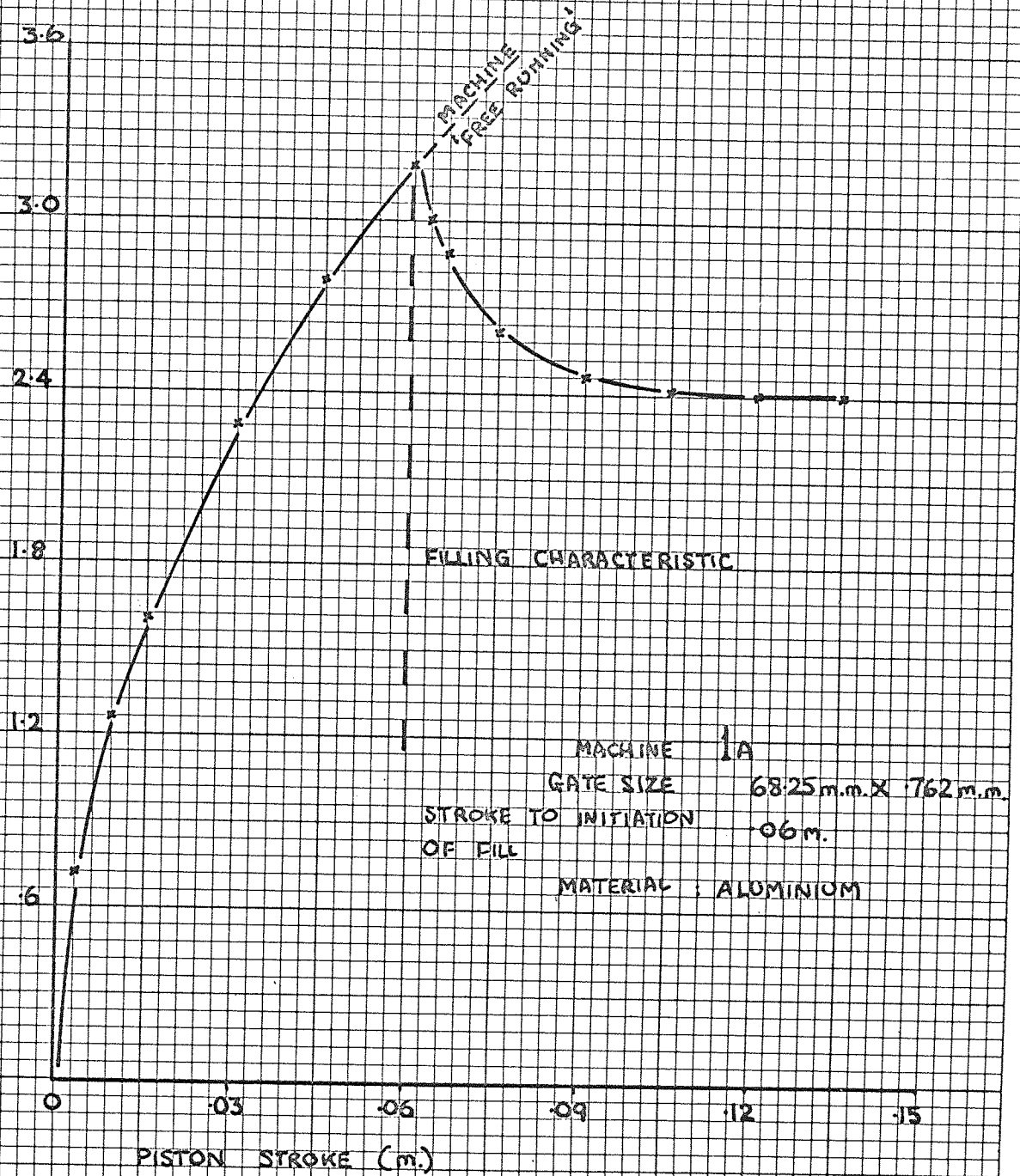


FIG 32(b)
EFFECT ON FILLING TIME OF GATE AREA CHANGES AND OF CHANGES
IN METAL PISTON DIA. GIVING THE SAME RESISTANCE EFFECT USING
MACHINE NUMBER 1A (CAVITY SIZE ASSUMED EQUAL TO EXPERIMENTAL
DIE B-6)

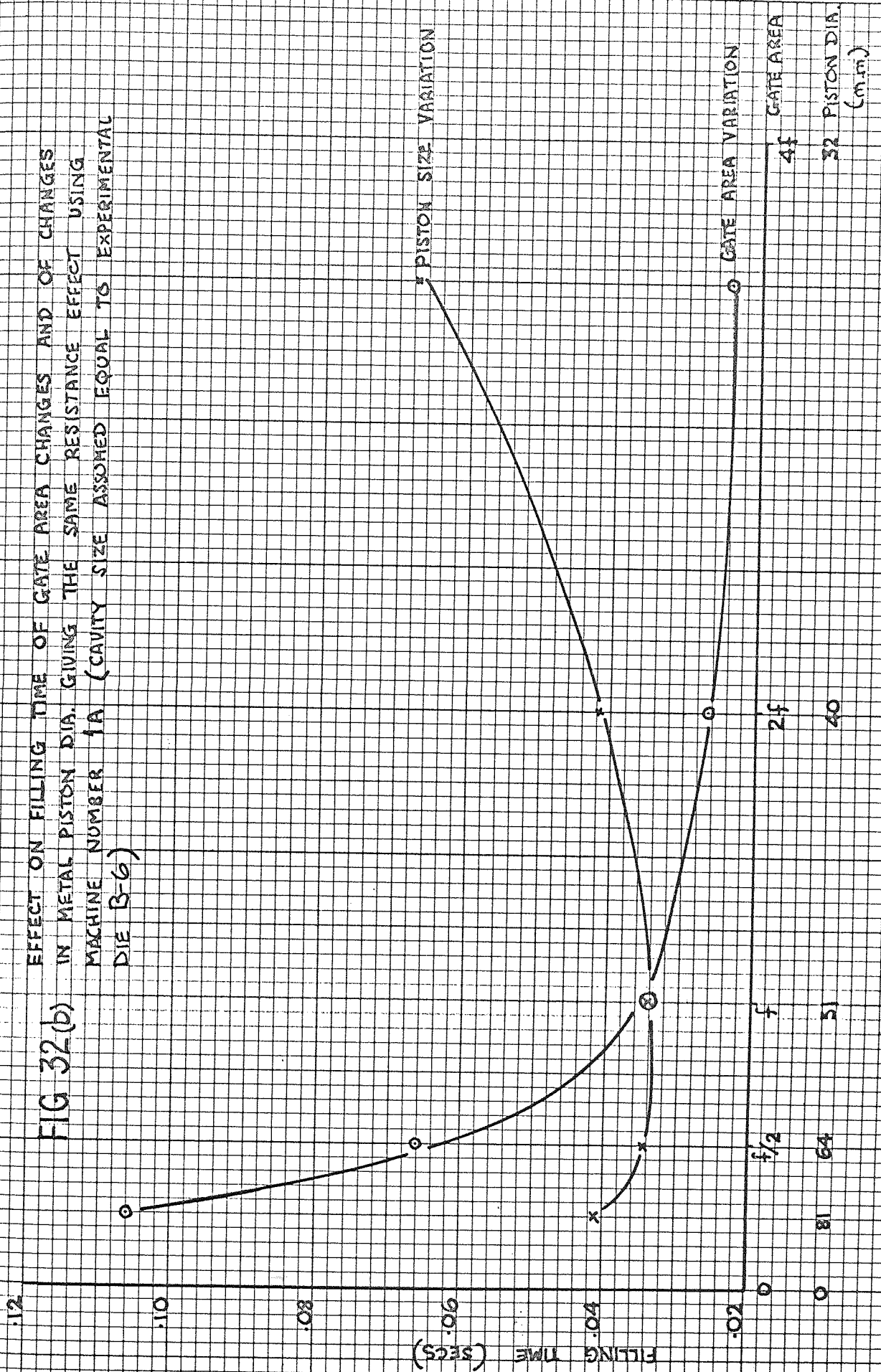


FIG 33(a) FILLING CHARACTERISTICS, ZERO VENTING,
MACHINE NUMBER 1A

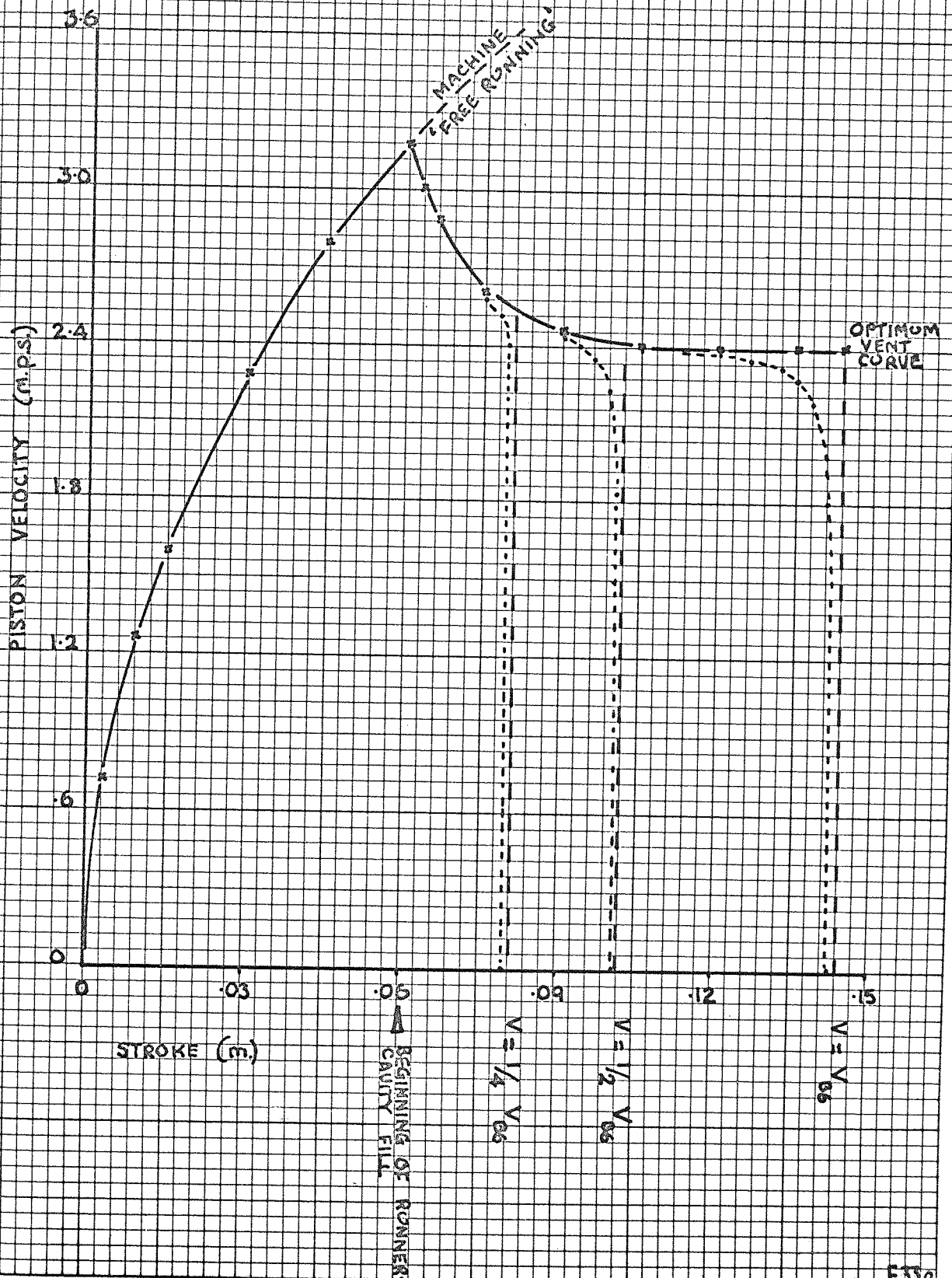


FIG 33b COMPARISON OF STEADY STATE OPTIMUM VENT, ZERO VENT
FILL TIMES USING MACHINE 1A

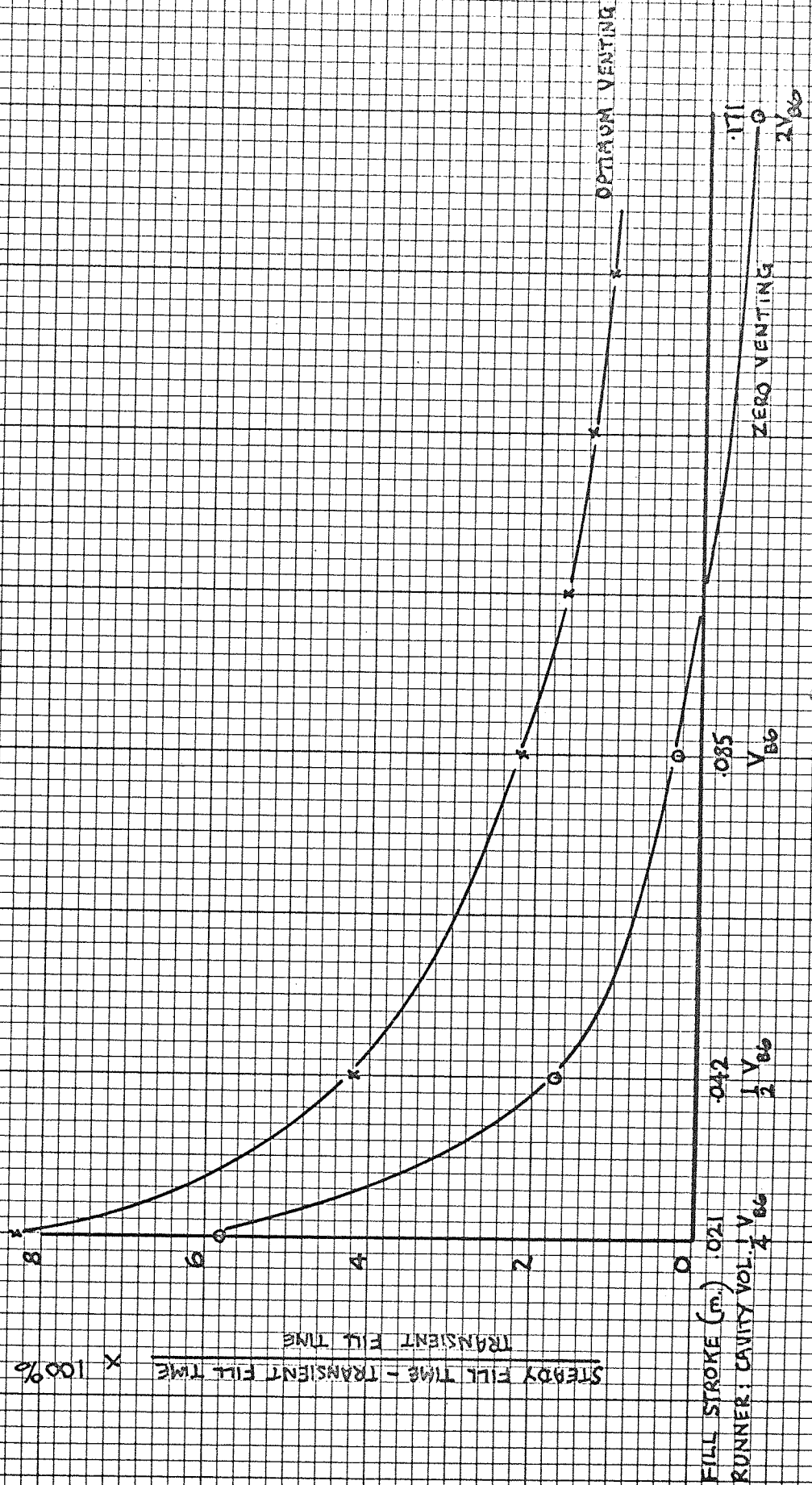


FIG 33C PERCENTAGE DIFFERENCE BETWEEN OPT. VENT, ZERO VENT
FILL TIMES USING MACHINE 1A

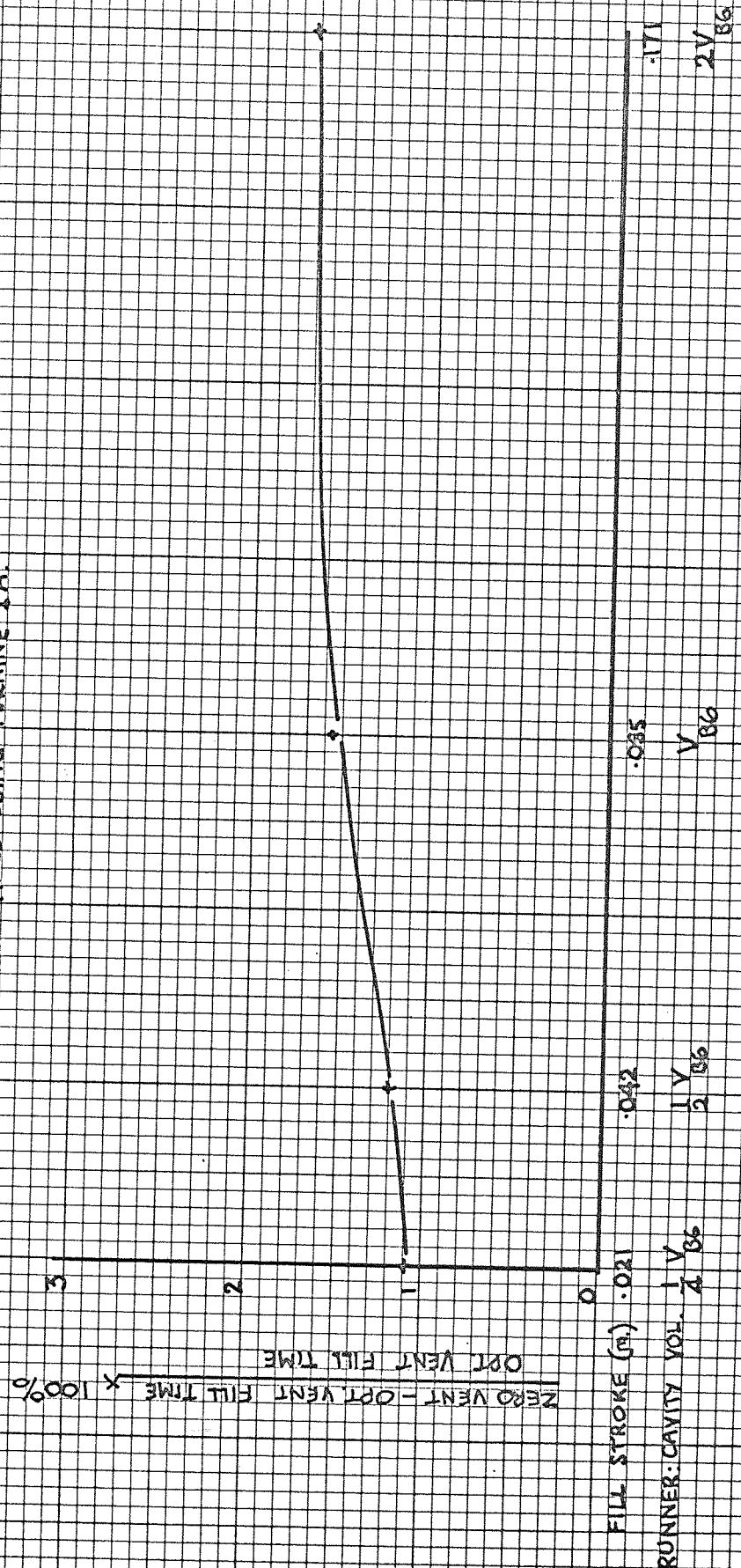


FIG 34a

FILLING CHARACTERISTICS IN ZERO VENTING CONDITIONS USING MACHINE NUMBER 1

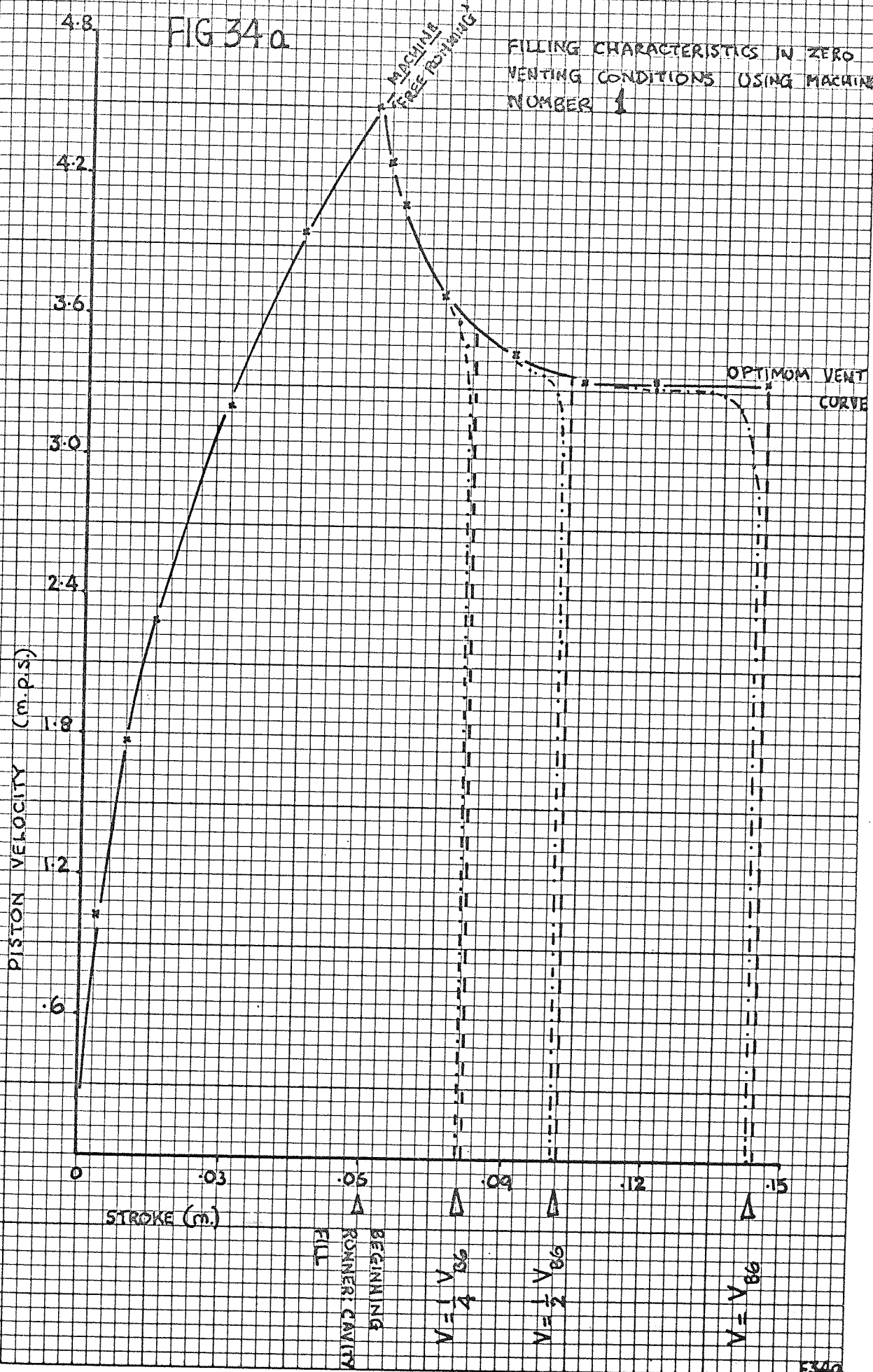


FIG 34b COMPARISON OF STEADY STATE, OPTIMUM VENT AND ZERO VENT FILL TIMES USING MACHINE NUMBER 1

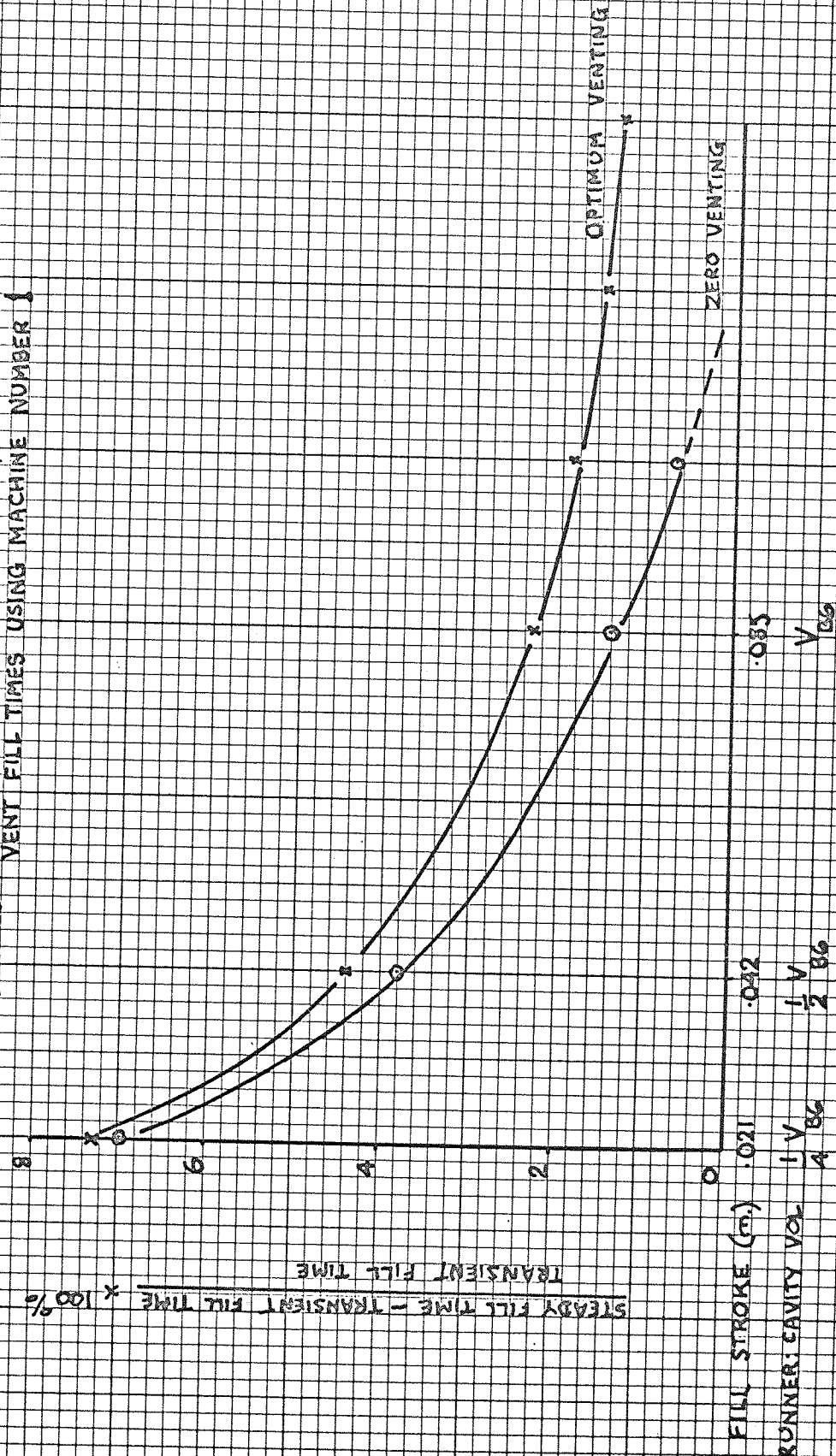


FIG 34c PERCENTAGE DIFFERENCE BETWEEN OPTIMUM VENT AND ZERO VENT FILL TIMES USING MACHINE NUMBER 1

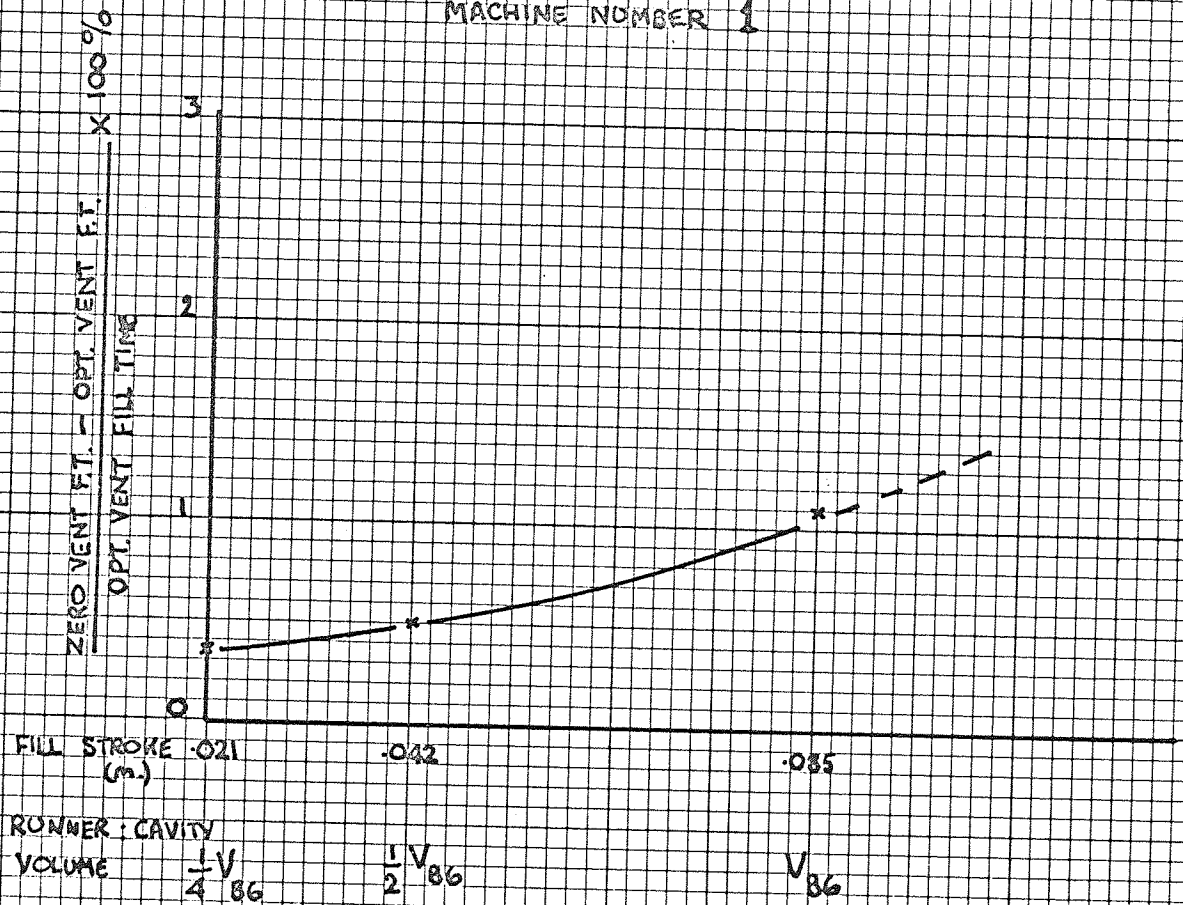


FIG 35 VOLUME COMPRESSION UNDER
ADIABATIC CONDITIONS FOR
OPTIMUM AND ZERO VENTING

PERCENTAGE POROSITY BY VOLUME

8

7

6

5

4

3

2

1

0

1.5

.575

.288

.144

.12

($\times 10^6$)

DRIVING FORCE ON 51 mm. DIA. PISTON (N/cm^2)

OPT. VENTING

ZERO VENTING

FIG 36 COMPARISON OF FILLING CHARACTERISTICS FOR FIXED AND FOR VARIABLE CAVITY RESISTANCE USING MACHINE NUMBER 2

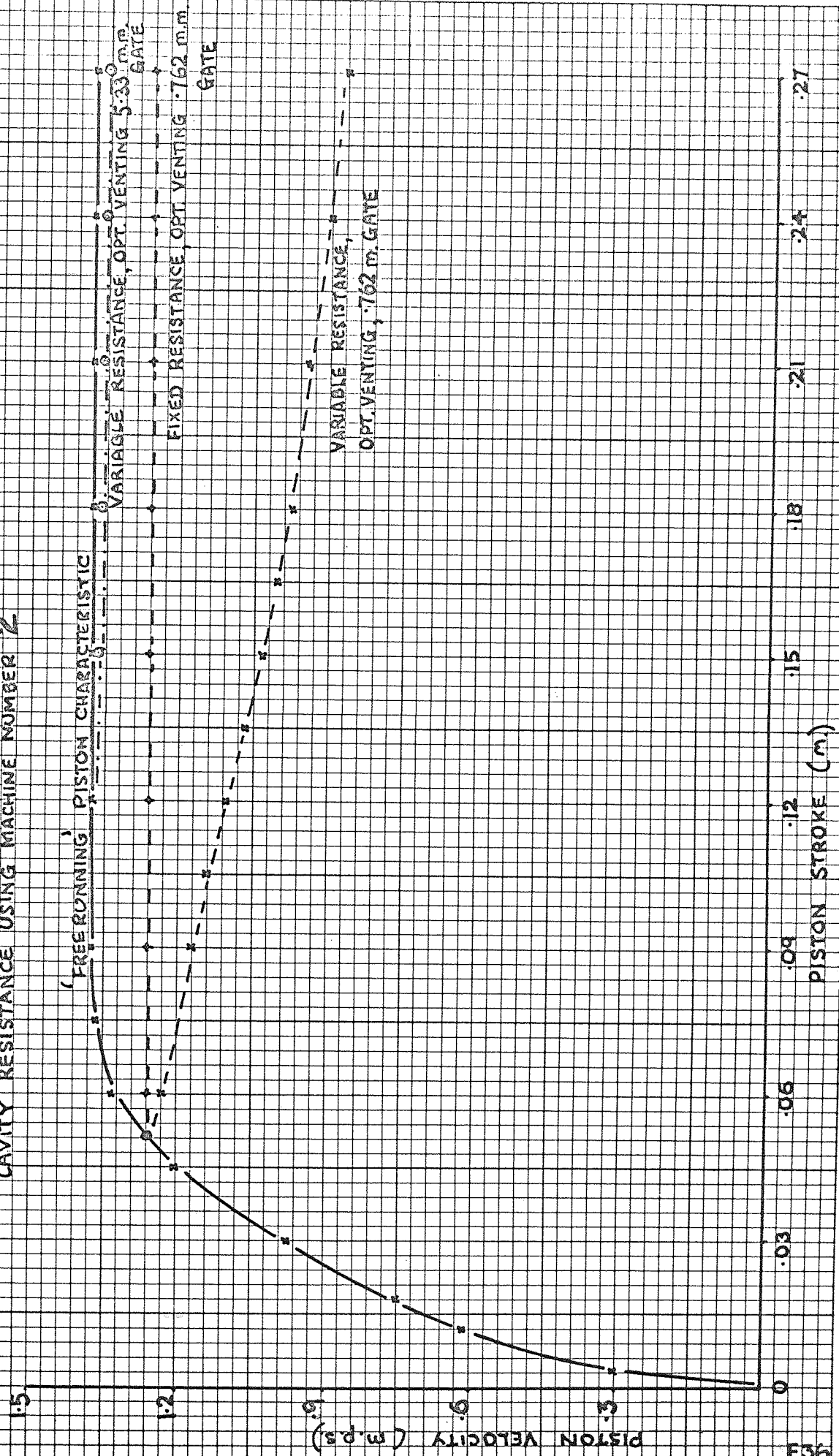


FIG 37 COMPARISON OF FILLING CHARACTERISTICS FOR FIXED
AND FOR VARIABLE CAVITY RESISTANCE USING TWO
GATE SIZES ON MACHINE NUMBER 5

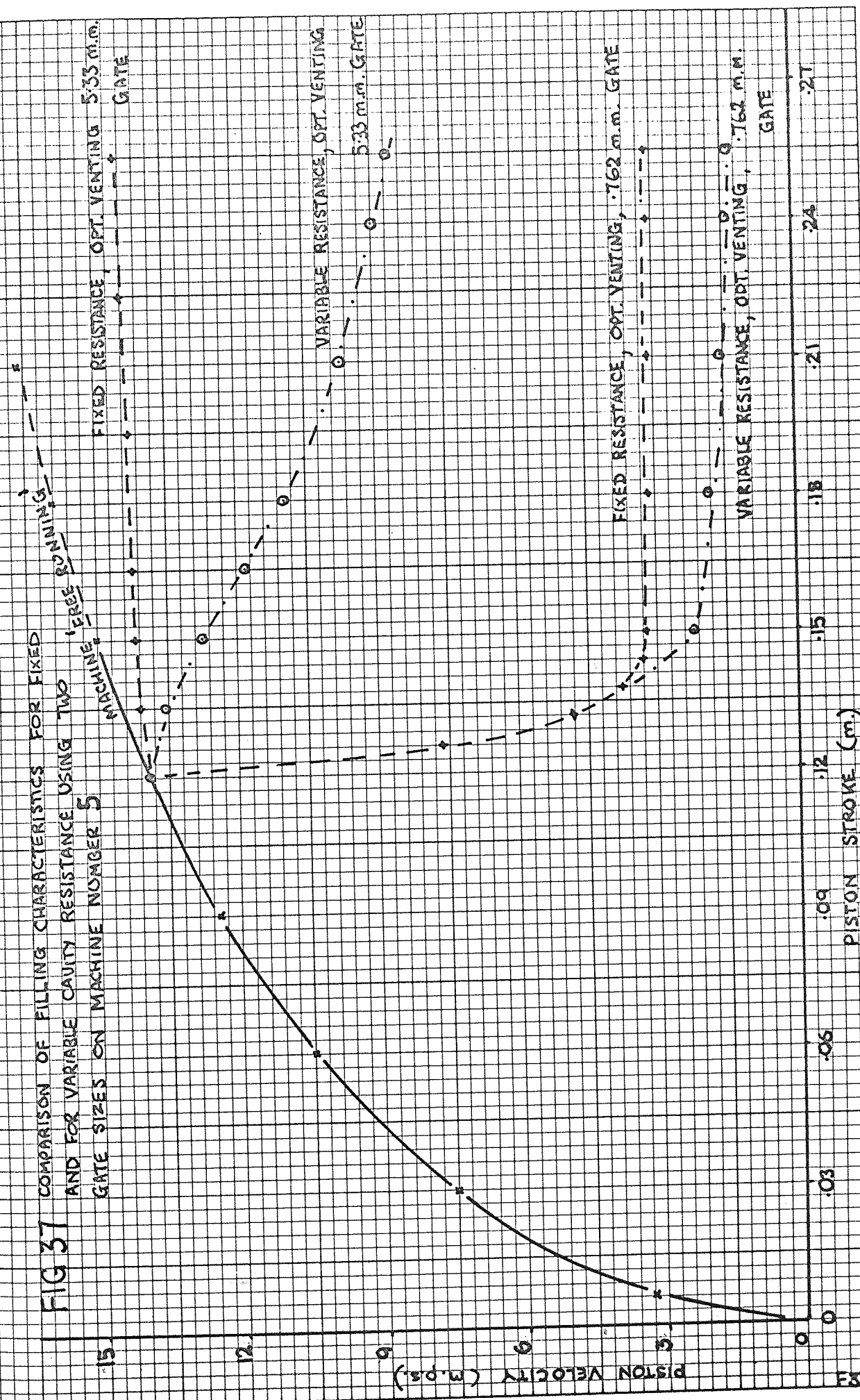


FIG 38

COMPARISON OF FILLING TIMES FOR FIXED AND FOR VARIABLE CAVITY RESISTANCE USING MACHINES NUMBERS 2 AND 5 FOR COMPARISON

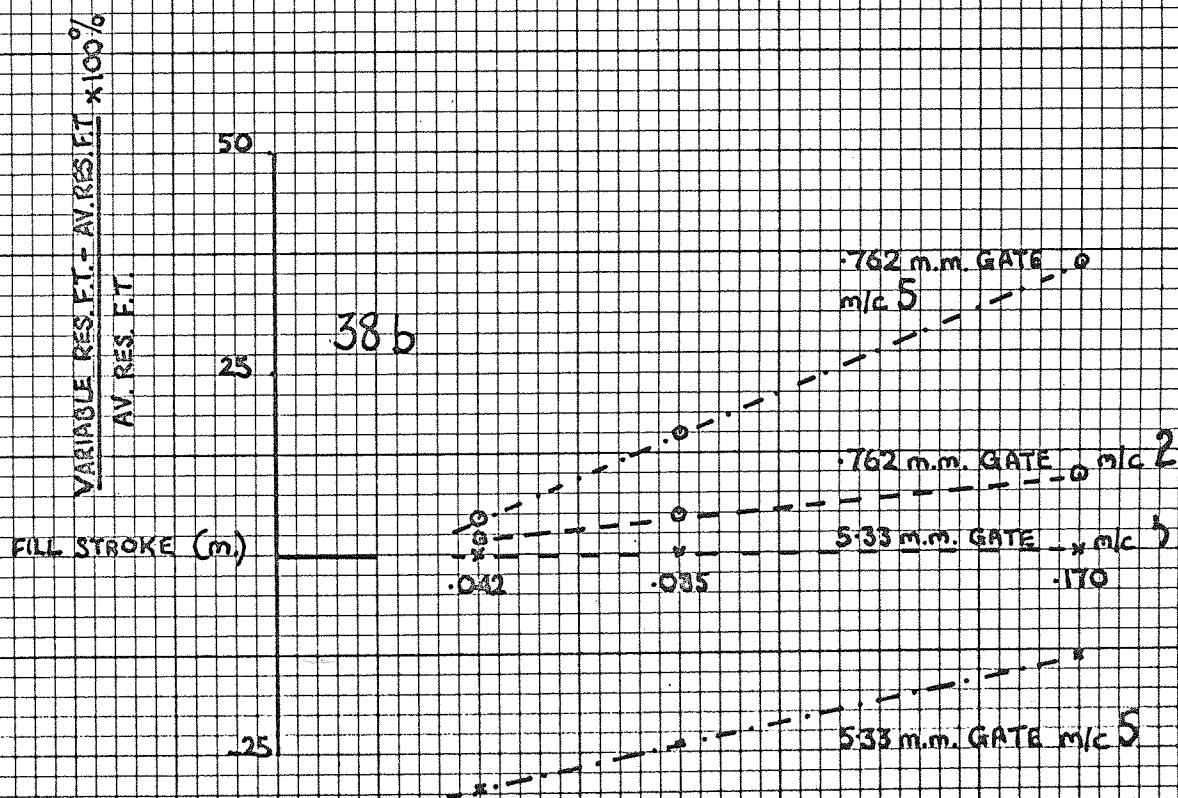
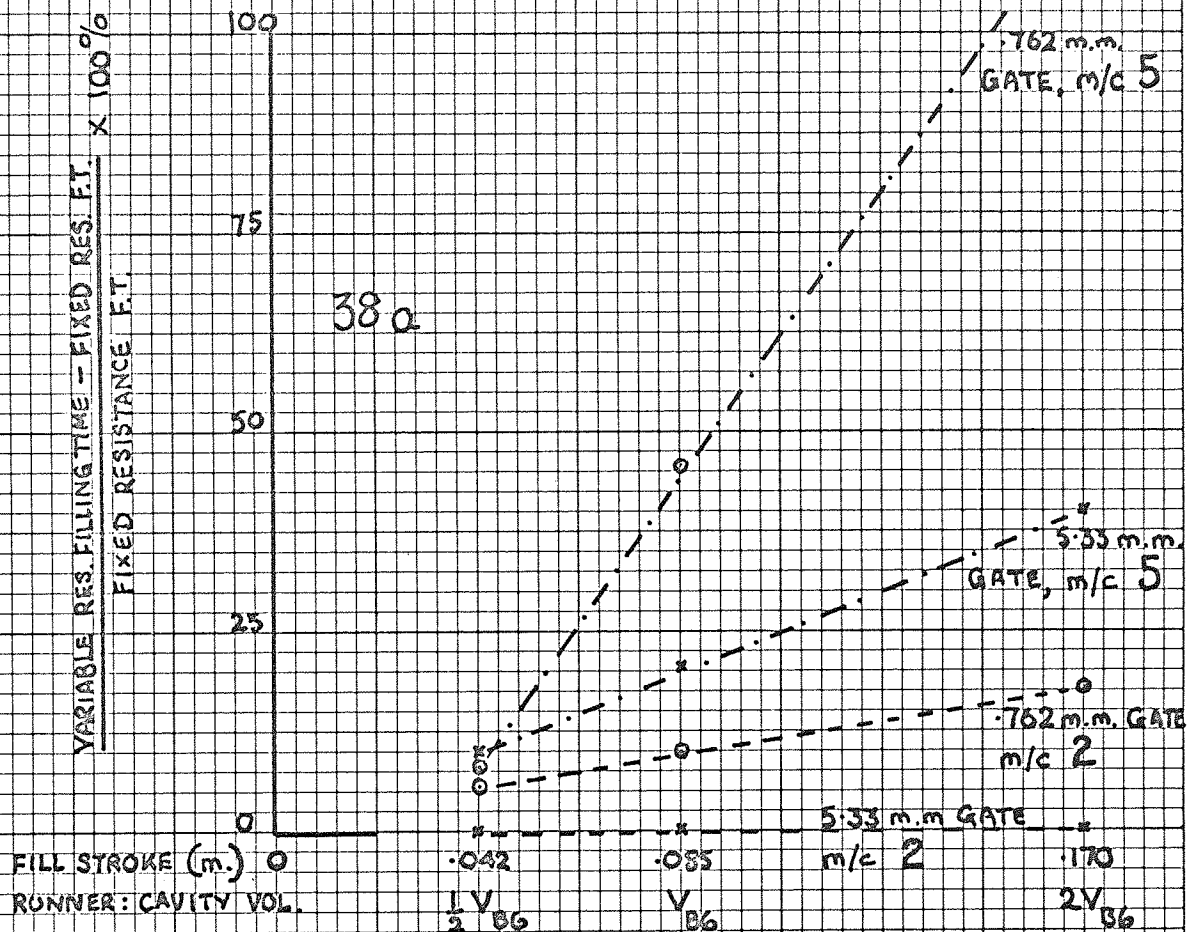


FIG 39 DIAGRAMMATIC ILLUSTRATION OF TWO STAGE PISTON VELOCITY CHARACTERISTICS FOR HIGH AND LOW RATIOS OF RESISTANCE TO INERTIAL FACTOR

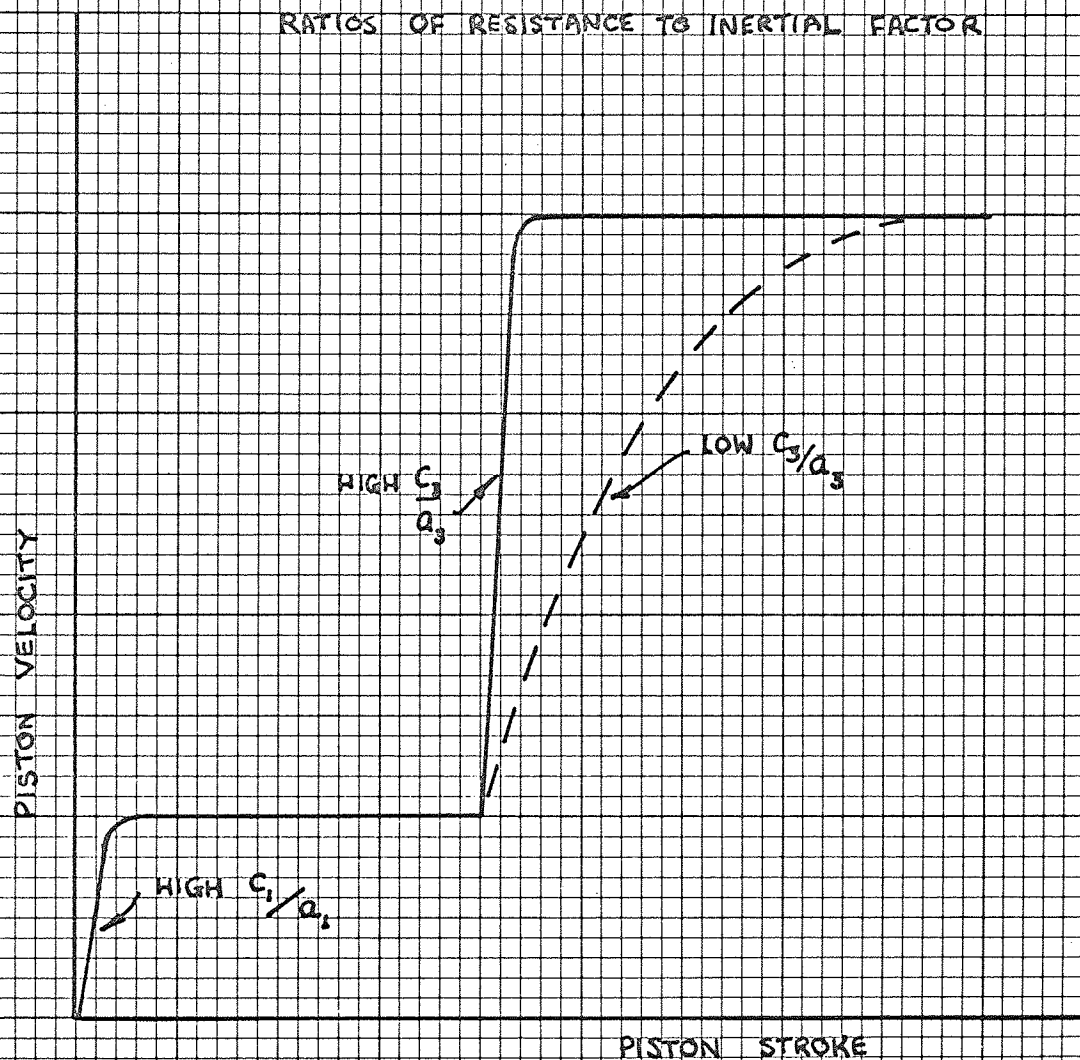


FIG 40 'FREE RUNNING' PISTON VELOCITY CURVES FOR
HYPOTHETICAL TWO-STAGE INJECTION SYSTEM.

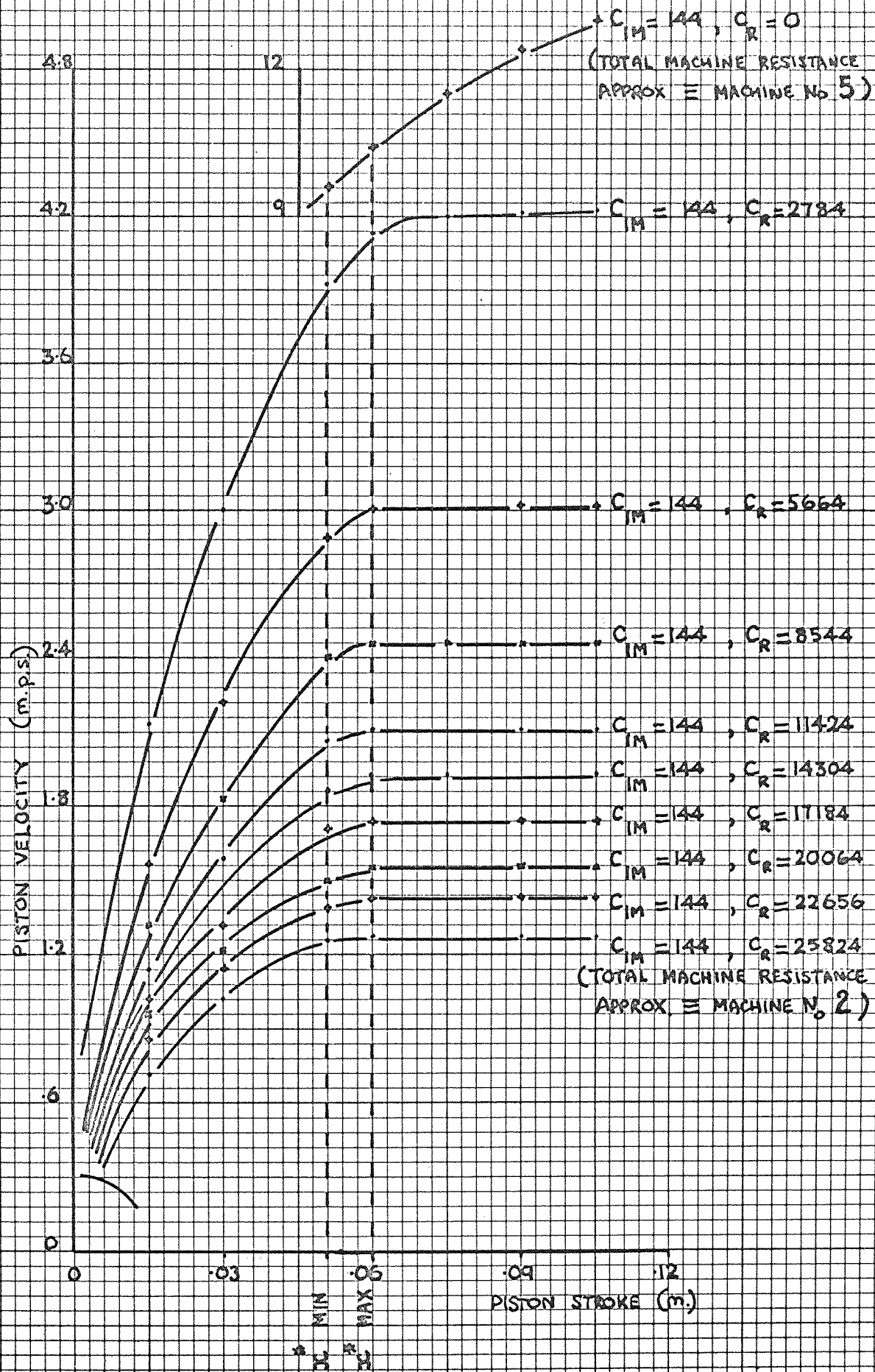


FIG 4] PISTON VELOCITY CHARACTERISTICS FOR A RANGE OF GATE SIZE AND CHANGEOVER POSITIONS USING MACHINE NUMBER 1A

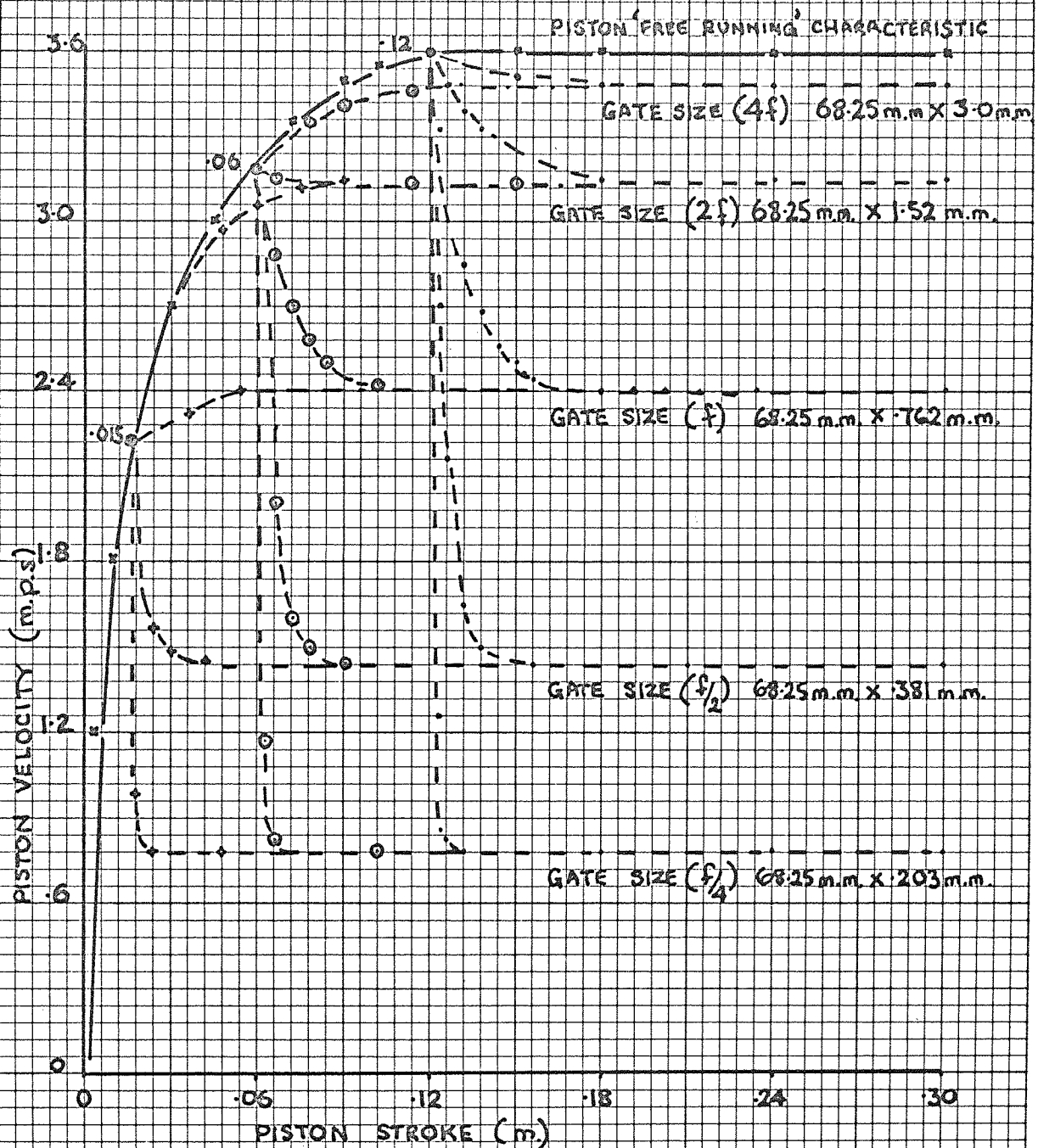


FIG 42

PISTON VELOCITY CHARACTERISTICS FOR A RANGE OF GATE SIZE AND CHANGEOVER POSITIONS USING MACHINE NUMBER 2

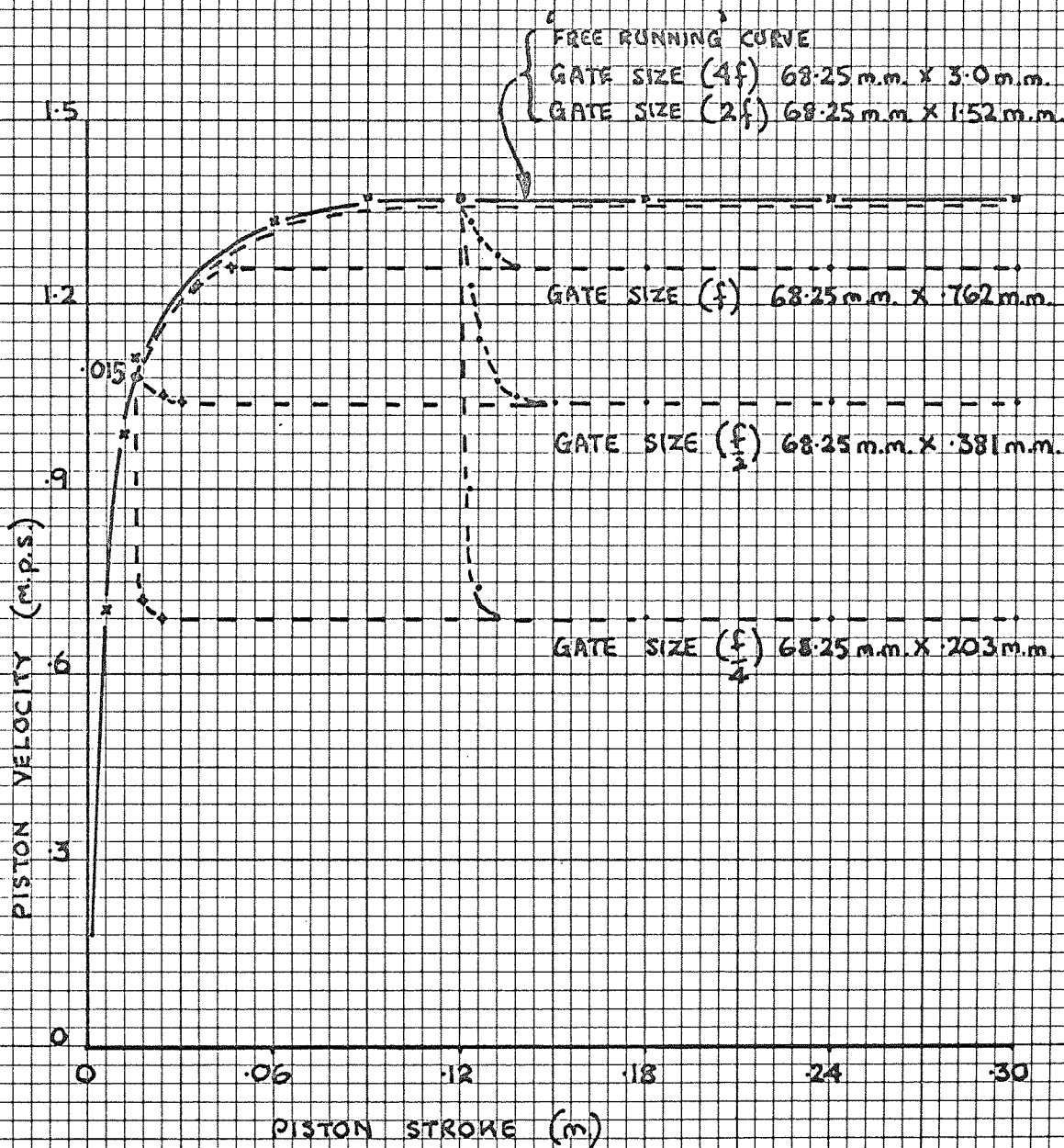


FIG 43 PISTON VELOCITY CHARACTERISTICS FOR A RANGE OF GATE SIZE AND CHANGEOVER POSITIONS USING MACHINE NUMBER 5

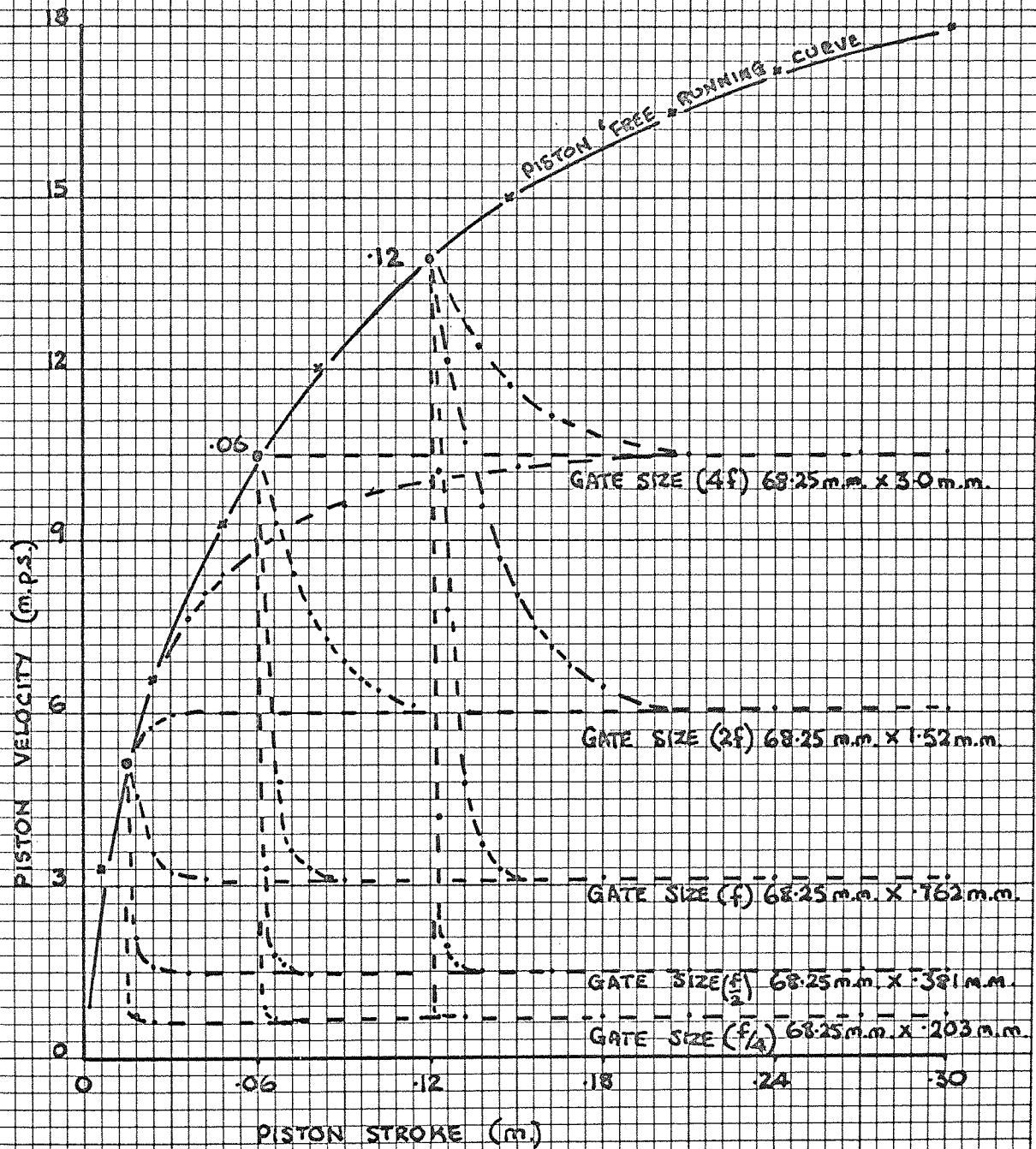


FIG 44a

CHANGES IN ENERGY RATE VS. GATE
SIZE FOR MACHINE NUMBER 1A
AT A CHANGE OVER POSITION AT
.015 m. OF PISTON MOVEMENT

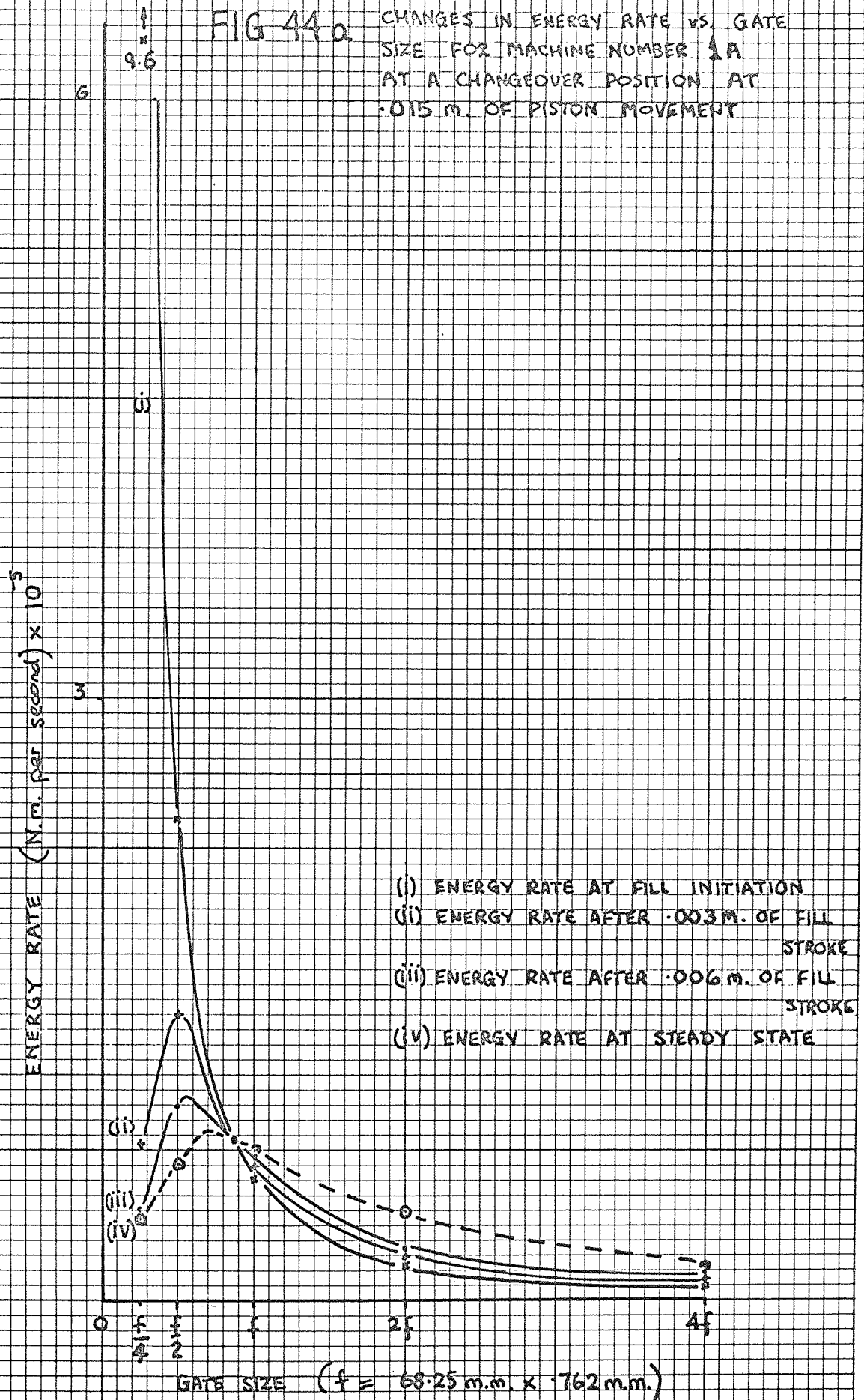


FIG 44b

CHANGES IN ENERGY RATE VS. GATE SIZE FOR MACHINE NUMBER 1A AT A CHANGE OVER POSITION AT .06 m. OF PISTON MOVEMENT

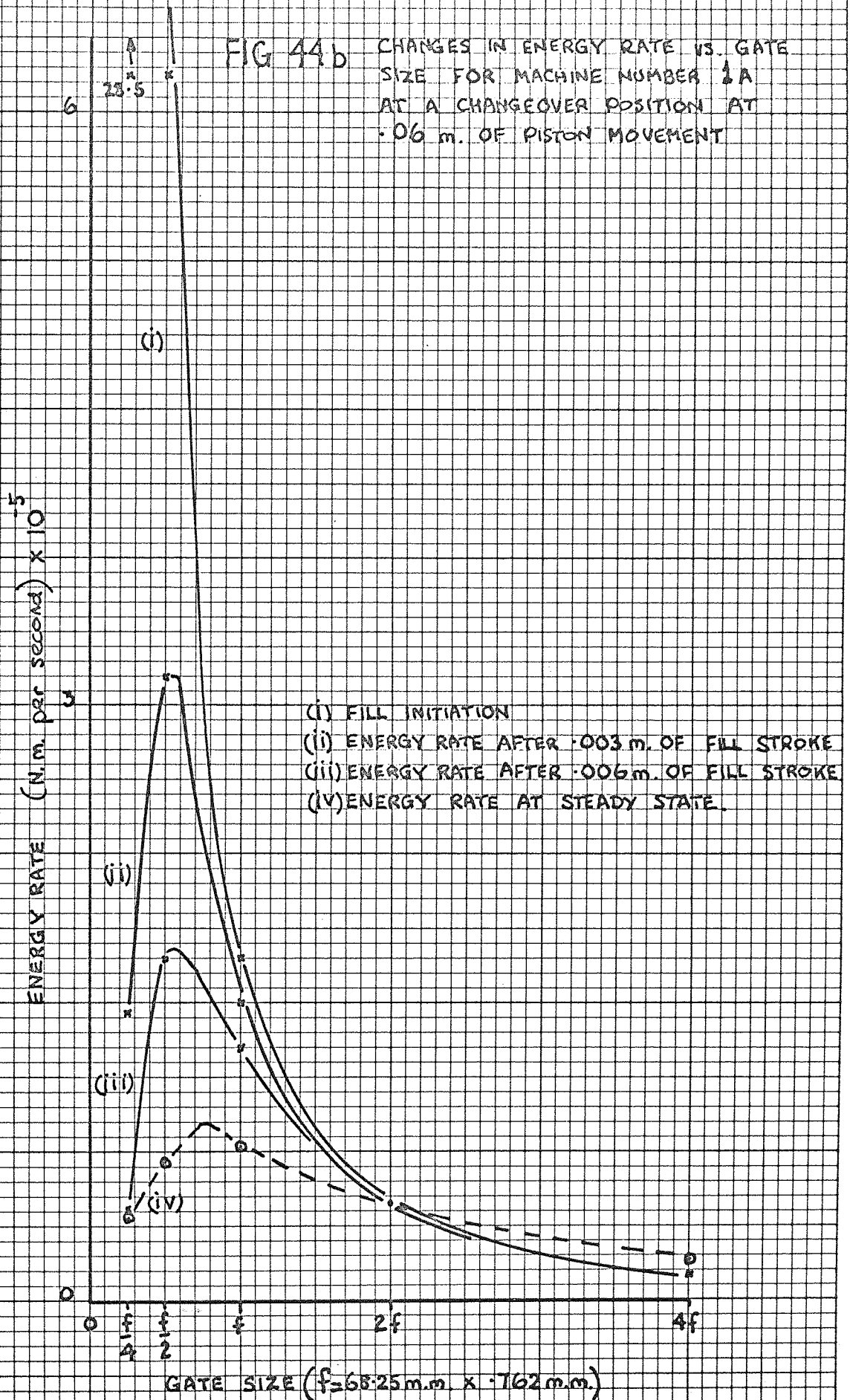


FIG 44c CHANGES IN ENERGY RATE VS GATE SIZE FOR MACHINE NUMBER 1A AT A CHANGE OVER POSITION AT .12 M. OF PISTON MOVEMENT

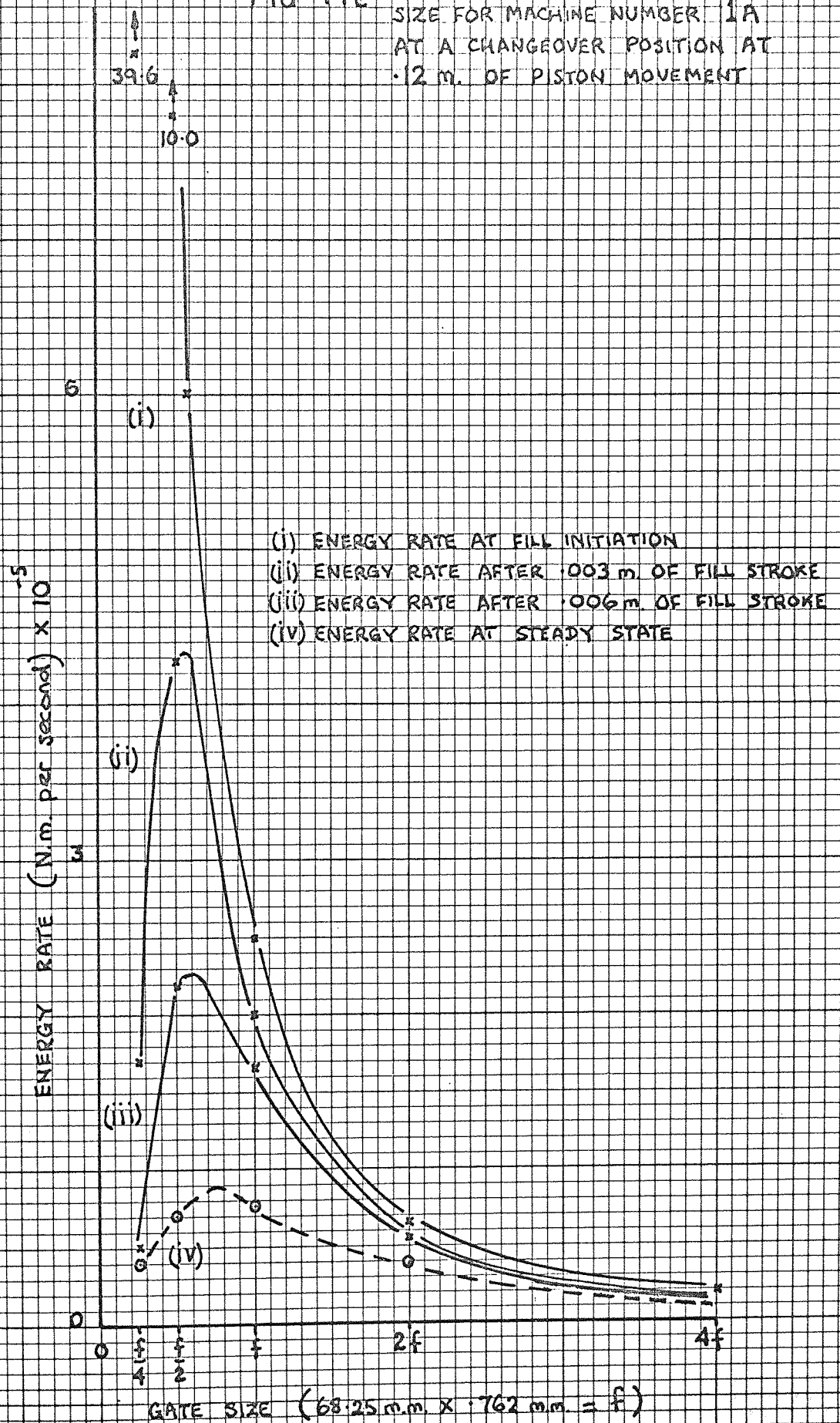


FIG 4.5 MAXIMUM AND STEADY STATE ENERGY RATES VS. GATE SIZE
FOR MACHINE NUMBER 1A

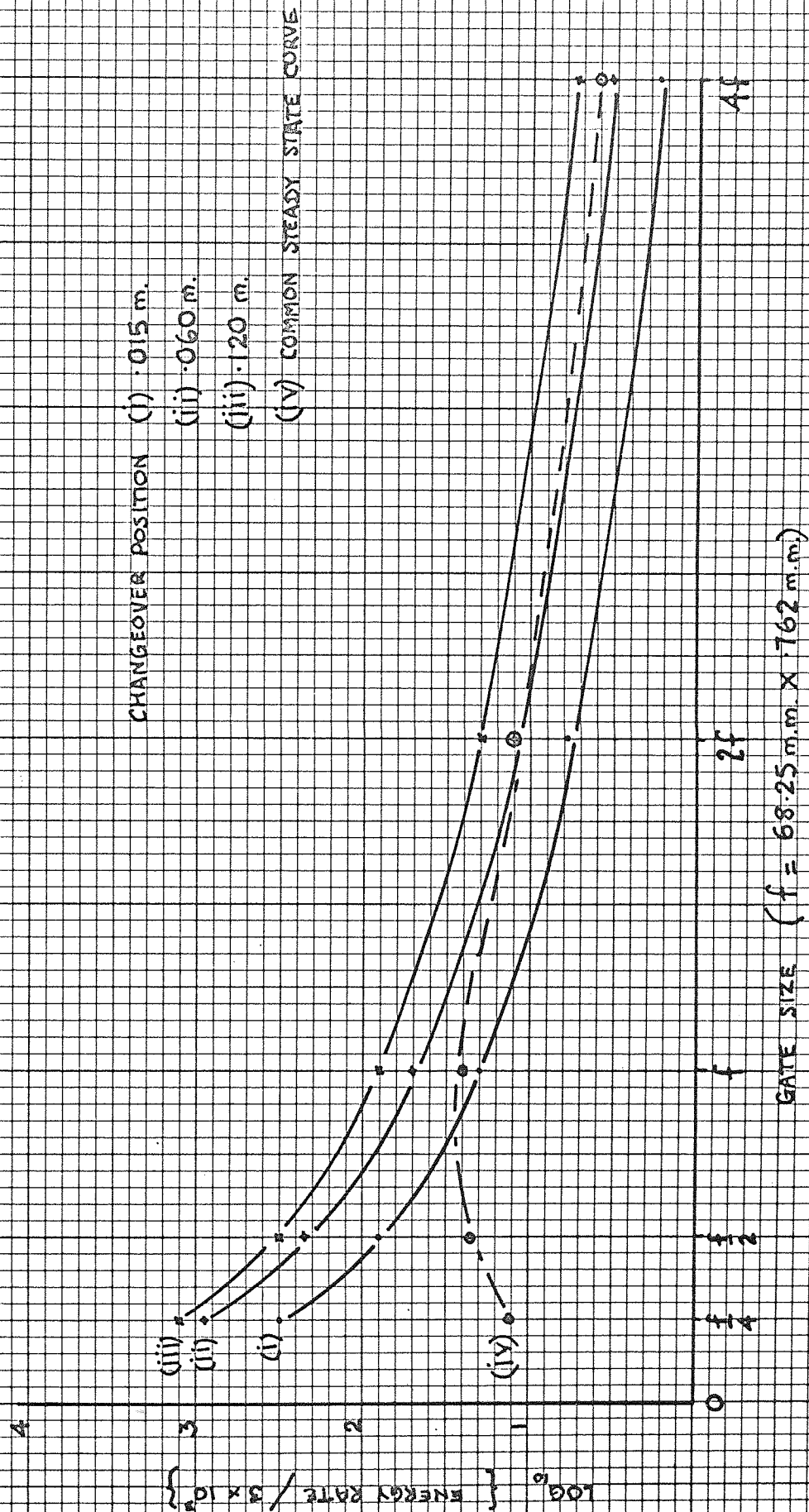


FIG 46 MAXIMUM AND STEADY STATE ENERGY RATES VS. GATE SIZE
FOR MACHINE NUMBER 2

CHANGEOVER POSITION (i) 015 m.
(ii) 060 m.
(iii) 120 m.
(iv) STEADY STATE CURVE

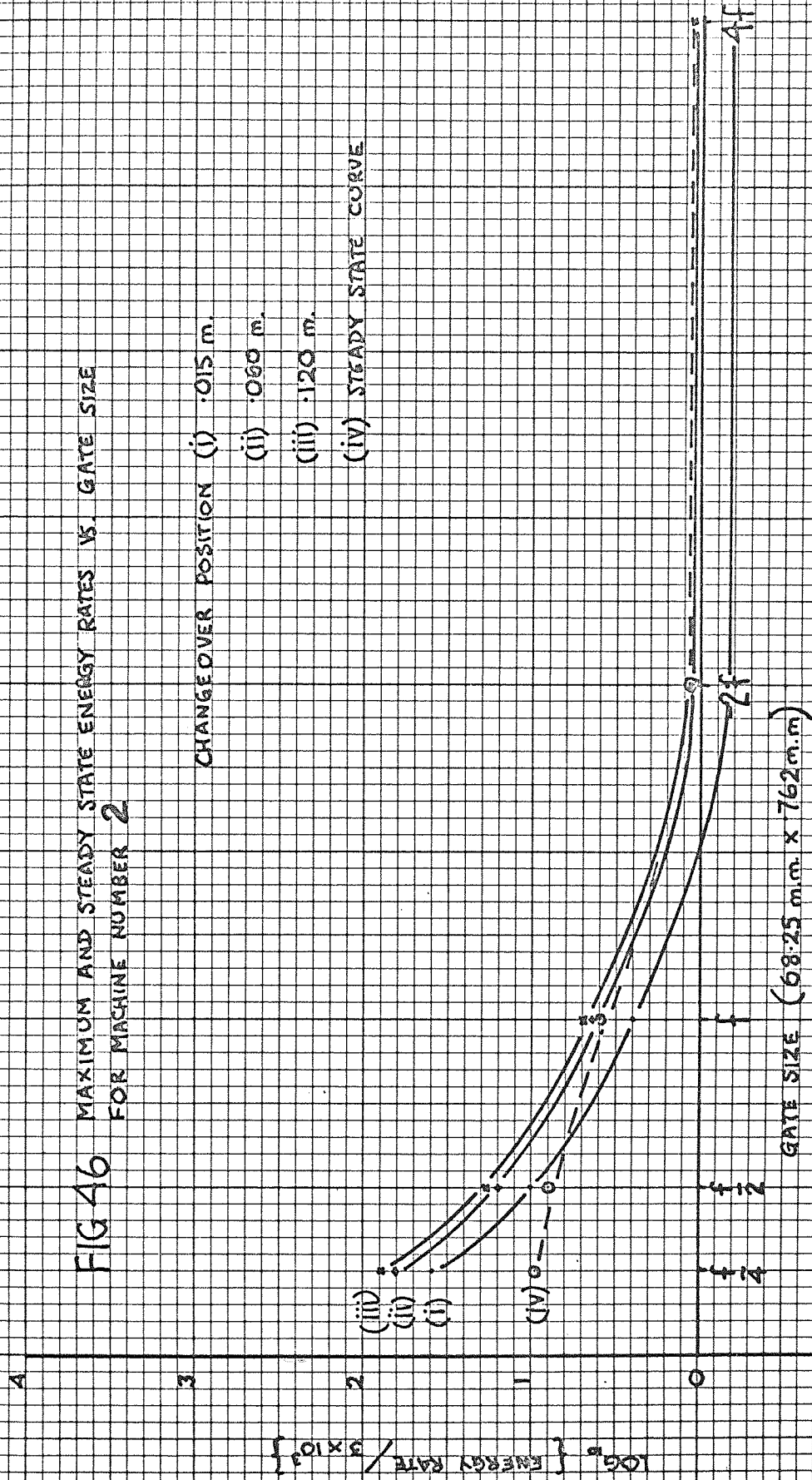


FIG 47 MAXIMUM AND STEADY ENERGY RATES VS. GATE SIZE
FOR MACHINE NUMBER 5

CHANGEOVER POSITION (i) .015 m.

(ii) .06 m.

(iii) .12 m.

(iv) COMMON STEADY STATE CURVE

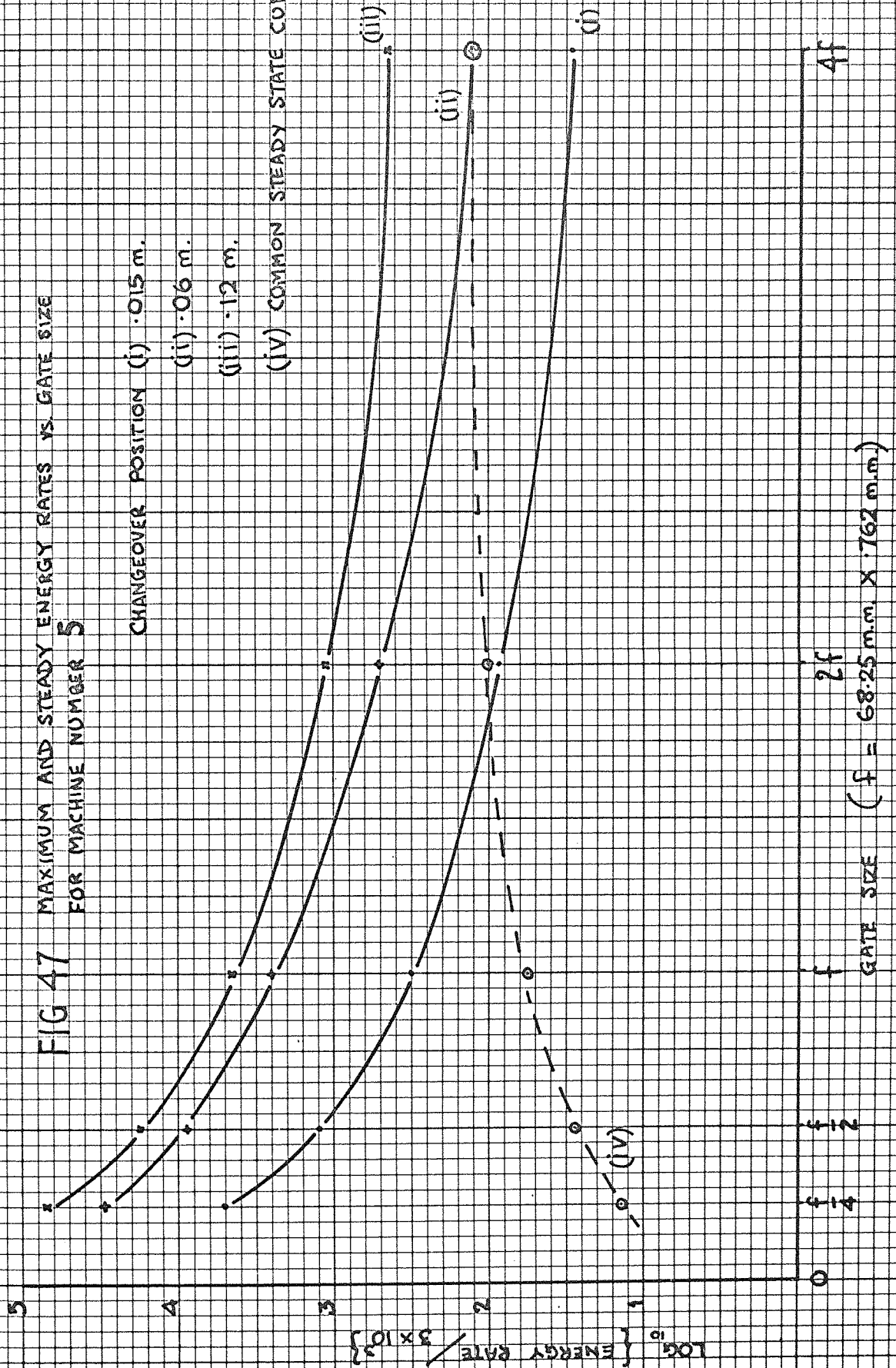
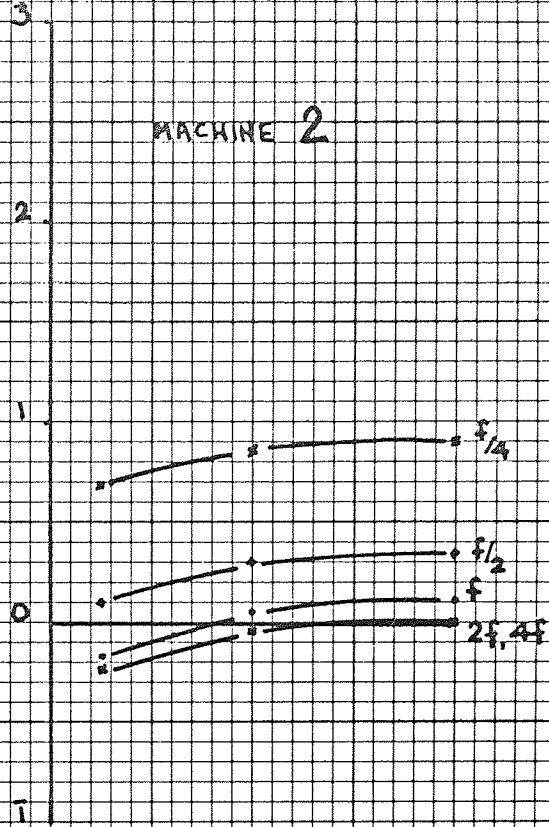
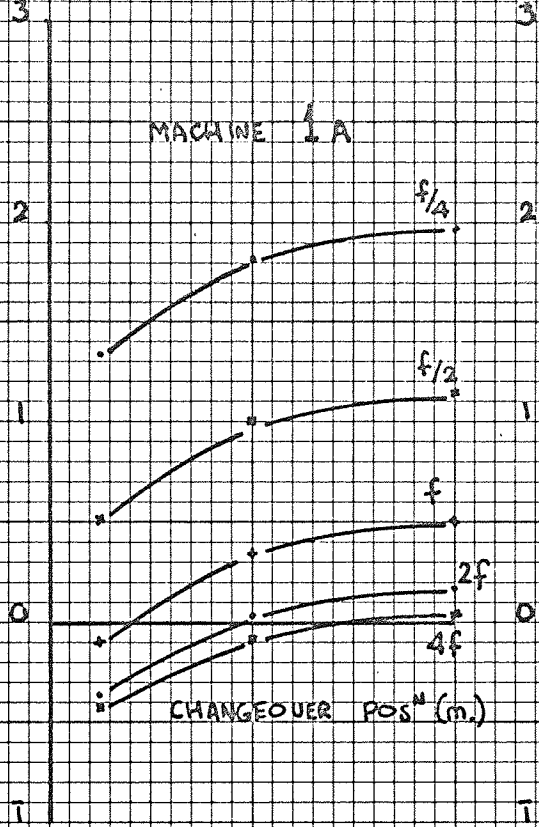


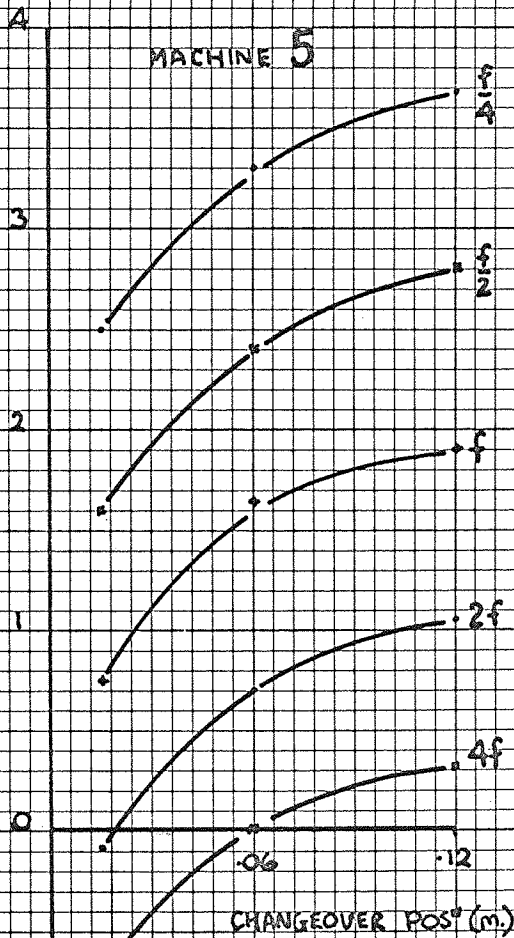
FIG 48

PLOTS OF ENERGY RATE RATIO AGAINST CHANGEOVER POSITION FOR MACHINES 1A, 2 AND 5

$\log_{10} \left\{ \frac{\text{INITIAL ENERGY RATE INPUT TO METAL SYSTEM}}{\text{STEADY STATE ENERGY INPUT}} \right\}$



$\log_{10} \left\{ \frac{\text{INITIAL ENERGY RATE INPUT TO METAL}}{\text{STEADY STATE ENERGY INPUT}} \right\}$



MACHINE CHANGE OVER POSITION (m.)		ENERGY RATE RATIO				
		$\frac{f}{4}$	$\frac{f}{2}$	f	$2f$	$4f$
1A	.120	96	14	3.3	1.5	1.06
	.060	67	10	2.3	1.1	.8
	.015	23	3.4	.7	.4	.4
2	.120	7.8	2.3	1.3	1.0	1.0
	.060	7.1	2.1	1.1	1.0	1.0
	.015	4.4	1.2	.7	.6	.6
5	.120	4700	590	78	11	4
	.060	2000	250	43	5	1
	.015	327	41	5.6	.9	.2

FIG 49 ENERGY RATE VS. FILLING STROKE CASTING IN ALUMINIUM AND IN ZINC

[GATE SIZE = 68.25 m.m. x 762 m.m., CHANGE OVER POS^m .06 m.]

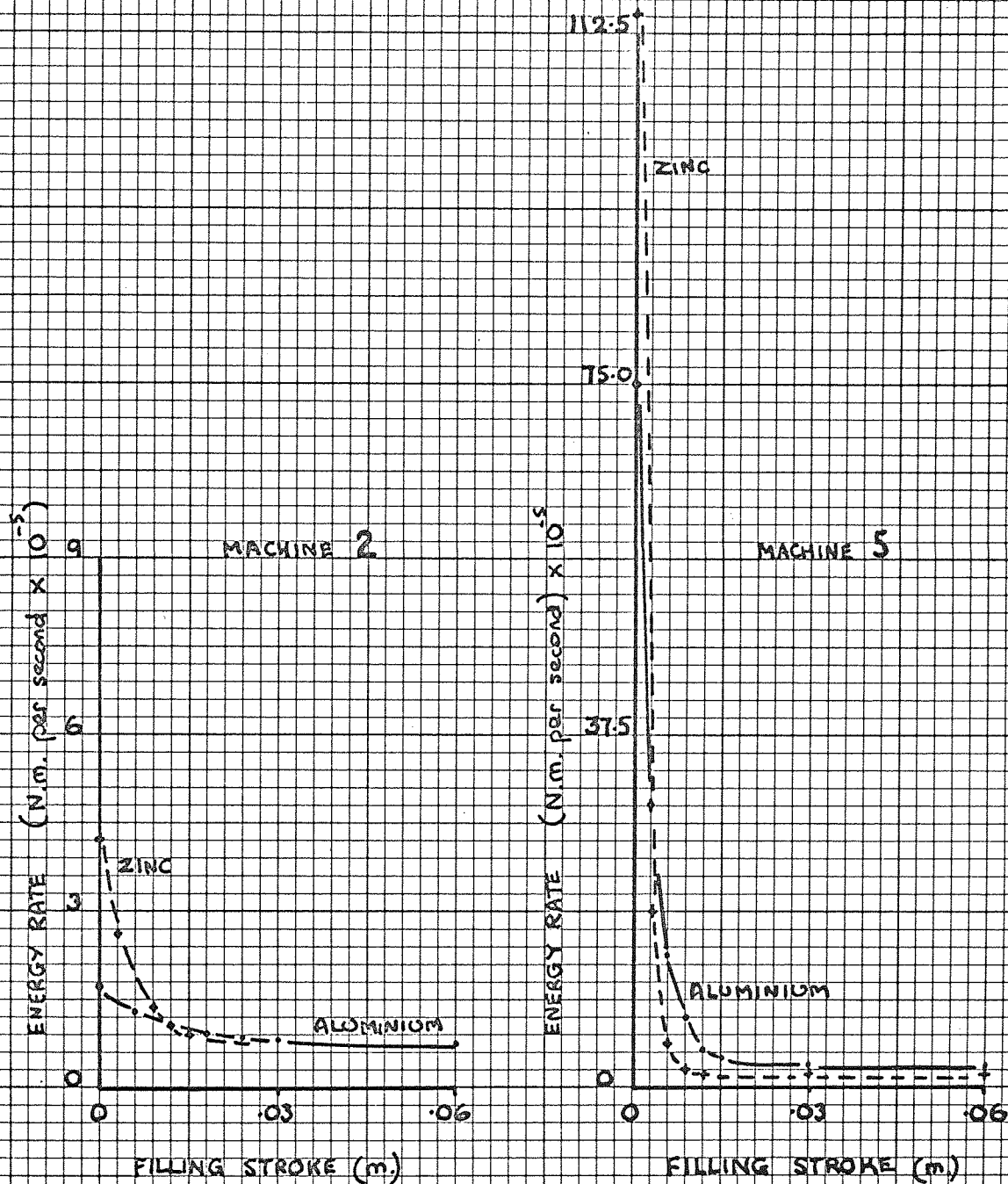


FIG 50

ENERGY RATE, PISTON VELOCITY VS. NET DRIVE FORCE
[MACHINE NUMBER 5, GATE SIZE 68.25 mm. X 762 mm,
CHANGE OVER POSITION .06 m.]

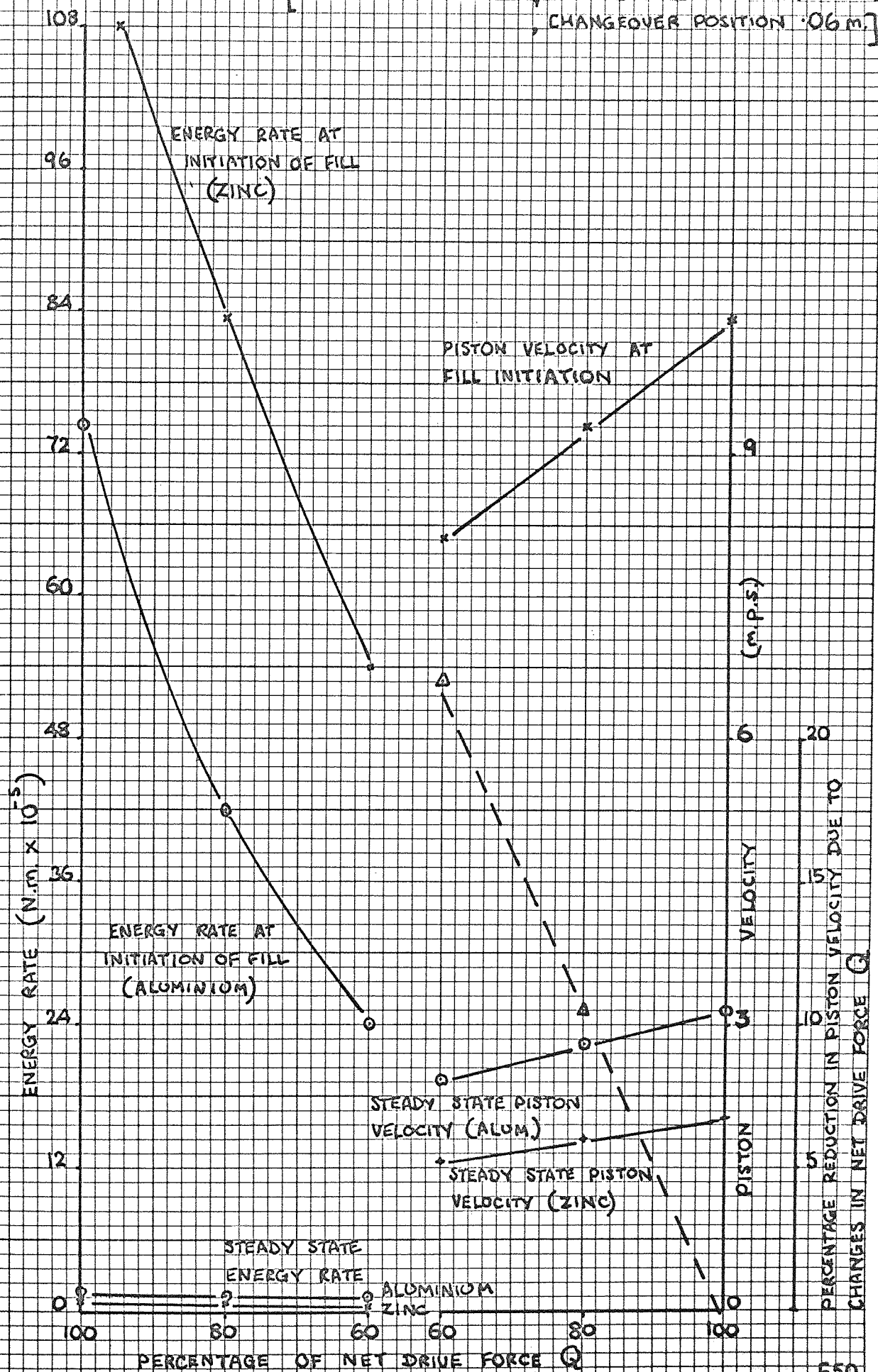
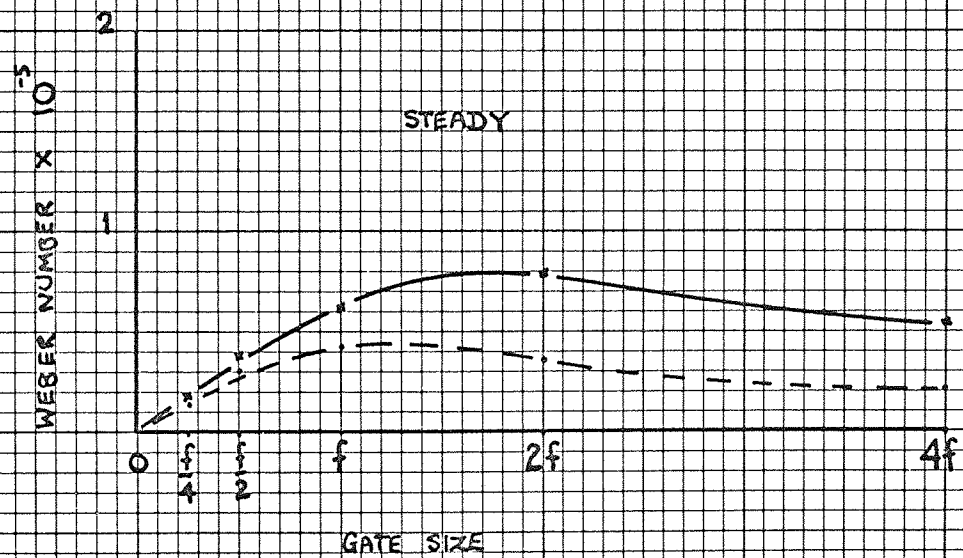
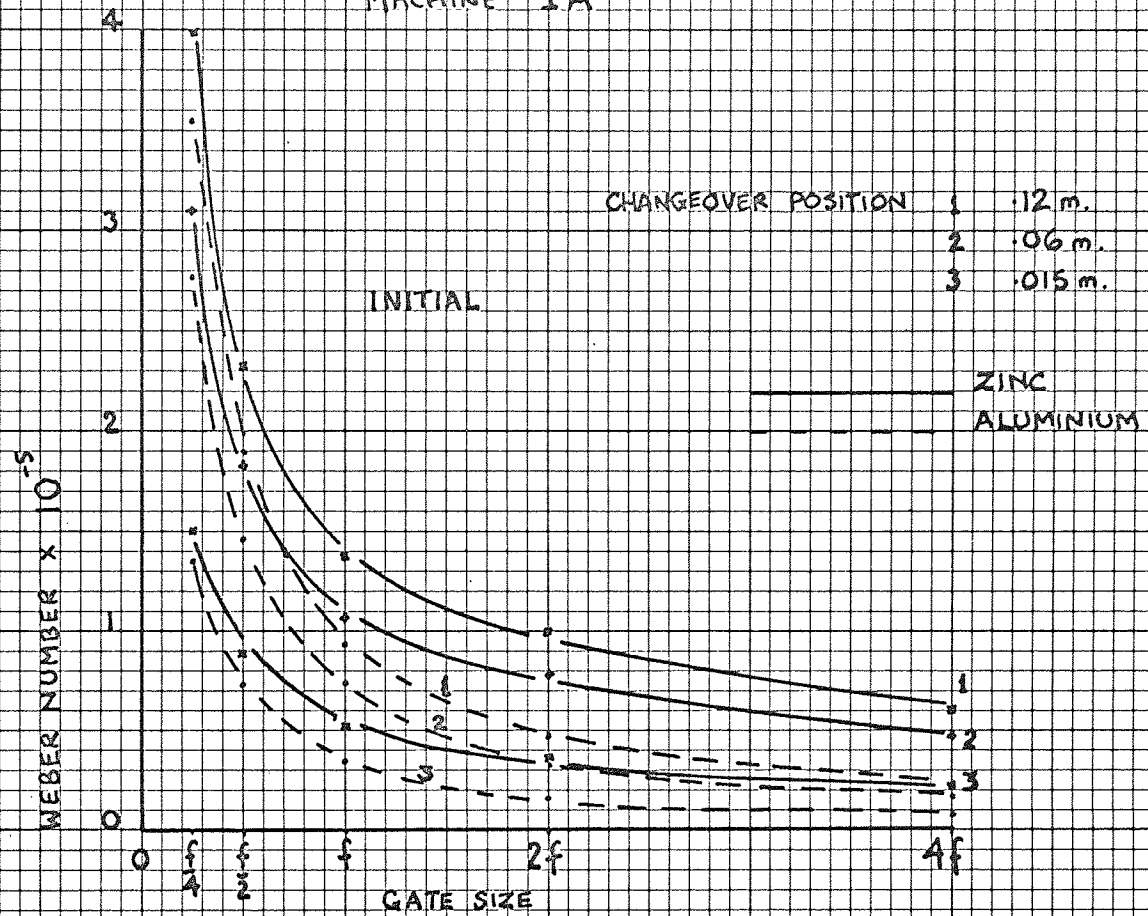


FIG 51 GRAPH OF WEBER NUMBER AGAINST GATE SIZE FOR A RANGE OF CHANGEOVER POSITION USING MACHINE 1A



$$(f = 68.25 \text{ m.m.} \times .762 \text{ m.m.})$$

FIG 52 GRAPH OF WEBER NUMBER AGAINST GATE SIZE FOR A RANGE OF CHANGEOVER POSITIONS USING MACHINE NUMBER 2

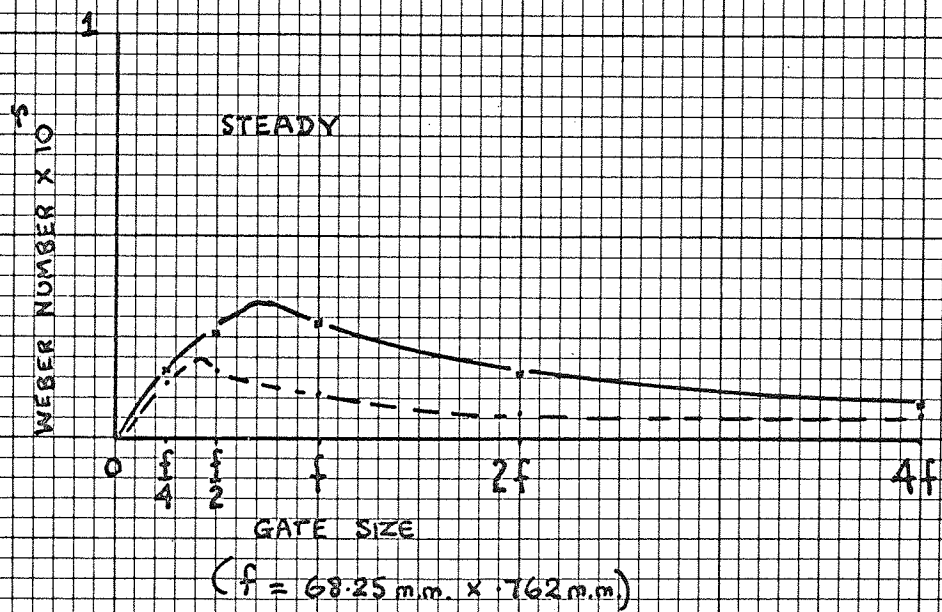
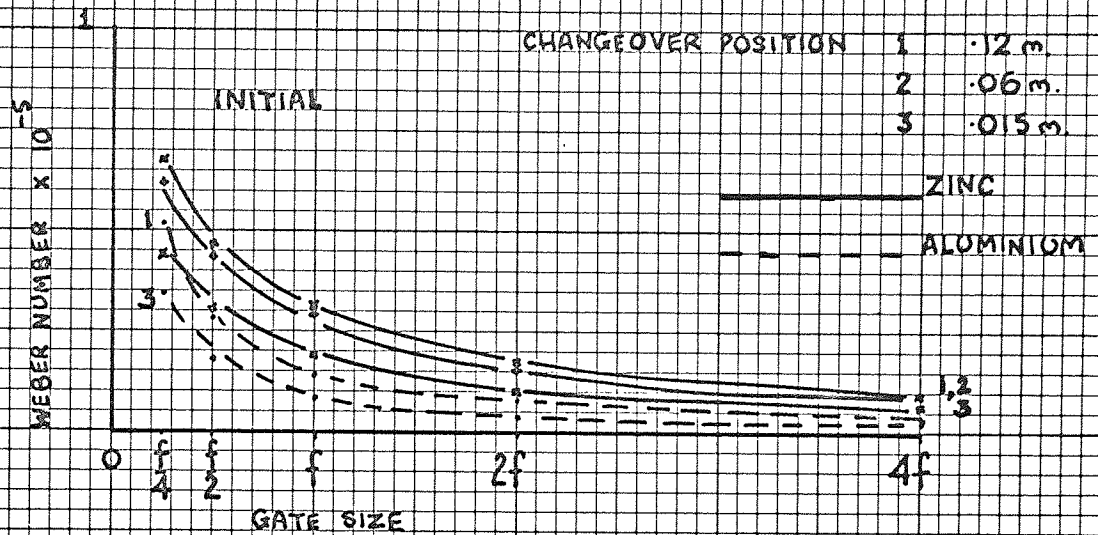


FIG 53

GRAPH OF WEBER NUMBER AGAINST GATE SIZE
FOR A RANGE OF CHANGEOVER POSITION
USING MACHINE NUMBER 5

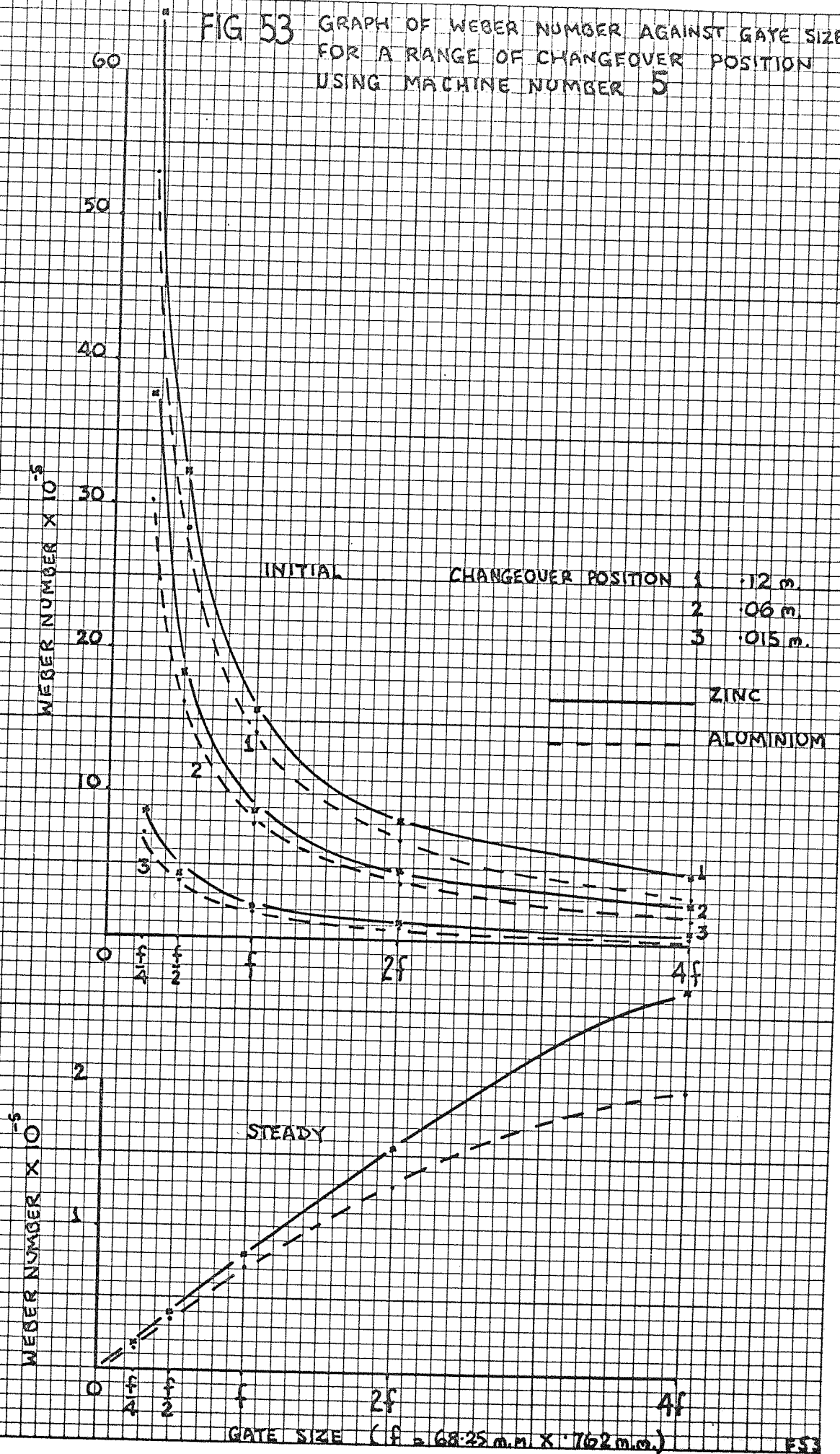
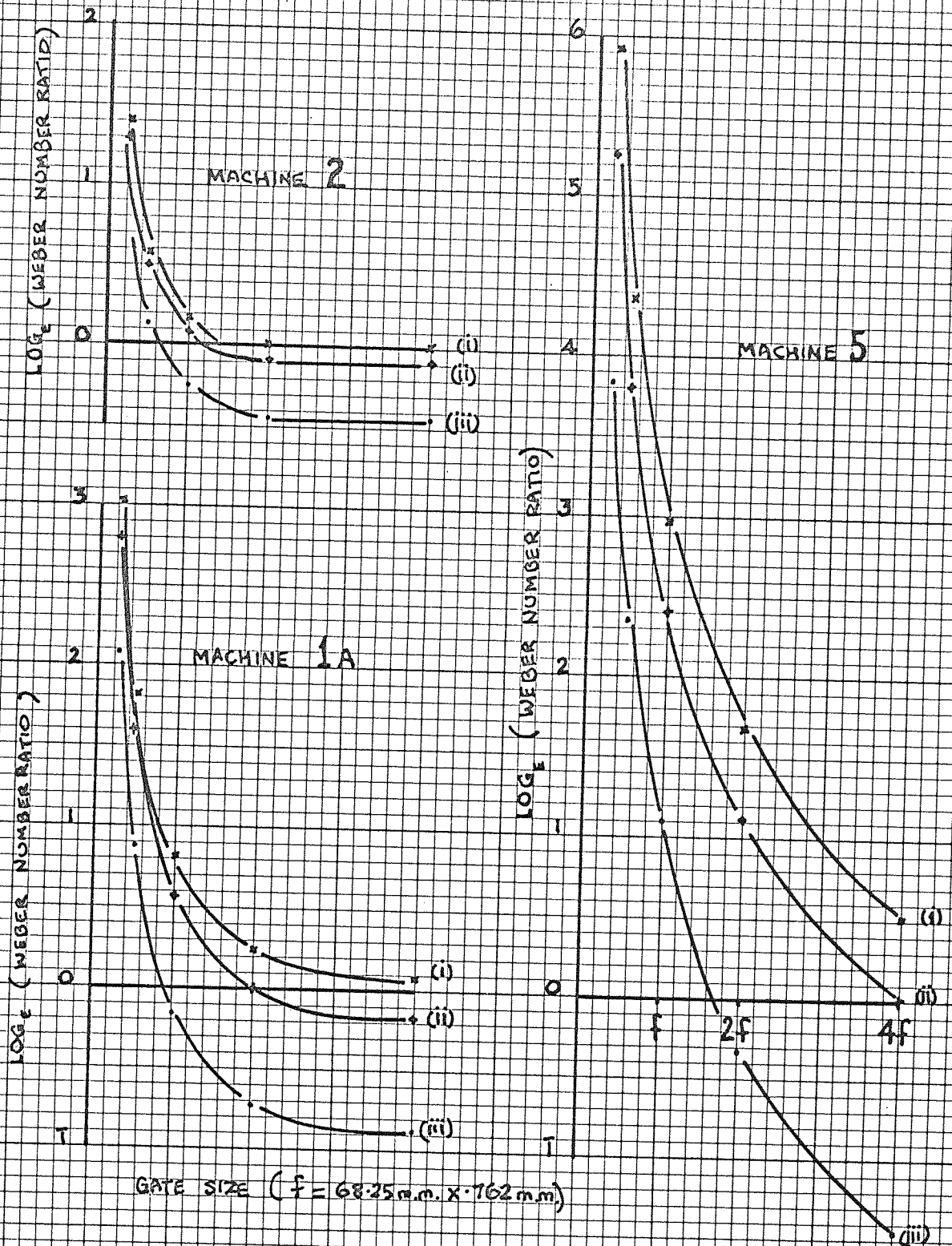


FIG 54 GRAPH OF WEBER NUMBER INITIAL / STEADY FLOW RATIO FOR A RANGE OF CHANGEOVER POSITIONS AND MACHINES



CHANGEOVER POSITION (i) .12 m.
(ii) .06 m.
(iii) .015 m.

FIG 55 VIEWS OF CASTING ILLUSTRATING RUNNER : GATE : CAVITY LAYOUT

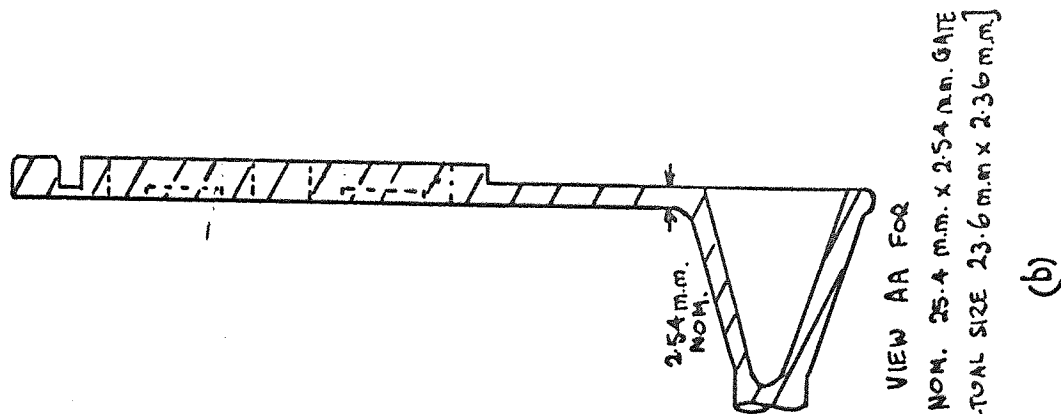
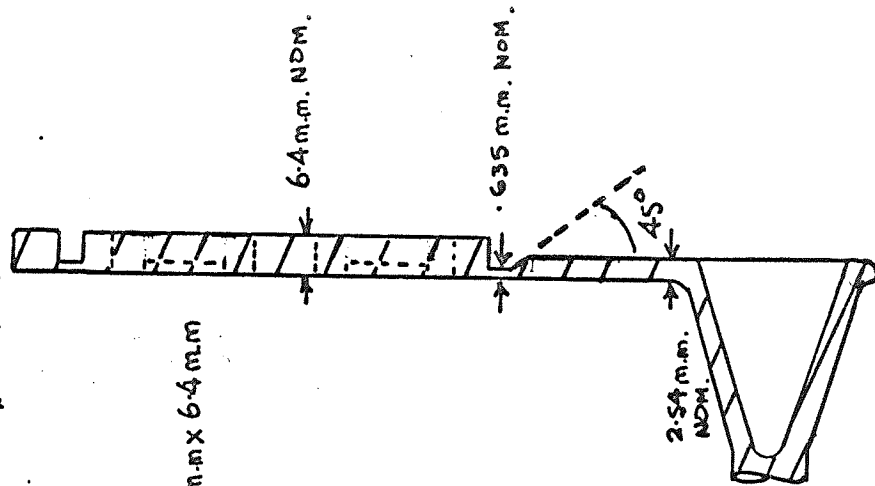
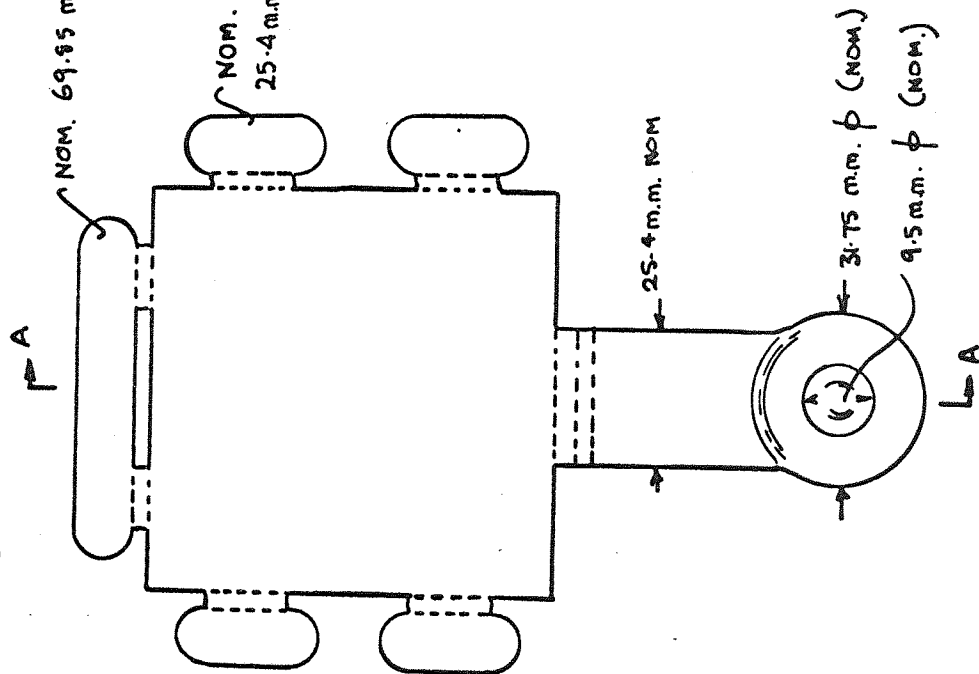


FIG 56 DIAGRAMMATIC LAYOUT OF EMB 10
INJECTION CYLINDER

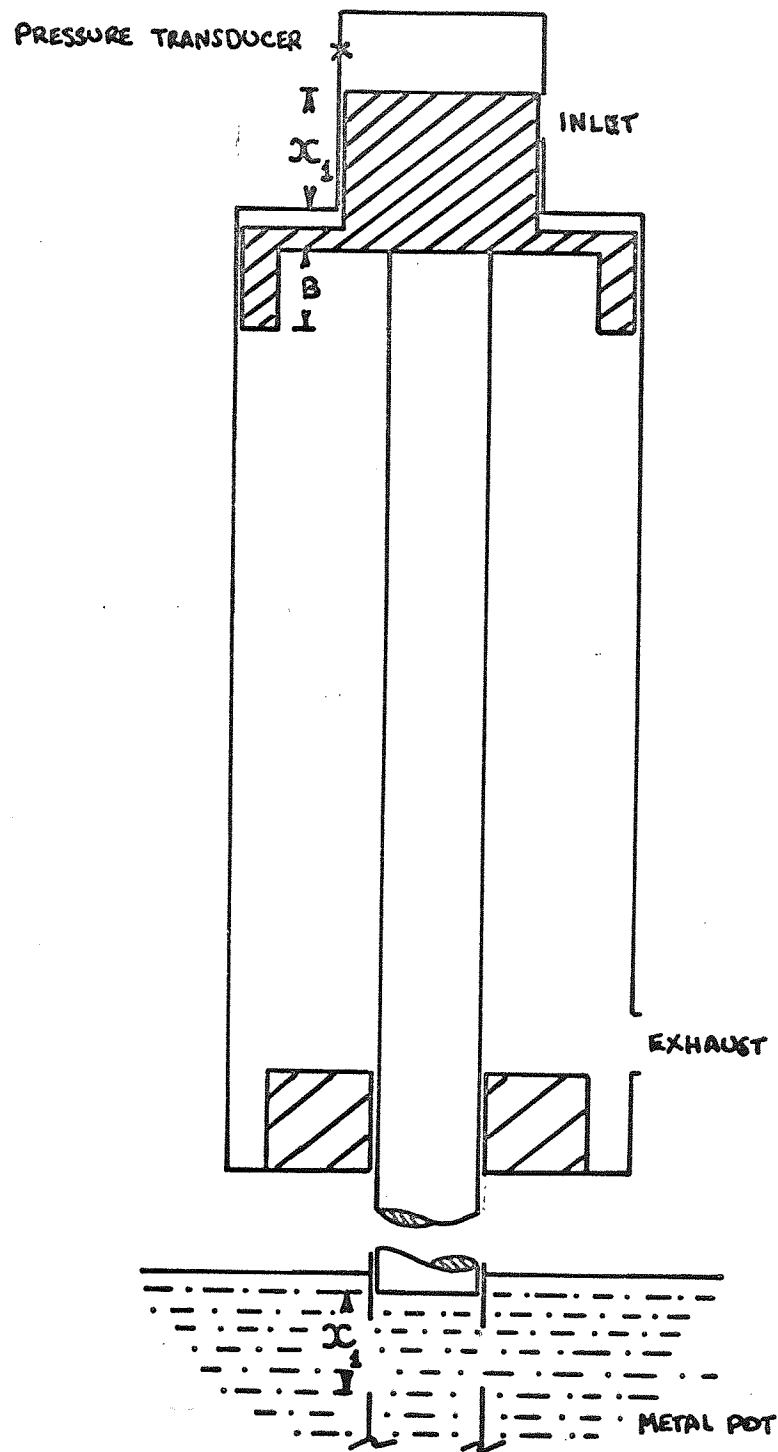
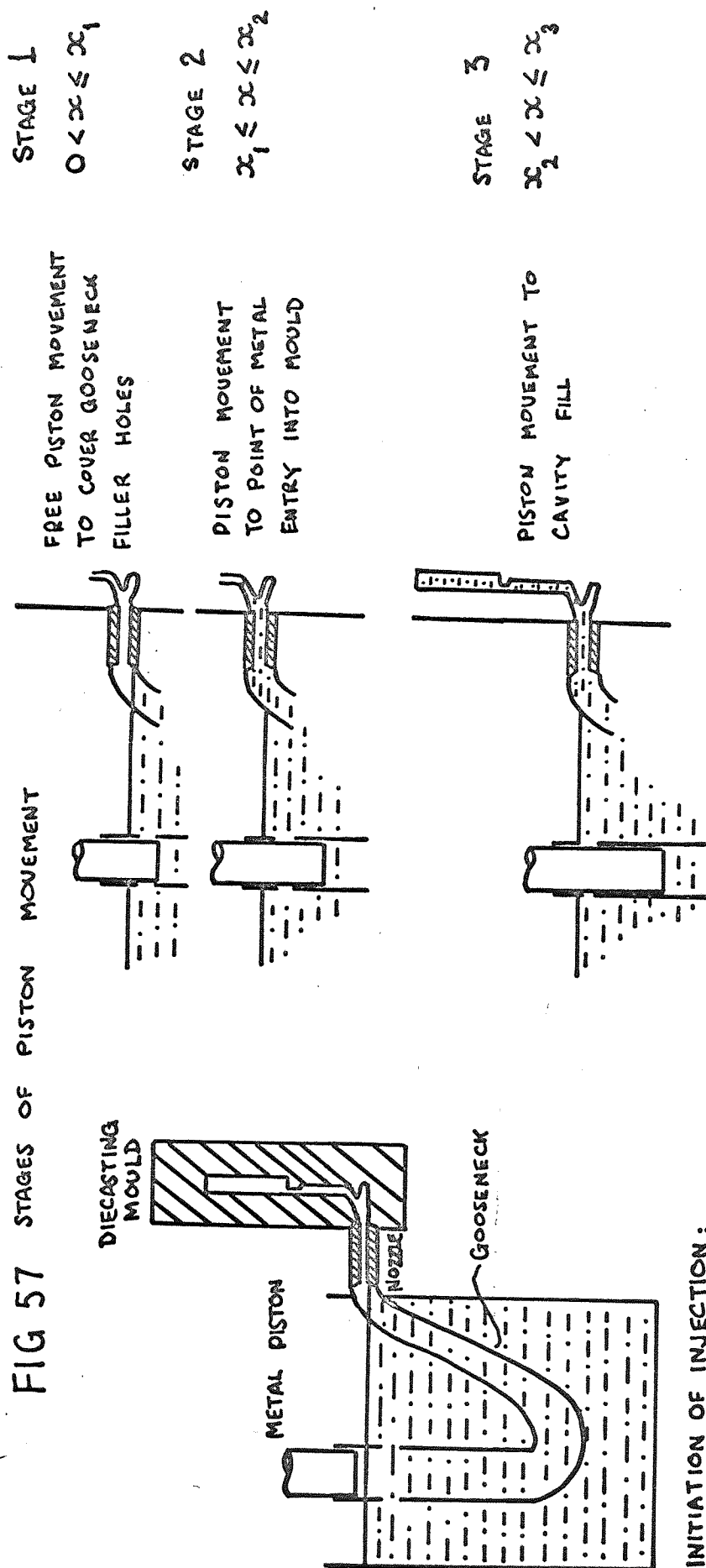


FIG 57 STAGES OF PISTON MOVEMENT



INITIATION OF INJECTION:
 PISTON IN FULLY RETURNED
 POSITION ($x=0$)

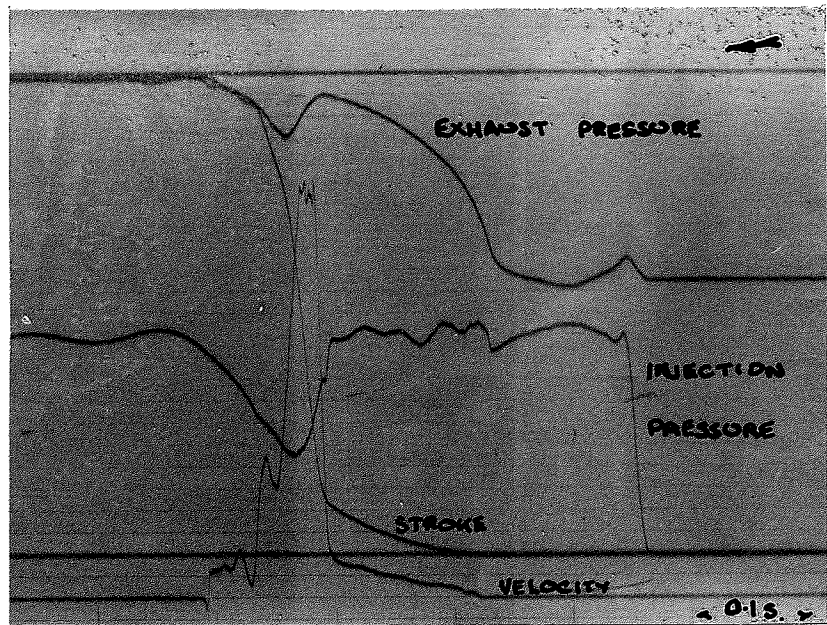


FIG 58 PISTON CHARACTERISTIC - 'FREE RUNNING'

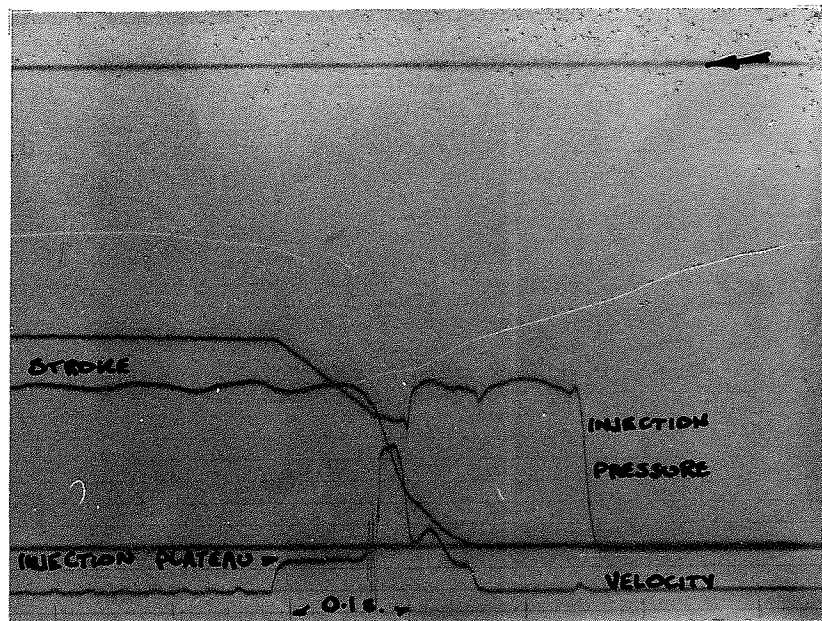


FIG 59 PISTON CHARACTERISTIC - INJECTION

FIG 60

COMPARISON OF CALCULATION OF PISTON SPEED
WITH MEASURED VALUES FOR EMB 10 MACHINE

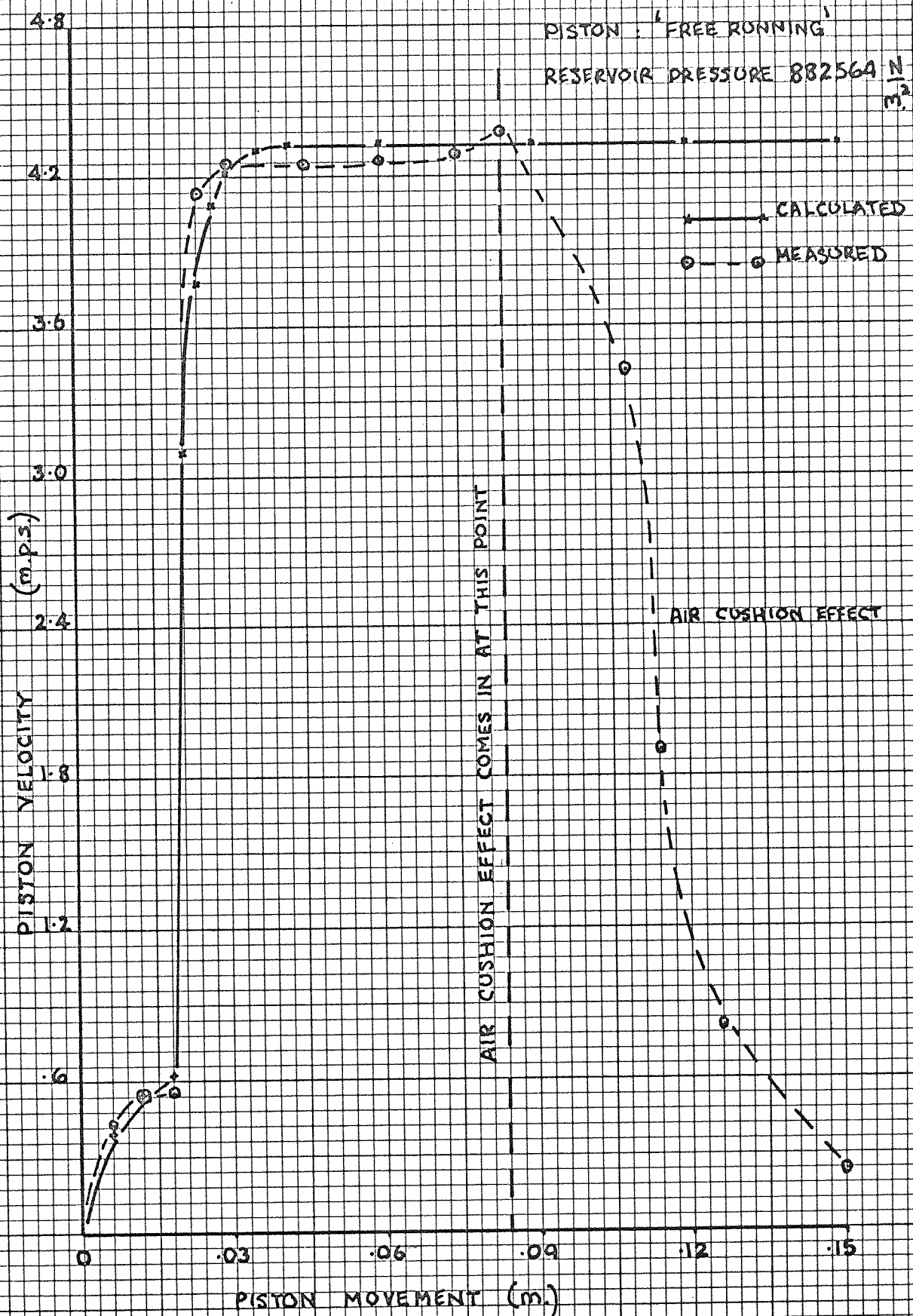


FIG 61a

CALCULATED AND MEASURED PISTON VELOCITY
CHARACTERISTICS FOR THE EXPERIMENTAL
TOOL ON THE EMB10 DIECASTING MACHINE

CAVITY SIZE 762mm x 762mm.
x 6.35mm.

GATE SIZE 25.4mm. x 58mm.

RESERVOIR PRESSURE 950000 N/m^2

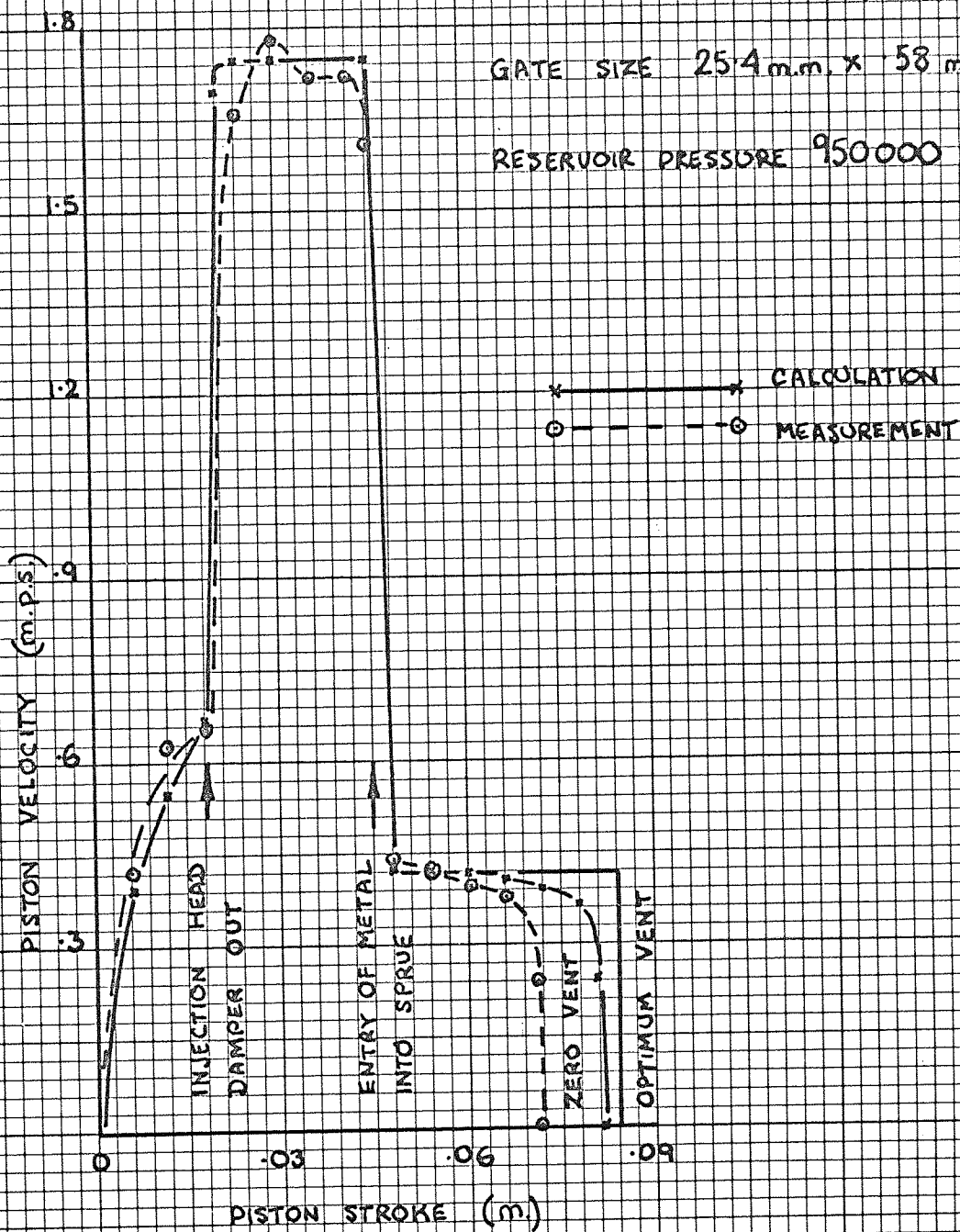


FIG 61b

CALCULATED AND MEASURED PISTON VELOCITY
CHARACTERISTICS FOR THE EXPERIMENTAL
TOOL ON THE EMB 10 DIECASTING MACHINE

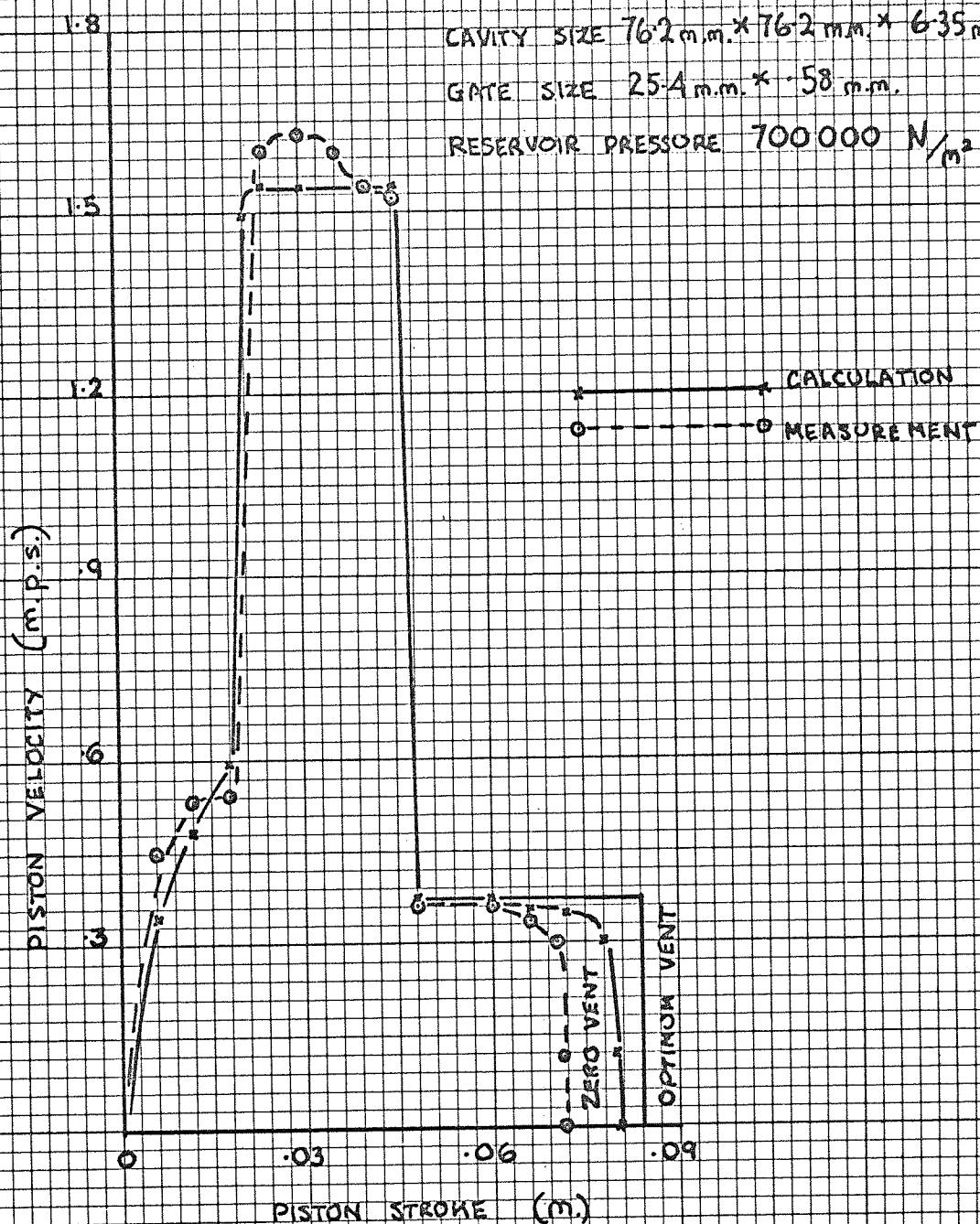


FIG 61c CALCULATED AND MEASURED PISTON VELOCITY CHARACTERISTICS FOR THE EXPERIMENTAL TOOL ON THE EMB10 DIECASTING MACHINE

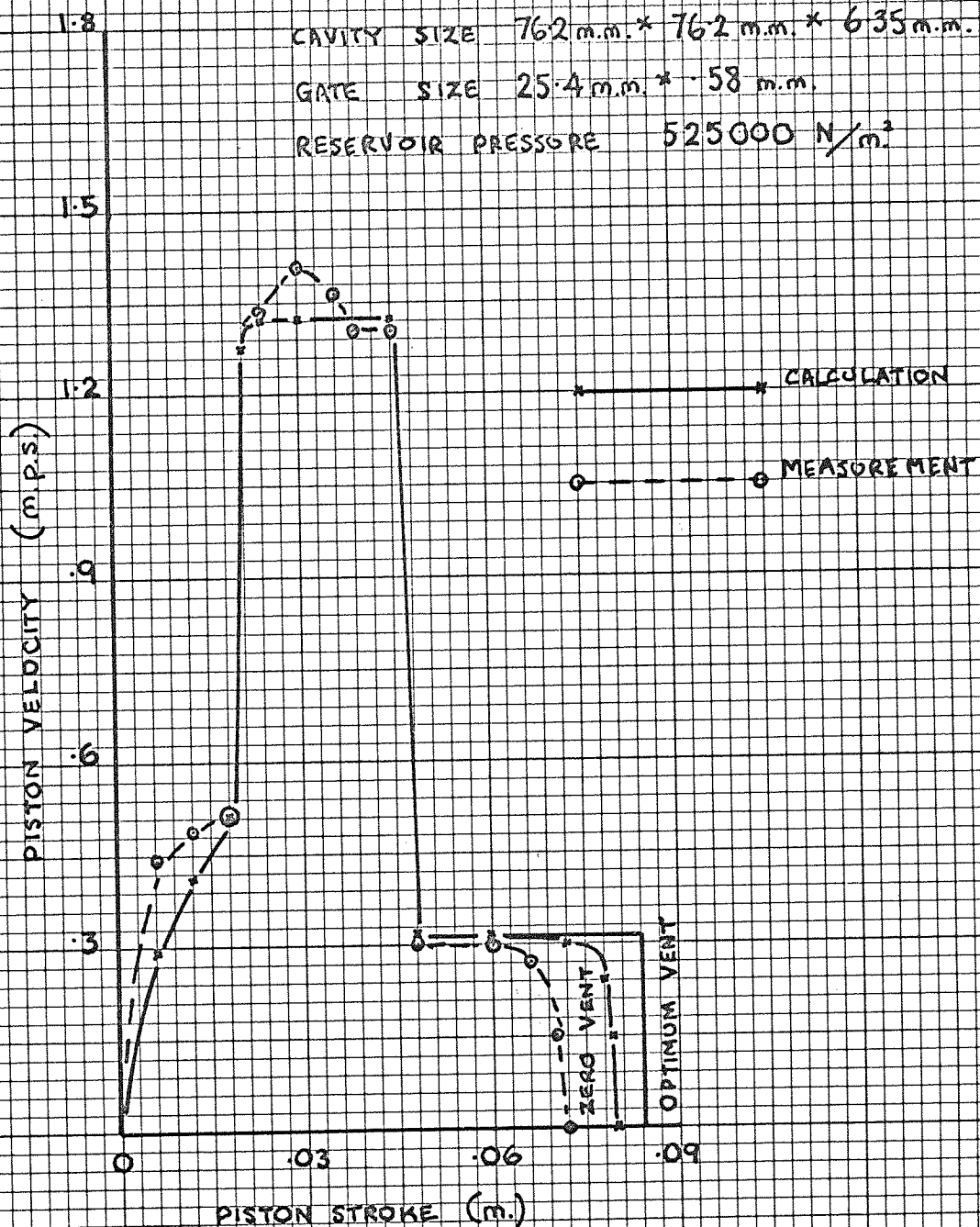


FIG 62a

CALCULATED AND MEASURED PISTON
VELOCITY CHARACTERISTICS FOR THE
EXPERIMENTAL TOOL ON THE EMB 10
DIECASTING MACHINE

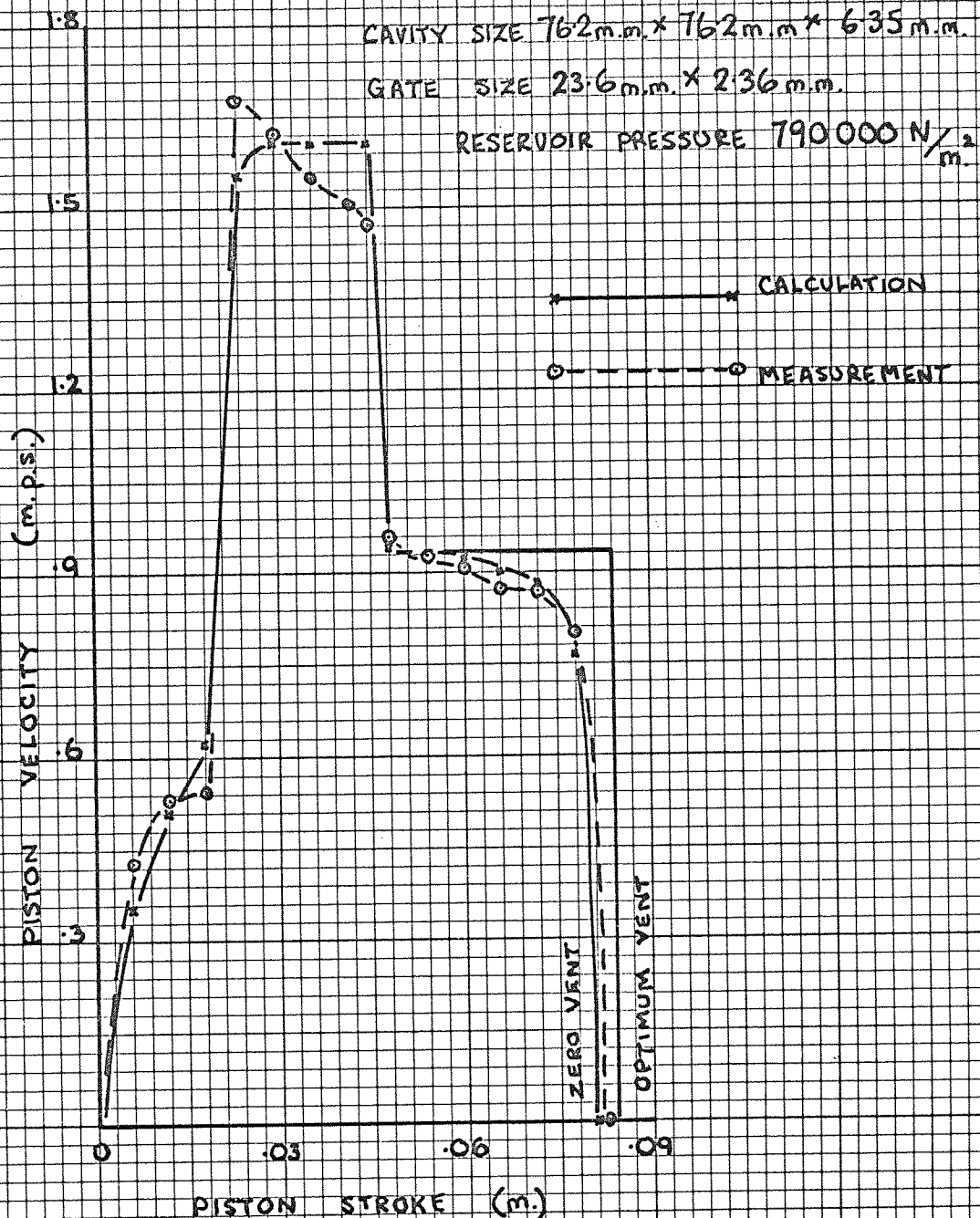


FIG 62 b

CALCULATED AND MEASURED PISTON VELOCITY
CHARACTERISTICS FOR THE EXPERIMENTAL
TOOL ON THE EMB 10 DIECASTING MACHINE

CAVITY SIZE 76.2 mm. x 76.2 mm. x 6.35 mm.

GATE SIZE 23.6 mm. x 2.36 mm.

RESERVOIR PRESSURE 670 000 N/m²

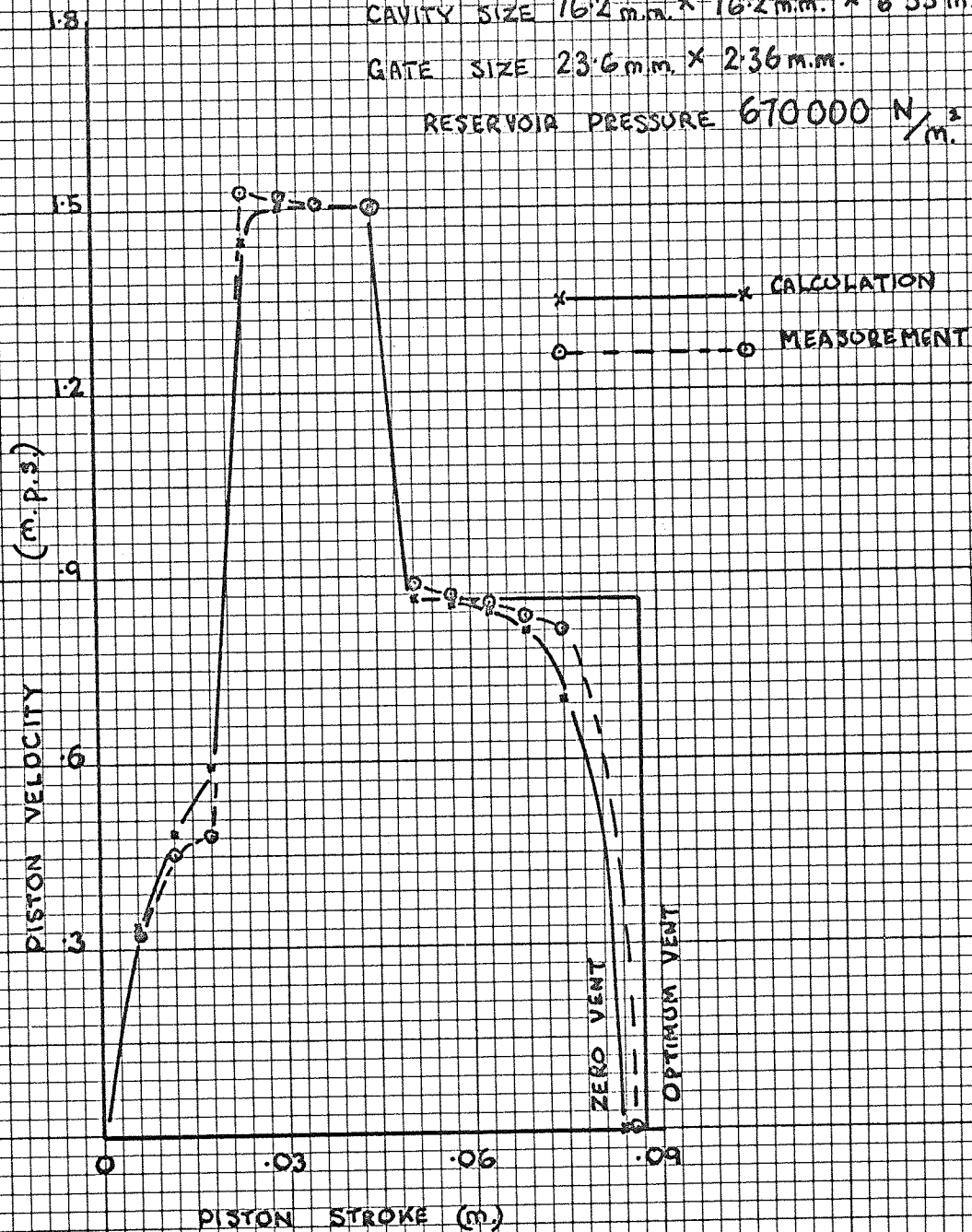


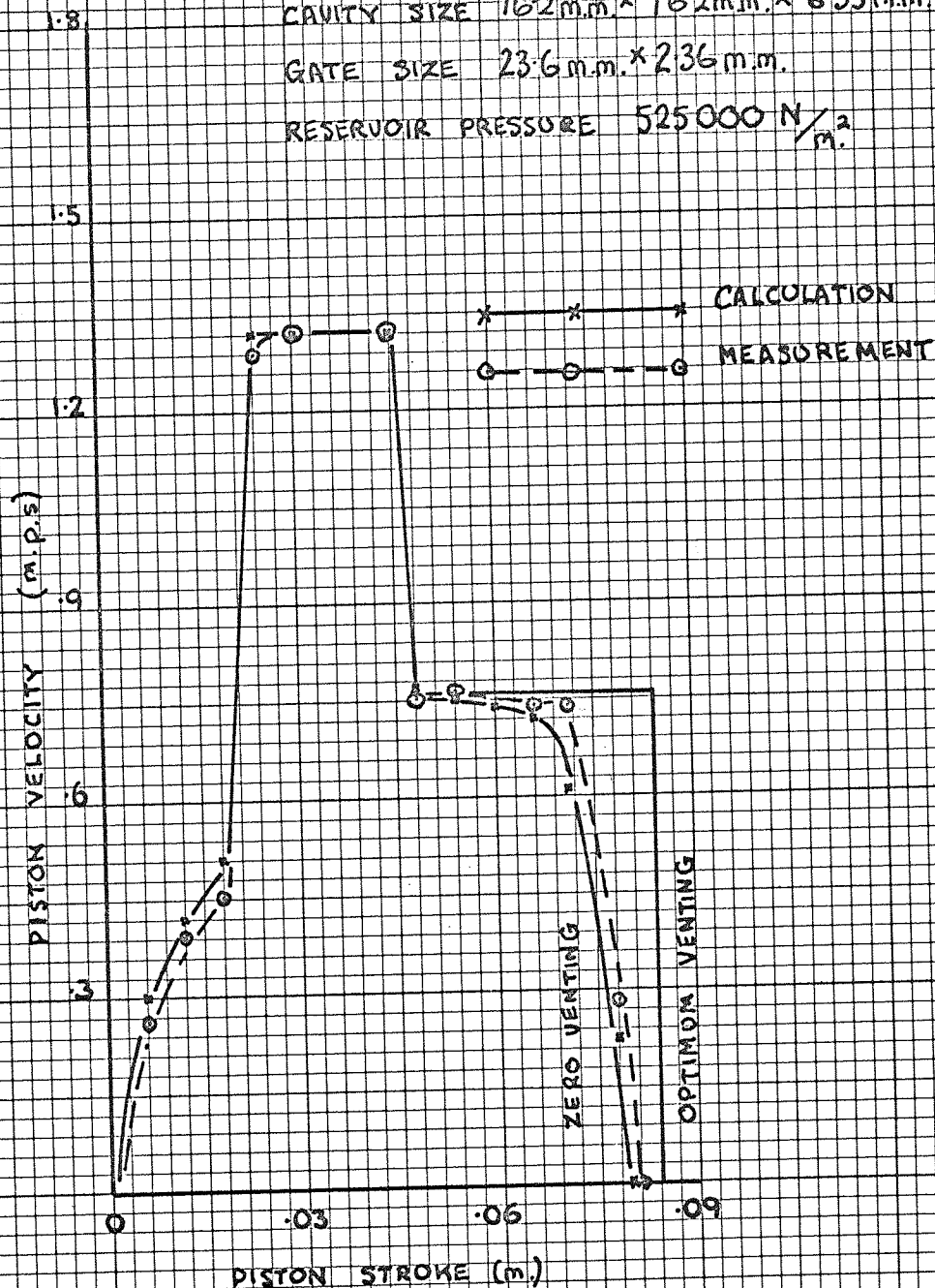
FIG 62C

CALCULATION AND MEASURED PISTON VELOCITY
CHARACTERISTICS FOR THE EXPERIMENTAL TOOL
ON THE EMB 10 DIECASTING MACHINE

CAVITY SIZE 76.2mm x 76.2mm x 6.35mm.

GATE SIZE 23.6mm x 23.6mm.

RESERVOIR PRESSURE 525000 N/m²



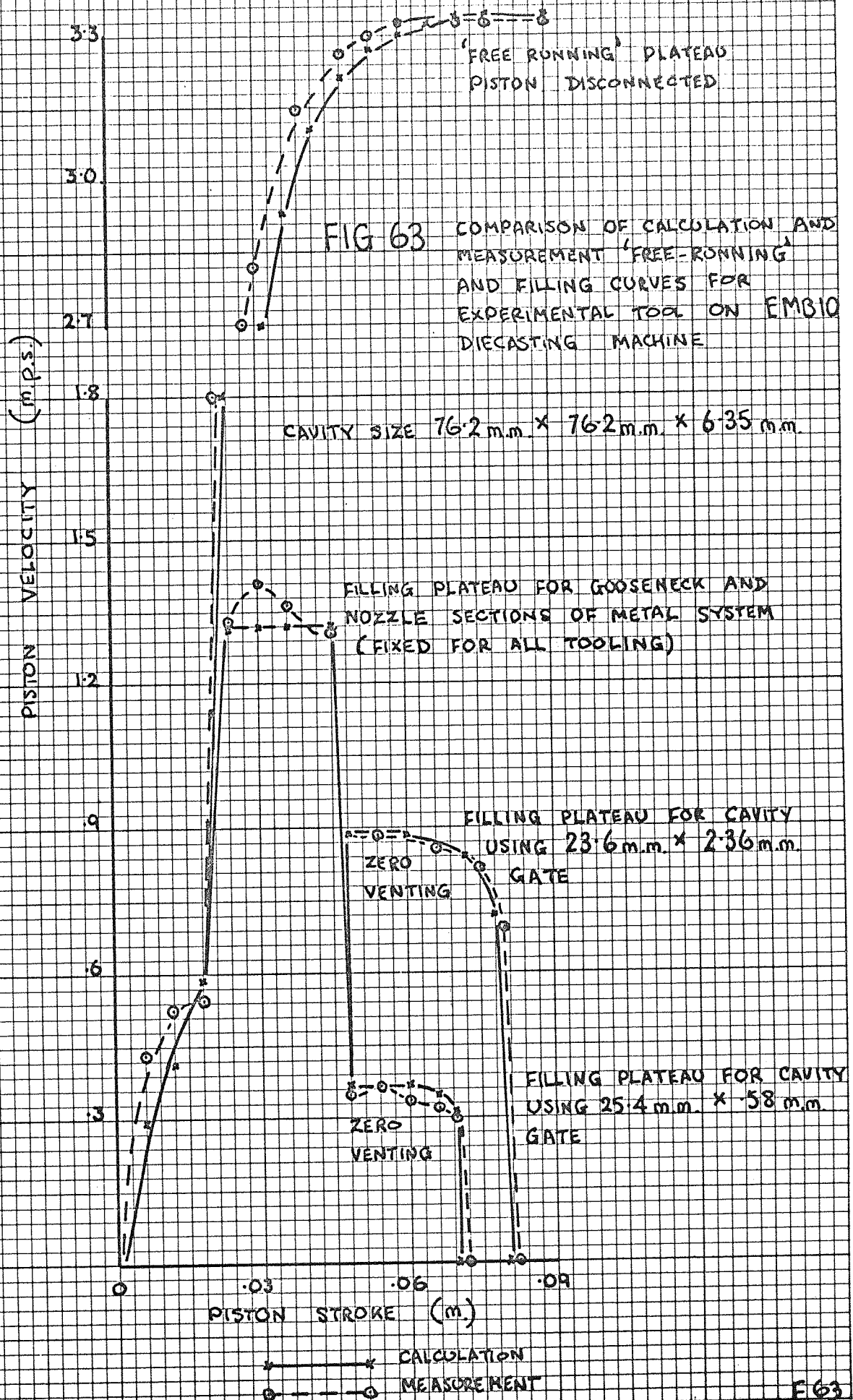


FIG 64 COMPARISON OF CALCULATION AND MEASUREMENT OF ELAPSED TIME VS. STROKE FOR EXPERIMENTAL TOOL ON EMBIO (GATE SIZE 25.4 m.m. X 58 m.m.)

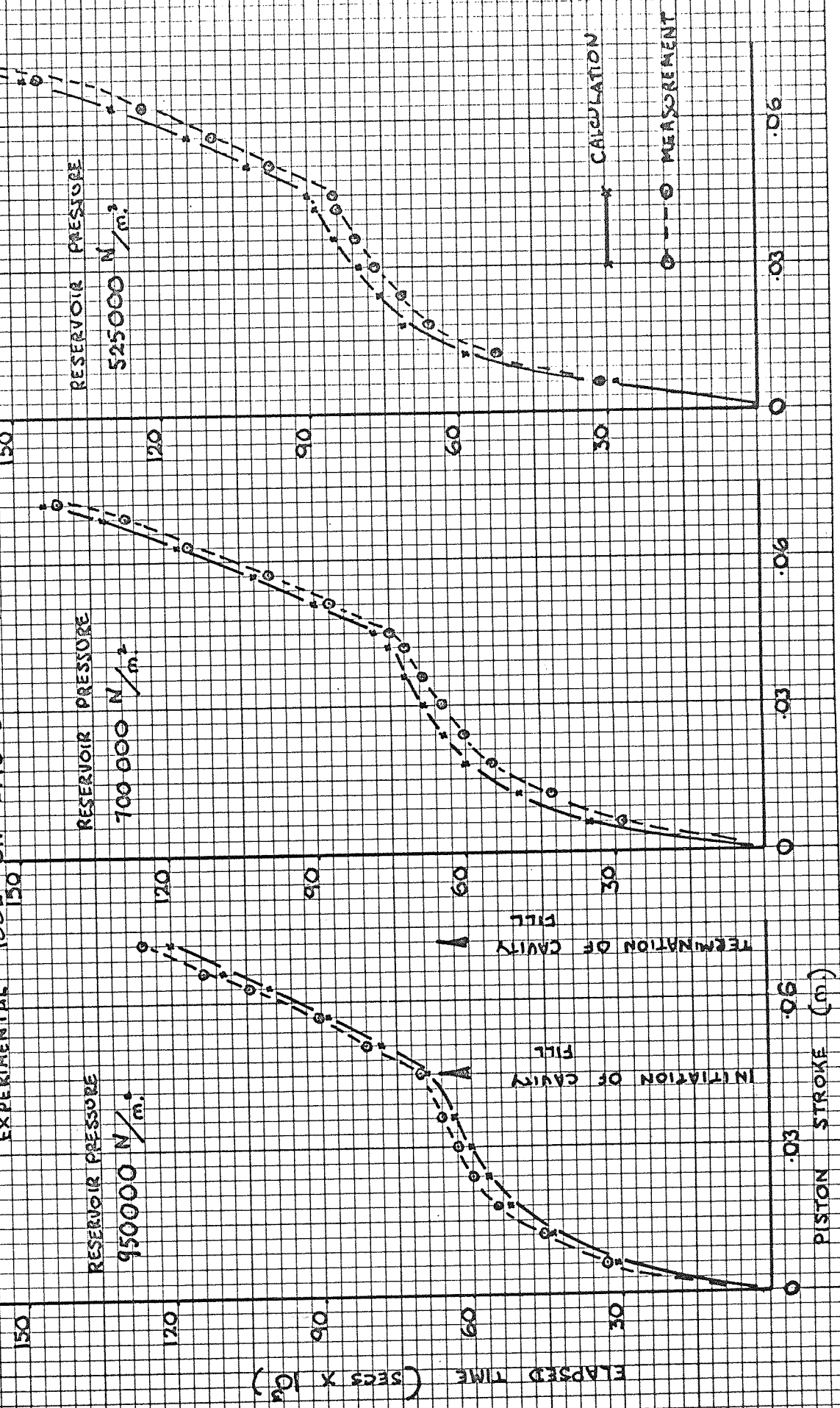


FIG 65 COMPARISON OF INJECTION CYLINDER DRIVE PRESSURE VS. STROKE BY CALCULATION AND MEASUREMENT FOR 140 EXPERIMENTAL TOOL ON EMB10

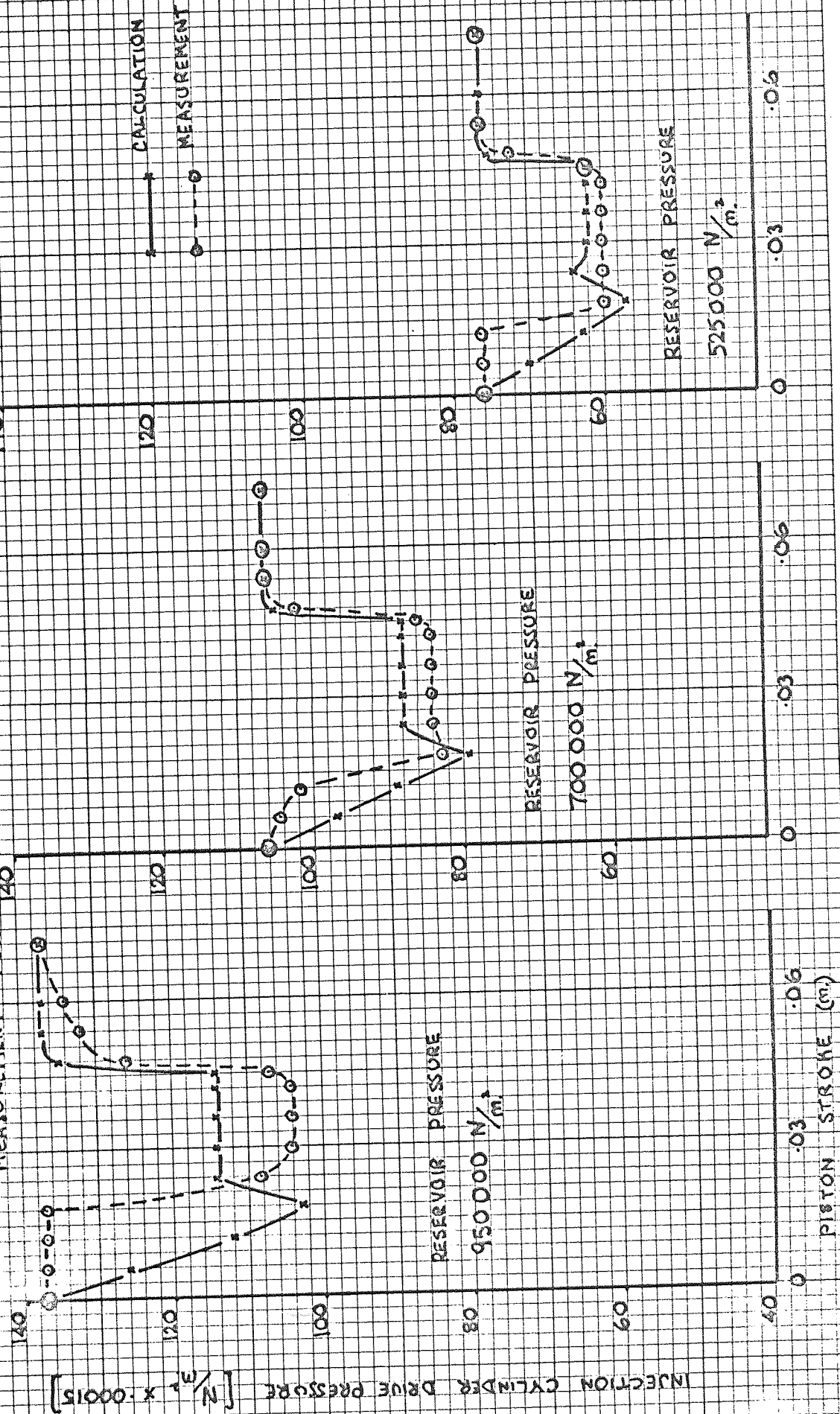


FIG 66a ENERGY RATE VS. GATE AREA

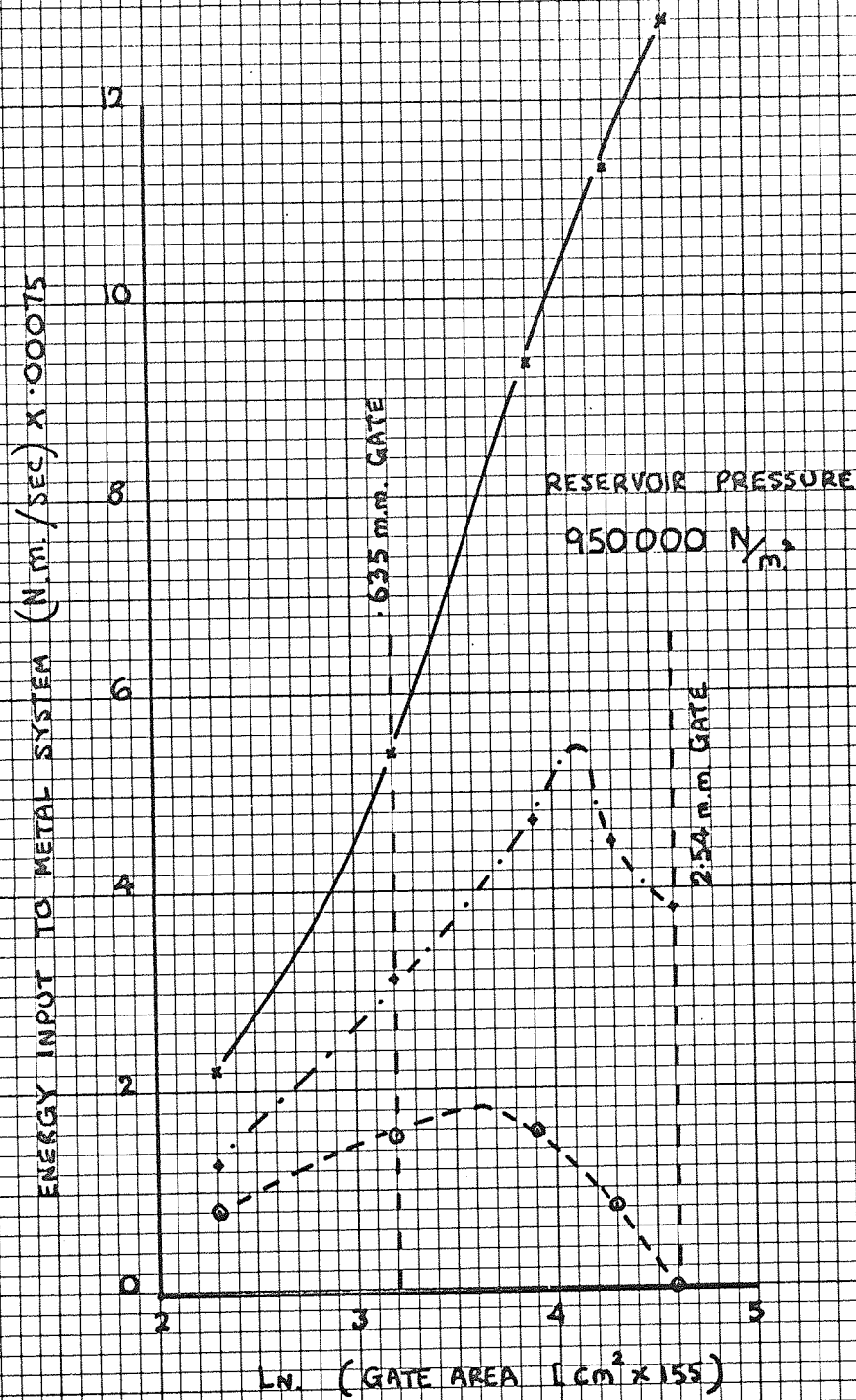


FIG 66b ENERGY RATE vs. GATE AREA

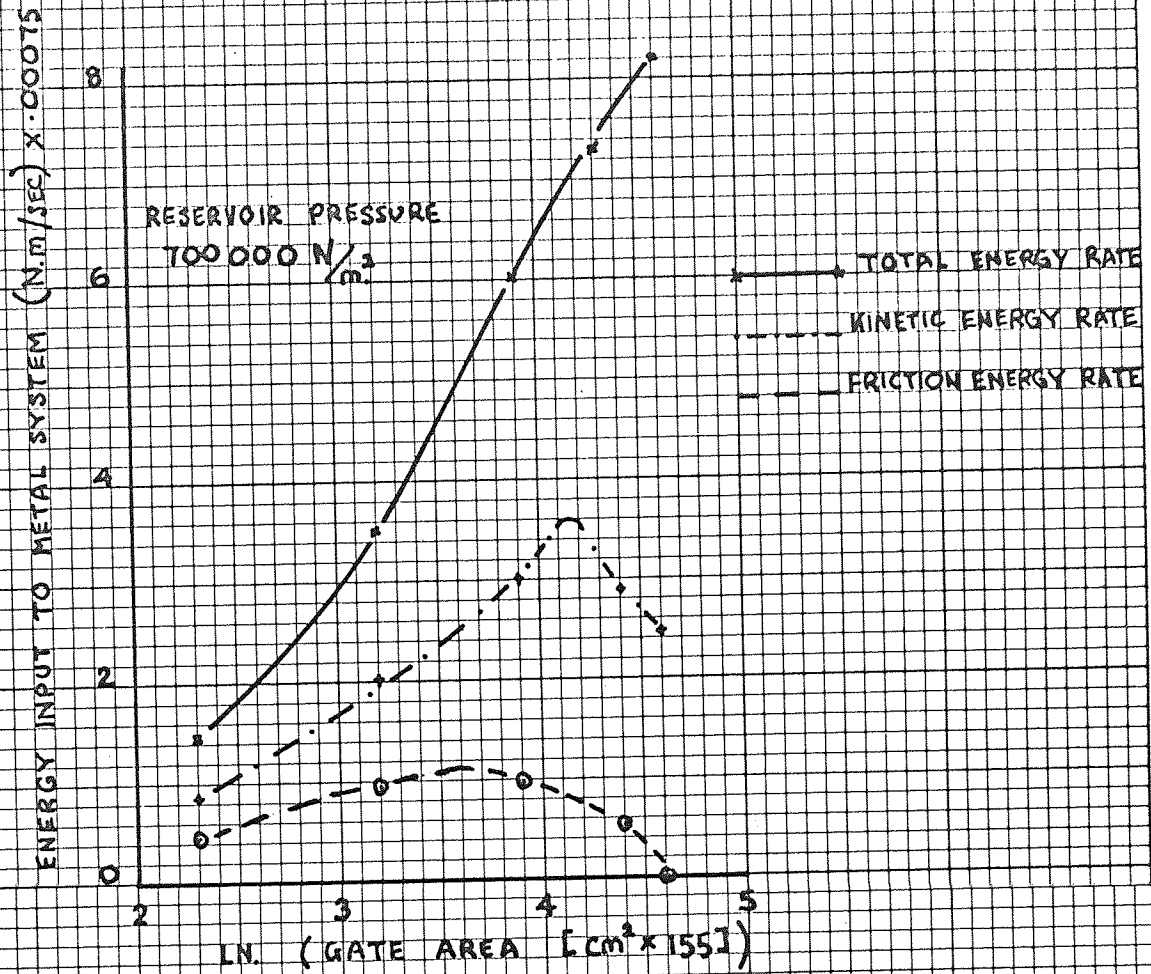
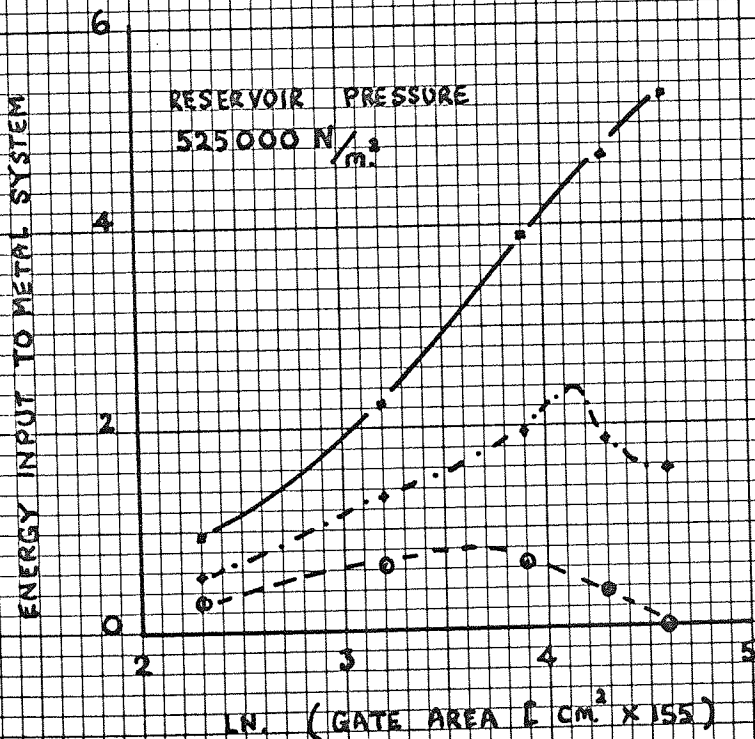
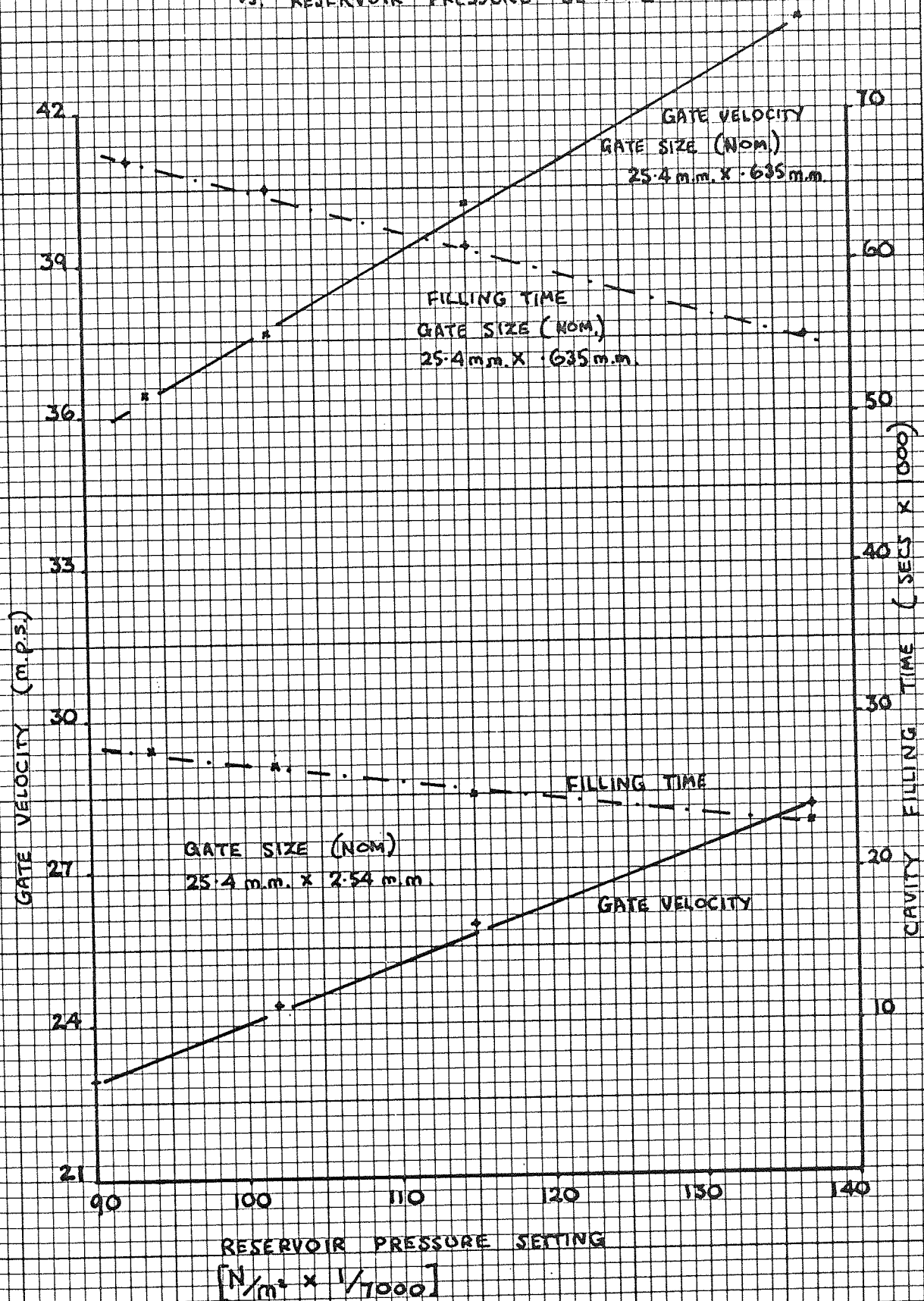


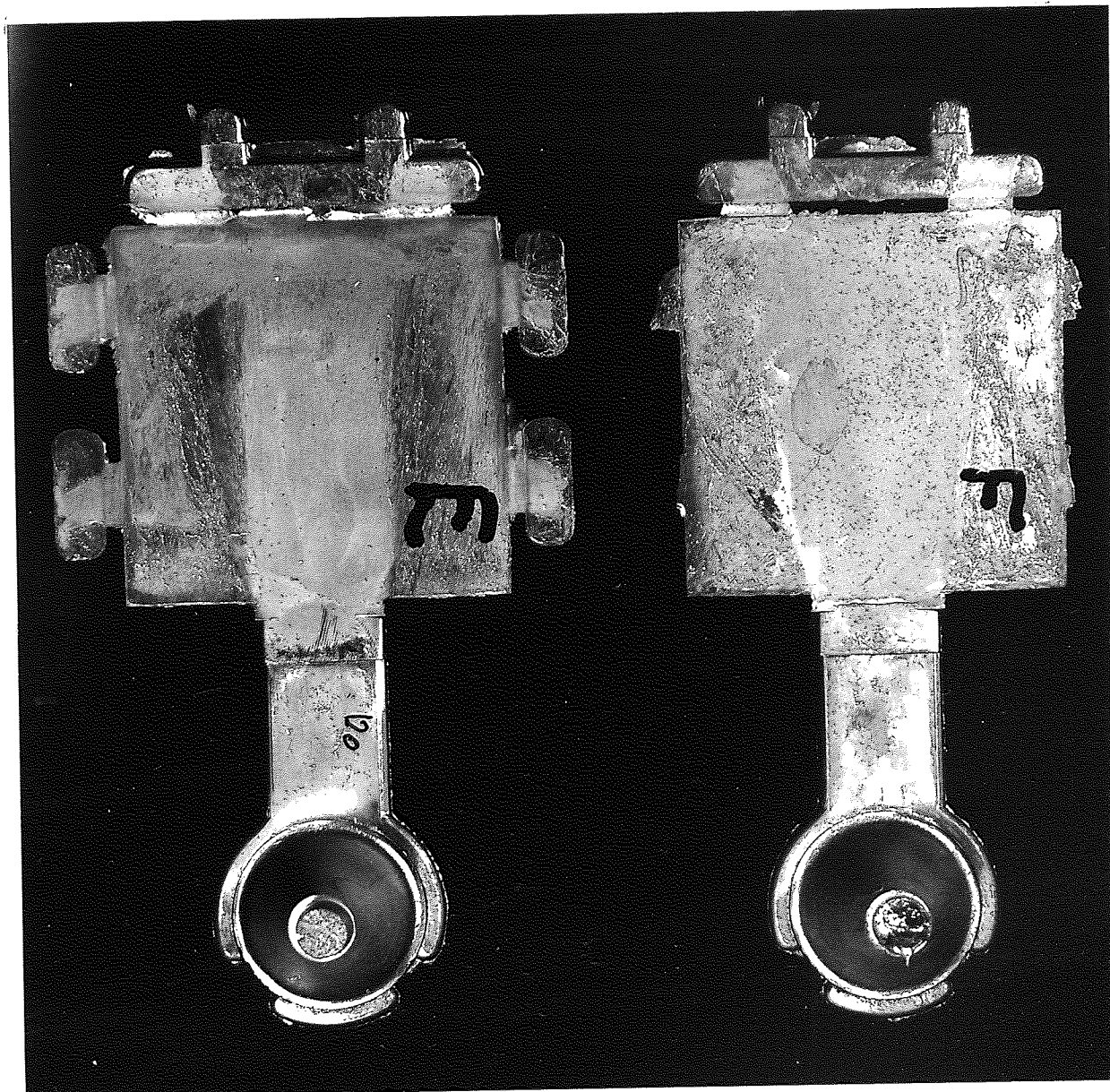
FIG 66c



F66b
F66c

FIG 67 CAVITY FILL TIME, PISTON VELOCITY
VS. RESERVOIR PRESSURE SETTING





a) 25.4 mm x 2.54 mm GATE

b) 25.4 mm x 0.635 mm GATE

FIG 68

FIG 69 TOTAL ENERGY INPUT VS. GATE AREA

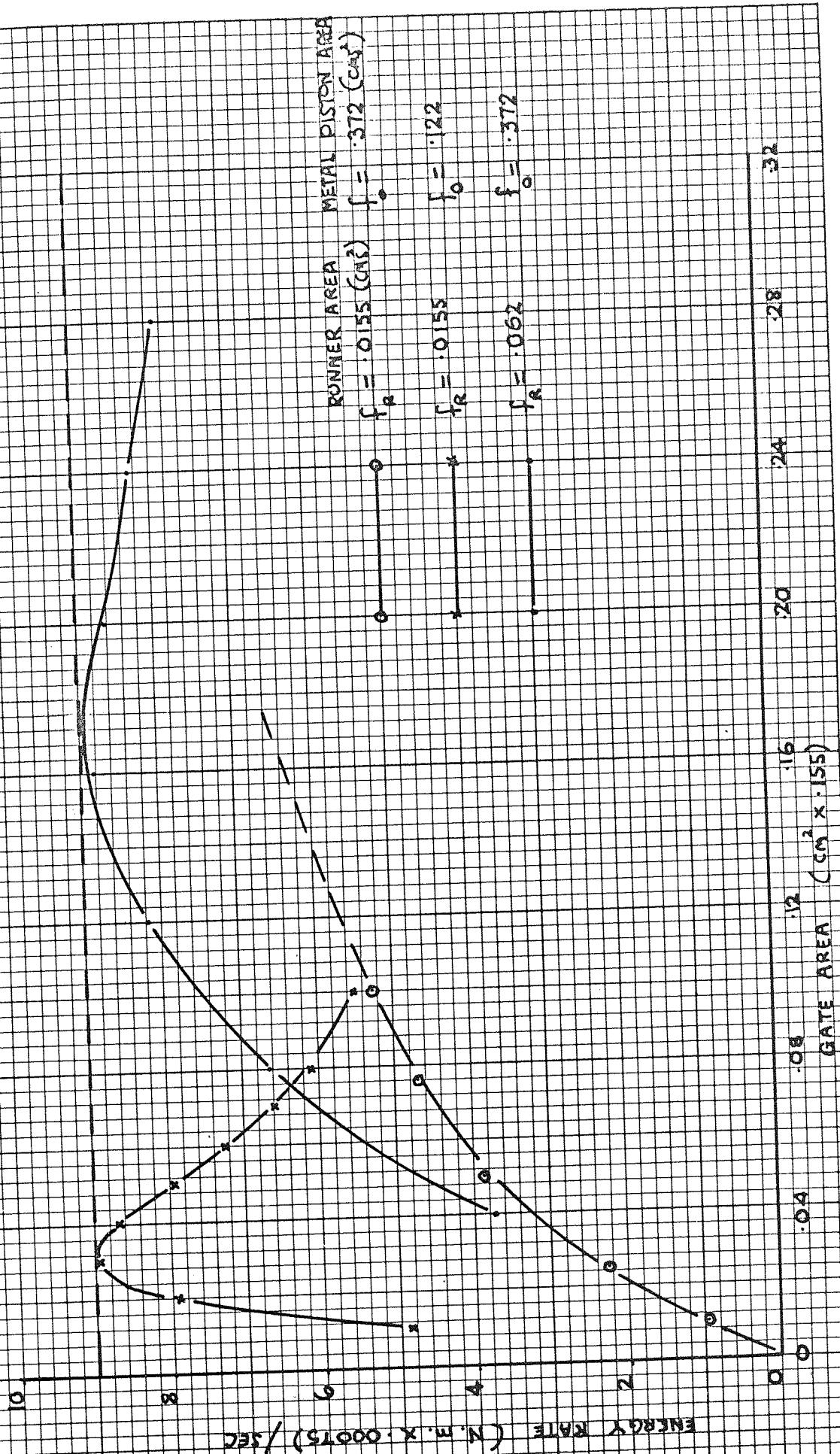
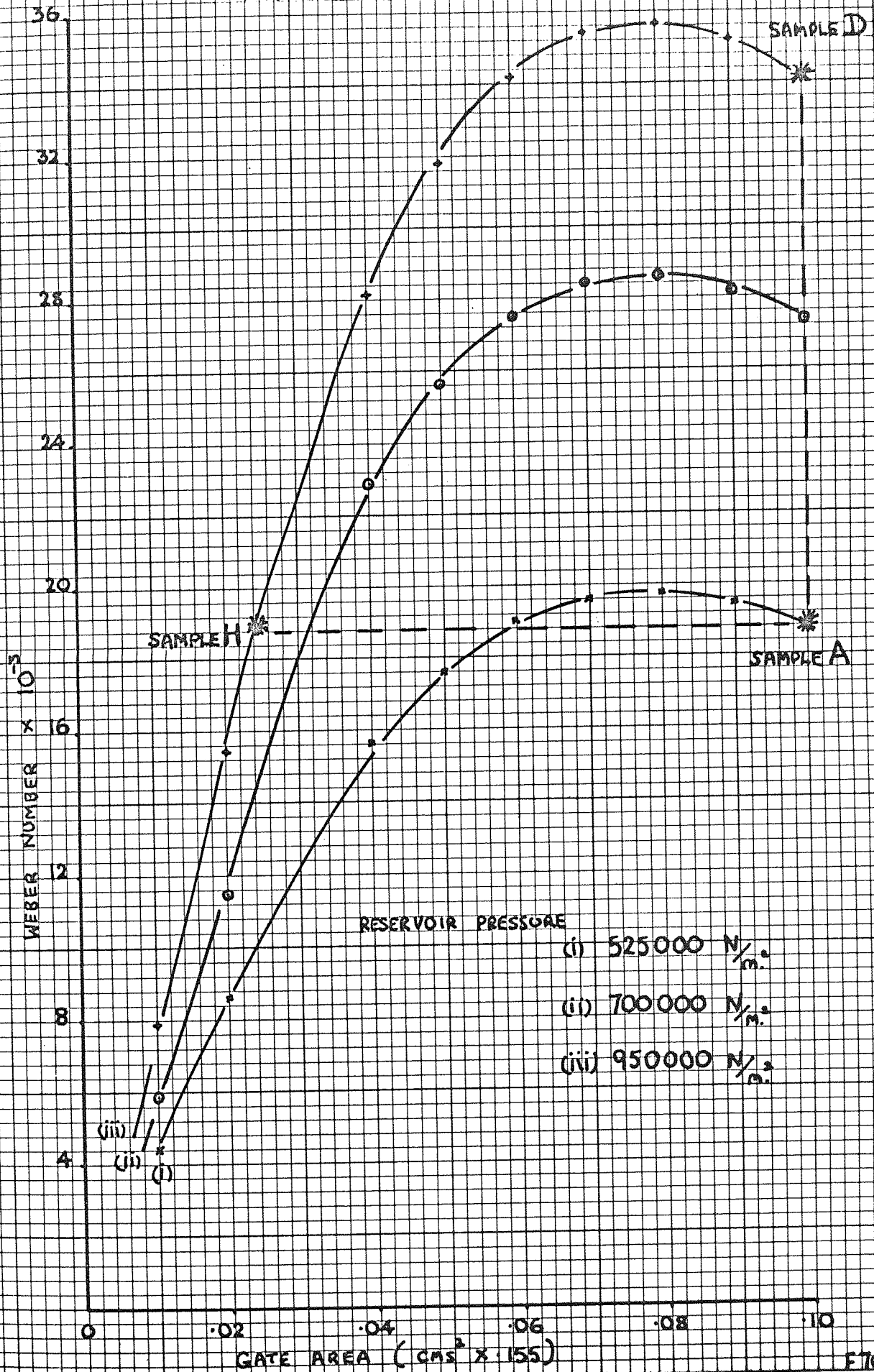
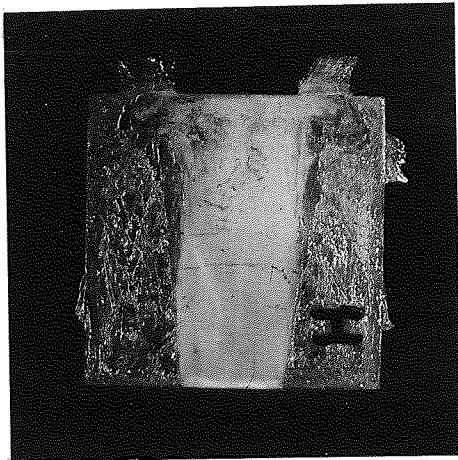


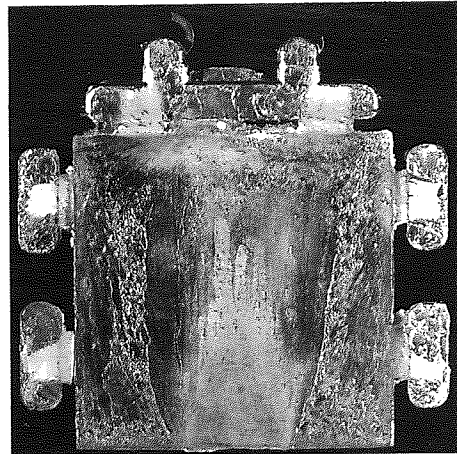
FIG 70

WEBER NUMBER VS. GATE AREA FOR STEADY FLOW
CONDITIONS ON EXPERIMENTAL MACHINE: MOULD



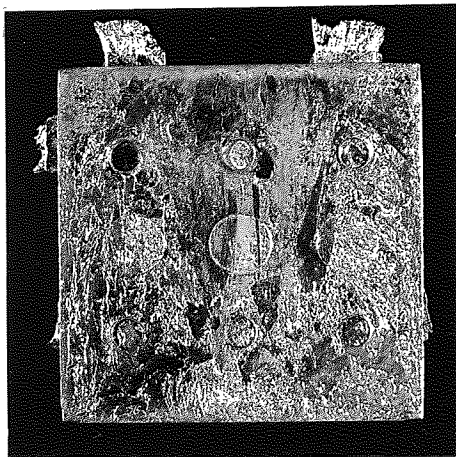


H

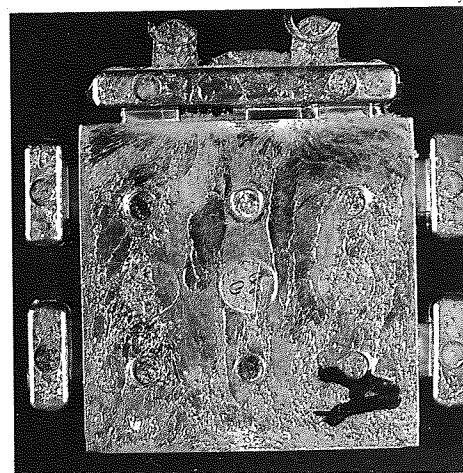


A

FIG 71 FRONT FACE, CASTINGS H AND A

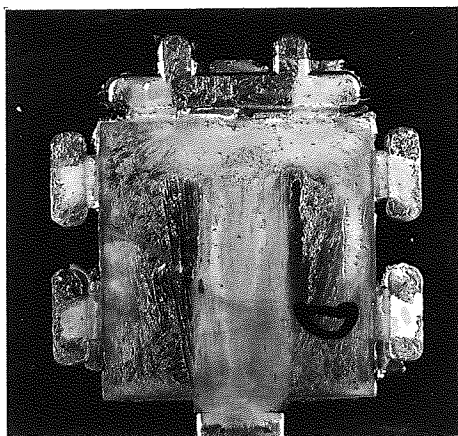


H



A

FIG 72 BACK FACE, CASTINGS H AND A



FRONT



BACK

FIG 73 FRONT AND BACK FACE, CASTING D

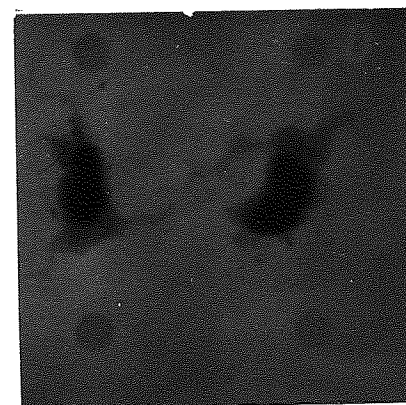
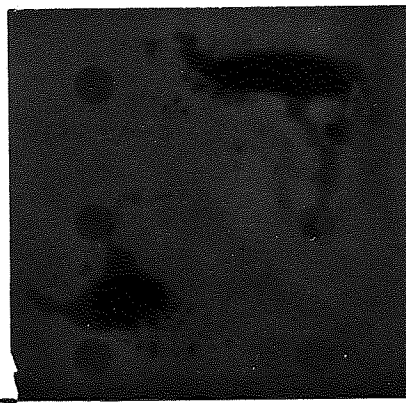
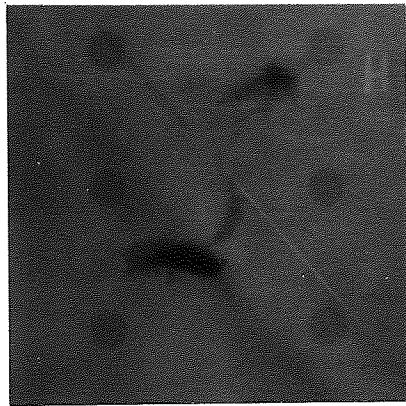


FIG 74 X-RAY PICTURES CASTINGS H, A AND D

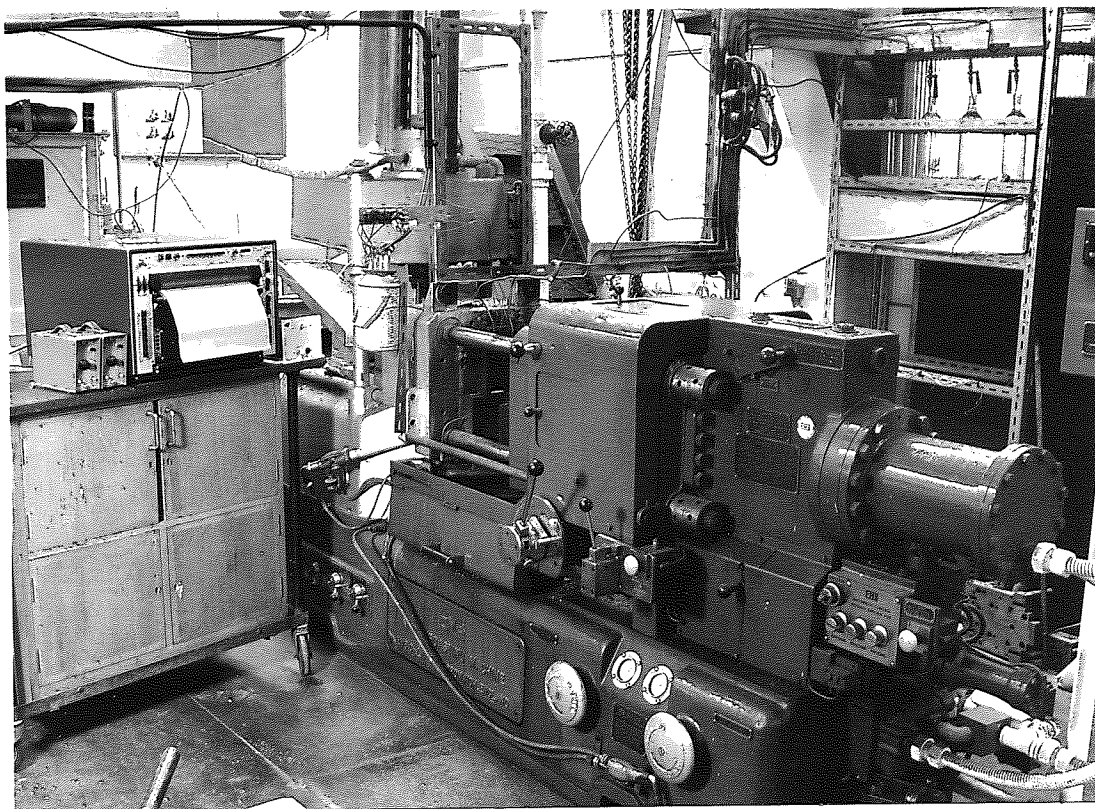


FIG 75 GENERAL VIEW DIECASTING MACHINE AND INSTRUMENTATION

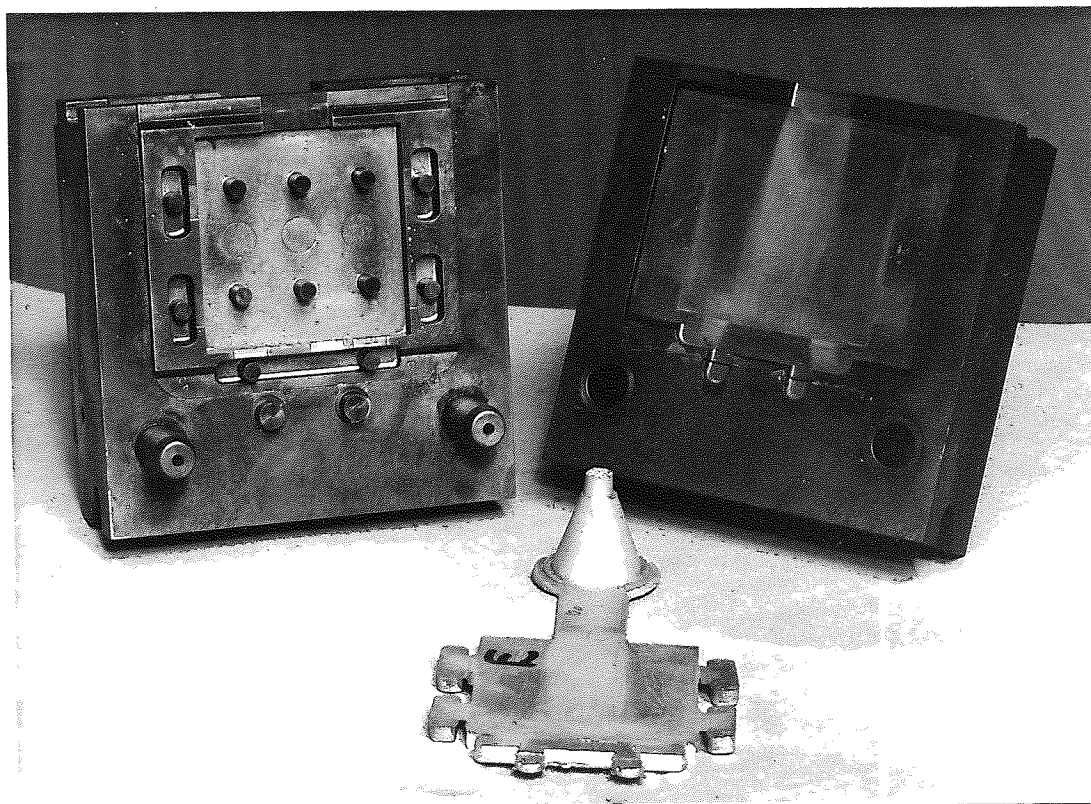


FIG 76 EXPERIMENTAL TOOLING FOR DIECASTING MACHINE

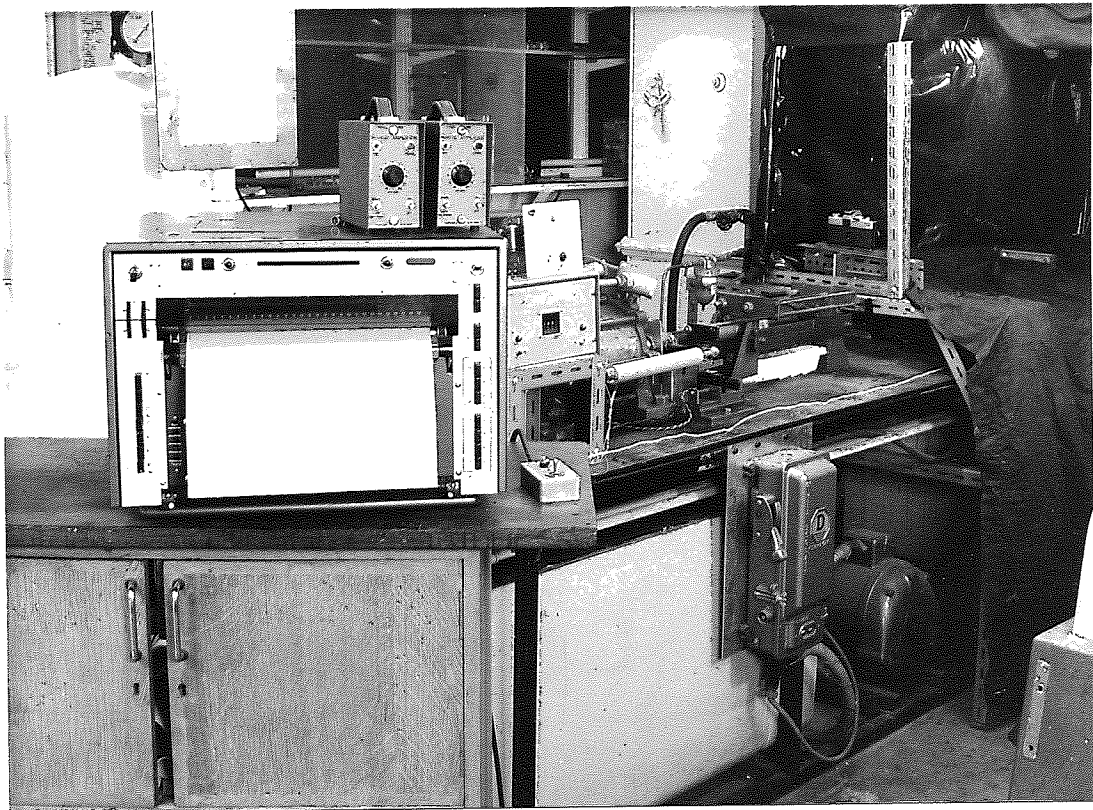
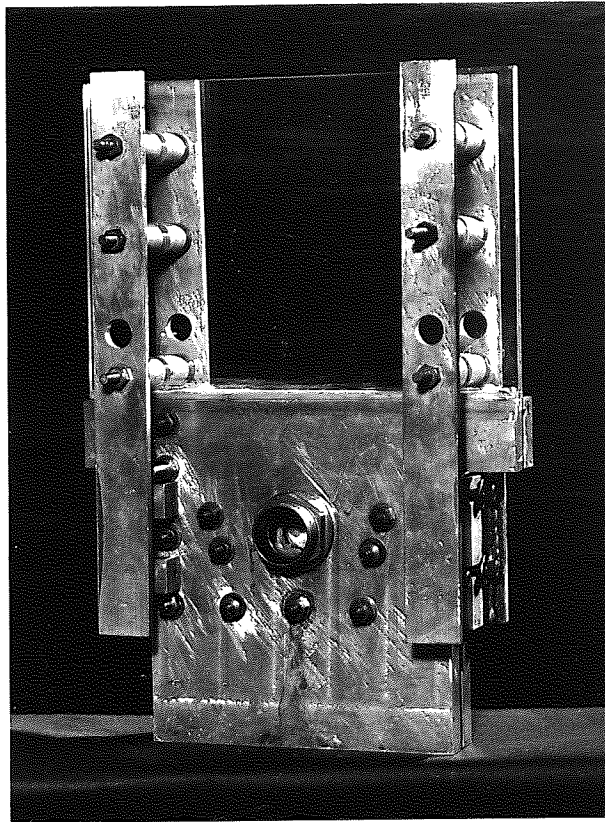
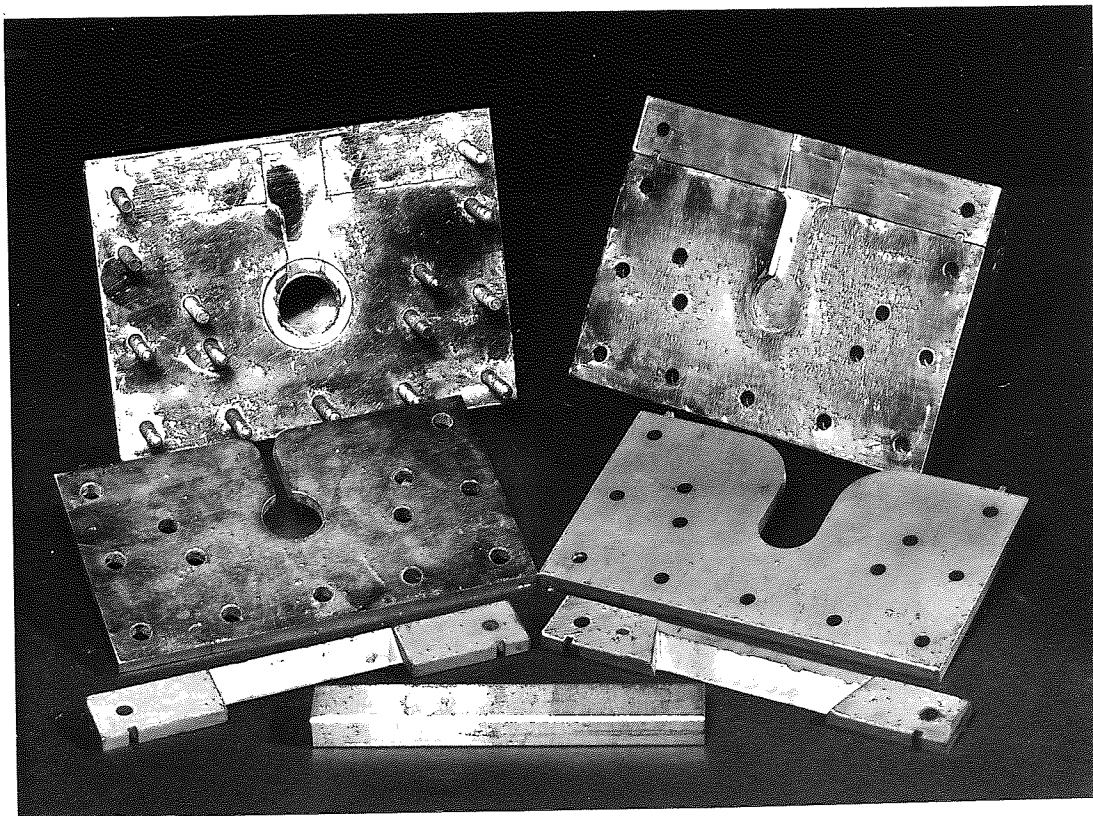


FIG 77 GENERAL VIEW WATER FLOW
RIG AND INSTRUMENTATION



EXPERIMENTAL DIE SET UP FOR PARALLEL
PLATE TESTS



SAMPLES OF RUNNER AND GATE PLATES

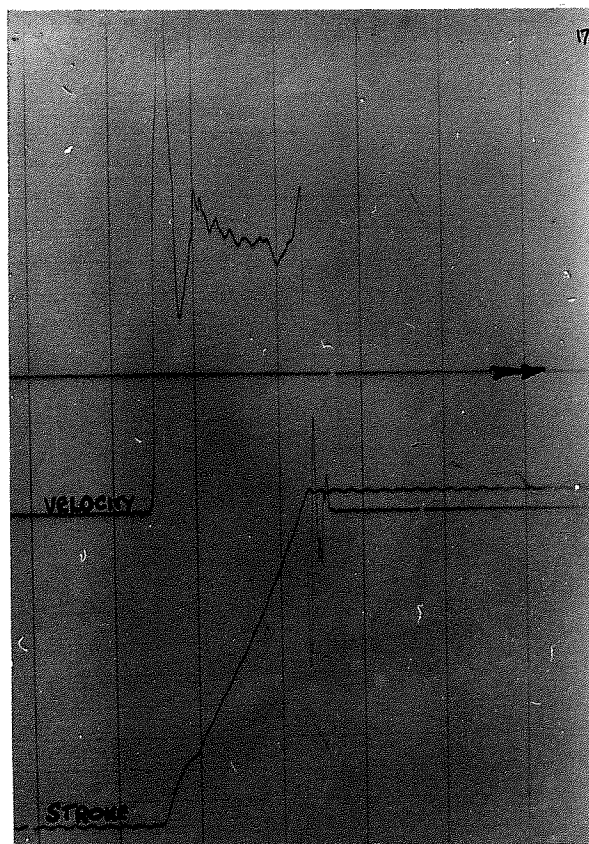


FIG 79 FREE PISTON VELOCITY CHARACTERISTIC
FOR WATER FLOW RIG

FIG 80 COMPARISON OF CALCULATION AND MEASUREMENT
OF PISTON VELOCITY ON THE EXPERIMENTAL RIG
SINGLE STAGE

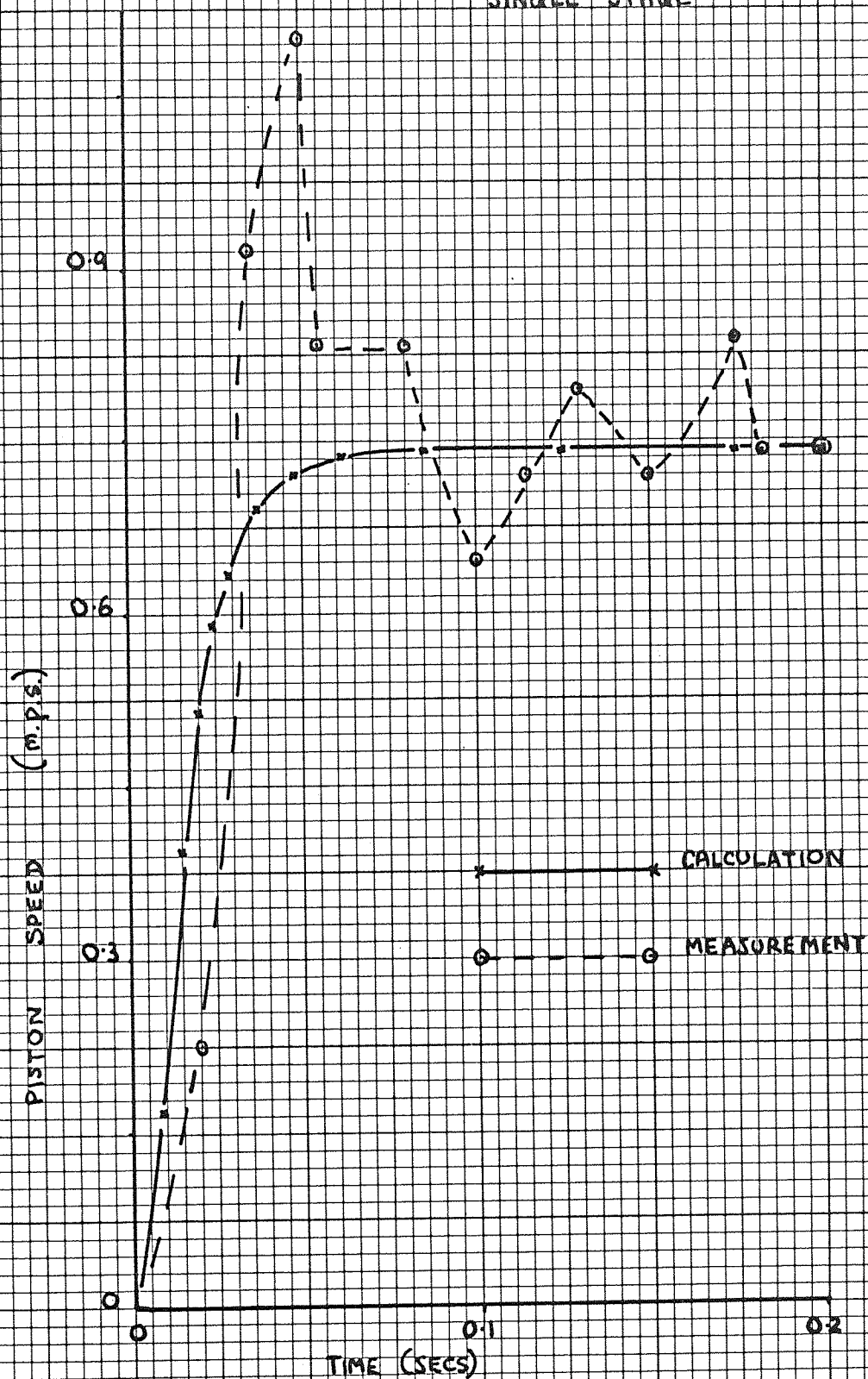
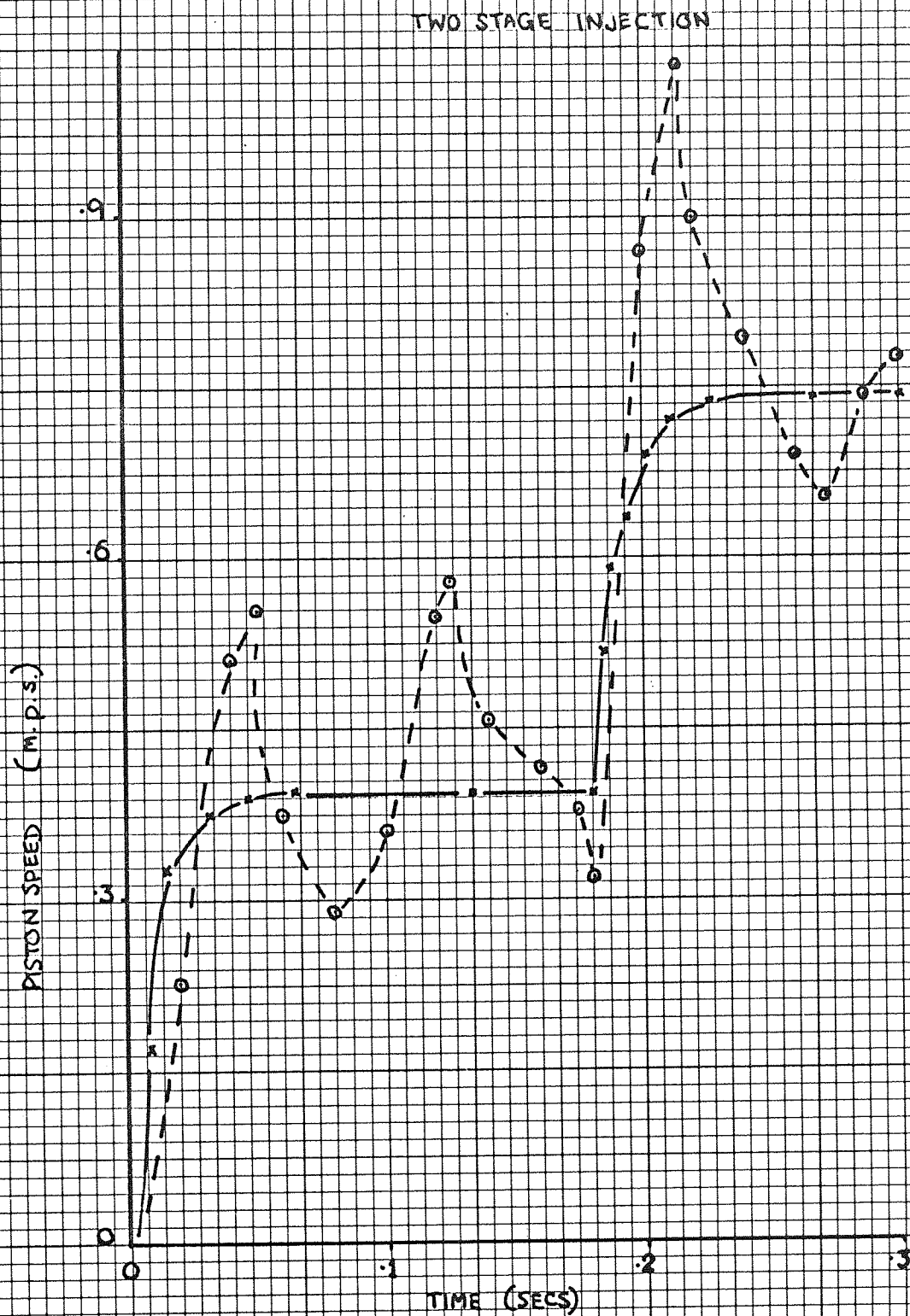


FIG 81 COMPARISON OF CALCULATION AND MEASUREMENT
OF PISTON VELOCITY ON THE EXPERIMENTAL RIG



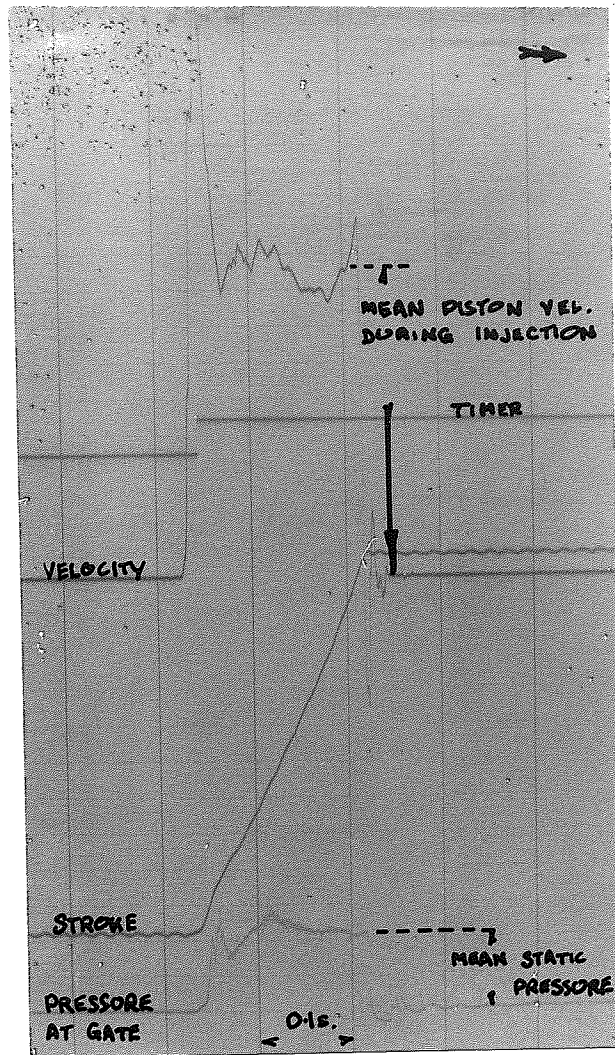


FIG 82 TYPICAL RIG TRACE

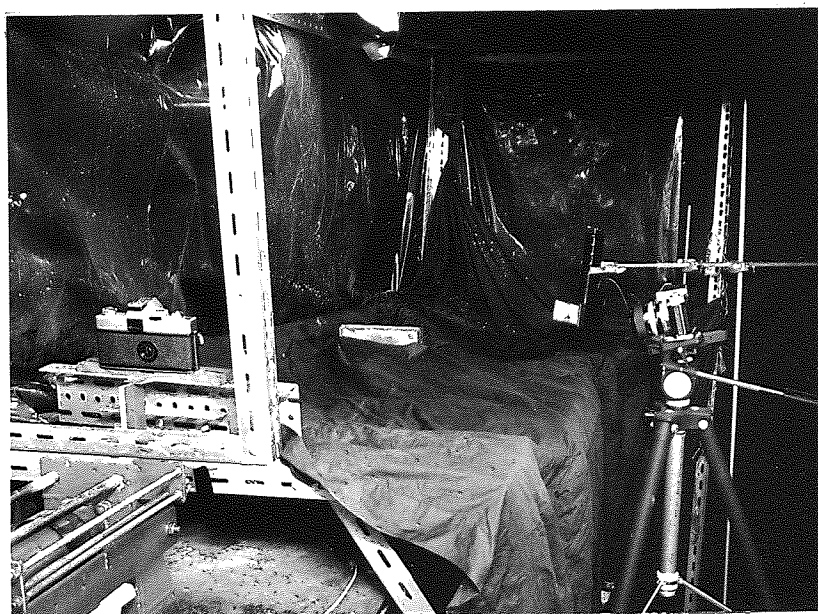
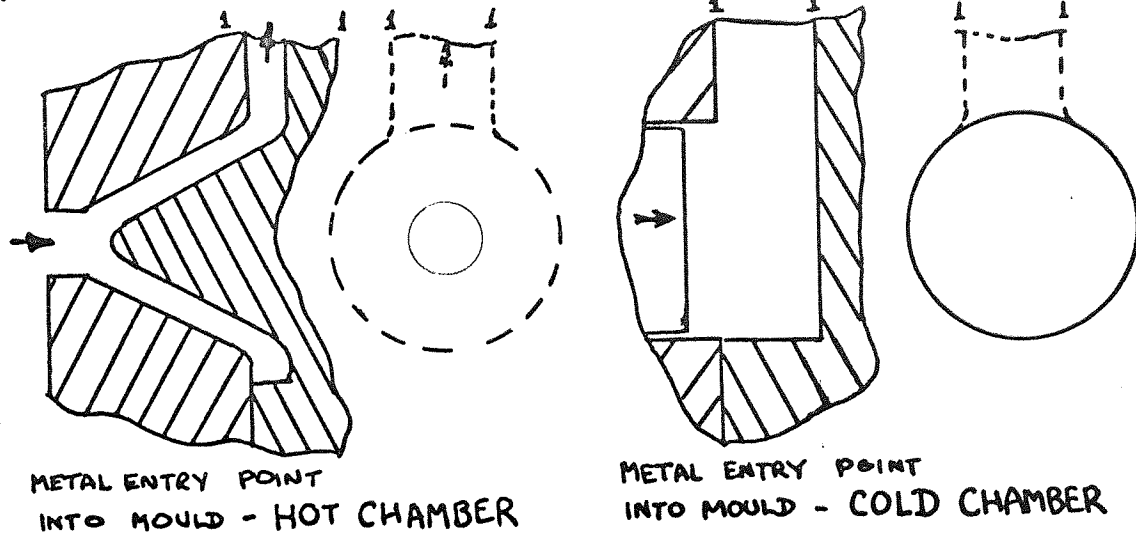
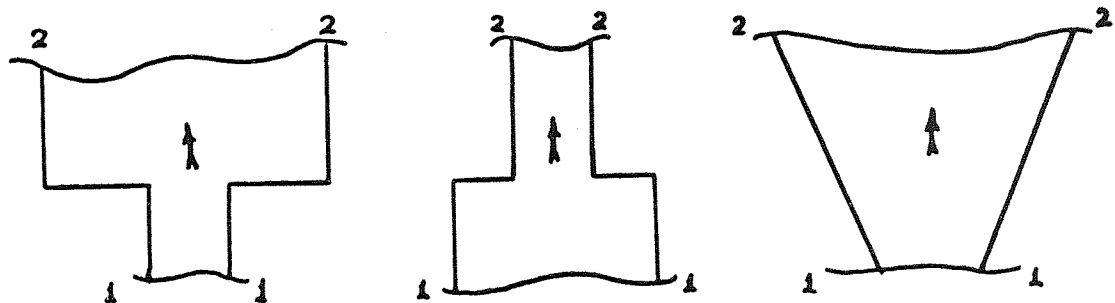


FIG 83 STILL PHOTOGRAPHIC SET-UP

(i)

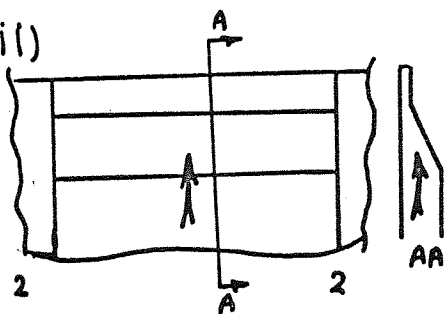


(ii)

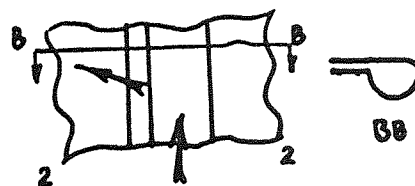


TYPICAL LOSS FEATURES ENCOUNTERED IN RUNNER : GATING SYSTEMS ADJACENT TO METAL ENTRY POINT. NOTE : FOR EASE OF MACHINING ETC., THE THIRD DIMENSION OF THESE FEATURES WOULD BE FIXED

(iii)



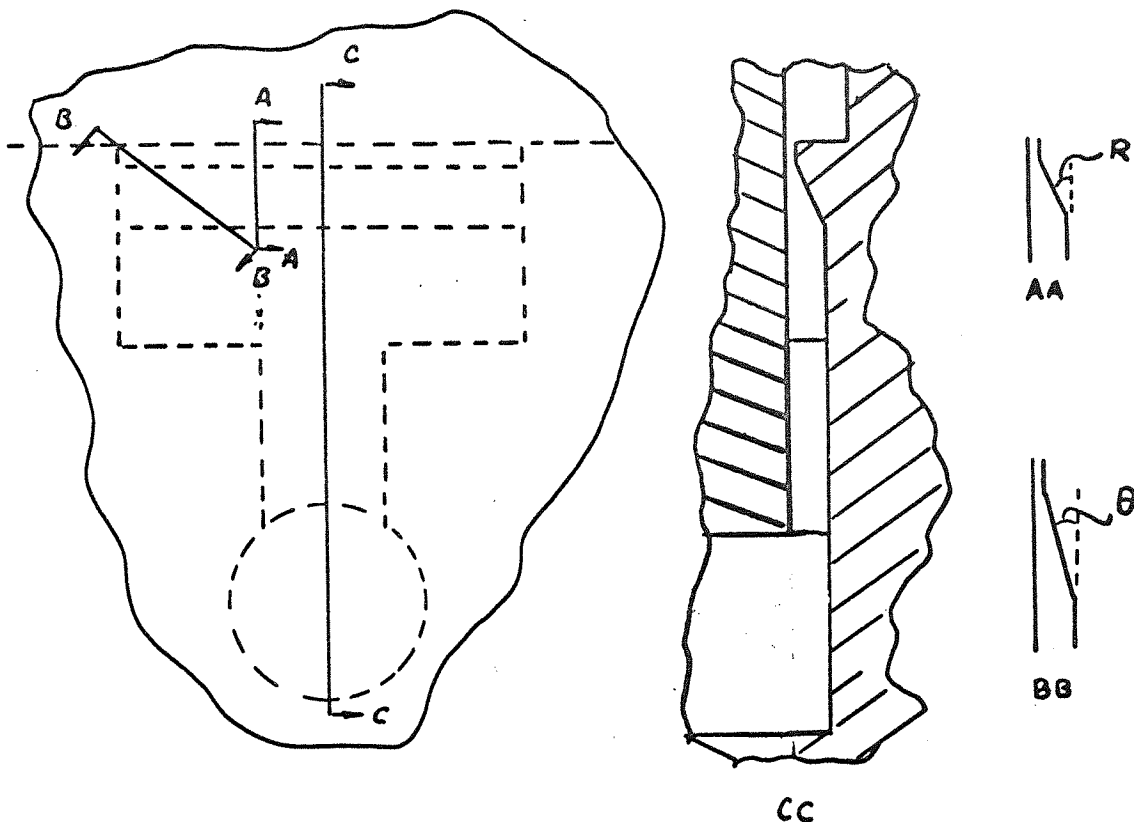
END-ON TYPE GATES



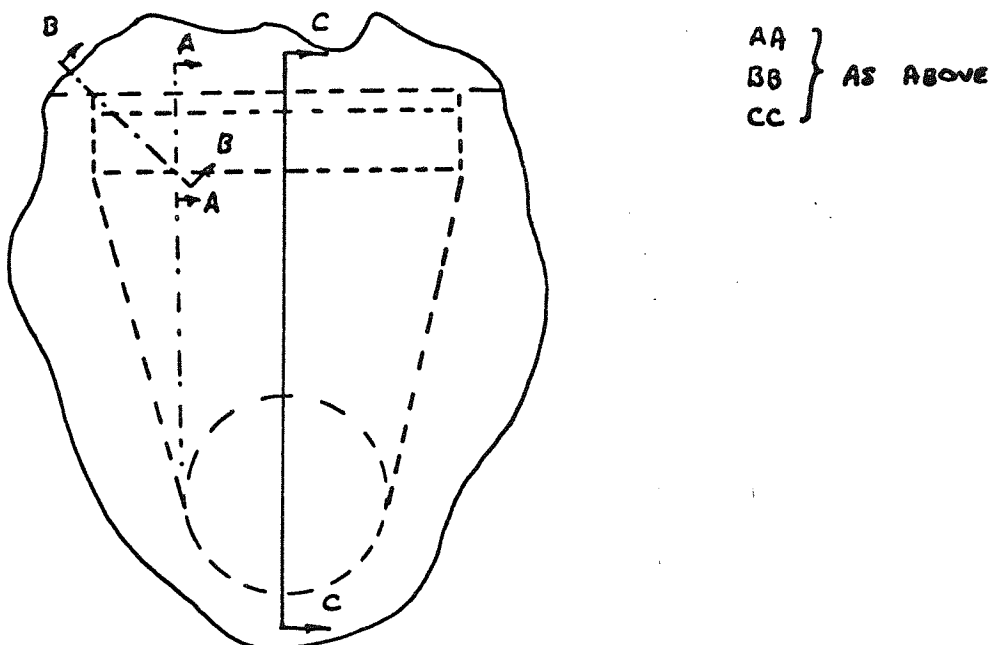
SIDE-ON TYPE GATES

CONTRACTION POINTS OF ATTACHMENT OF RUNNER TO CAVITY

FIG 84 TYPICAL HYDRAULIC LOSS FEATURES ENCOUNTERED IN RUNNER : GATING SYSTEMS



a) SYSTEM COMPRIZING BEND: CONTRACTION, SUDDEN EXPANSION AND GATE CONTRACTION



b) SYSTEM COMPRIZING BEND: CONTRACTION, TAPERED EXPANSION AND GATE CONTRACTION

FIG 85 EXAMPLES OF LOSS FEATURE COMBINATIONS COMPRIZING TYPICAL RUNNER: GATE COMBINATIONS

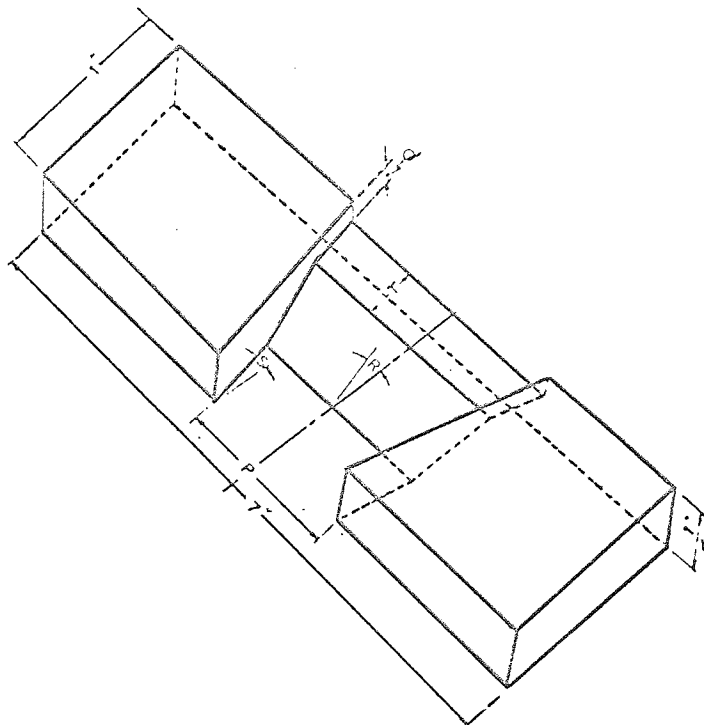


FIG 86 Gate geometry (after Nussey¹⁹)

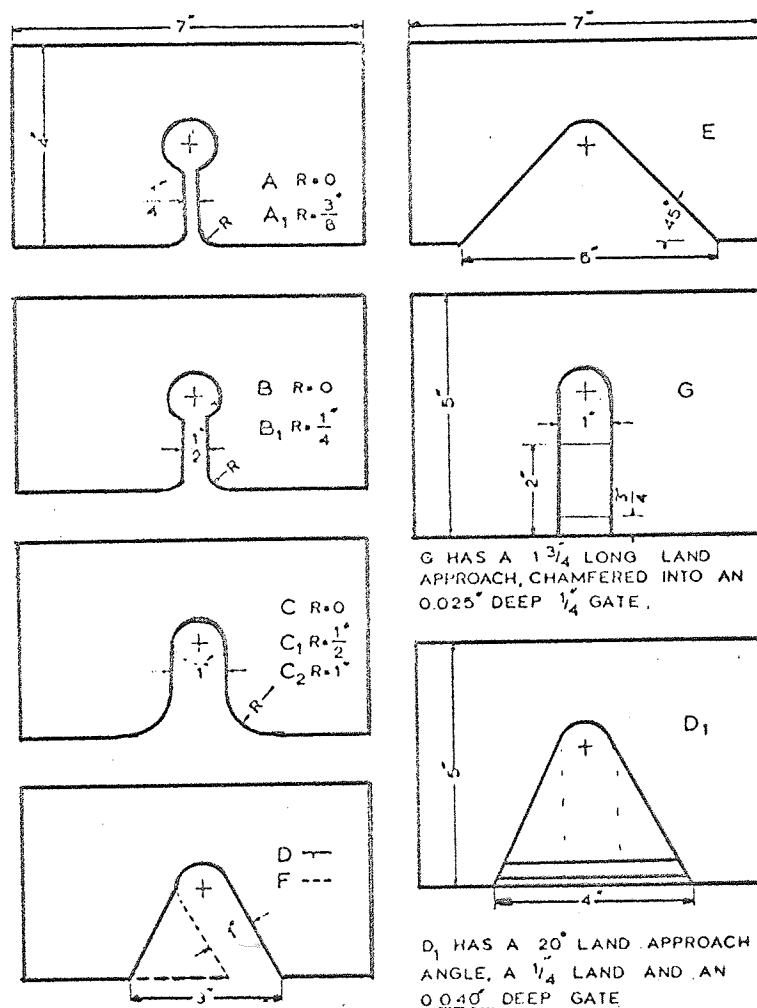


FIG 87 Runner geometry (after Nussey¹⁹)

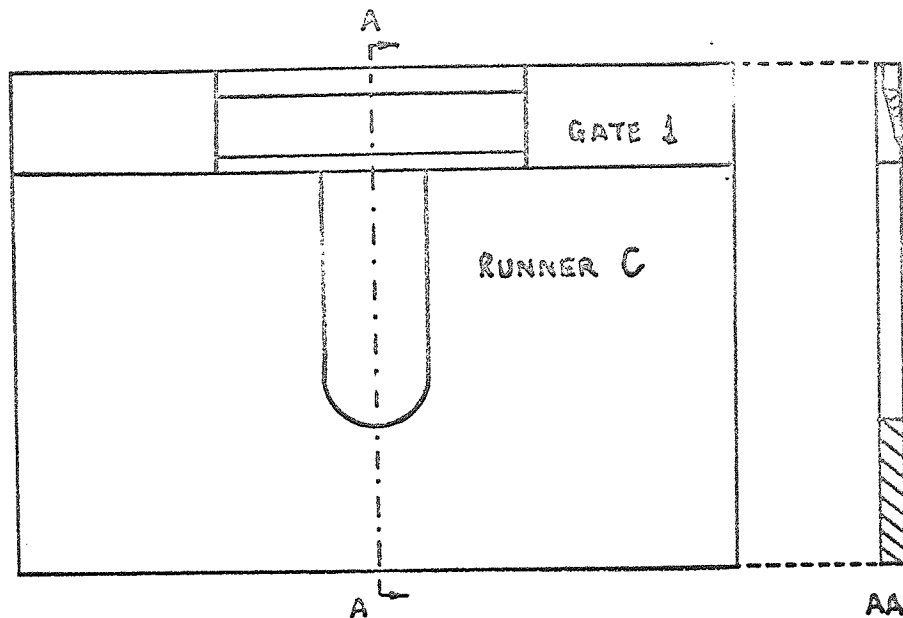


FIG 88 Typical runner : gate combination

Parameter	P	Q		R	S	T	gate exit area minimum runner area		
	gate width inches	gate depth		Land approach angle degrees	gate exit semi-angle degrees	Land length inches	A, A ₁	B, B ₁ , B ₂	C, C ₁ , C ₂
		nominal 10 ⁻³ inches	actual 10 ⁻³ inches						
1	3.00	25	26.7	20	0	.25	1.28	0.64	0.32
2	3.00	25	28.5	20	0	.125	1.37	0.68	0.34
3	3.00	25	24.2	20	0	.062	1.16	0.58	0.29
4	3.00	25	25.8	20	0	.00	1.24	0.62	0.31
5	0.50	25	24.9	20	0	.25	0.20	0.10	0.05
6	1.00	25	25.7	20	0	.25	0.41	0.20	0.10
7	3.00	25	27.6	20	0	.25	1.33	0.66	0.33
8	4.00	25	29.0	20	0	.25	1.86	0.93	0.46
95	5.00	25	26.3	20	0	.25	2.11	1.05	0.57
10	3.00	25	25.2	16.5	0	.25	1.21	0.60	0.30
11	3.00	25	24.5	30	0	.25	1.18	0.59	0.30
12	3.00	25	25.9	40	0	.25	1.25	0.62	0.31
13	3.00	25	26.4	50	0	.25	1.27	0.63	0.32
14	0.50	10	10.0	20	0	.25	0.08	0.04	0.02
15	0.50	40	39.6	20	0	.25	0.32	0.16	0.08
16	0.50	60	60.1	20	0	.25	0.40	0.24	0.12
17	1.00	10	12.4	20	0	.25	0.20	0.10	0.05
18	1.00	40	43.0	20	0	.25	0.69	0.35	0.17
19	1.00	60	60.2	20	0	.25	0.96	0.48	0.24
20	3.00	10	12.8	20	0	.25	0.61	0.30	0.15
21	3.00	40	44.4	20	0	.25	2.12	1.06	0.53
22	3.00	60	64.0	20	0	.25	3.45	1.72	0.86
23	3.00	80	83.6	20	0	.25	4.00	2.00	1.00
24	5.00	10	11.0	20	0	.25	0.88	0.44	0.22
25	5.00	40	42.0	20	0	.25	3.35	1.68	0.84
26	5.00	60	62.8	20	0	.25	5.00	2.50	1.25
27	5.00	40	43.3	20	-14	.25	1.73	0.86	0.43
28	3.00	40	42.1	20	-7	.25	1.85	0.92	0.46
29	3.00	40	40.1	20	+7	.25	2.08	1.04	0.52
30	3.00	40	44.6	20	+14	.25	2.49	1.25	0.62
31	3.00	40	44.0	20	+21	.25	2.70	1.35	0.67
32	1.00	25	26.8	20	-7	.25	0.32	0.16	0.08
33	1.00	25	26.4	20	+7	.25	0.53	0.26	0.13
34	1.00	25	25.6	20	+14	.25	0.61	0.30	0.15
35	3.00	25	28.8	20	0	.25	1.39	0.70	0.35
36	3.00	25	26.7	20	0	.25	1.28	0.64	0.32
37	3.00	25	27.0	20	0	.25	1.30	0.65	0.32

FIG 89

Table 6 (after Nussey¹⁹)

FIG 90(i) COMPARISON OF CALCULATION AND MEASUREMENT OF GATE WIDTH VS. EFFICIENCY

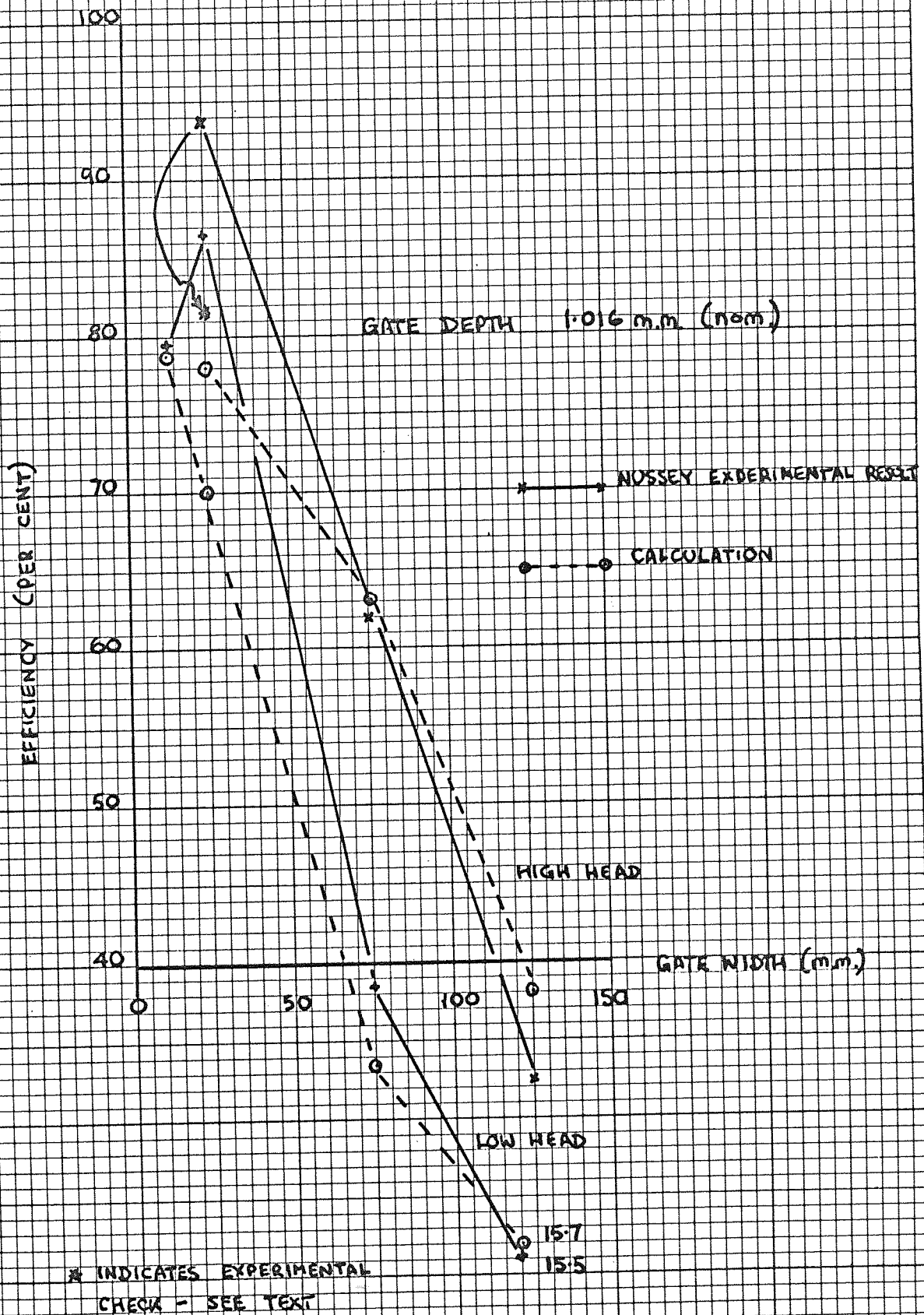


FIG 90 (ii)

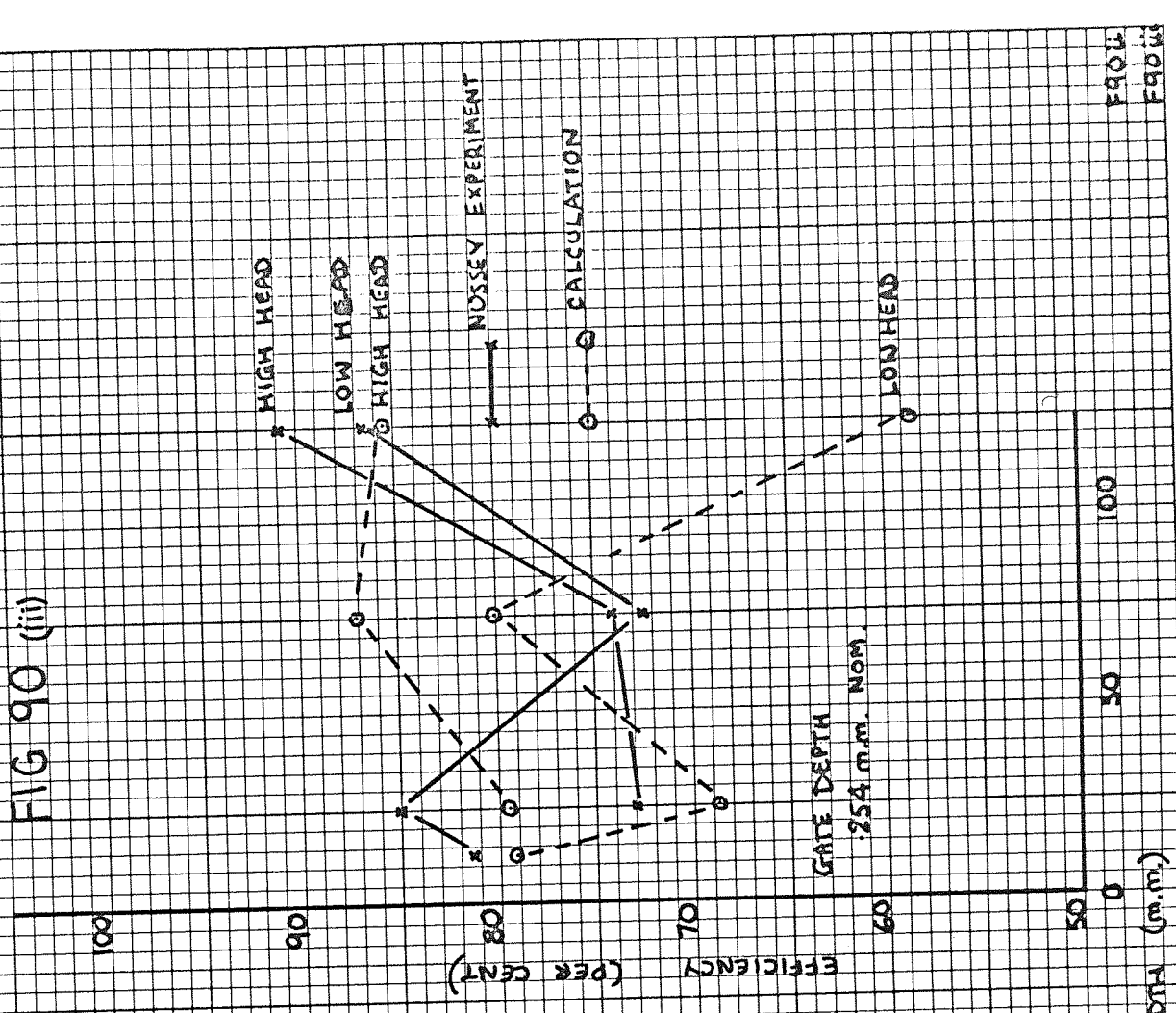


FIG 90 (ii)

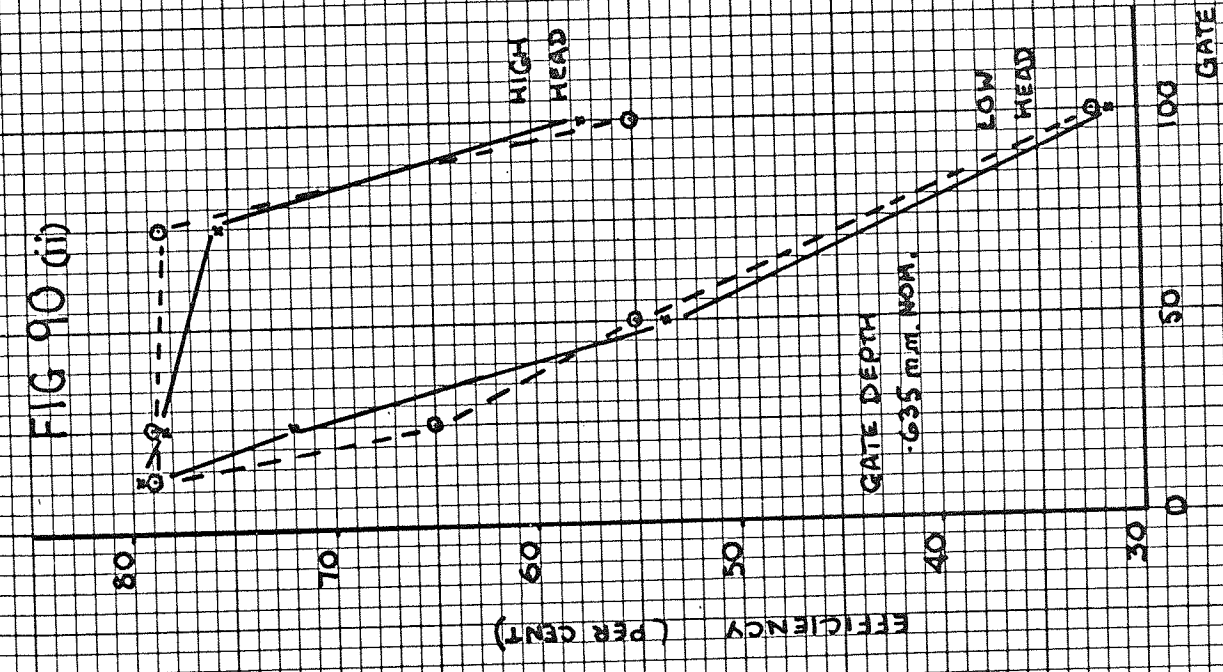


FIG 91 COMPARISON OF CALCULATION AND MEASUREMENT OF GATE DEPTH (Q) VS EFFICIENCY

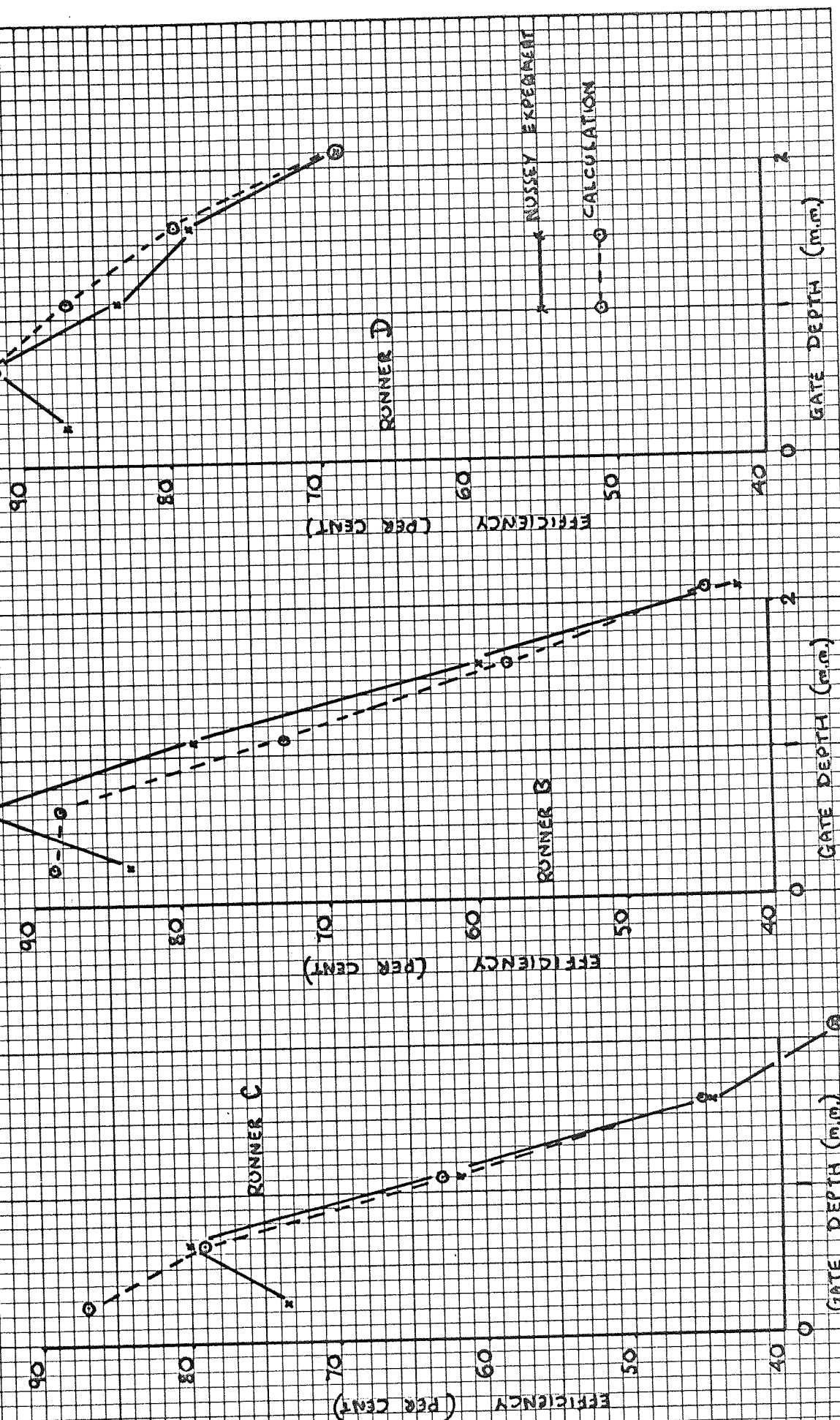
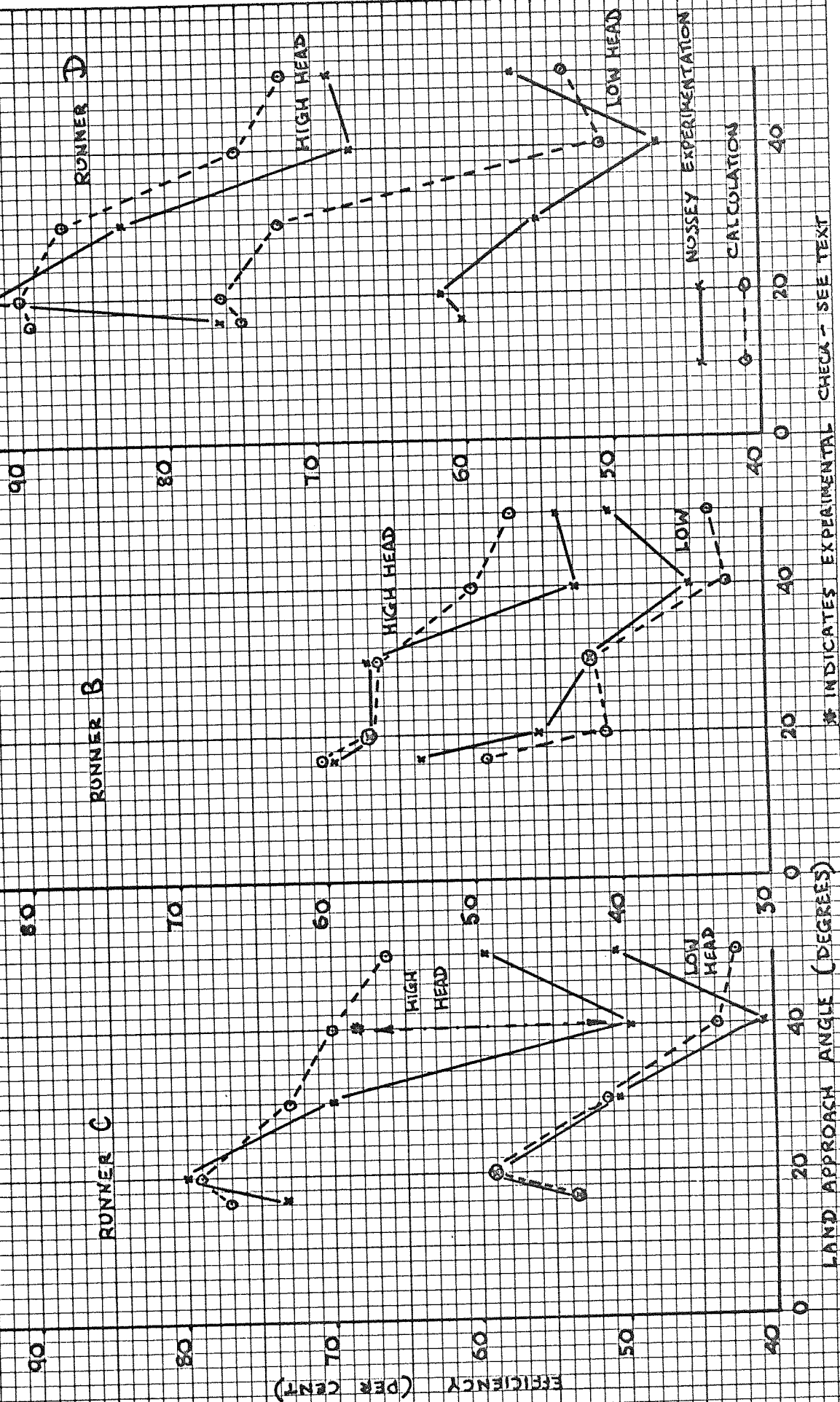


FIG 92 COMPARISON OF CALCULATION AND MEASUREMENT OF LAND APPROACH ANGLE (R) VS. EFFICIENCY



* INDICATES EXPERIMENTAL CHECK - SEE TEXT

FIG 93 COMPARISON OF CALCULATION AND MEASUREMENT OF GATE EXIT SEMI ANGLE (S) VS. EFFICIENCY

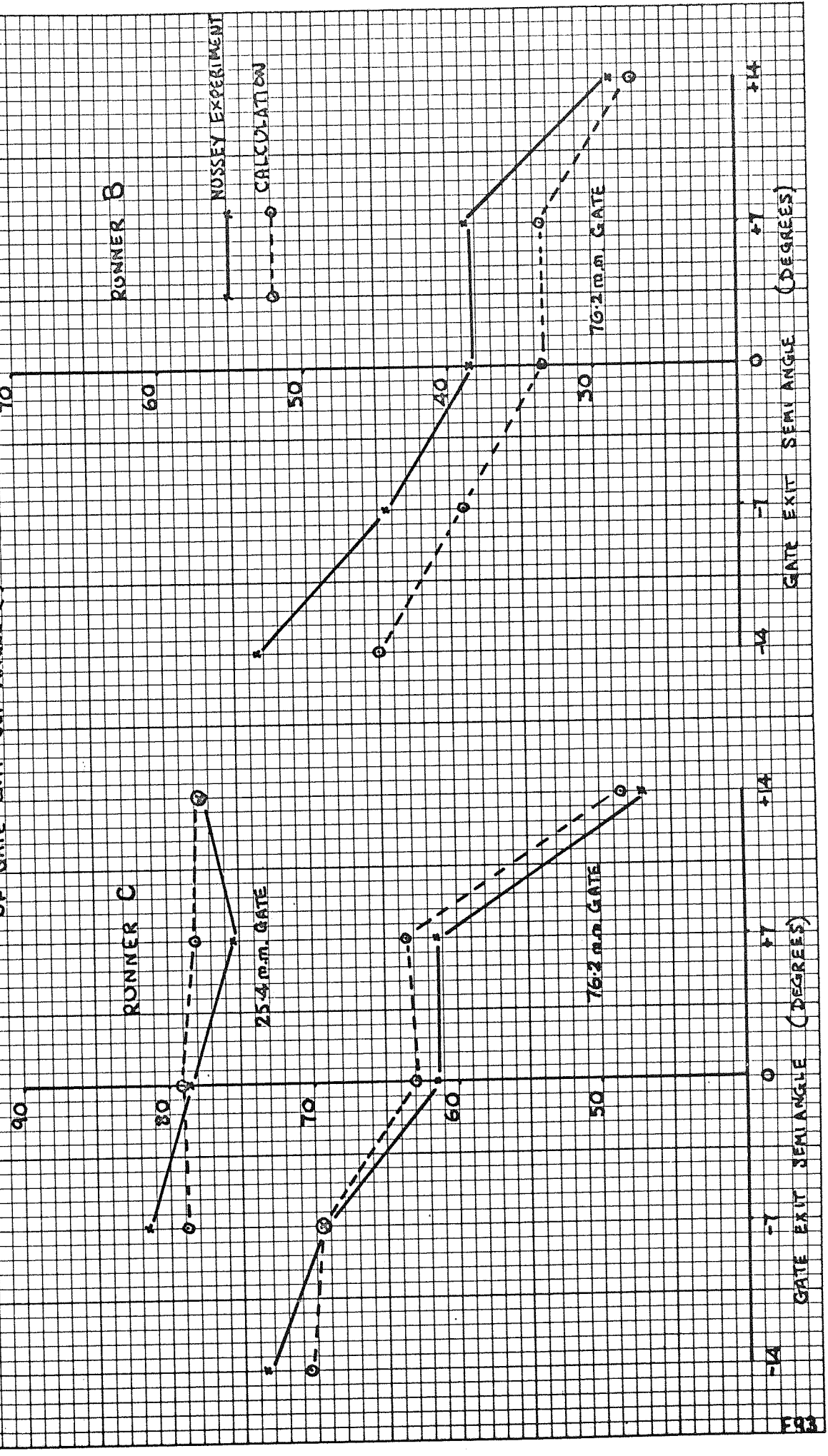
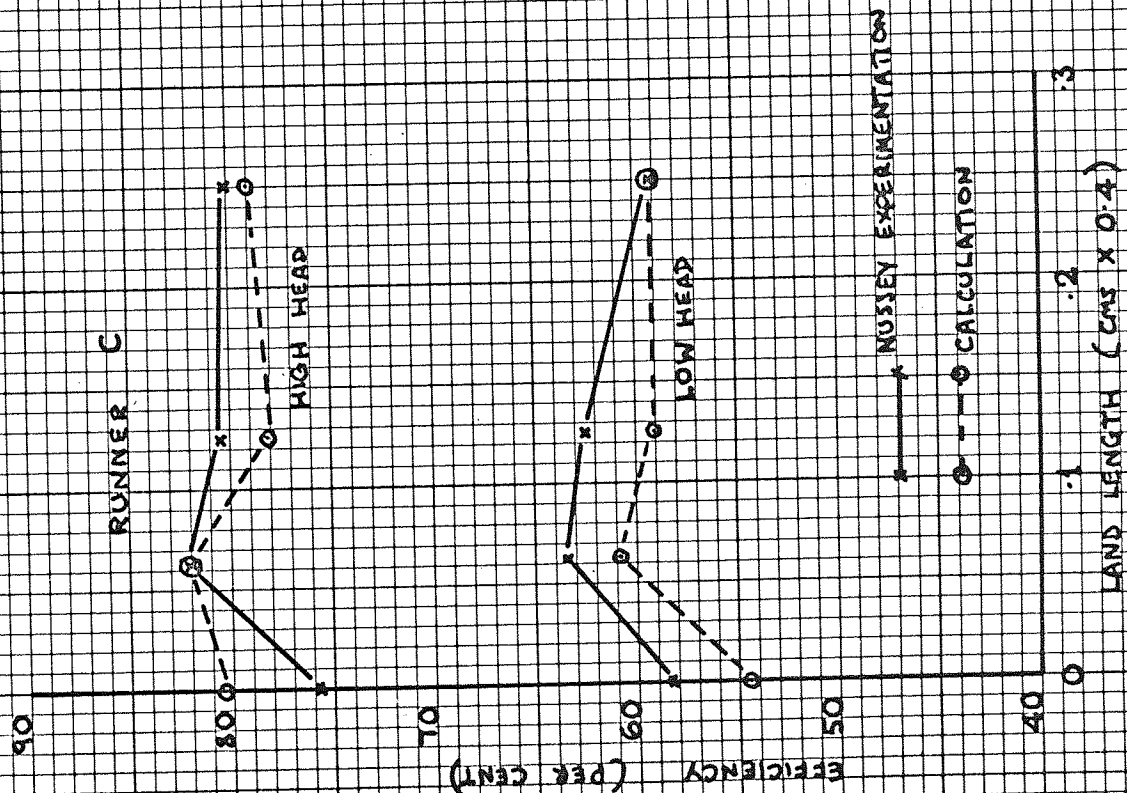
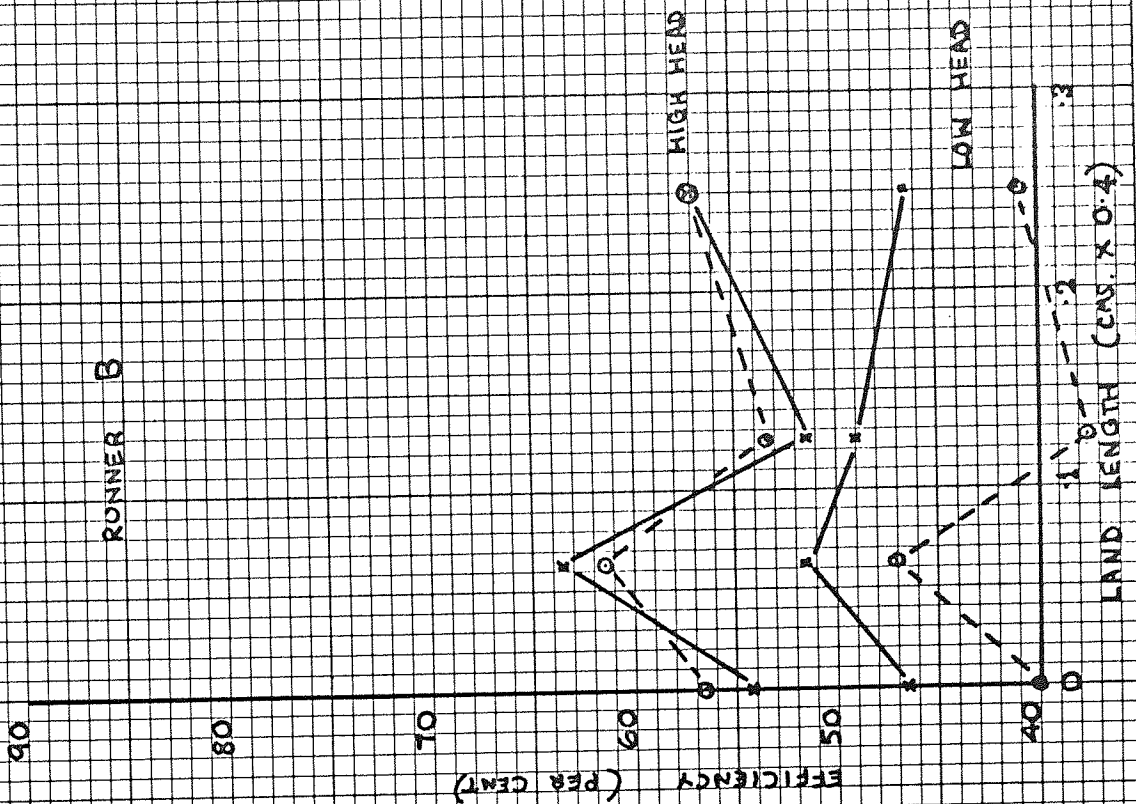


FIG 94 COMPARISON OF CALCULATION AND MEASUREMENT OF LAND LENGTH (T) VS EFFICIENCY



	Diameter inches	Slot length along tube inches	Slit depth		Slit location outside bend: O inside bend: I	angle of embrace degrees	Slit Area Tube Area (choke factor.)
			nominal 10 ⁻³ inches	actual 10 ⁻³ inches			
1	∞	5	15.6	16	-	0	0.54
2	∞	5	31.2	37	-	0	1.28
3	∞	5	62.5	61	-	0	2.11
4	32	5	15.6	16	I	90	0.54
5	32	5	31.2	39	I	90	1.35
6	32	5	62.5	71	I	90	2.48
7	32	5	15.6	16	O	90	0.54
8	32	5	31.2	38½	O	90	1.33
9	32	5	62.5	69	O	90	2.40
10	16	5	15.6	16	I	180	0.54
11	16	5	31.2	38	I	180	1.31
12	16	5	62.5	71½	I	180	2.49
13	16	5	15.6	16½	O	180	0.55
14	16	5	31.2	36	O	180	1.24
15	16	5	62.5	68	O	180	2.35
16	8	5	15.6	17	I	180	0.50
17	8	5	31.2	42	I	180	1.45
18	8	5	62.5	72	I	180	2.50
19	8	5	15.6	16	O	180	0.54
20	8	5	31.2	38½	O	180	1.33
21	8	5	62.5	70	O	180	2.43
22	4	3	15.6	16	I	180	0.33
23	4	3	31.2	41	I	180	0.63
24	4	3	62.5	71	I	180	1.40
25	4	3	15.6	15	O	180	0.31
26	4	3	31.2	35	O	180	0.73
27	4	3	62.5	64½	O	180	1.35

FIG. 95 Table 7 dimensions of side runners (after Nussey¹⁹)

FIG 96 LEAST SQUARE REGRESSION PLOT OF EFFICIENCY AGAINST THE INVERSE OF BEND RADIUS FOR CURVED SIDE RUNNER RANGE

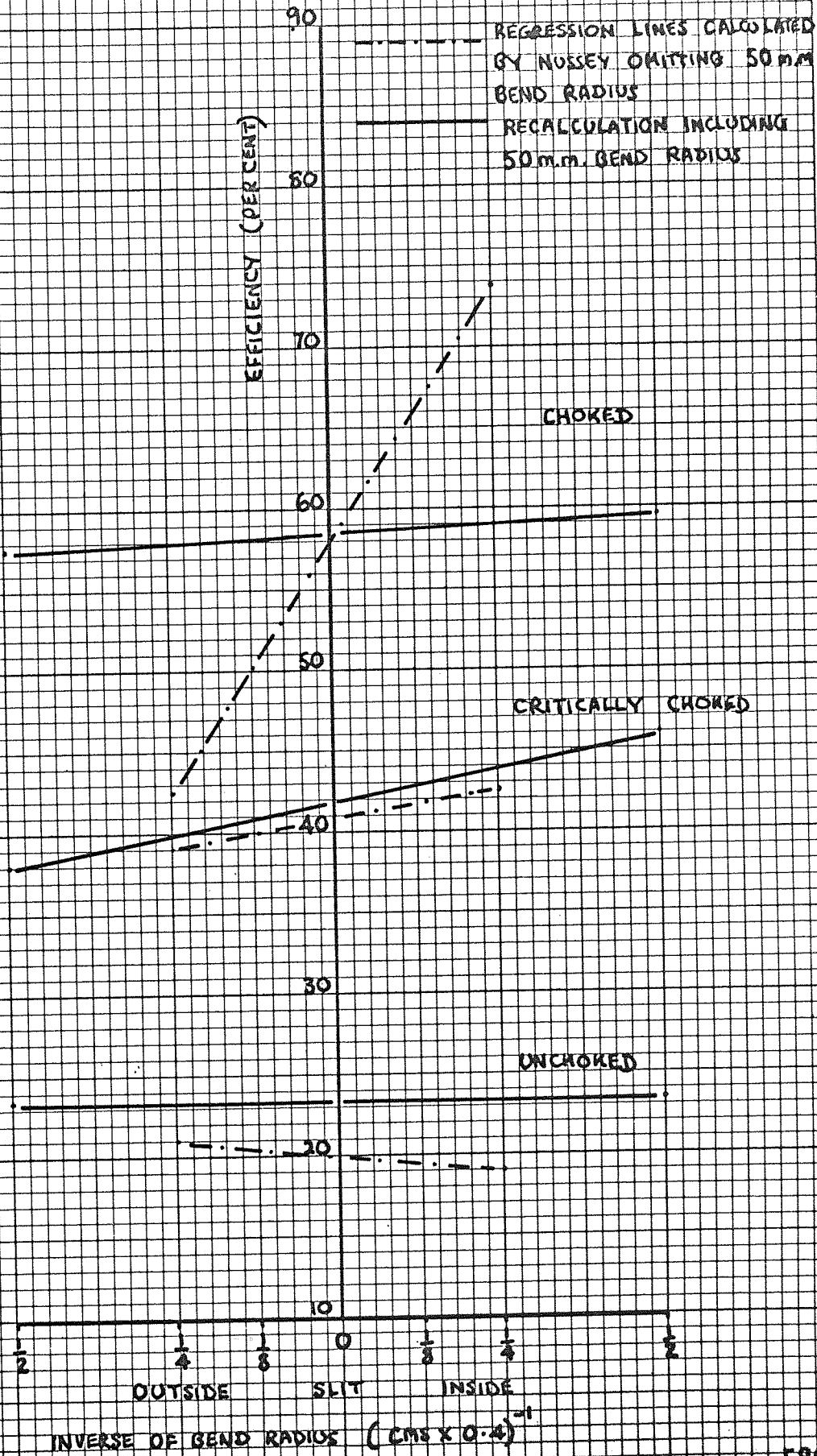
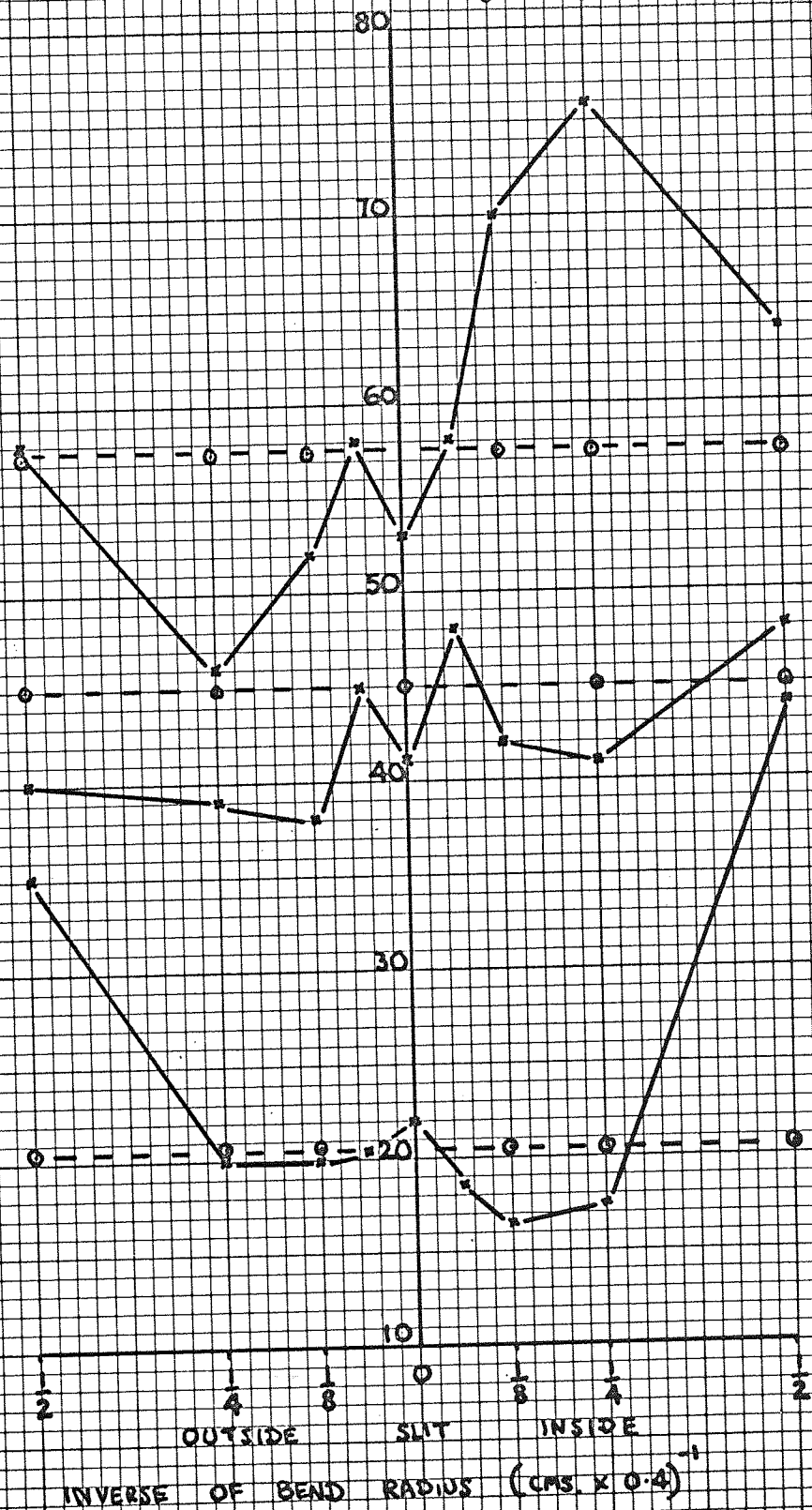


FIG 97

COMPARISON OF CALCULATED AND MEASURED
EFFICIENCIES FOR SIDE RUNNER RANGE

* — * NUSSEY MEASUREMENT
o — o CALCULATION



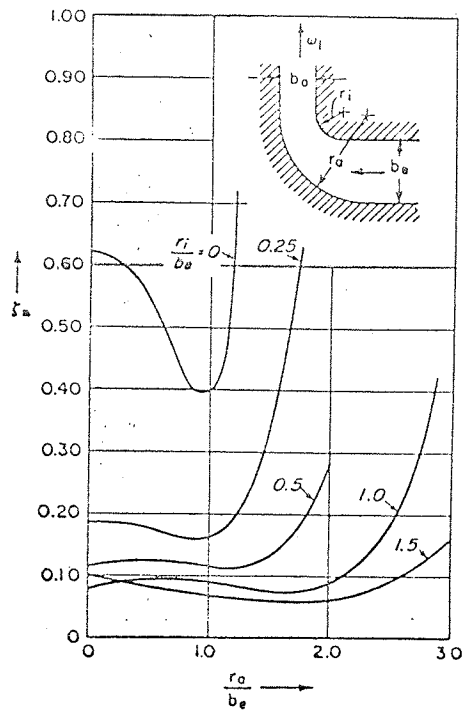


FIG 98 Bend loss coefficient curve (after Sachs¹²)

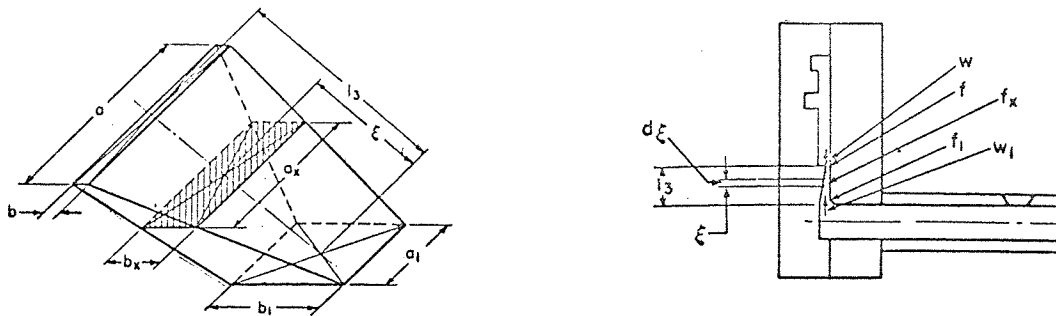
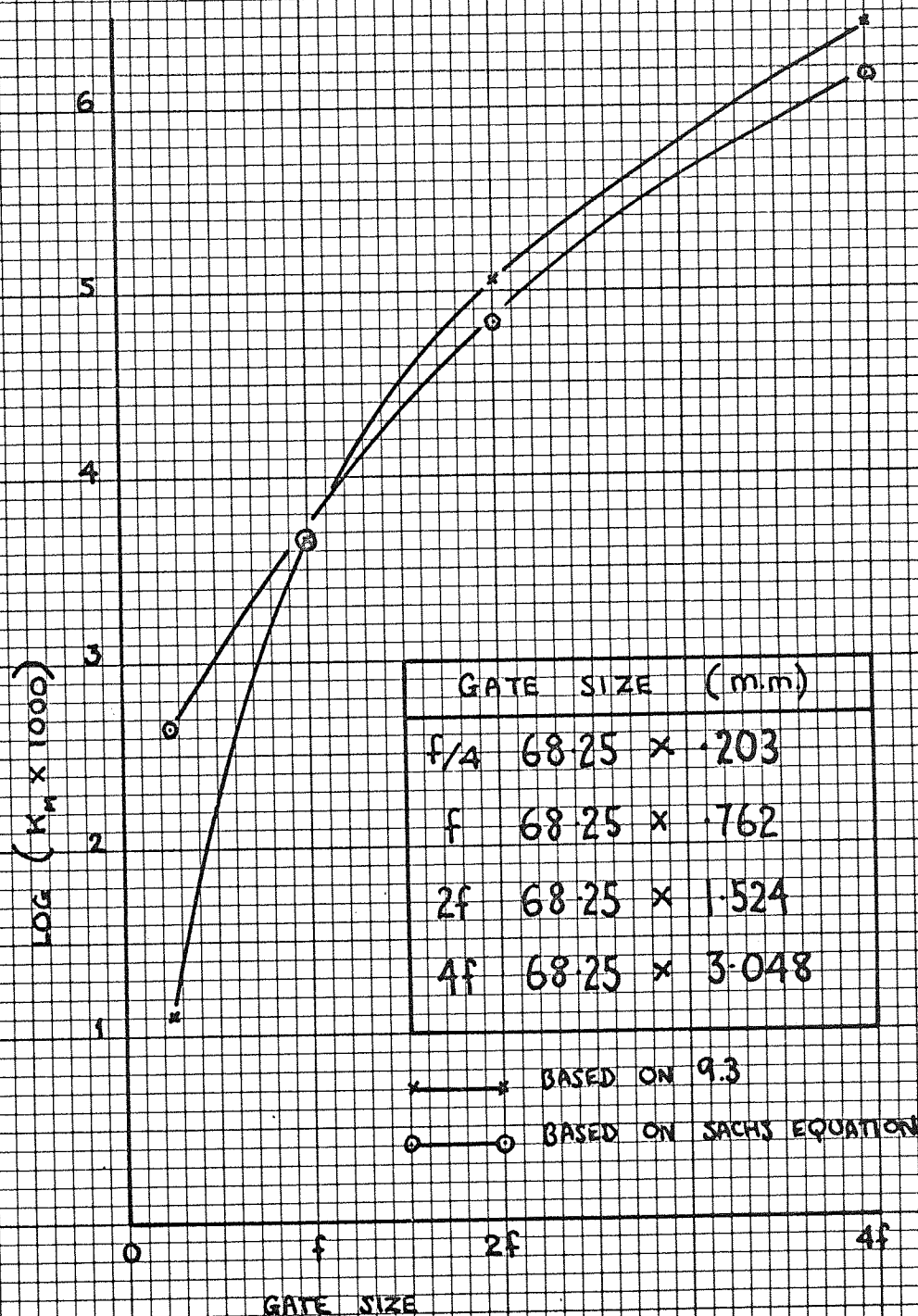


FIG 99 Taper gate (after Sachs¹²)

FIG 100

COMPARISON OF LOSS COEFFICIENT EQUATIONS
FOR GATE RANGE CONSIDERED.



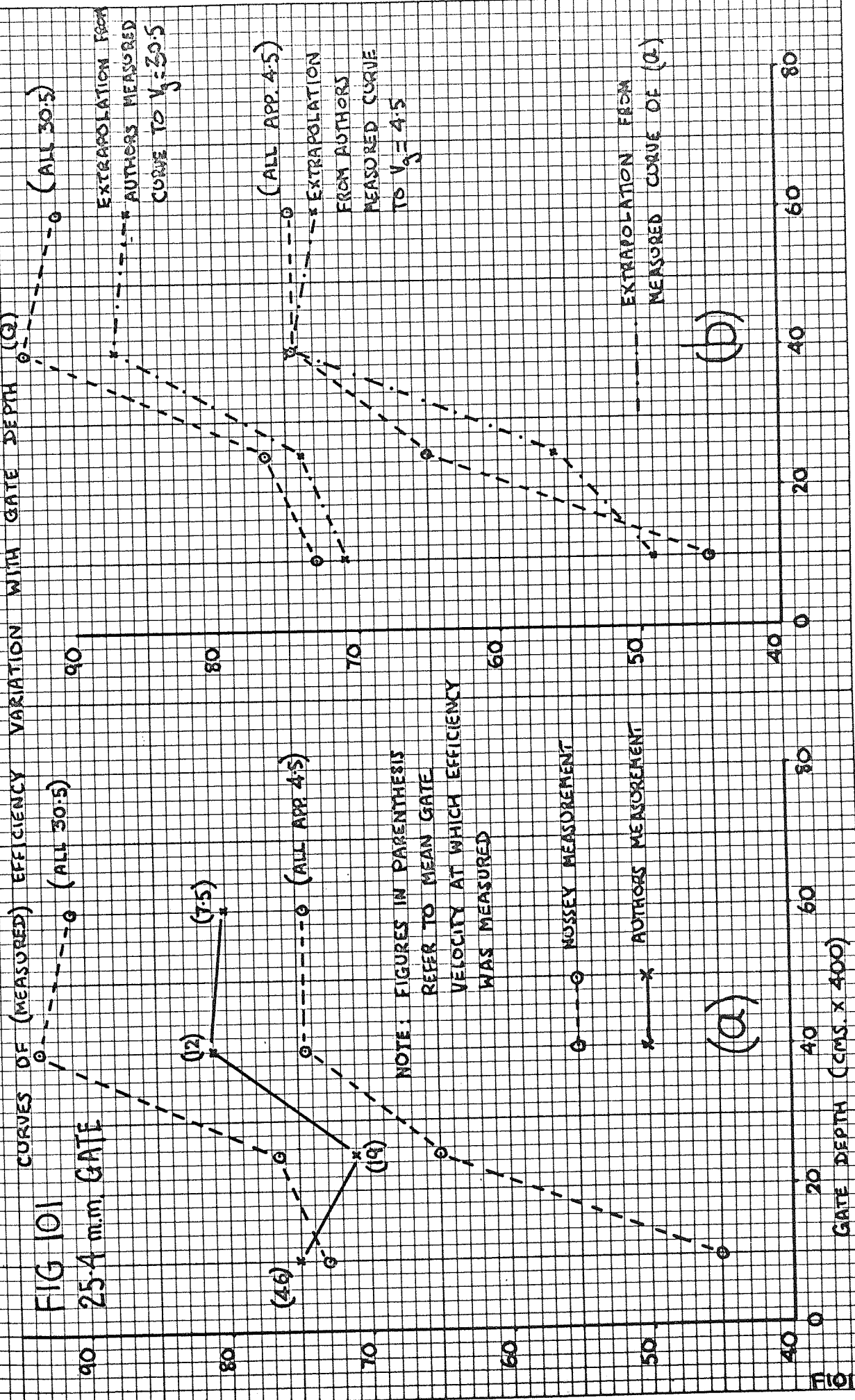


FIG 102 MEASUREMENTS OF EFFICIENCY VARIATION WITH GATE DEPTH

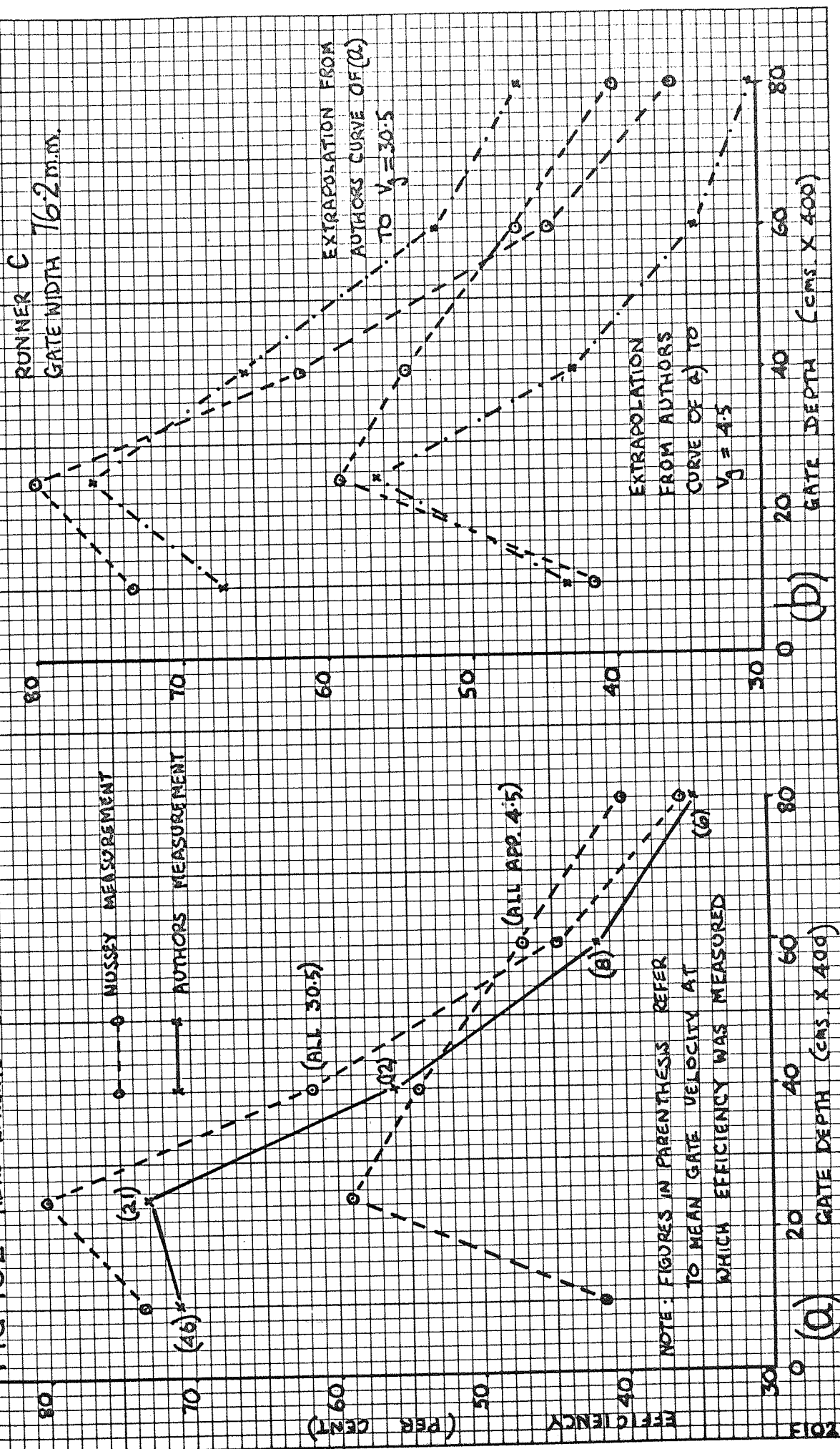


FIG 103 MEASUREMENTS OF EFFICIENCY VARIATION WITH LAND APPROACH ANGLE

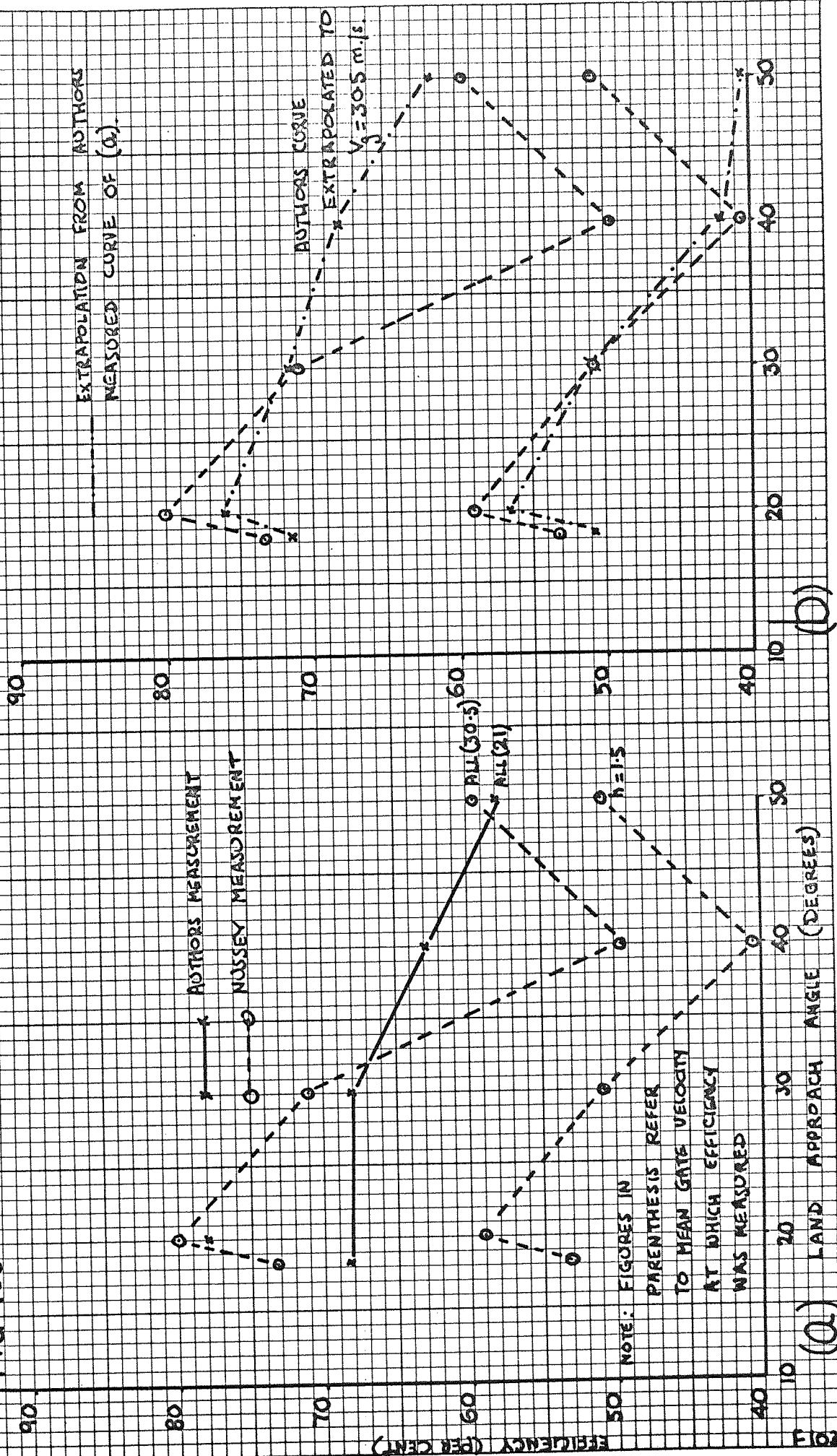
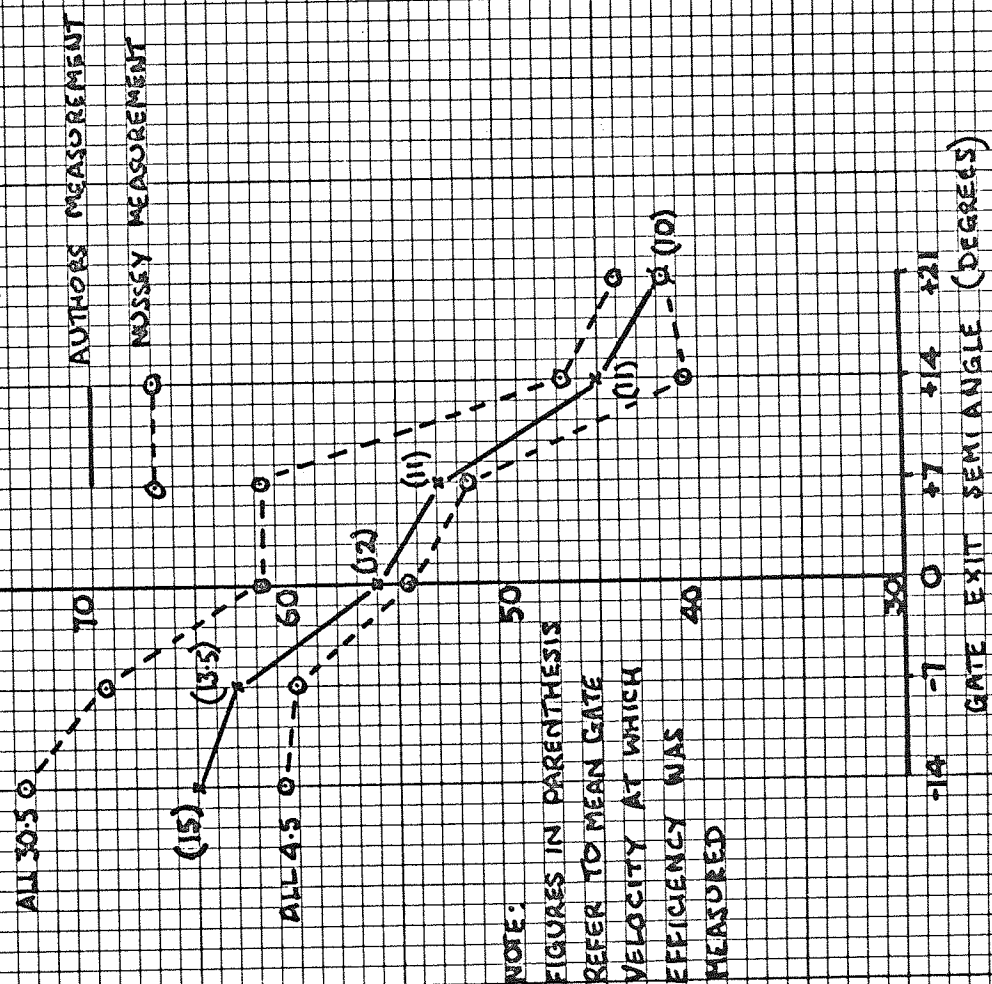


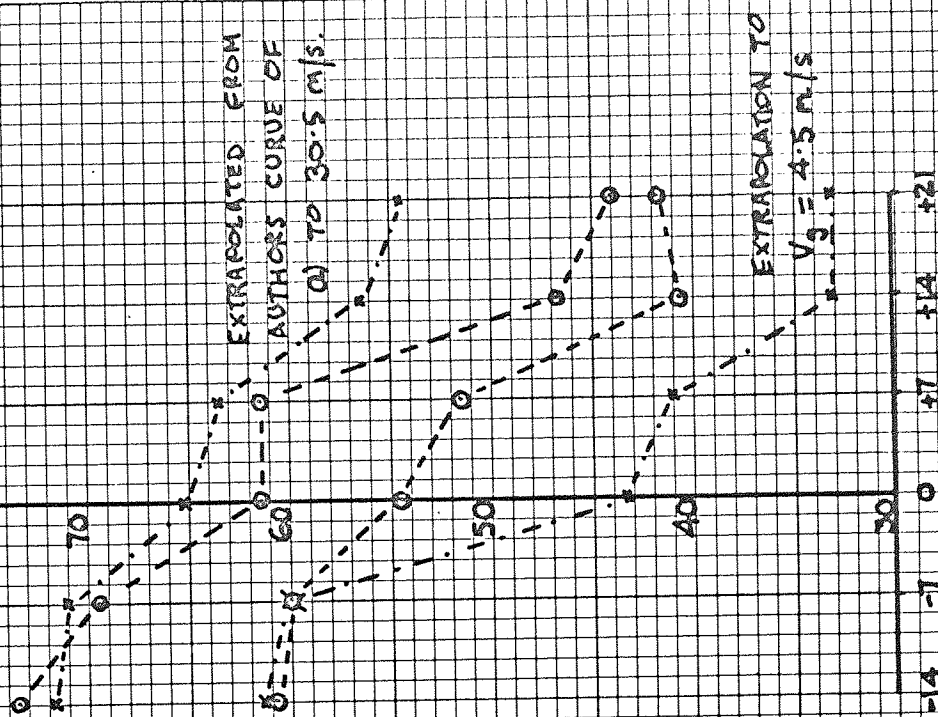
FIG 104 MEASUREMENTS OF EFFICIENCY VARIATION WITH GATE SEMI ANGLE
RUNNER C

(a)



NOTE:
FIGURES IN PARENTHESIS
REFER TO MEAN GATE
VELOCITY AT WHICH
EFFICIENCY WAS
MEASURED

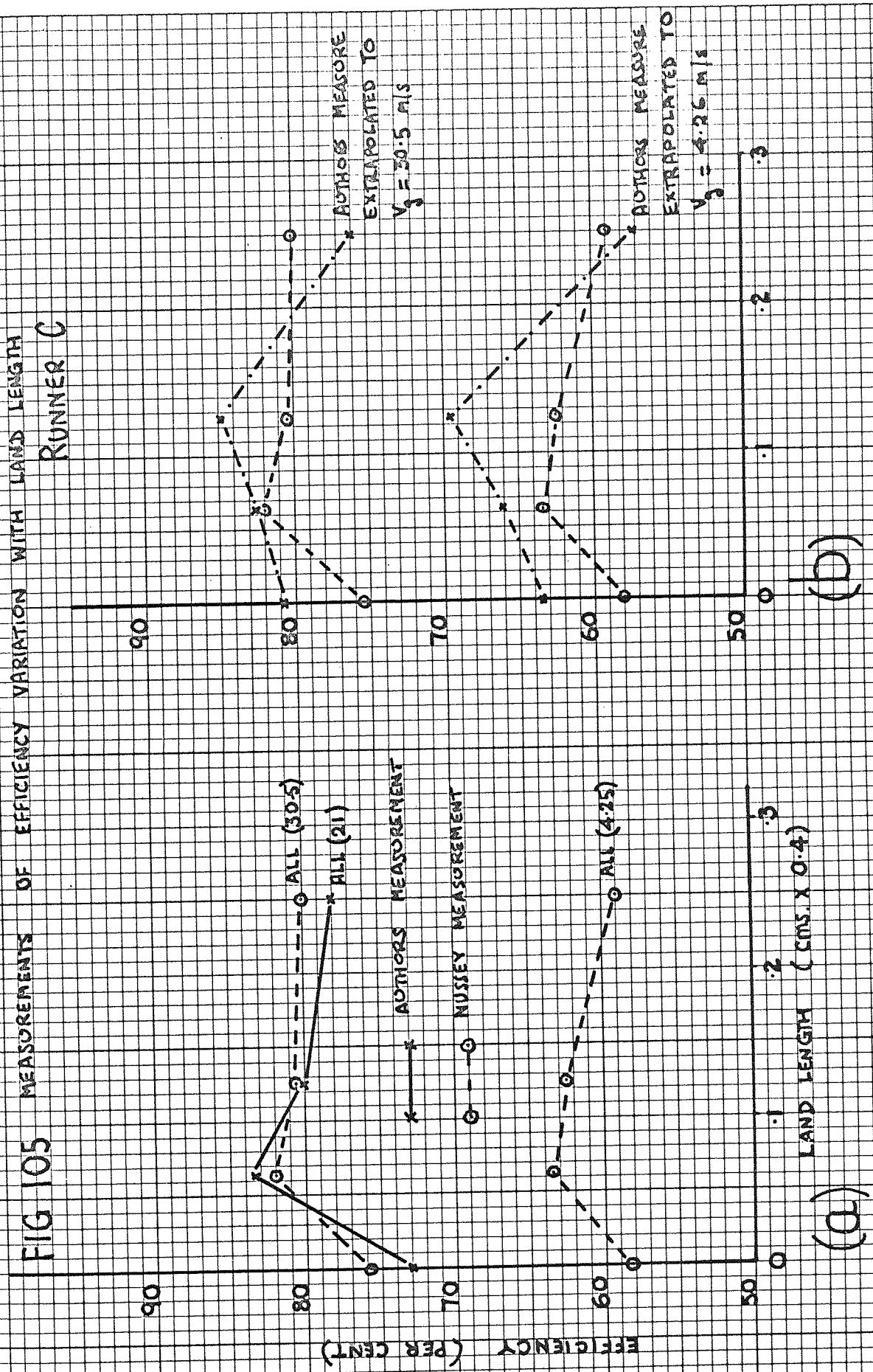
(b)

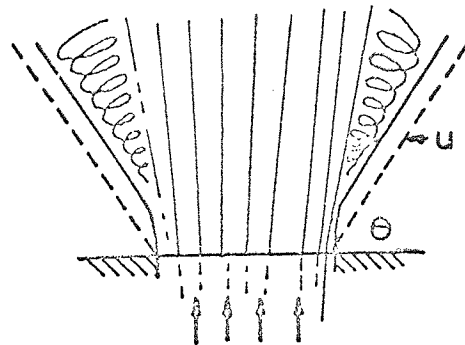


EXTRAPOLATION TO
 $V_g = 4.5 \text{ m/s}$

GATE EXIT SEMI ANGLE (DEGREES)

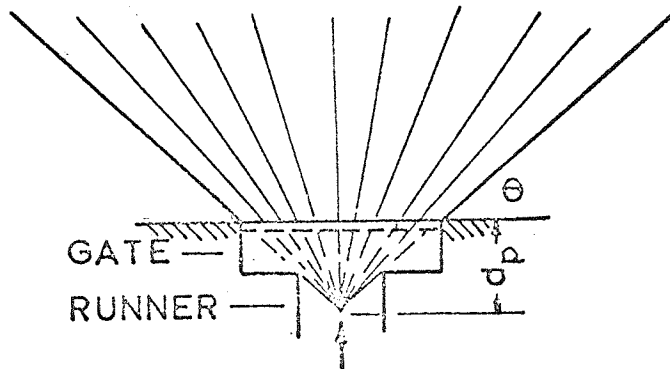
FIG 105 MEASUREMENTS OF EFFICIENCY VARIATION WITH LAND LENGTH
RUNNER C





LINE SOURCE I

(b)



GATE

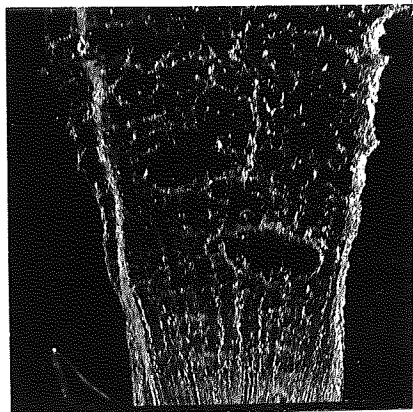
RUNNER

POINT SOURCE P

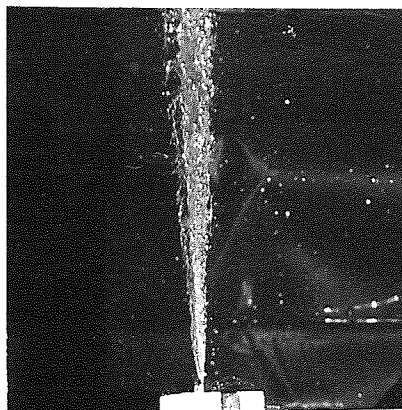
(a)

FIG 106 Diagrammatic representation of 'line' and 'point' source flow (after Nussey¹⁹)

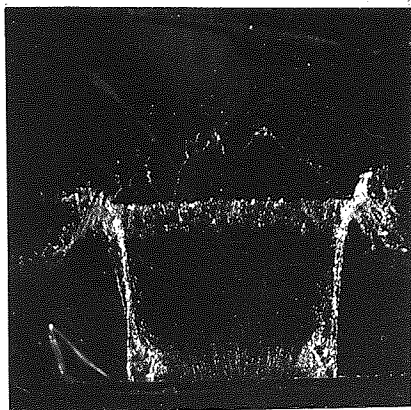
FRONT



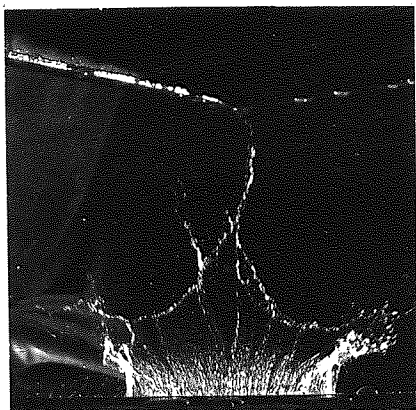
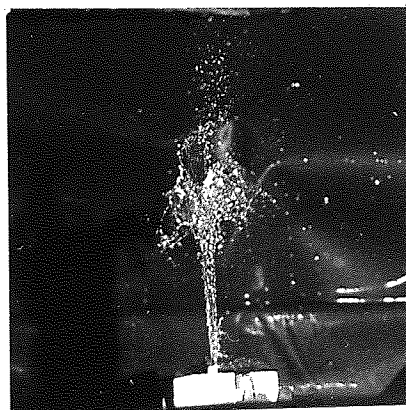
SIDE



STEADY



20 MS.



10 MS.

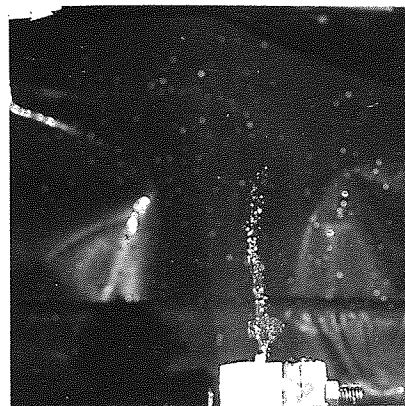


FIG 107

RUNNER : GATE COMBINATION C1 (choked)
Gate velocity at full flow app. 22 m/s

Note: elapsed times refer to photo cell
closure, not initiation of flow through
gate

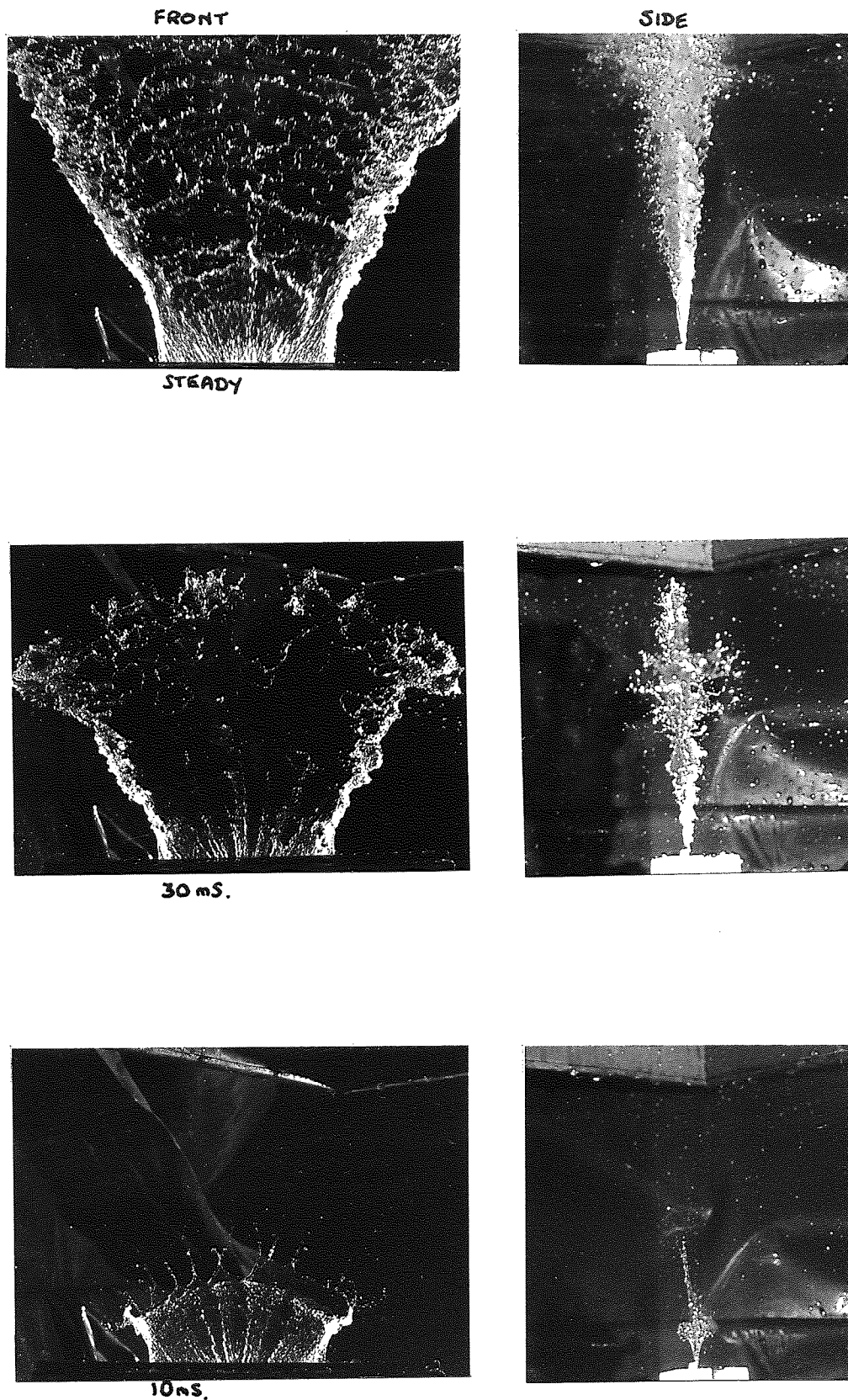


FIG 108

RUNNER : GATE COMBINATION A1 (unchoked)
Gate velocity at full flow app. 22 m/s

Note: elapsed times refer to photo cell closure,
not initiation of flow through gate

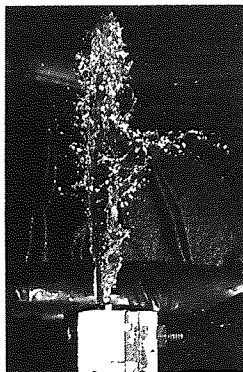


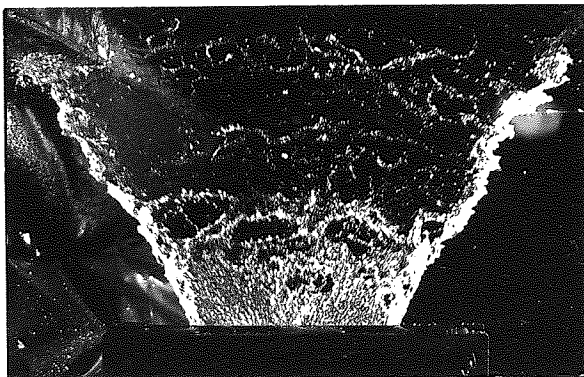
FIG 109

RUNNER : GATE COMBINATION A2
SIDEVIEW

Gate velocity at full flow app 22 m/s

Note: elapsed times refer to photo cell closure,
not initiation of flow through gate

FRONT



SIDE

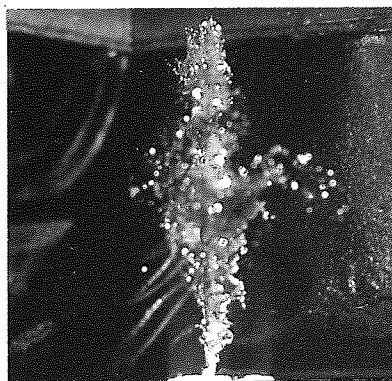


FIG 110

RUNNER : GATE COMBINATION C31 (unchoked)
FULL FLOW

Gate velocity at full flow app 22 m/s

Note: elapsed times refer to photo cell closure,
not initiation of flow through gate

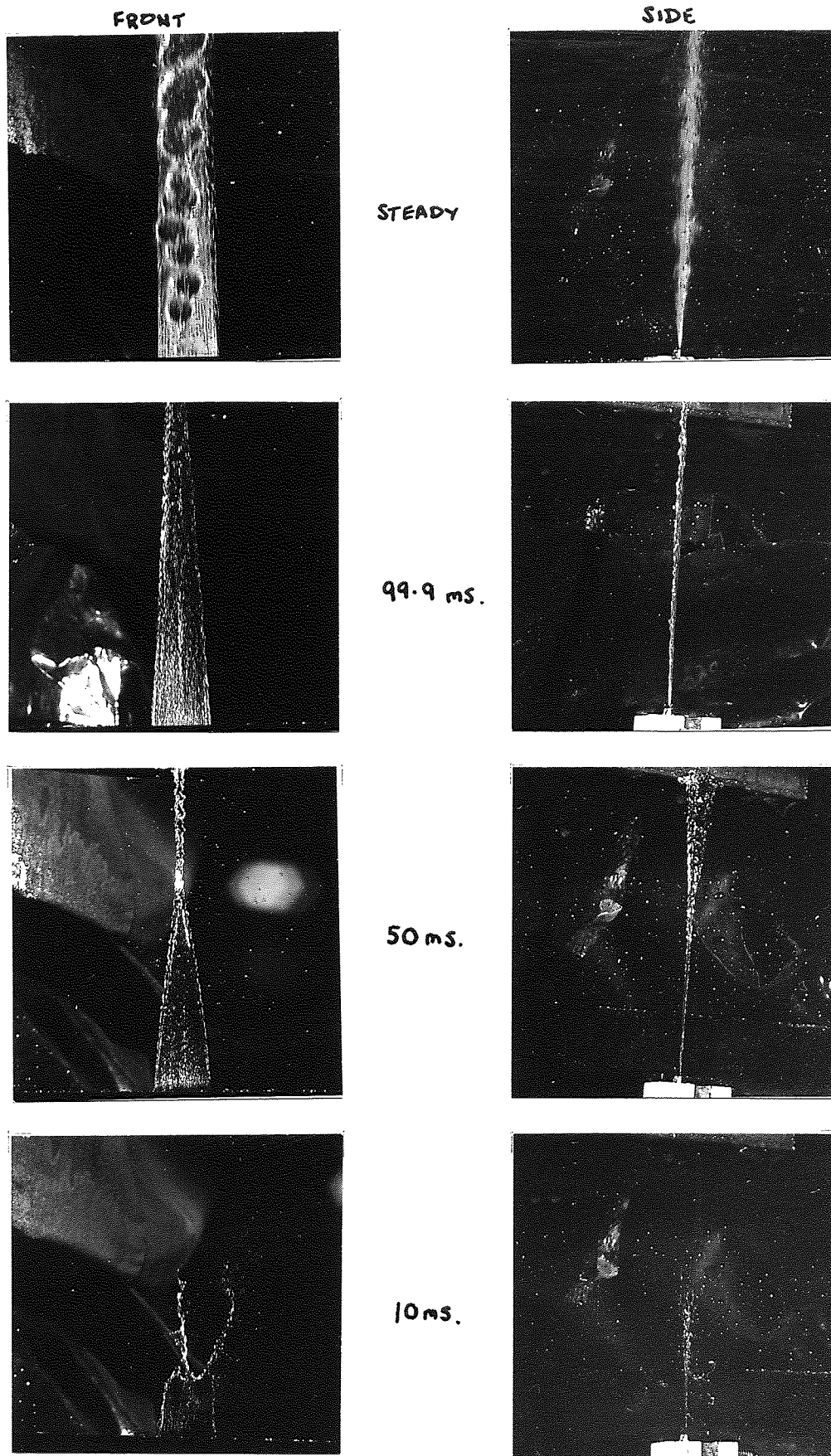
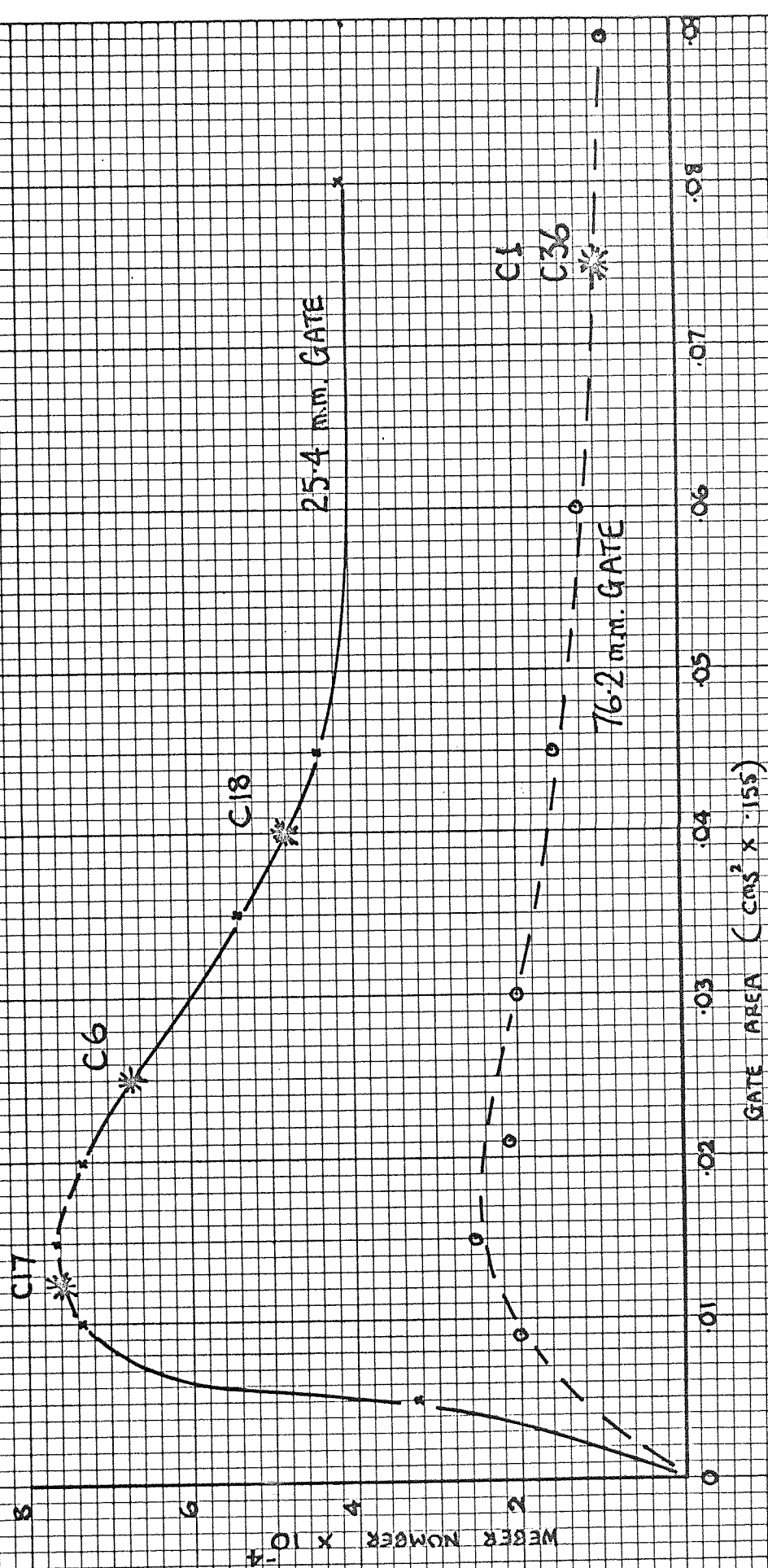


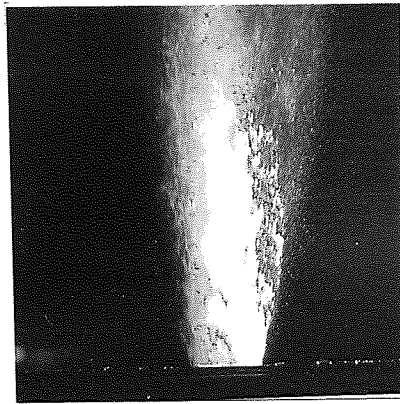
FIG 111 RUNNER : GATE COMBINATION C17 (choked)
Gate velocity at full flow app. 46 m/s

WEBER NUMBER VS GATE AREA
FOR FLOW RIG.

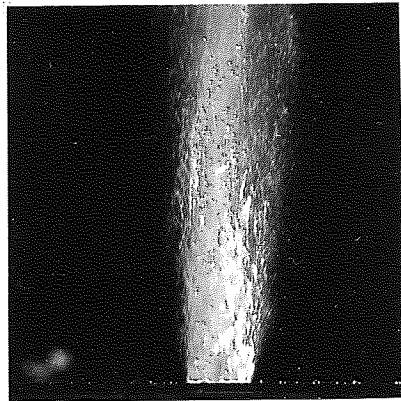
FIGURE 113



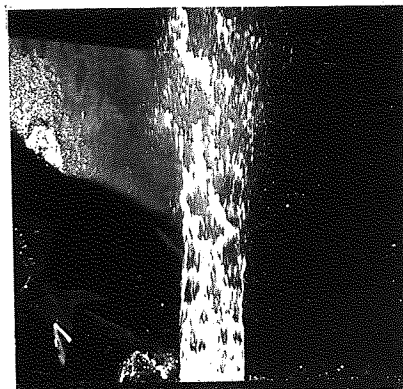
FRONT



C17



C6



C18

FIG 114 FULL FLOW CONDITIONS FOR VARIOUS
RUNNER : GATE COMBINATIONS (c.f. fig 113)

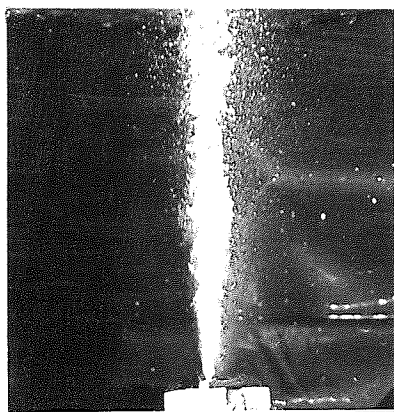
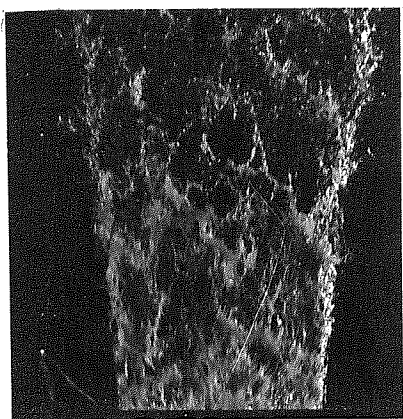
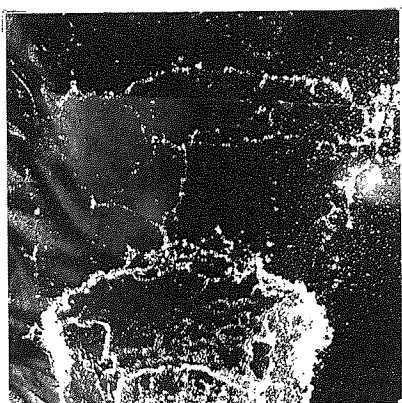
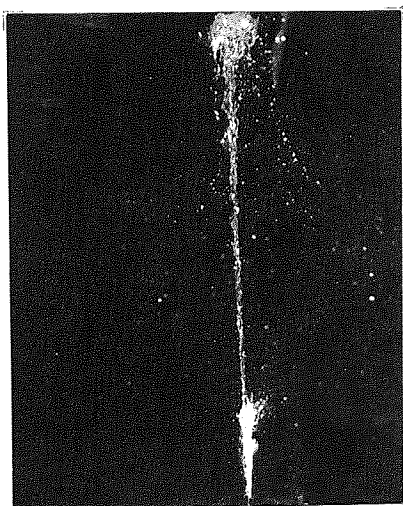
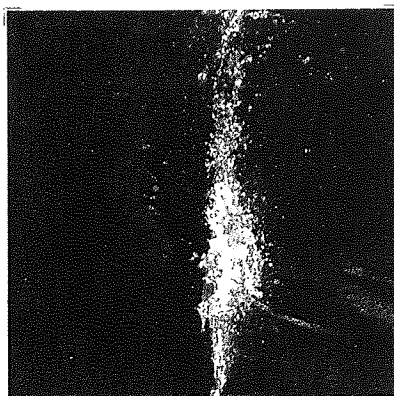


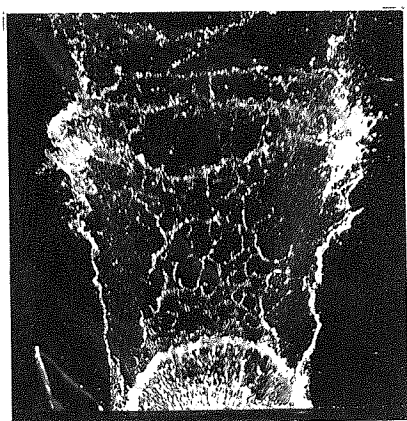
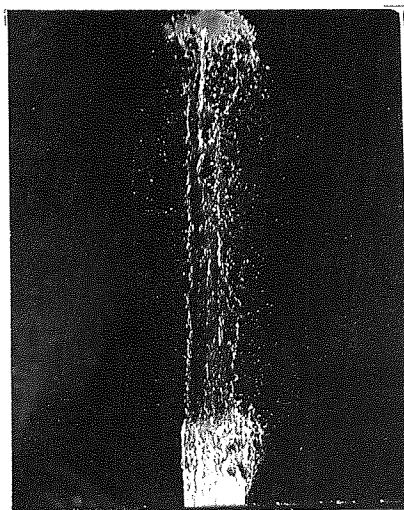
FIG 115 EFFECT OF AIR : FLUID MIXING
RUNNER : GATE COMBINATION C1



B9



C17



A1

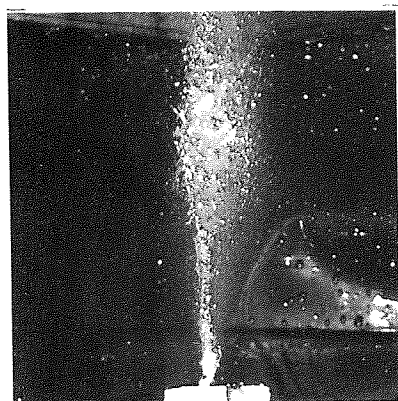


FIG 116 'EXPLOSIVE' BREAKDOWN IN FLOW THROUGH
VARIOUS RUNNER : GATE COMBINATIONS

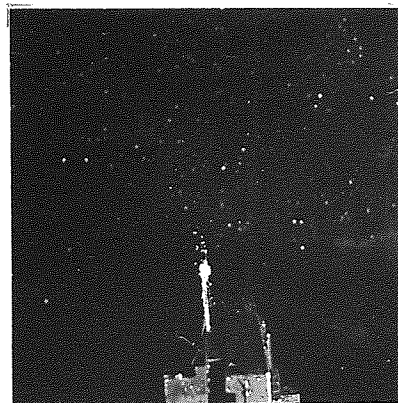
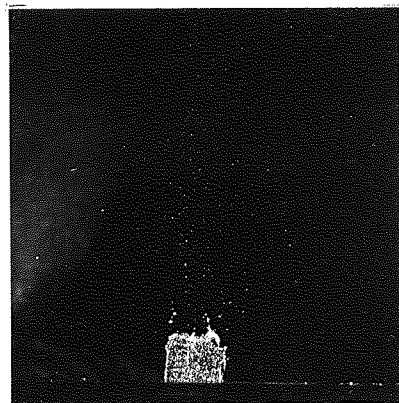
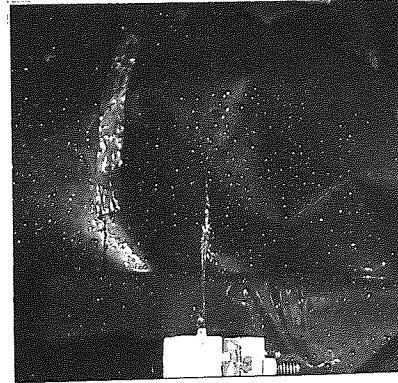
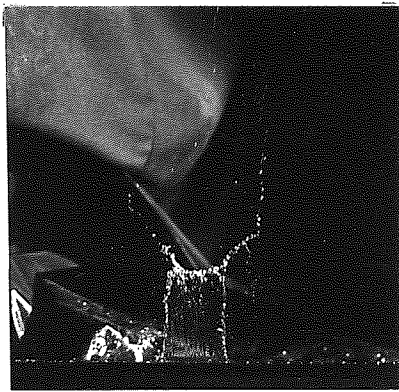
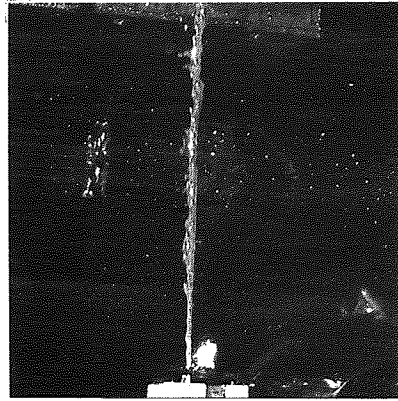
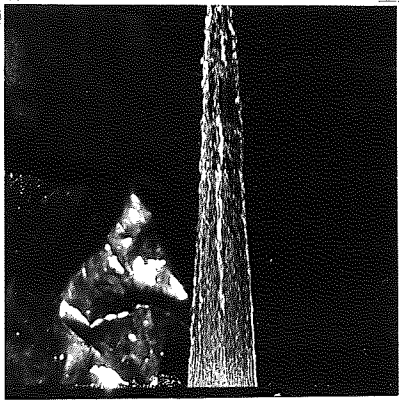


FIG 117 a) TRANSITION STAGES, UNRESTRICTED FLOW
THROUGH RUNNER : GATE COMBINATION C6

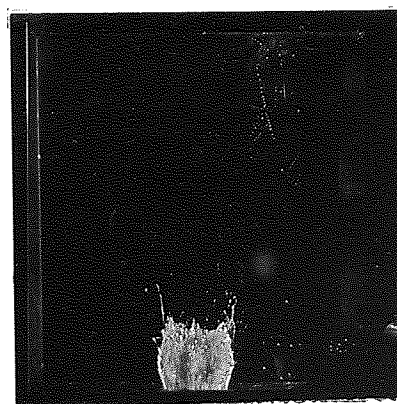
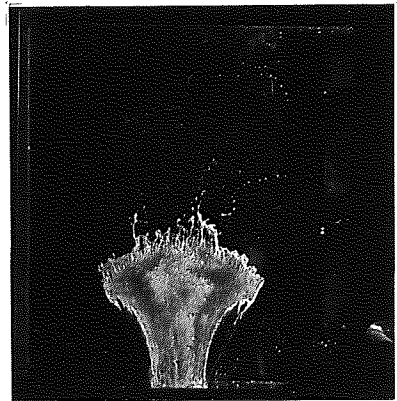
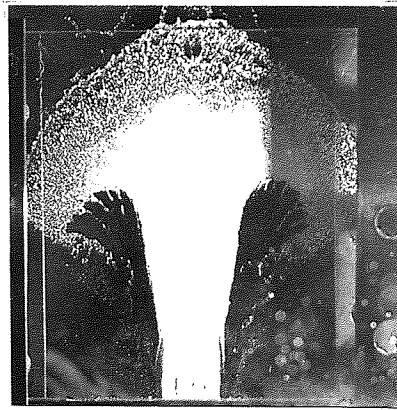
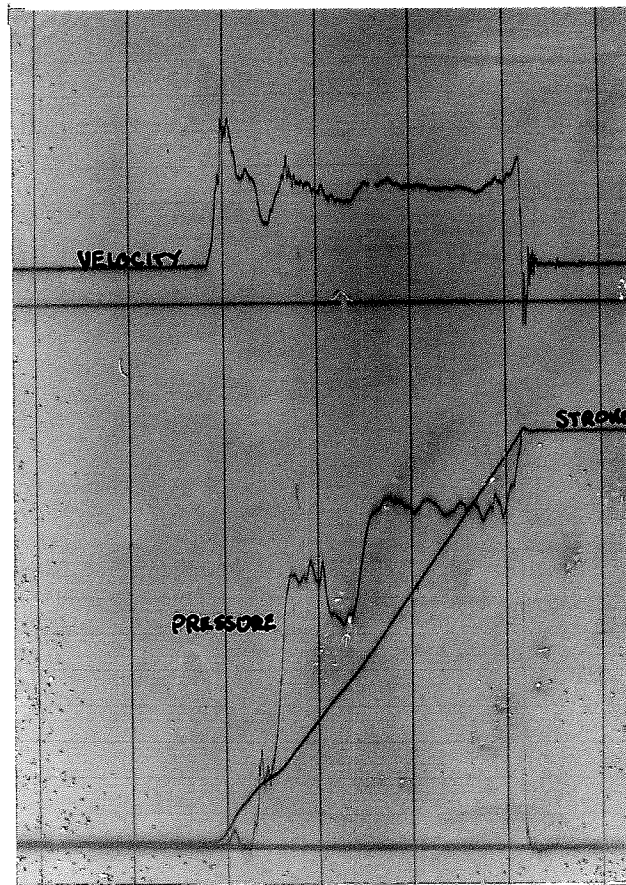
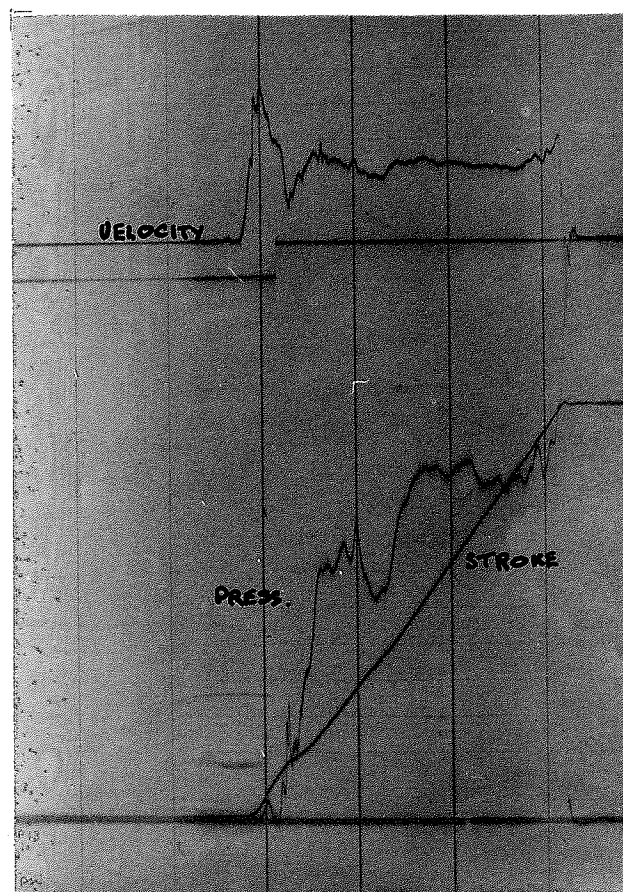


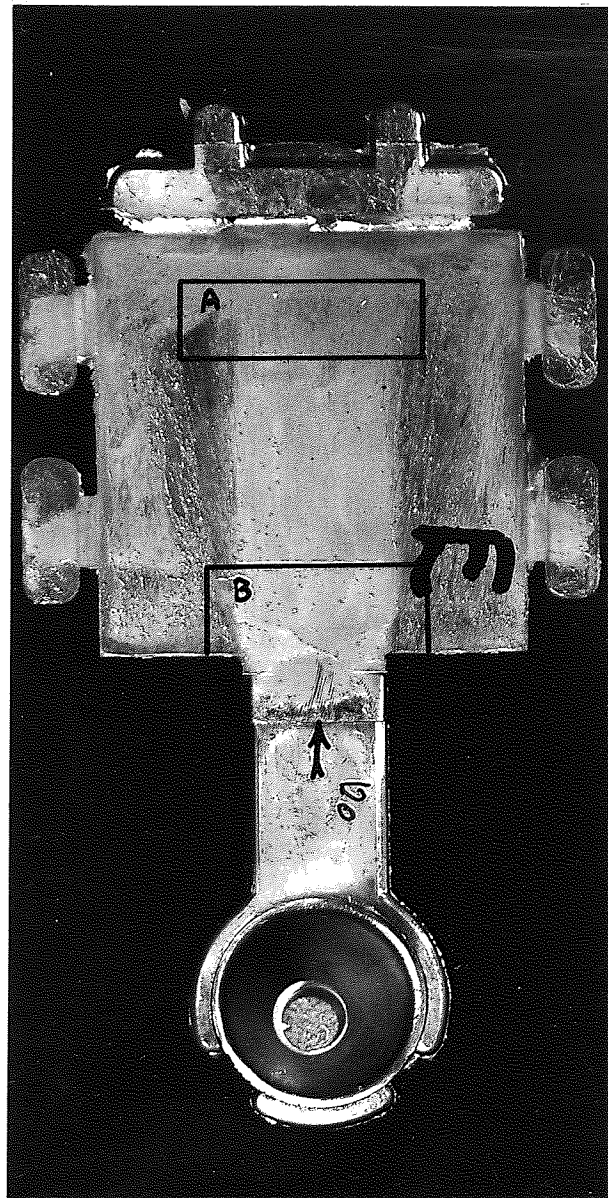
FIG 117 b) TRANSITION STAGES, FLOW RESTRICTED BY
PARALLEL PLATES RUNNER : GATE COMBINATION
C6



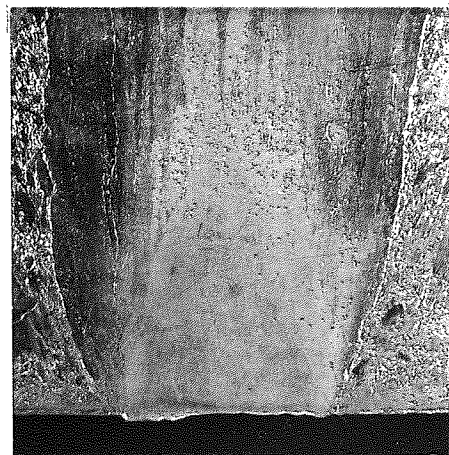
a) TRACE RECORD FOR UNRESTRICTED FLOW



b) TRACE RECORD, FLOW RESTRICTED BY PARALLEL PLATES

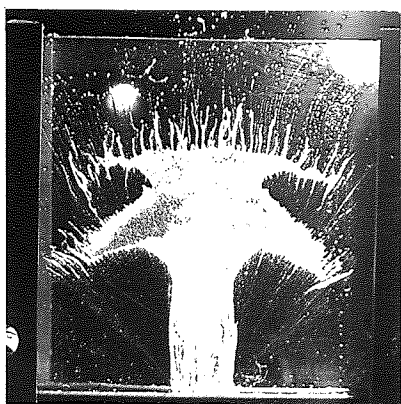


ENLARGEMENT AREA A

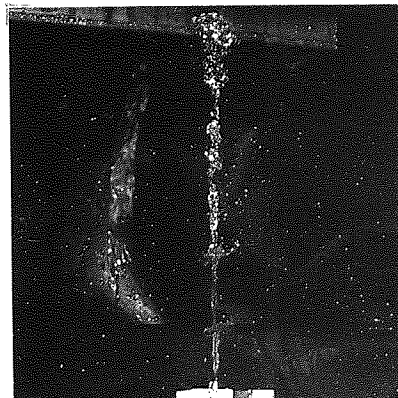
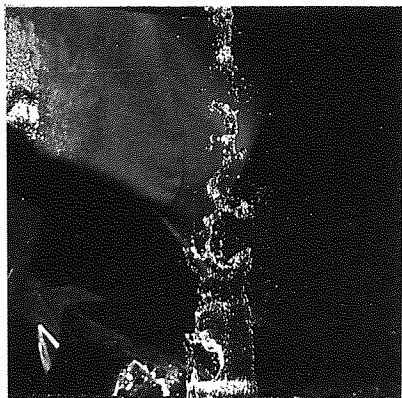


ENLARGEMENT AREA B

FIG 118 FLOW DEFECTS OF FIG 117a, b



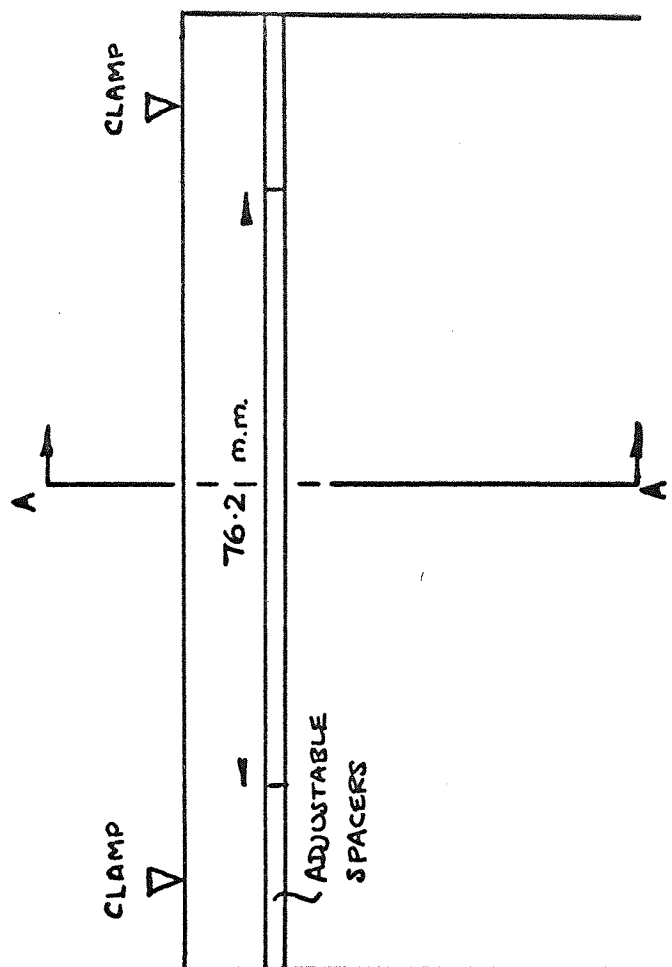
EXPLOSIVE BREAKDOWN RESTRICTED FLOW



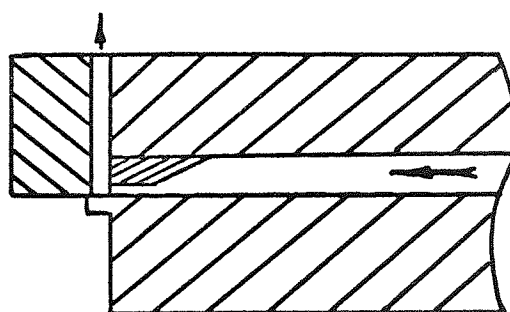
EXPLOSIVE BREAKDOWN UNRESTRICTED FLOW

FIG 119 RUNNER : GATE COMBINATION C6 **CP** FIG 117

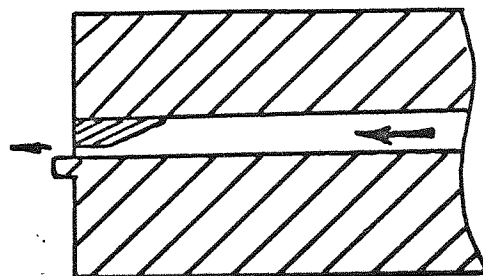
FIG 120 DIAGRAMMATIC REPRESENTATION OF OBSTACLE CONFIGURATION.



NOT TO SCALE



RESTRICTED
(VIEW AA)



UNRESTRICTED

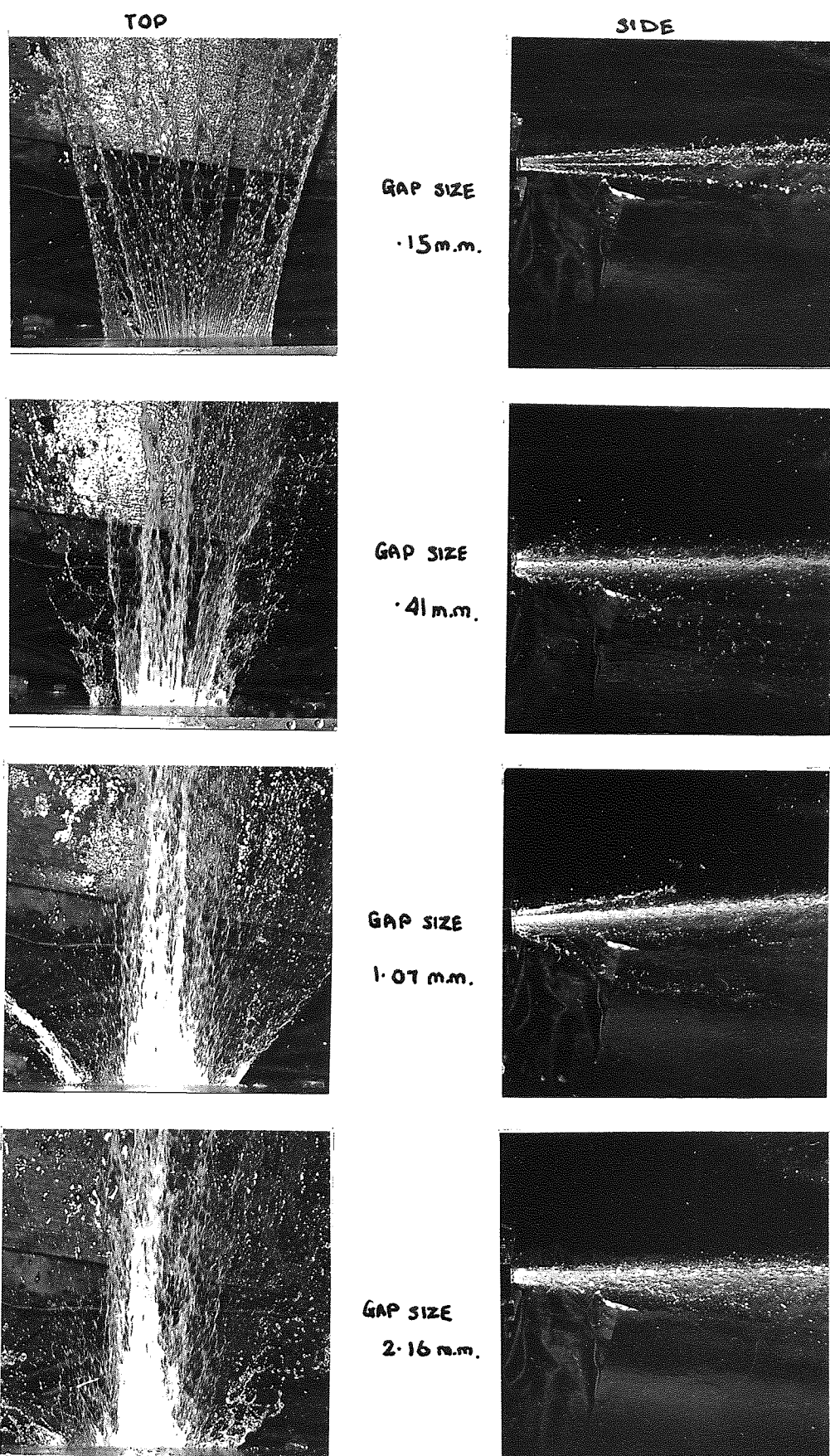
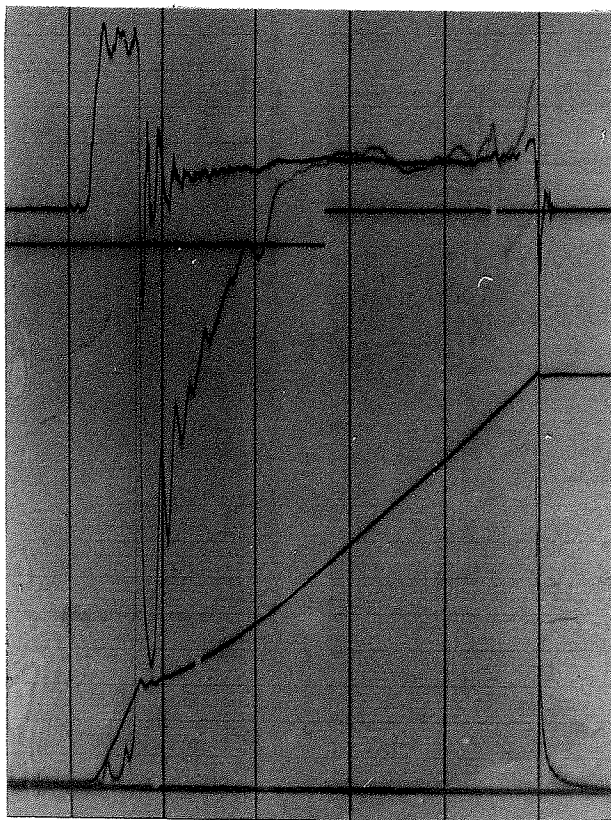
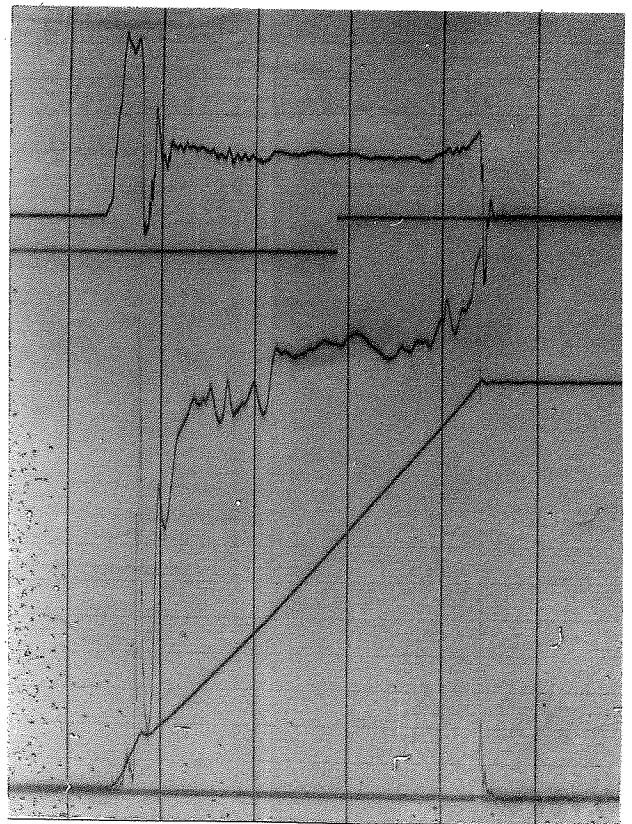


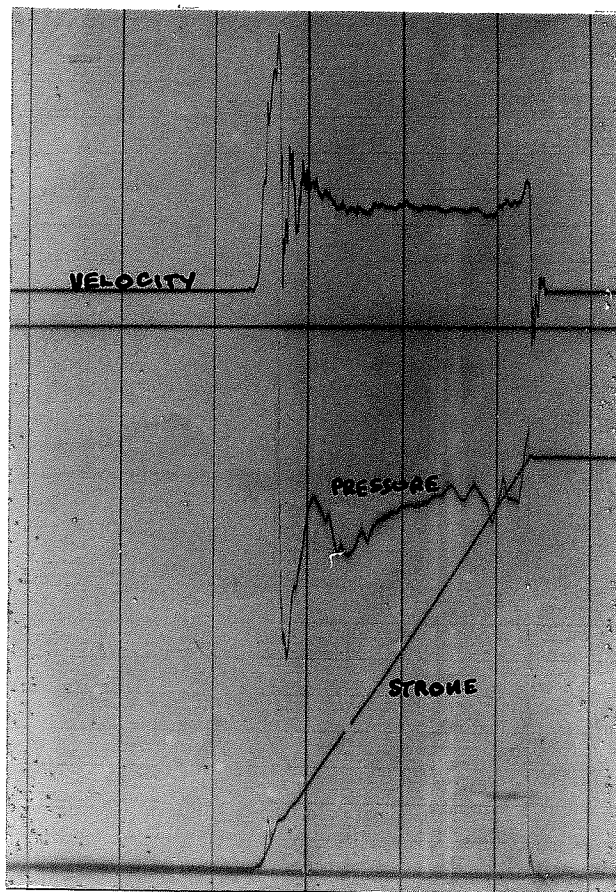
FIG 121a EFFECTS OF PLATE OBSTACLE PERPENDICULAR TO
FLOW FROM RUNNER : GATE COMBINATION C6



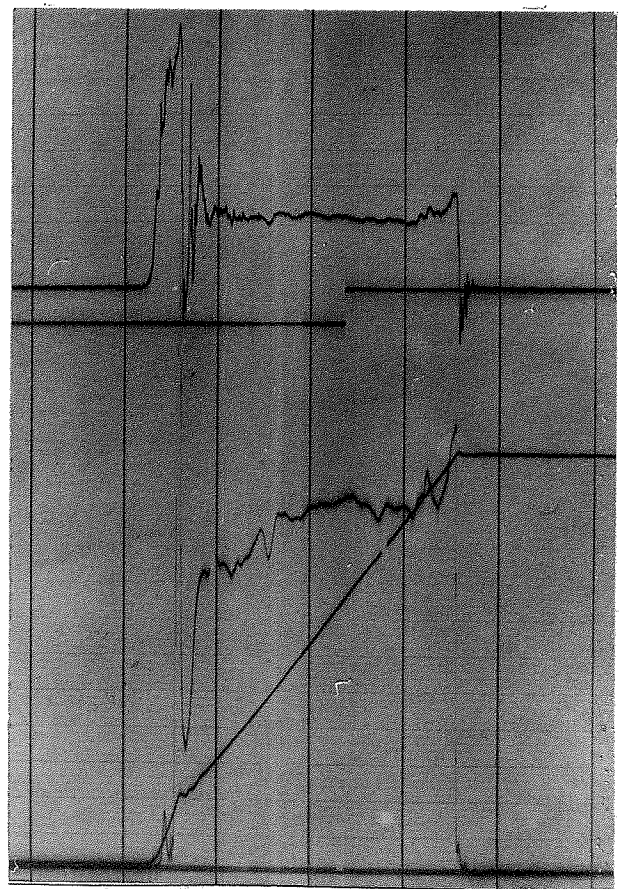
GAP SIZE 15 mm.



GAP SIZE 41 mm.



GAP SIZE 2.16 mm.



GAP SIZE 1.07 mm.

FIG 121b TRACE RECORDS SHOWING EFFECTS OF PLATE OBSTACLE PERPENDICULAR TO FLOW FROM RUNNER - GATE COMBINATION C6

